UNIVERSIDADE D
COIMBRA

Pedro Gonçalo Banza Gonçalves

MONITORING AND IMPROVEMENT OF A MULTI-PHASE REACTION SYSTEM

Tese no âmbito do Programa Doutoral em Engenharia da Refinação, Petroquímica e Química, orientada pelo Professor Doutor Nuno Manuel Clemente de Oliveira, coorientada pela Professora Doutora Carla Isabel Costa Pinheiro, coordenada pela Doutora Dulce Cristina Martins da Silva e apresentada ao Departamento de Engenharia Química da Faculdade de Ciências e Tecnologia da Universidade de Coimbra.

Outubro de 2021

work finantially supported by:

under the program *Bolsas de Doutoramento em Empresas* PD/BDE/113542/2015

MONITORING AND IMPROVEMENT OF A MULTI-PHASE REACTION SYSTEM

Pedro Gonçalo Banza Gonçalves

Dissertação apresentada à Faculdade de Ciências e Tecnologia da Universidade de Coimbra, para obtenção do grau de Doutor em Engenharia da Refinação, Petroquímica e Química.

outubro de 2021

Orientação académica: Professor Doutor Nuno Manuel Clemente de Oliveira

Co-orientação académica: Professora Doutora Carla Isabel da Costa Pinheiro

Coordenação empresarial: Doutora Dulce Cristina Martins da Silva

Dedico este trabalho à minha família.

Obrigado por tudo.

Agradecimentos

Em primeiro lugar, gostaria de expressar a minha sincera gratidão ao meu orientador académico Professor Doutor Nuno Oliveira, por todo o apoio dado ao longo deste projeto, pela sua paciência e pelo conhecimento transmitido. A sua orientação permitiu-me que persistisse em pensar “fora da caixa”, perante os resultados obtidos durante esta investigação.

Em segundo lugar, gostaria de agradecer à minha coorientadora académica, Professora Doutora Carla Pinheiro por sempre persistir na importância da relação estreita entre a indústria e a academia. A sua proatividade neste assunto guiou-me na escrita desta tese, considerando a gestão dos conteúdos abordados.

Em terceiro lugar, o meu sincero apreço à Doutora Dulce Silva, a minha coordenadora empresarial, pelo seu incansável apoio e orientação durante este projeto. A sua vasta experiência e pragmatismo encorajou-me a aplicar e desenvolver o meu próprio espírito crítico na Bondalti Chemicals S.A. Aqui, eu tive a oportunidade de ter uma experiência única na minha formação, ao contactar com a realidade dos processos industriais. À empresa, expresso o meu sincero agradecimento por me ter facultado a acomodação e as condições de trabalho necessárias para realização desta investigação em ambiente industrial. O meu especial apreço aos departamentos de Inovação, Desenvolvimento e Engenharia de Processo, Produção, e de Controlo de Qualidade, por toda a cooperação e partilha de conhecimentos. O meu especial agradecimento ao Doutor Paulo Araújo e ao Eng. Mário Jorge Pinho por terem impulsionado as condições para a criação deste projeto de doutoramento em ambiente industrial – o seu rigor e ambição foram essenciais no decorrer deste trabalho.

Um agradecimento especial à Bondalti Chemicals S. A. e à FCT – Fundação para a Ciência e Tecnologia, pelo seu apoio financeiro na bolsa de doutoramento PD/BDE/113542/2015. De realçar também o apoio financeiro disponibilizado pela PRODEQ – Associação para o Desenvolvimento da Engenharia Química durante os últimos meses de realização desta tese.

Gostaria também de expressar o meu agradecimento ao Professor Doutor José Paixão, do Departamento de Física da Universidade de Coimbra, por todo o apoio e

disponibilidade durante os últimos meses do estudo de caraterização de materiais realizado neste trabalho.

Um especial agradecimento aos meus colegas da “Família Palacete”, donde construí fortes laços para a vida. Muito obrigado por todas as alegrias e lágrimas partilhadas neste período. Obrigado por toda a amizade, apoio e crescimento pessoal.

Por último, mas não menos importante, gostaria de agradecer à minha família e amigos pelo seu apoio incondicional, pela inteligência emocional e pela força dadas durante toda esta etapa.

Acknowledgements

Firstly, I would like to express my sincere gratitude to my academic advisor Professor Doctor Nuno Oliveira for the continuous support over the course of this project, for his patience, and immense knowledge. His guidance helped me to persist on thinking *beyond the box* towards the results obtained during this research.

Secondly, I would like to say thanks to my joint academic advisor Professor Doctor Carla Pinheiro by always persisting on the importance of close partnership between the industry and the academia. Her proactiveness on this issue guided me to write this thesis, concerning the management of contents.

Thirdly, I am pleased to express my appreciation to Doctor Dulce Silva, my entrepreneurial coordenator, for her tireless support, advice, and guidance throughout this project. Her vast experience and pragmatic view on the industry encourage me to believe and develop my own critical thinking at Bondalti Chemicals S. A. Here, I had the opportunity to have a *hands-on experience* by directly contacting with large-scaled processes. To the company, I would like to express my special gratitude of providing me the accommodation and the working conditions needed for the course for this investigation. My special appreciation also to the departments of R&D/Process Engineering, Production, Quality Control Laboratory, for all the cooperation given and knowledge shared. My special appreciation to Doctor Paulo Araújo and Eng. Mário Jorge Pinho for driving the conditions to initiate this PhD project in entrepreneurial environment – their rigor and ambition were essential in the course of this work.

A special thankfulness to Bondalti Chemicals S. A. and FCT – Fundação para a Ciência e Tecnologia, for their financial support to the PhD grant PD/BDE/113542/2015. In addition, a worth mention to PRODEQ – Associação para o Desenvolvimento da Engenharia Química, for the financial support given in the last months of this thesis.

I would like also to express my gratitude to Professor Doctor José Paixão, from the Department of Physics of the University of Coimbra, for all the support and availability given during the last months of the characterisation study performed in this investigation.

A special gratitude to all my fellow colleagues of “*Familia Palacete*”, from where I created strong bonds for life. Thank you so much for all the joys and tears shared in the same period. Thank you for all the friendship, support, and personal growth.

Last but not the least, I would like to thank my family and friends for their unconditional support, providing me the emotional intelligence and strength to overcome all the obstacles throughout my life.

Resumo

Nesta tese abordou-se a operação de um sistema reacional multifásico utilizado para a produção industrial de anilina, onde a hidrogenação do nitrobenzeno em fase líquida ocorre usando um catalisador de níquel suportado em sílica. Foi desenvolvido um modelo matemático para o reator industrial, tendo sido testado numa gama representativa de condições operatórias. Atendendo à análise dos dados industriais, foi possível confirmar que a velocidade da reação é controlada pela transferência de massa de nitrobenzeno. Posto isto, aponta-se que a produtividade do sistema dependa da estabilidade da suspensão de catalisador, de forma a promover a transferência de massa na mistura reacional.

Dado que a política de adição de catalisador fresco ao sistema pode afetar significativamente o desempenho da unidade, realizou-se um estudo de caracterização do catalisador através de recolha de amostras no sistema industrial. Este estudo visou a avaliação das eventuais alterações físico-químicas deste material ao longo do tempo. Os resultados da caracterização indicaram, em geral, que o catalisador tende a perder o seu suporte de sílica, possivelmente devido ao efeito abrasivo induzido pela agitação do reator. Em paralelo, verificou-se que o catalisador usado apresenta uma fração significativa de níquel cristalino, quando comparado com os catalisadores frescos. Este resultado motivou a caracterização magnética deste material, tendo-se confirmado que o catalisador tende a aumentar a sua resistência à desmagnetização (coercividade).

Adicionalmente, procedeu-se ao acompanhamento da operação do reator industrial, onde se realizaram várias medições de concentração de catalisador no mesmo período de observação. Durante este período, registaram-se vários eventos onde a concentração de catalisador diminuiu de forma significativa, independentemente da quantidade de catalisador fresco adicionada ao sistema. Este comportamento foi avaliado através de vários testes industriais que indicaram que a deposição/acumulação de catalisador no interior do reator seria a causa mais plausível para explicar este fenómeno. Esta hipótese foi também sustentada pela redução do desempenho dos dispositivos de transferência de calor observada no mesmo período. Posteriormente, a existência de depósitos de catalisador foi confirmada durante um procedimento de manutenção do reator industrial. Assim, recomenda-se que o coeficiente global de transferência de calor do sistema seja monitorizado, visando o planeamento de paragens do sistema e de limpeza do equipamento.

A caracterização magnética dos catalisadores frescos também evidenciou que estes apresentavam distintos valores de coercividade. Tendo em conta as implicações relativas à deposição de catalisador no sistema, propôs-se a adição de catalisador fresco de menor coercividade no reator industrial. Após a limpeza do sistema, o reator foi apenas alimentado com catalisador fresco de baixa coercividade, tendo-se verificado que a concentração de catalisador em suspensão aumentou. Esta observação sugere que a adição de catalisador fresco com uma dada coercividade pode ser bastante eficaz no controlo da concentração de catalisador. Uma vez que a política de adição de catalisador fresco pode afetar significativamente o desempenho do sistema, desenvolveu-se uma ferramenta de monitorização com base nos resultados validados pelo modelo. Deste modo, o efeito da adição de catalisador na previsão da conversão de nitrobenzeno pode ser considerado de uma forma mais precisa. Além disso, desenvolveu-se uma nova estratégia de controlo do reator que visa o controlo do tempo de retenção hidráulico do reator. Esta abordagem contrasta com a atual estrutura de controlo aplicada à alimentação do reator, onde o valor de referência da corrente de anilina reciclada por intermédio de um rácio preestabelecido em função do caudal de entrada de nitrobenzeno. Em resultado desta alteração, a conversão do nitrobenzeno melhorou, tendo-se mantido estável posteriormente.

Por fim, propôs-se um procedimento de monitorização e controlo do reator industrial, considerando as melhorias efetuadas ao longo deste trabalho. Este procedimento envolve o controlo estatístico do reator com base no modelo do processo desenvolvido. Caso o estado do processo se encontre fora dos limites de controlo estatístico ou se prevejam elevadas concentrações de nitrobenzeno no vaso reacional, sugere-se, como medida corretiva, o ajuste do tempo de retenção hidráulico do reator. Caso esta solução seja ineficaz, sugere-se a avaliação da concentração de catalisador no reator - se esta for elevada, recomenda-se a adição de catalisador fresco para promover a transferência de massa de nitrobenzeno, caso contrário, aconselha-se a avaliação do estado da transferência de calor do reator. Uma vez confirmado o bom desempenho dos dispositivos de permuta de calor, a adição de catalisador fresco deve ser assegurada para manter a concentração de catalisador dentro da gama de operação e, por conseguinte, a transferência de massa de nitrobenzeno; caso contrário, a deposição de catalisador no sistema é identificada como ocorrendo, sugerindo o planeamento da paragem do sistema para ações de limpeza numa escala significativa.

A aplicação da modelação matemática no presente trabalho, permitiu o desenvolvimento de uma abordagem sistémica de condução da operação industrial. Deste modo, foi possível estruturar uma nova ferramenta de monitorização e de diagnóstico que pode ser continuamente atualizada através da incorporação de novos dados operatórios. Desta forma, o processo industrial poderá tornar-se mais robusto, estando em melhores condições para operar dentro de limites operatórios que maximizem a sua produtividade.

PALAVRAS-CHAVE: Reator multifásico, catalisador, monitorização do processo

Abstract

This thesis addresses the operation of a multi-phase reaction system applied to the industrial production of aniline, where the liquid-phase hydrogenation of nitrobenzene occurs using a nickel supported on silica catalyst. A mathematical model of the industrial reactor is here developed and tested under a representative range of operating conditions. Through the analysis of industrial data gathered, it was possible to confirm that the reaction rate is limited by the mass transfer of nitrobenzene. Consequently, maintaining a stable catalyst concentration in the suspension is important to guarantee the regular operation of the unit.

Since the catalyst addition policy can significantly influence the behaviour of the unit, a detailed characterisation of the catalyst was considered. This study addressed the physico-chemical changes of this material with time. The characterisation results indicate that the catalyst tends to lose its silica support, possibly due to the abrasive effect induced by the reactor agitation. In parallel, a higher fraction of crystalline nickel in the used catalyst samples was verified, in comparison with the fresh catalysts. This result motivated the magnetic characterisation of this material, where the increasing resistance to demagnetisation (coercivity) of the catalyst was confirmed. Additionally, the process operation was followed, where several measurements of catalyst concentration were performed during an extended period. Various events were detected where the concentration of catalyst suffered significant decreases, irrespective of the quantity of fresh catalyst added to the system. This behaviour was evaluated through several industrial trials that indicated that the catalyst accumulation/deposition in the internals of the reactor was appeared as the most plausible cause to explain this phenomenon. This hypothesis was further sustained by observing that the performance of the heat exchanging devices also decayed in the same period. Later, the existence of catalyst deposits was confirmed during a maintenance procedure performed to the industrial unit. Because of this, the monitoring of the overall heat transfer coefficient is recommended to plan future shutdowns and cleaning of the equipment.

The magnetic characterisation also evidenced that the fresh catalysts depicted distinct coercivity values. Considering the underlying implications related to the catalyst deposition in the industrial reactor, the addition of a low-coercivity catalyst to the system was proposed; after cleaning the system, this was attempted, noticing that the catalyst concentration had increased afterwards. This observation indicates that the catalyst

addition could be significantly effective on controlling the catalyst concentration. Since the catalyst addition policy can significantly influence the performance of the system, a process monitoring tool was developed based on the validated model results. This allows the effects of catalyst additions to be considered in a more precise form. In addition to this, a new control strategy of the reactor was developed, where the control of the hydraulic retention time of the reactor was considered. This approach contrasts the current control strategy applied to the reactor feed, where the reference value of the recycled aniline flowrate is based on a predefined ratio as function of the nitrobenzene feed flowrate. This modification led to the improvement of the nitrobenzene conversion afterwards.

Finally, a procedure for process monitoring and control is proposed, considering the advances made in the present work. This procedure involves the statistical control of the industrial reactor supported by a process model. If the state of the process is diagnosed to be near or outside the operational limits, or if high nitrobenzene bulk concentrations are detected in the reaction mixture, the adjustment of the hydraulic retention time of the industrial reactor is recommended, as a corrective measure. If the latter solution is not effective, the catalyst concentration needs to be revaluated – if this value is small and outside the desired range, a catalyst make-up is advised to promote the mass transfer of nitrobenzene, otherwise an evaluation of the heat transfer of the reactor is recommended. Once confirmed the good performance of the heat exchanging devices, the addition of fresh catalyst should be performed that the desired range of catalyst concentration is maintained and, in turn, the expected mass transfer and conversion of nitrobenzene; otherwise, the shutdown of the industrial unit should be timetabled for cleaning procedures.

The application of mathematical modelling in the present work allowed the development of a systematic approach for the operation of the industrial unit. This enabled the establishment of a new tool for process monitoring and diagnosis, which can be continuously updated through the incorporation of updated data. This allows a more robust operation, guaranteeing that the operating limits can be maintained through longer time periods, improving the productivity of the unit.

KEYWORDS: Multiphase reactor, catalyst characterisation, catalyst addition, process monitoring

Science, my lad, is made up of mistakes, but they are mistakes which it is useful to make, because they lead little by little to the truth.

Jules Verne (1828–1905)

Contents

List of Figures

List of Tables

Nomenclature

Roman letters		Greek letters	
a	External area	α	Solubility
a*	Specific external area	ρ	Density
C	Concentration	β	Conversion factor
c	Specific heat	μ	Dynamic viscosity
D	Diffusivity	ν	Kinematic viscosity
d	Size	ϵ	Holdup
Q	Volumetric flowrate	ϑ	Stochiometric coefficient
f	Fraction of available cat. sites	η	Electric motor efficiency
Fr	Froude number	λ	Thermal conductivity
G	Mass flowrate	φ	Related to power factor
g	Gravitational acceleration	κ	Factor (Equation 2.11)
H	Enthalpy	Subscripts	
h	Heat transfer coefficient	ANL	Aniline
He	Henry constant	AS	Active site
I	Current Intensity	AST	Total active sites
K	Adsorption constant	b	Bubbles
k	Kinetic constant/Mass Transfer Coeff./Cat .activation constant	cat	Catalyst
MTR	Maximal mass transfer rate	CD	Complete dispersion state of gas bubbles
MW	Molecular Weight	CG	Gas induction
N	Agitator speed	cw	Cooling Water
n	Overall molar consumption rate	C	Condensate
Nu	Nusselt number	D	Dispersion (Three phase mixture)
P	Pressure	f	Related to Cat. Activation constant
Pot	Power	G	Gas phase
Pv	Vapour Pressure	GL	Gas-Liquid interface
Q	Volumetric flowrate	HS	Headspace
R	Ideal gas constant	H_2	Hydrogen
r	Reaction Rate	H_2O	Water
Re	Reynolds number	I	Impeller
S	Submergence	i	Component
Sc	Schmidt number	in	Inlet
Sh	Sherwood number	JS	“Just suspended” state of catalyst particles
T	Temperature	L	Liquid (or gas-liquid interface)
U	Voltage	LS	Liquid-Solid interface

u	Superficial gas velocity	MNB	Nitrobenzene
V	Volume	obs	Observed value
w	Mass fraction	out	Outlet
X	Mass percentage of catalyst	R	Reactor
x	Molar fraction	R	Reference value
		S	Solid
		SG	Complete suspension of catalyst particles (under gassed conditions)

1. Introduction

This thesis addresses the operation of a multiphase reaction system applied to the industrial production of aniline. In the present work, a model of the industrial reactor is developed, to predict the performance of the system under a broad range of operating conditions. In addition to this, a characterisation study of the catalyst used in the process and an analysis of the process operation are presented. This analysis comprises the follow-up of the catalyst concentration, together with additional key process variables during an extensive period of observation. Moreover, a framework for process monitoring and control is proposed, where the establishment of improved practices and conditions for process diagnosis and maintenance is aimed.

The project motivation is briefly addressed in section 1.1. Next, the historical background, market outlook, and a survey of aniline manufacturing processes are presented, respectively, in sections 1.2, 1.3 and 1.4. The main objectives and thesis outline are considered in section 1.5.

1.1 Motivation

Bondalti Chemicals S.A. represents one of the major producers of organic and inorganic chemicals in the Portuguese industry. Over the recent years, the company has invested in various R&D projects which involved laboratorial studies, together with the execution of industrial trials, and the development of mathematical modelling approaches aimed to better understand the processes installed. The present investigation aims to follow these efforts by addressing the industrial production of aniline, where the liquid-phase catalytic hydrogenation of nitrobenzene is carried. Here, it is intended to exploit a considerable amount of data from the operation of an industrial reaction unit to validate a process model. This mathematical framework should be capable of describing the system performance, providing the means to drive the process towards its operating limits to maximise its productivity.

Since the catalyst behaviour directly influences the performance of the reaction system, an assessment of the catalyst management policy should be considered, to clarify its impact on the performance of the unit. For this purpose, it is convenient to investigate in detail the various aspects related to the presence of the catalyst in the reactor, the

modifications in its structure and properties, and its availability to participate in the mass transfer and reaction phenomena. Such information should also be related to the effects of other process variables relevant to the operation of the unit, in a complete mathematical framework. This framework should be able to provide an evaluation of the interactions between these different factors, and their relative strengths, to allow quantitative predictions relative to the behaviour of the unit, and hence allowing its operational diagnosis and optimisation.

1.2 Historical background of aniline production

The beginning of the Modern Age is marked by the dominance of Europe in the world trade of imported goods. The consequence of such economic prosperity was obviously the exponential growth of the population, along with the increasing standards of living. However, this scenario quickly became unsustainable, thus leading to the development and improvement of anthropogenic solutions on site to satisfy such demand [1].

An example of such effort was the production of synthetic dyes. One of the foremost attempts started in the 1800s with the reproduction of the natural *anil dye*, originally shipped to Europe from the port of Malacca by the Portuguese back in the 16th century [1]. In 1826, Unverdorben was the first to obtain the latter substance through the destructive distillation of indigo which he named *crystallin.* In 1840, Fritzsche studied the distillation of indigo-caustic potash mixture. The result was a colourless liquid that quickly also turned blue coloured when mixed with strong acids; owing to its final appearance and botanical origin, Fritzsche called this substance *anilin.* Two years later, Zinin treated benzonitrile with hydrogen sulphide which resulted in a basic compound that he referred to as *benzidam*. In 1843, Hoffman confirmed that the latter substances were in fact identical. Hoffman and Zinin worked together in the development of the first large-scaled process of aniline production, which consists in reacting benzene with nitric/sulphuric acids followed by a reduction step with iron fillings and comprising an acidic catalyst [1] – this last step discloses the reduction of nitrobenzene that was first described by Béchamp in 1854 (which came to be known as the *Béchamp Process*) [2]. This chemical route was then upgraded to the industrial scale by Perkin, in 1856, an assistant to the Hoffman's group at the Royal College of Chemistry in London, who developed a synthetic dye that he called *mauvedine* when oxidising aniline sulphate with a dichromate solution. This product was known as *Purple Aniline*. This

discovery had propelled the dye industry in the ensuing years with the foundation of *Badische Anilin und Soda-Fabrik* (BASF) [1].

Later, in 1873, Nicholson improved the industrial scheme for aniline production also by improving the Béchamp Process. The related process involved the introduction of steam into the reaction mixture and assembling a hollow stirrer tube. The reduction encompassed iron fillings and hydrochloric acid thus obtaining aniline production yields up to 90-95% [2].

The rapid breakthroughs achieved in the dye industry by the end of the 19th century led to the replacement of all the natural dyes. In fact, over 700 aniline-derived dyes have been developed so far. Notwithstanding its legacy in the industrial production of dye/pigments, aniline is currently used as an intermediate for major manufacturing sectors including the pharmaceutical and the petrochemical [1].

1.3 Aniline market outlook

According to Imarc [3], the global aniline market is expected to achieve a yearly growth of approximately 5.3% between 2018-2023 reaching a volume of 10.1 Mt of production by 2023. The major drivers of such economic growth include:

1. Increasing demand of methylene diphenyl diisocynate (MDI), an aniline derivative, used as a raw material in the production of coatings, insulation, adhesives, sealants, automotive interiors, and consumer goods.
2. An accelerated rate of urbanisation, demanding greater usage of polyurethanes in the civil construction as a reliable thermic isolation material.
3. The growing manufacture of pharmaceutic and rubber processing chemicals.

As reported by Technavio [4], in 2019 almost 80% of the aniline consumed worldwide was used in the production of MDI. In the same year, about half of the aniline global consumption will be related to the production of insulation products (Figure 1.1).

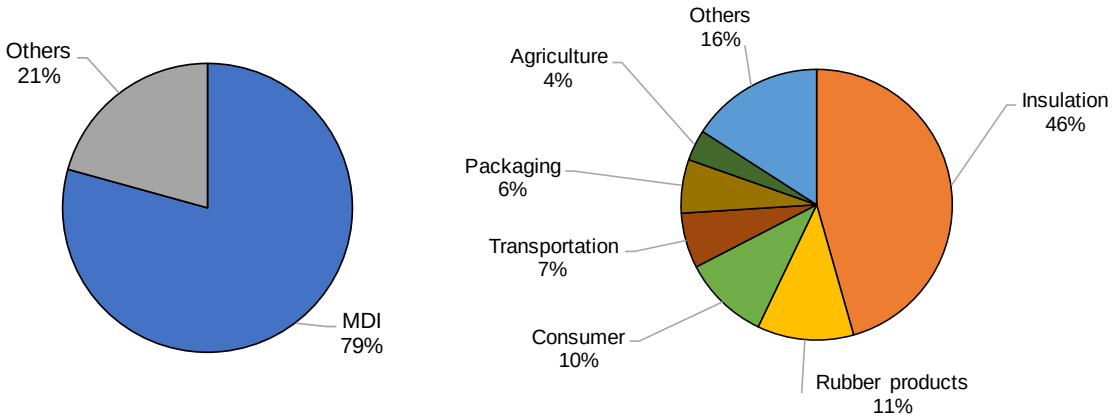

Figure 1.1 - Aniline global market share by application and end-use in 2019 (adapted from [4]).

As stated by IHS Markit [5], the aniline world consumption is foreseen to exhibit an annual growth rate of 4.9% between 2017-2022. Figure 1.2 outlines the distribution of the worldwide aniline consumption per region in 2017, presenting China as the main consumer. In addition, a report [6] confirms that the Asia-Pacific region, in 2017, also appeared as the top producer and consumer of polyurethane products, representing 45% of the corresponding global demand.

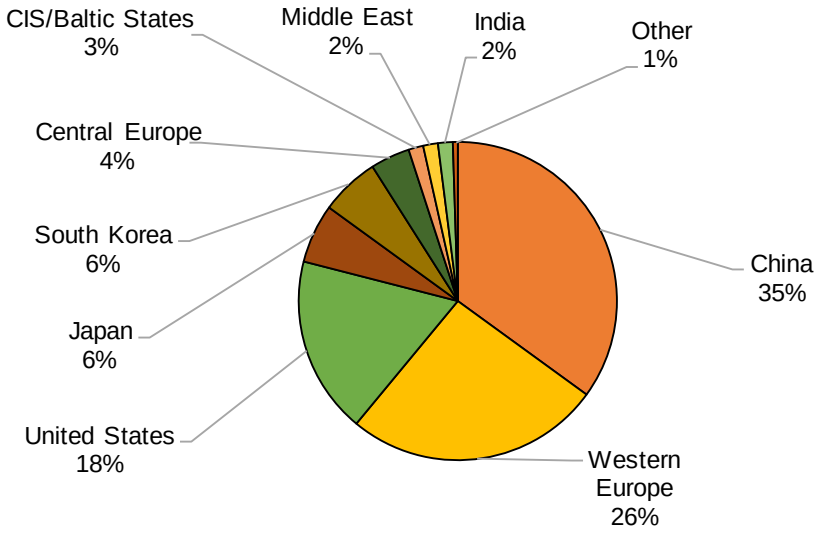

Figure 1.2 – Aniline global consumption by region (2017) (adapted from [5]).

As referred by Afshar [7], the global aniline capacity is expected to be almost 10 Mt in 2019. Figure 1.3 outlines the Asia Pacific and Western Europe regions, in 2013, with the largest shares of global aniline capacity with 40%, and 29%, respectively. It should be noted that the top position of the Asia Pacific region in the global aniline capacity has been influenced by companies like BASF and Jillin Connel, which installed units with annual capacities of 300 kt and 360 kt, in 2014, respectively.

Relatively to the Western European region (see Figure 1.4), 72% of the aniline production capacity in 2013 belonged to BASF, Covestro and Huntsman, that together represented more than 1.2 Mt. In 2013, Bondalti Chemicals, S.A. represented 11% of the aniline total production capacity in this region and 3% worldwide [7].

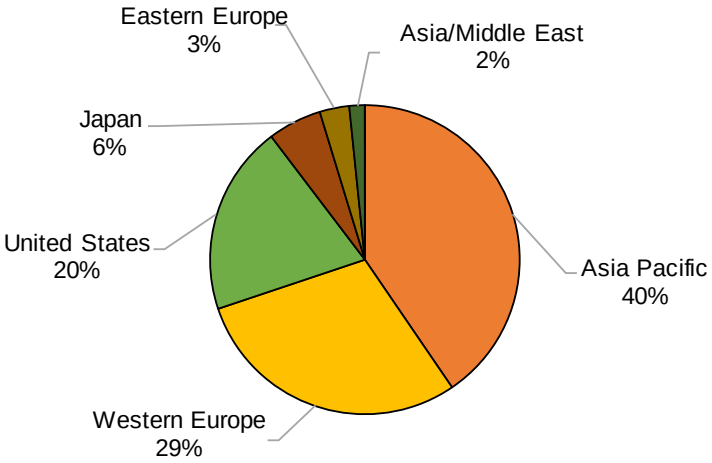

Figure 1.3 – Aniline global production capacity by region in 2013 (adapted from [7]).

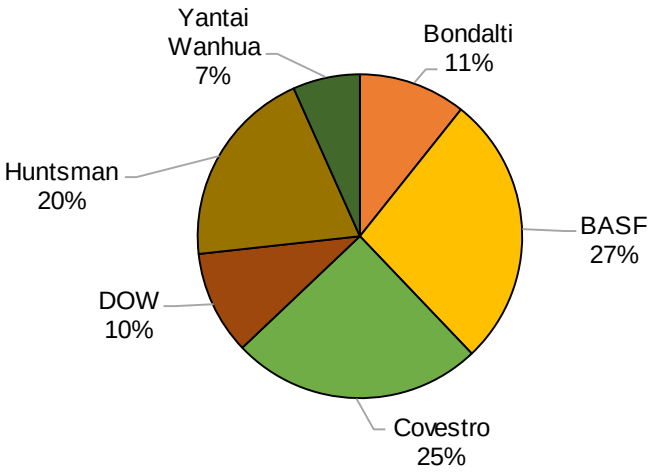

Figure 1.4 – Aniline production capacity in Western Europe in 2013 (adapted from [7]).

1.4 Aniline manufacturing

As mentioned before in section 1.2, the commercial success derived from the process developed by Perkin around 1860 propelled the industrial golden age of synthetic dyes, and especially the aniline manufacture, on the century that followed. During the 1970s, the industry had to develop new processes showing new applications in the pharmaceutical and agrochemical sectors; this evolution, together with the more extensive use of petrochemical feedstocks, stimulated the expansion of novel manufacturing technologies, also including the continuous processes for aniline production [8].

Figure 1.5 outlines the major pathways for aniline production currently used in industry. Discontinuous processes include the nitrobenzene reduction catalysed with hydrochloric acid and iron turnings. Continuous processes embody the nitrobenzene hydrogenation and ammonolysis of phenol or chlorobenzene. The latter processes will be described in more detail in the next sections.

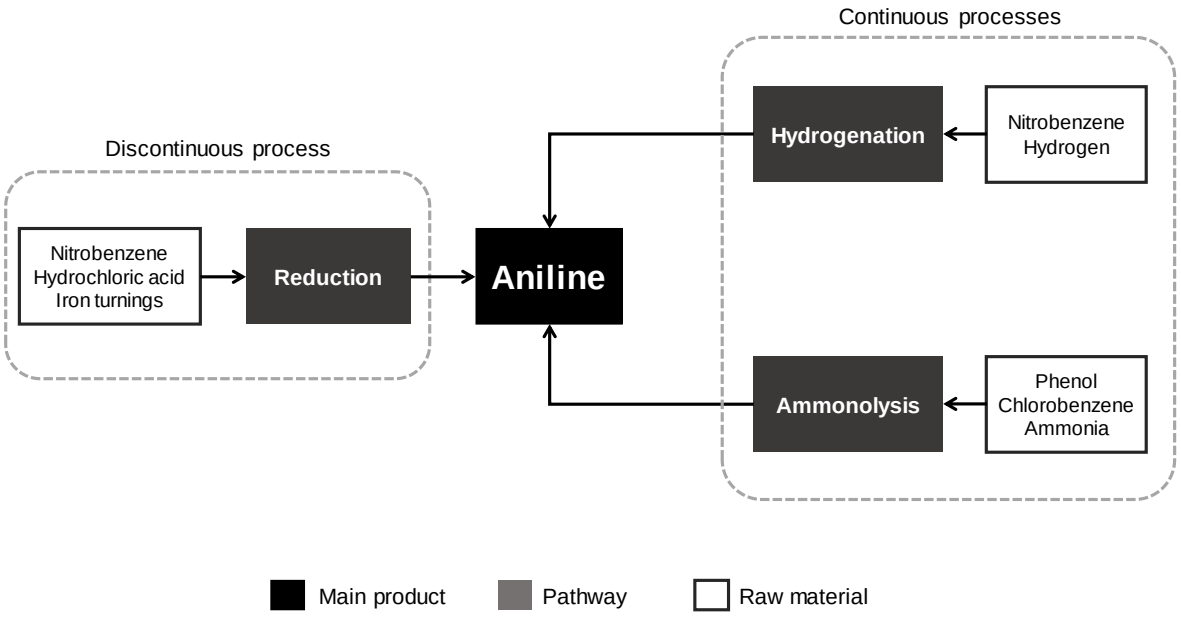

Figure 1.5 – Main pathways for aniline production.

1.4.1 Discontinuous processes

As previously said, the first process used for nitrobenzene reduction is known as the *Béchamp Process*. Until the 1960s, the production of aniline and other aromatic amines was almost exclusively derived from this route (Figure 1.6). This reaction is straightforward

and is generally carried in a batch stirred reactor with hydrochloric acid and iron fillings. It should be noted that the handling and disposal of the spent iron can bring some difficulties when the operation is performed at a large scale. Nevertheless, Bayer still applies this process in West Virginia by using waste iron filings from the automobile industry to produce iron-oxide pigment [8] [9].

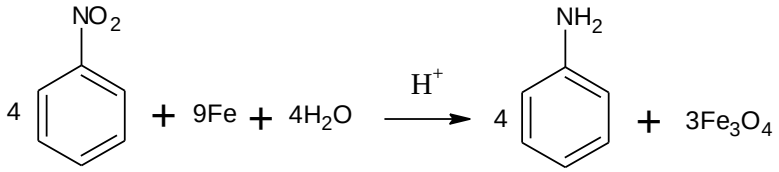

Figure 1.6 – Nitrobenzene Reduction to Aniline (Béchamp Process) [8].

1.4.2 Continuous processes

The growing demand from the rubber and the polyurethane industries, along with the manufacturing of other petrochemical-based products, was a major driving force in the development of large-scale aniline production units that operate continuously.

Nitrobenzene is the main feedstock for aniline industrial production through catalytic hydrogenation that can be carried either in the gas or liquid phases:

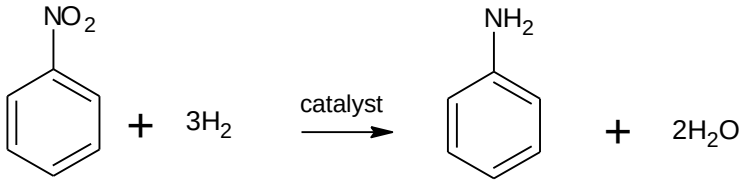

Figure 1.7 – Nitrobenzene hydrogenation to Aniline.

In both cases of nitrobenzene hydrogenation for producing aniline, the reaction is highly exothermic, thus demanding the removal of considerable amounts of heat. The yield and product quality obtained in both cases are virtually identical. The gas-phase hydrogenation of nitrobenzene can be advantageous by providing an effective use of the reaction heat; however, the liquid-phase alternative has the benefit of presenting a higher space-time yield, thereby needing a smaller size of the reaction vessel, and smaller energy

requirements, since it discards the recycle gas loop. On the other hand, the gas-phase hydrogenation discards the step of catalyst separation from the reaction mixture, and it ensures a longer catalyst life [10].

Chlorobenzene, phenol, and benzene are alternative feedstocks for aniline production through amination processes, despite their minor usage.

Gas-phase catalytic hydrogenation of nitrobenzene

The gas-phase hydrogenation of the nitrobenzene can be performed either in fixed-bed or in fluidised-bed technologies. In late 1950s, American Cyanamid was the first to develop the continuous mode for aniline production by using a fluidised bed-based technology known as the *Catan Process* [11]. A variation is used by BASF [12] where the hydrogenation is performed under 250-300°C and 4-10 barg with excess of hydrogen, where a yield of 99% is claimed. The unreacted hydrogen is then compressed downstream and recycled back to the reaction vessel. Copper or nickel/molybdenum supported on active alumina are reported as suitable catalysts. The same inventors mentioned a procedure for catalyst regeneration, comprising a burning off step of the organic material, followed by its reduction at around 250 to 300°C. The reaction heat is then used to produce steam. Another BASF patent specifies improvements regarding mass transfer phenomena within the reaction vessel by presenting a cross-channel packing with gas-permeable cells [13]. Haase and its co-workers [14] presented an apparatus for carrying out the hydrogenation of nitroaromatics, equipped with a chromatography recording system to determine the bulk concentration of nitro and nitroso compounds in the reaction mixture; moreover, the latter invention also includes a regulator unit for catalyst addition, depending on the online measurements of the unreacted species.

Covestro presented another example of fluidised-bed technology [15] that can also be employed for aniline production, where a fraction of the used catalyst is replaced periodically whenever the catalyst selectivity goes below 99.5%. Table 1.1 outlines an overview of the process examples mentioned.

Table 1.1 - Fluidised-bed technology of nitrobenzene hydrogenation in the gas-phase.

Patent No.	Assignee	Ref.	Temperature [°C]	Pressure [barg]	Catalyst
US 2891094	American Cyanmid Co	[11]	250-300	N/A	Copper on silica
US 3136818	BASF	[12]	250-300	4-10	Copper or nickel/molybdenum supported on active alumina
US 2012/0215029A1	BASF	[14]	120	25	Nickel supported on silica, zirconia, or alumina
US 2010/0280271 A1	Covestro	[15]	220-280	2-10	Palladium, platinum, ruthenium, iron, cobalt, or nickel supported on alumina, silica, titanium oxide, iron oxide/alumina mixture, or copper oxide/chromium oxide mixture

Relatively to the use of fixed-bed technology, First Chemical Corporation (since 2002 a subsidiary of DuPont) uses the *Lonza Process,* where the feed stream, containing a mixture of hydrogen and vaporised nitrobenzene, passes over a fixed-bed catalyst of cooper on pumice. A molar ratio of nitrobenzene to hydrogen of 2.5-6.0 to 1.0 and a conversion to aniline of 96% is claimed [16]. Covestro operates a similar process with a palladium catalyst on an alumina support, modified with vanadium and lead. The system operates under adiabatic conditions including the recycle of unreacted hydrogen back to the reaction vessel [17]. In 1998, Langer and its co-workers [18] highlighted difficulties within the fixed bed technology related to the dissipation of heat from the reaction caused by a non-uniform residence time distribution. Moreover, the attrition of the catalyst was also referred as a drawback. However, the claimed conversion to aniline is 99.8%. Table 1.2 shows examples of fixed-bed technology applied to the industrial production of aniline through continuous gas-phased hydrogenation of nitrobenzene.

Table 1.2 – Fixed-bed technology examples of nitrobenzene hydrogenation in the gas-phase.

Patent No.	Assignee	Ref.	Temperature [°C]	Pressure [barg]	Catalyst
US 3636152	DuPont	[16]	150-300	2-15	Copper supported on pumice
US 7692042 B2	Covestro	[17]	250-300	2-50	Palladium supported on alumina
US 9533939 B2	Huntsman	[19]	240-280	30-40	Nickel, platinum, or palladium supported on alumina

Liquid-phase catalytic hydrogenation of nitrobenzene

The liquid-phase nitrobenzene hydrogenation process, developed by Imperial Chemical Industries Ltd [20] (today Huntsman), offers higher productivity, along with better use of the heat produced when compared to the gas-phase hydrogenation processes. These authors claimed that the activity of the catalyst is promoted when aniline is used as solvent and “present in preponderating concentration in the solution”. Moreover, they stated that under these conditions it is possible to operate at or near the boiling point of aniline at the prevailing pressure thus performing the hydrogenation rapidly and safely, as well as enhancing the removal of heat produced by the reaction. Nickel on kieselguhr is preferred as a catalyst.

To reduce the catalyst consumption and the energy usage, DuPont [21] developed a plug-flow technology where a platinum-palladium catalyst supported on carbon was used. This catalyst formulation includes iron as a modifier, in order to provide a longer catalyst life, high activity and protection against hydrogenation of the aromatic ring. The conversion of nitrobenzene per pass is practically total. Unreacted hydrogen present in the effluent stream is vented and the reactor product is treated downstream to remove the water produced by the reaction followed by a purification step.

In 1997, Nagata and its co-workers [22], in collaboration with Mitsui Toatsu Chemicals, Inc., developed a slurry-type reactor to perform the nitrobenzene hydrogenation in the liquid phase. These authors recommend the use of large amounts of a solvent to facilitate the removal of the reaction heat. The latter implies keeping a low content of nitro-compounds within the mixture; otherwise, it can severely affect the overall performance by

promoting the accumulation of heavy by-products that, in turn, could hinder catalyst activity and lifetime. In this invention, the use of catalyst promoters such as zinc oxide and carbonate or bicarbonate of an alkali metal are claimed. In addition, these authors referred to the importance of removing the water produced by the reaction, as it decreases the catalyst activity and increases the content of by-products. This is accomplished through evaporation of the reaction product, using the reaction heat as a source of energy. Afterwards, a fraction of the aniline produced can be recycled to the reaction vessel with the intention of maintaining the solvent content at a desired content. The latter process uses a platinum and palladium mixture supported on carbon and the hydrogenation is carried between 150-250°C and 3-7 barg.

Bondalti also implements a liquid-phase hydrogenation of nitrobenzene for aniline production. The underlying process uses a stirred slurry reactor that operates at a pressure between 10 and 60 barg, at a temperature of 90-200°C. In this case, powdered nickel supported on silica is applied. Conversions of 98-99% are normally achieved [23]. Table 1.3 shows a comparison between the major processes for nitrobenzene hydrogenation in liquid-phase.

Table 1.3 - Examples of nitrobenzene hydrogenation processes in the liquid-phase.

Patent No	Assignee	Ref	Temperature [°C]	Pressure [barg]	Catalyst
US 3270057	Huntsman	[20]	160-175	<10	Nickel supported on kieselguhr
US 4415754	DuPont	[21]	100-300	4-21	Platinum-Palladium and iron supported on carbon
US 5616806	Mitsui Toatsu	[22]	150-250	3-7	Palladium and platinum supported on carbon

Other processes

Besides the nitrobenzene hydrogenation route, aniline can be manufactured through ammonolysis. In this case, the feedstocks of chlorobenzene, phenol, or benzene are used. However, the number of related industrial applications of this process route is scarce due to their high operating costs (high temperature/pressure) and lower yields when compared to the processes mentioned previously.

Methods for producing aniline through amination of chlorobenzene are reported in various patents [24] [25] [26]. Copper-/Zinc-containing catalysts are typically used. Operating conditions comprise reaction temperatures at around 250-500°C and reaction pressures at around 30-400 barg.

Alternative production routes for aniline that use phenol as main feedstock are also patented [27] [28]. The operating conditions used include temperatures ranging between 400-480°C and pressures at around 15-56 barg. Metal oxides supported on alumino-silicates are preferred.

Direct amination of benzene has also been developed in various patents [29] [30] [31] [32]. However, this route was only tested on a laboratorial scale, thus needing further investigation on an industrial scenario.

Table 1.4 outlines the main industrial routes for aniline production through amination processes.

Table 1.4 – Amination industrial process for aniline manufacturing.

Patent No	Assignee	Ref	Feedstock	Temp. [°C]	Pressure [barg]	Catalyst
US 2432552	DOW	[24]	Chlorobenzene	180-220	N/A	Copper
US 3231616	ExxonMobil Oil Co.	[25]	Chlorobenzene	300-500	400	Copper or zinc catalyst supported on mordenite (alumino-silicate)
US 2001284	Raschig AG	[26]	Chlorobenzene	250-450	30	Cuprous salt
US 4404399	Halcon	[27]	Phenol	400-480	22-56	Metal oxides supported on alumino-silicates
US 4987260	Mitsui Petrochemical	[28]	Phenol	425	15	Sodium and iron oxide supported on γ-alumina

In 2017, a new breakthrough was announced by Covestro with the development of a new bio-based route for aniline production, thus offering an alternative for the conventional petroleum based raw materials. Although the latter process was only proven at a laboratorial scale, Covestro plans to develop an industrial upgrade. This project involves a cooperation

between Covestro, the University of Stuttgart, the CAT Catalytic Centre (Aachen University) and Bayer [33].

1.5 Thesis objectives and outline

This Thesis aims to achieve the following goals:

- ✓ To enhance the process understanding by developing a mathematical model able to predict the reaction conversion within a defined range of operating conditions. This mathematical framework should be adapted by including updated process data to ensure the optimisation of the industrial unit towards new operating conditions that maximises productivity.
- ✓ To characterise the physico-chemical changes that the industrial catalysts material might exhibit during its usage.
- ✓ To develop a detailed monitorisation tool for the industrial unit, providing the means to identify the influence of external disturbances on the inherent variability of the process. This way, the preventive maintenance of the operation is promoted by providing a set of corrective measures to the industrial practice.
- ✓ To enhance the steadiness of the reaction conversion through the improvement of the regulatory control system already installed. The development of this control layer should promote the reduction of the catalyst make-ups and of the processing costs related to the purification of the final product.

Giving these main objectives, Figure 1.8 presents the strategy defined for this project. Here, a literature review was essential to survey the main features involved in the modelling of multiphasic reactors. This includes the prediction of the hydrodynamic parameters, of the mass transfer phenomena, and of the physico-chemical properties related to the compounds involved. In addition, previous kinetic studies developed at the

laboratorial scale are addressed, where the predicted reaction and maximal mass transfer rates are compared; based on this exercise, the expected limitations of the reaction rate at the industrial scale are also identified. To confirm this, the industrial operation is analysed, while attending to a specific period where the steadiness of the catalyst concentration and of the nitrobenzene conversion are verified. By these means, the global reaction rate can be correlated based on the industrial data gathered.

Once this mathematical framework was obtained, the model validation is provided considering the deviation between the predicted and measured values of the quality variable (nitrobenzene bulk concentration) during an extensive observation period performed to the process operation. To evaluate the influence of the catalyst state on the model predictions, a characterisation study is performed to describe the possible physico-chemical changes that this material might undergo during its lifetime in the process. This study gave important highlights regarding the improvement of the catalyst addition policy, preventing the advent of operating issues that might compromise the reaction stability.

The validated model results are used to develop a process monitoring tool, based on the principles of statistical process control. This way, the diagnosis of external disturbances can be performed, providing the preventive maintenance tool for the catalyst utilisation. In addition, the reaction steadiness is also addressed through the improvement of the regulatory control system.

In resume, this project provides a mathematical framework, which can be updated with future sample data sets to enhance the model predictability towards the reaction outcome. This way, a process monitoring tool is provided, where its continuous improvement opens an opportunity for process optimisation by evaluating new operating conditions that maximises the productivity of the industrial unit.

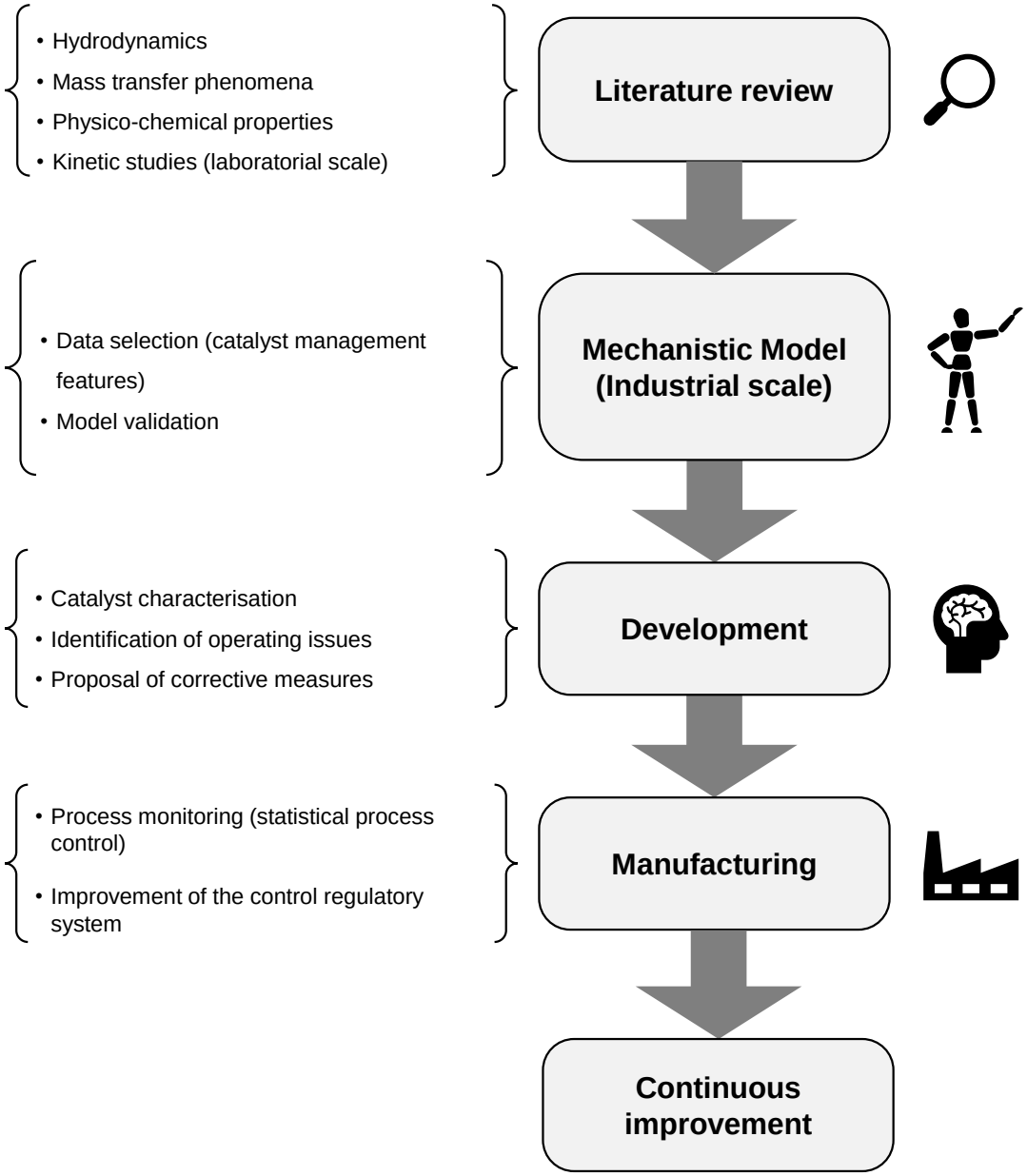

Figure 1.8 – Representation of the defined strategy in the present work.

This Thesis is organised as follows. Chapter 2 includes a modelling study of the industrial reactor. A description of the system studied is presented, together with a survey of the hydrodynamic parameters, transport parameters useful in the modelling of multiphase reactors. In addition, the previous laboratorial kinetic studies in this area are addressed, assuming the limitations that are likely to occur at that scale. Next, a mechanistic model developed for the industrial unit is presented, where its validation with industrial data is

discussed. In addition, a sensitivity analysis is also addressed, considering the effect of key process variables on the reaction conversion.

Chapter 3 presents a characterisation study of the catalyst used in the process. Here, the physico-chemical differences between fresh and used catalyst samples are discussed. In addition, a specific blend of fresh catalysts is investigated to improve the stability of catalyst concentration in the reaction vessel.

Chapter 4 presents the analysis of the operation of the industrial reactor. This includes the realisation of industrial trials to evaluate the interdependencies between the process variables and the catalyst behaviour in the system. In addition, a process monitoring tool is presented, including the statistical control of the process operation based on the model developed. Afterwards, an improvement to the regulatory control system is advanced, alongside with the results achieved with its implementation. Finally, a procedure for process monitoring and control is suggested presenting corrective measures to keep the operation steadiness.

2. Modelling of an industrial liquid phase hydrogenation reactor

In this chapter, a modelling study of the industrial reactor used in the production of aniline at Bondalti Chemicals S.A. is presented.

Firstly, an outlook on the use of multiphasic reactors in the chemical industries is given, focusing on the technology used in the underlying process. A general description of the reaction system is also included.

Secondly, a review concerning the modelling multiphasic reactors is presented, including the prediction of hydrodynamic parameters, and the mass transfer phenomena. Previous kinetic studies regarding the nitrobenzene hydrogenation in the liquid phase are also addressed.

Thirdly, the mechanistic model of the industrial unit is described, detailing the mass and energy balances related to the triphasic reaction system. Considering the catalyst used in the present case-study, the reaction rate was also predicted based on the analysis of process data. The model was used to perform a sensitivity analysis where the effect of the major process variables on the conversion of nitrobenzene was assessed. These results provide important conclusions relative to the operation and monitoring of the industrial unit.

2.1 Catalytic hydrogenation and related reactor technology

As previously mentioned, catalytic hydrogenation is recognised as the most used pathway for reducing organic compounds and one of the major processes applied in industry. Examples of both large- and small-scale hydrogenation processes include the production of (i) fine chemicals, (ii) commodity chemicals for the pharmaceutical industry, (iii) precursors used in the polymer industry, and (iv) intermediates for the fats and oils industry. Considering that 10-20% of all fine chemical and pharmaceutical products manufactured derive from hydrogenations, this explains the greater diversity of hydrogenation catalysts commercially available, when compared to other catalytic processes [34].

Most of the hydrogenation catalysts can be divided into two main clusters: (a) precious metals (e.g. Pt, Pd, Rh, and Ru), (b) and transition base metals (e.g. Co, Fe, and

Ni). Although both ensembles can perform similar hydrogenation functions, selecting the best option is mainly based on an economic point of view. Although precious metal catalysts usually display higher activity and selectivity, their higher price requires the use of very effective downstream units to prevent significant losses. Base metal catalysts are less expensive but also display lower activities, and their underlying processes require higher operating costs as they demand more severe process conditions, as well as higher catalyst loads. Therefore, the design of a hydrogenation unit should consider a trade-off between the initial and the operating costs when selecting a proper catalyst [34]. Catalyst stability and mechanical strength are also important criteria for process design and operation [35]. Depending on the type of reactor technology used, the associated timescale of the catalyst decay could vary from seconds to days in vessels with moving catalyst beds, or from weeks to years when a fixed-catalyst bed is considered [36].

Hydrogenations are often strongly exothermic reactions. Hence, the operation of such systems requires strict control of the temperature, and additional measures to prevent the related hazards of hydrogen handling and the pyrophoric properties of the catalysts used. These reactions encompass (a) the reduction of nitro compounds to amines, (b) saturation of multiple bonds, and (c) production of nitriles through reduction [37].

Hydrogenation units are usually multiphasic systems. Among these, triphasic systems are known to correspond to the most widely used class, where the liquid phase (often including a reactant to be processed) is combined with a gaseous component (hydrogen), in operating conditions that, in turn, require the presence of a solid phase (heterogeneous catalyst). These systems can be categorised by two modes of solid-reaction mixture contact: one where the solid phase is maintained packed (fixed-bed), and another one where the catalyst particles are kept in suspension throughout the reaction vessel (moving bed). While the fixed-bed option is more appropriate for reaction systems with intrinsically slow kinetics, the moving bed solution is preferred for cases where diffusional phenomena hinder the overall reaction rate [38]. Since the present case-study addresses a moving-bed type reactor, the fixed-bed technology is not considered in this study.

The moving-bed triphasic reactors are broadly known as “triphasic slurry reactors” and they are widely used for a variety of chemical processes (e.g. hydrogenation, oxidation, chlorination, hydroformylation, and bioremediation) [38]. From this type of reactors three

main categories can be distinguished: slurry bubble columns, fluidised beds, and agitated tanks.

For a given reaction, the selection of a suitable reaction technology should consider the operating features that each reactor type provides beforehand. For instance, in the case of slurry bubble columns and fluidised beds, the conversion of the gas phase can be affected by reducing the area available for gas-liquid mass transfer caused by the coalescence of the gas bubbles. To achieve this, a higher height-to-diameter ratio in the reaction vessel is used. On the other hand, in the case of agitated slurry reactors, the homogeneity of bubble size is rapidly achieved, as mechanical agitation ensures the dispersion of gas bubbles throughout the reaction medium.

Considering the capability to chemically convert the liquid reactants, the agitated slurry reactors may present a lower performance because of back-mixing, in comparison with slurry bubble column and fluidised bed technologies, where this issue is not pointed as significant. Nonetheless, agitated slurry reactors are preferred in terms of temperature uniformity [38].

The selection of a multiphasic reaction vessel should be oriented towards reducing the mass transfer resistances to achieve greater catalyst activities, and therefore promote the overall conversion [38]. The gas-liquid mass transfer and the reaction heat removal are major issues to overcome, while designing and implementing a hydrogenation process on a large scale [37]. Common design configurations used in hydrogenation units are outlined in Figure 2.1.

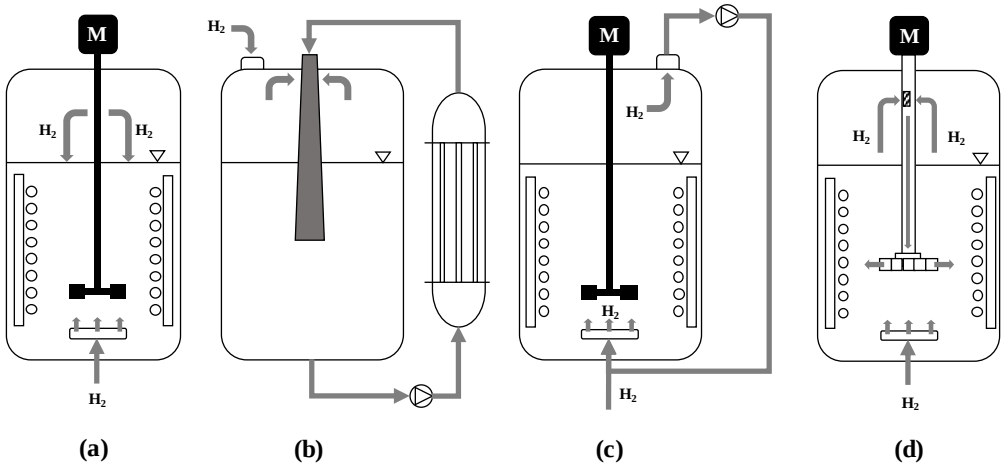

Figure 2.1 - Different reactor configuration designs for hydrogenation processes: (a) surface gassing, (b) and (c) reactor with external recirculation, and (d) gas-inducing reactor (adapted from [37]).

For instance, in Figure 2.1-(a), hydrogen is fed through a sparger located at the bottom of the vessel and the undissolved gas accumulates in the headspace of the reactor, leading to the increase of the local pressure. Once the maximum pressure is reached, the hydrogen intake is stopped, allowing the excess gas to be absorbed from the headspace into the mixture to be consumed. This solution, however, was proven to be inefficient regarding mass transfer restricting severely the overall reaction rate [37]. As such, alternative designs were proposed – Figures 2.1-(b) and 2.1-(c) –, with the intention of reducing the gas-liquid mass transfer limitations. Figure 2.1-(b) displays the external recirculation of the mixture via an injector, together with the use of an external heat exchanger. This technology presents several disadvantages namely [37]:

- the mismatch between the rate of reaction heat production and the rate of heat removal in the external heat exchanger can result in local hotspots, thus hindering selectivity
- the unequal distribution of hydrogen throughout the system, thereby causing the formation of by-products and catalyst deactivation
- a deficient distribution of catalyst particles
- additional costs and maintenance issues associated with the external devices used.

Figure 2.1-(c) exhibits another hydrogenation configuration that enables the recirculation of gas from the headspace to the bottom of the vessel through an external compressor. Still, this design shows a major drawback of using a compressor to perform the recirculation of gas, leading to increased maintenance and energy consumption relative costs [37]. An improved solution is presented in Figure 2.1-(d), where the agitator works as a gas-inducing impeller. This technology is currently used in the underlying hydrogenation process of Bondalti. In this case, the impeller works itself as a gas dispersion-device. The rotation of the agitator creates a pressure difference between the headspace and the impeller zone allowing the descent of gas through the hollow shaft of the agitator. If the agitation rate is above a critical point, the head loss at the vanes of the impeller is greater than hydrostatic head allowing the gas flow to be induced into the reaction mixture. If further contact of the gas-phase is desired, a gas sparger can be also installed. The unconsumed gas goes to the headspace, where it can be recirculated through the hollow shaft of the impeller.

Advantages attributed to the gas-inducing system, in comparison with the previous gas-liquid configurations include [37]:

- a higher homogeneity of the reaction medium providing a more controlled temperature and an extended lifetime of the catalyst
- an enhanced dissipation of the reaction heat, thereby reducing the need of using external heat changing devices
- a reduction of the maintenance costs as the recycle compressor for the gas phase is not required.

Nevertheless, some drawbacks related to gas-inducing reactors have been reported by [39] [40]:

- as the agitation energy requirements for gas induction increase with the impeller submergence, the installation of the impeller closer to the liquid surface level might be required, and this might reduce the total the gas-liquid contacting area
- a careful maintenance of the impeller sealing is needed when the gas phase is inflammable (e.g. hydrogen) and high reaction pressures are used (>10 barg).

2.2 Reactor-decanter system

The reaction equipment used at Bondalti Chemicals S.A. comprises a stirred slurry reactor coupled with a decanter, as shown in Figure 2.2. The reactor contains two independent heat exchanger devices (**A**), tube bundles and helical coils that allow the temperature control of the exothermic reaction. Furthermore, the reactor is equipped with a gas-inducing impeller (**B**) that promotes the direct contact between the gas and liquid phases, the uniform suspension of the catalyst particles and contributes to the removal of the reaction heat.

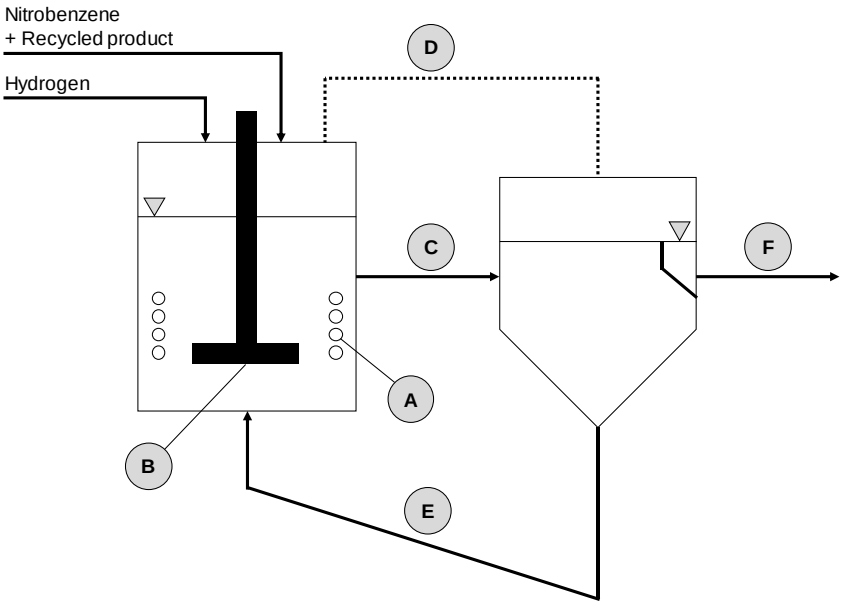

Figure 2.2 – Scheme of the reactor-decanter system.

The reaction mixture flows to the decanter through pipe **C**, where it is introduced in a downward flowing tube to promote the separation of each phase. Pipe **D** guarantees equal pressures in these two vessels. The catalyst material is recovered in the decanter, from where it is recycled back to the reactor through the recirculation stream (**E**). The decanter overflow (**F**) is a liquid stream almost free of solids, corresponding to the output stream of the unit [41].

2.3 Review of modelling information

In this section, an overview of significant issues relative to the mathematical modelling of multi-phase reactors is presented, oriented towards the description of agitated multiphasic vessels. This allows the description of the hydrodynamic and transport phenomena that occur in the industrial system considered. Available information relative to the kinetics of nitrobenzene hydrogenation is also reviewed.

The transport phenomena involved in a gas-liquid-solid reaction system can be represented using the film model as the basis (see Figure 2.3). This includes a combination of diffusional resistances in series describing the transport of gaseous and/or liquid compounds to the catalyst active sites in the solid phase, where the chemical reaction takes

place. Considering the present case-study, the gas-side film resistance can be ignored, due to the low solubility of hydrogen in the liquid phase. Here, C_{G,H_2} corresponds to the hydrogen concentration in the gas phase, C^*_{G,H_2} is the saturation concentration of hydrogen in equilibrium with the liquid phase, C_{L,H_2} is the hydrogen concentration in the liquid phase, and C_{S,H_2} is the hydrogen concentration in the solid phase, which can vary along the particle radius, in the case of porous catalysts (intraparticle mass transfer) [34] [38] [42].

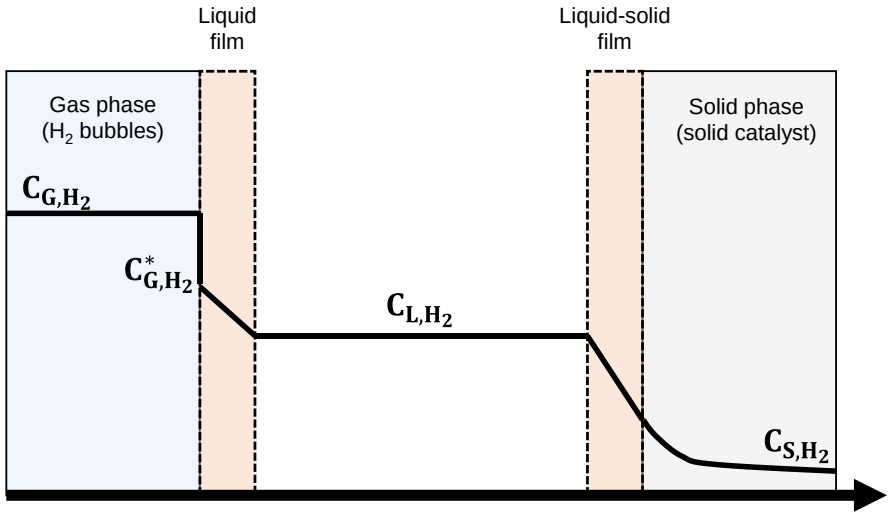

Figure 2.3 – Hydrogen concentration profiles involved in the gas-liquid-solid system under study.

In contrast to the intrinsic kinetics that depend only on the operating conditions used, the mass transfer phenomena are also dependent on the reactor type, size, and geometry [43]. As mentioned in section 2.1, the moving-bed technology used in the present-case is preferred for cases where mass transfer limitations exert an influence on the overall reaction rate. Therefore, an accurate description of the mass transfer phenomena is significantly relevant in the present case-study.

2.3.1 Mass transfer phenomena

Early studies on mass transfer in multiphase reactors included the development of purely empirical correlations based on the operating parameters used and the geometrical features of the systems studied. Consequently, these correlations were system-dependent and valid within a limited operating window. Because of this, these expressions did not provide an attractive solution for scale-up design, where the corresponding hydrodynamics

and operating regime could differ significantly. Improved mass transfer correlations were further developed based on the similarity criteria among multiphase systems. The development of mass transfer correlations for multiphase systems was first addressed by attending to the mechanical similarity criterium. This considers two main characteristics: dynamic and kinematic similarity. Dynamic similarity implies that geometrically comparable systems should also exhibit equal ratio of forces affecting the fluid motion. Kinematic similarity implies that geometrically analogous systems should also present comparable hydrodynamic paths in a related interval of time [44]. Given these criteria, Froessling [45] and Ranz and Marshall [46] [47] were the first authors to propose empirical correlations by using dimensionless numbers as

$$\mathrm{Sh} = \mathrm{A} + \mathrm{B}\,(\mathrm{Re})^{\alpha}(\mathrm{Sc})^{\beta} \tag{2.1}$$

where Sh is the Sherwood number that describes the ratio between the convective and diffusive terms in mass transfer, Re is the Reynolds number representing the ratio between the inertial and viscous forces, and Sc is the Schmidt number representing the ratio between the momentum and the molecular diffusivities.

The previous approach has, though, an intrinsic drawback: the assumption that the dimensionless groups are invariant in space. For instance, in the case of agitated vessels, it is observed that the inertial force decreases as the fluid distances itself from the impeller zone. Thus, using the Re number based on the impeller tip speed $\left(\mathrm{N}\mathrm{d}_{\mathrm{I}}^{2}\rho/\mu\right)$ may represent a gross simplification of the true phenomena [44].

Kolmogorov [48] assessed the turbulence behaviour on mixing systems through a dimensional analysis. In his theory, the turbulent motion of the fluid is described by a succession of eddies, where the larger ones, formed due to the impeller rotation, transfer their energy to smaller receiving eddies through viscosity, as the fluid is moved away from the impeller zone. The author claimed that, at sufficiently high Re numbers, the smallest eddies are isotropic and thus independent of the fluid motion and equipment geometry. Under these conditions, the turbulence of the system reaches equilibrium and can be characterised by the power dissipated per unit mass ($^{\mathrm{Pot}}/_{\rho \mathrm{V}}$) and the kinematic viscosity (ν) [49]. Therefore, the Reynolds number is, in this case, defined as

$$\mathrm{Re_K} = \frac{\mathrm{d}^{4/3}\left(\mathrm{Pot}/\rho \mathrm{V}\right)^{1/3}}{\nu} \tag{2.2}$$

where d represents the size of the dispersed phase (e.g., gas bubbles, solid particles). The energy consumed per unit mass can be determined assuming that the nominal motor power of the agitator should be enough to support the energy transferred to the mixture, plus the energy losses of the operation [50]. Considering the industrial unit here studied, a triphasic electric motor supplies the power input to the agitator. In this case, the power input is given by expression [51]

$$\mathrm{Pot} = \eta\sqrt{3}\cos\varphi\, \mathrm{I}\, \mathrm{U} \tag{2.3}$$

where η is the motor efficiency, $\cos\varphi$ is the power factor, I is the current intensity of the agitator and U the line voltage.

The isotropic theory of Kolmogorov is widely accepted, due to its simplicity, enabling the relation of turbulence and power consumed in mixed systems with mass transfer. Several investigators [52] [53] [54] [55] [56] [57] [58] [59] [60] have used this approach to develop mass transfer correlations applied to multiphase systems. However, these correlations are still system-dependent by discarding the specific flow patterns and the turbulence intensity promoted by large-scale anisotropies in different geometric vessel configurations (e.g., gas dispersion or solid particles suspension) [61]. Therefore, this theory still provides a too simplistic view in the case of multiphase systems, where kinematic similarity (e.g., hydrodynamics and turbulence) need also to be considered.

Kinematic similarity states that geometrically similar systems should also have similar fluid dynamics in space and in time. This issue led to the development of mass transfer correlations applied to turbulent flows with suspended particles, where steady state forced convection is assumed. This concept is designated as the *slip velocity* approach, and it was first proposed by [62] [63] [64]. In this case, the Re number is defined through the terminal settling velocity of the particles ($\mathrm{u_t}$):

$$\mathrm{Re_T} = \frac{\rho_\mathrm{L} \mathrm{u_t} \mathrm{d_p}}{\mu_\mathrm{L}} \tag{2.4}$$

It should be noted, though, that the established assumption of steady state flows for the prediction of liquid-solid mass transfer discards the free-suspension behaviour of the solid particles in agitated vessels. This dynamic behaviour involves their random movement in space and in time, demanding its mathematical description through turbulent vector components, and mean flow currents of the liquid flow [65] [66] [67]. This, in turn, implies that slip velocity-based correlations hinder the selection of a proper value for the velocity term in the Reynolds number. In addition, it has been reported that the related empirical exponents may vary in the Reynolds and Schmidt numbers [67] [68]. Recall that the description of the particle-fluid slip velocity characteristics entails complex mathematics which, in turn, hinders a numerical solution. Further, it should be mentioned that the related information on these characteristics is still scarce thereby complicating the prediction of solid-liquid mass transfer in industrial-scaled reactors based on the slip-velocity approach [69].

These approaches, however, evidenced some difficulties in comparing different multiphasic systems with geometric and kinematic similarities. Owing to this, more recent investigations [67] [70] [71] [72] [73] [74] have developed a new type of correlations that defines the turbulence intensity of the system. In the case of agitated vessels, the turbulence intensity can be expressed through the ratios between the operating speed of agitation, N, and the corresponding critical speeds of agitation for complete dispersion of gas bubbles, $\mathrm{N_{CD}}$, and the just-suspended state of solid particles, $\mathrm{N_{JS}}$. The former parameter, $\frac{\mathrm{N}}{\mathrm{N_{CD}}}$, is denoted as the *relative gas dispersion* and the latter one, $\frac{\mathrm{N}}{\mathrm{N_{JS}}}$, is known as the *relative solid suspension*. Together, they can be used to describe the hydrodynamic regime for a given multiphasic system. The turbulence similarity between multiphasic systems is ensured, provided that the same hydrodynamic regime is achieved. The correlations developed under these similarity criteria have the advantage of being scale-independent towards a wide variety of impeller-vessel configurations. Logically, this feature is preferred for scale-up design. Therefore, the prediction of gas-liquid and liquid-solid mass transfer coefficients in the model developed for the underlying industrial system are based on this approach.

For the prediction of gas-liquid mass transfer coefficient, the correlation selected was developed by Yawalkar et al. [74] for a coalescing air-water system in an agitated vessel:

$$k_L a_b = 3.35 \left(\frac{N}{N_{CD}}\right)^{1.464} u_G \quad (2.5)$$

Here $\frac{N}{N_{CD}}$ is the ratio of the operating agitation rate to the corresponding critical value for gas dispersion (see Equation 2.9), u_G is the superficial gas velocity. These authors confirmed that this equation provided similar results when compared to other correlations developed by different researchers irrespective of the vessel size and geometry, impeller type and sparger type.

The liquid-solid mass transfer coefficient in multiphase agitated systems relies on the degree of suspension of the solid particles [75] [60] [70] [71] which, in turn, depends on the turbulence structure of the system. In two-phase systems the turbulence structure is influenced by the type of the impeller, the power input, the impeller-tank size ratio, the impeller location, physical properties of the particle and liquid, and the particle loading. However, in the case of three-phase agitated systems, additional factors should be considered, including the type and location of the sparger, and the gas flowrate [67], thereby explaining the lesser number of correlations available in this case. For the present industrial case-study the correlation proposed by Pangarkar et al. [67] was selected, which is applicable for three-phase systems, also covering the operating gas flowrate used in the present case-study:

$$k_{LS,i} = 1.8 \times 10^{-3} \left(\frac{N}{N_{SG}}\right) Sc^{-0.53} \quad (2.6)$$

Here $\frac{N}{N_{SG}}$ is the ratio of the operating agitation rate to the critical speed for solid suspension under aerated conditions.

However, it should be mentioned that Pangarkar and co-workers [67] claimed the importance of performing additional studies on large-sized vessels with diameters above 1 m to check the dependence of k_{LS} on additional geometric parameters and physical properties. Nonetheless, considering that this correlation is more likely to encompass the criteria of kinetic similarity, this will be included in the mechanistic model for the industrial reactor.

2.3.2 Hydrodynamic parameters

In the case of gas-inducing multiphase reactors, the agitation rate should be capable of promoting a good homogenisation of all phases involved. To accomplish that, the hydrodynamic regime developed needs to allow the induction of gas, as well as ensure the complete dispersion of the gas bubbles and the solid particles (see Figure 2.4). Each of the latter steps is attributed to a corresponding critical speed of agitation. Gas holdup is another hydrodynamic parameter to be considered in these systems, as it defines the gas-liquid interfacial area available for mass transfer. These parameters are analysed in the next sections, considering the system-impeller configuration of the reactor studied.

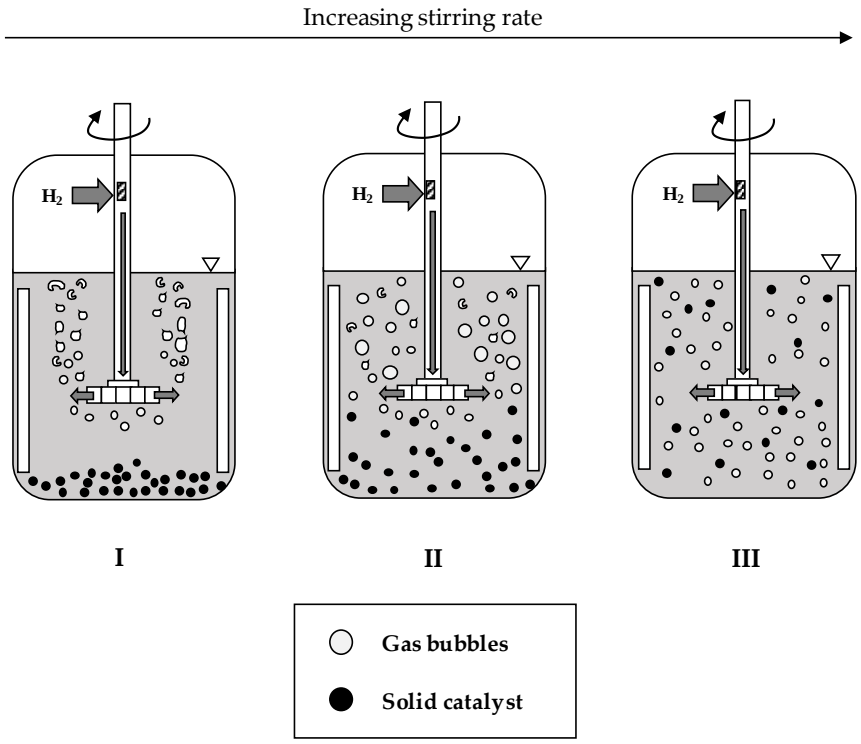

Figure 2.4 – Hydrodynamic regimes involved in a three-phase agitated reactor (adapted from [76]).

Critical speed of agitation for gas induction and rate of gas induction

As mentioned earlier, the process of gas induction in stirred vessels considers the entrance of gas through the hollow shaft of the agitator, from where it exits through a vane turbine. To promote this phenomenon, the operating speed of agitation should surpass a critical minimum value, when the kinetic energy creates a minimum pressure drop between

the impeller zone and the headspace to start the induction of gas into the liquid mixture [40]. The corresponding threshold is denoted as the critical speed for gas induction, N_{CG}. Therefore, in this case, that gas flow rate is influenced by the impeller rotation speed, in contrast to conventional sparged vessels, where these variables are independent [40].

The impeller submergence corresponds to the static head of liquid above the impeller needed to be overcome so that the gas can be induced. Several authors have reported the dependency of N_{CG} with the impeller submergence [77] [78] [79], together with the development of models that predict N_{CG} for different types of impeller [80] [81] [82] [83]. Poncin and co-workers [83] studied the hydrodynamics of the air-water system by using an agitated vessel equipped with a gas-inducing system similar to the one used in the industrial reactor studied. In this case, the critical speed of gas induction was defined through the modified critical Froude number, Fr_c^*, assuming ideal frictionless liquid motion

$$Fr_c^* = \frac{(N_{CG}\, d_I)^2}{gS} = 0.153 \tag{2.7}$$

where d_I is the impeller diameter, g the gravitational acceleration, and S the impeller submergence. These authors also correlated the gas induction rate by assessing the effect of different liquid levels (impeller submergence) and of the impeller speed as

$$Q_G = \frac{N d_I^3}{23\,[1 + (Fr^* - Fr_c^*)^{-1.7}]} \tag{2.8}$$

where Fr^* is the modified Froude number based on the operating agitation speed N.

Critical speed of agitation for complete gas and solid dispersion

The agitation rate of the impeller system must be enough to not only enable the induction of gas, but also to promote the homogenisation of the mixture; in the case of triphasic systems, this latter issue includes two distinct hydrodynamic regimes: complete dispersion of gas bubbles and the suspension of solid particles. Each of these corresponds to a specific threshold agitation that, in turn, is dependent on the physical properties of the fluid/solid phase (i.e. density, particle size), gas flow rate, impeller/vessel dimensions, impeller type and impeller submergence [76].

The minimum speed for complete dispersion of gas can be determined by the correlation proposed by Nienow and co-workers [84].

$$N_{CD} = \frac{4Q_G^{0.5} d_R^{0.25}}{d_I^2} \tag{2.9}$$

where N_{CD} is the critical speed for complete gas dispersion, d_R is the vessel diameter, and d_I is the impeller diameter. This correlation is appropriate for systems equipped with disc turbines similar to the ones used in the present case-study [74].

Besides the importance of guaranteeing a complete dispersion of the gas, the performance of mechanically agitated three-phase reactors entails that the solid particles must be maintained in suspension for an adequate liquid-solid contacting area. Concerning this issue, Zwietering [85] defined the minimum agitation speed at which every solid particle is in motion and kept suspended for more than 1-2 s, which he denoted as *just off-bottom suspension speed*, N_{JS}. This criterion is widely used owing to its simplicity and reproducibility, and it can be represented as

$$N_{JS} = \varphi \frac{\mu_L^{0.1} d_{cat}^{0.2} [(g(\rho_{cat} - \rho_L)/\rho_L)]^{0.45} X^{0.13}}{\rho_L^{0.1} d_I^{0.85}} \tag{2.10}$$

where $\varphi = 9$, considering the vessel-impeller geometric configuration of the present system studied [86]. μ_L is the absolute viscosity of the liquid phase, d_{cat} is the diameter of the catalyst particle, ρ_{cat} and ρ_L are the densities of the catalyst and the liquid phase, respectively, and X is the mass percentage of the solid phase.

Although the subject of solid suspension in agitated vessels is extensively reported by several authors [73] [85] [87] [88] [89] [90] [91] [92] [93] [94] [95] [96] [97] [98], fewer studies were developed for three-phase systems, because the presence of a gas phase in the mixing system increases the complexity of the behaviour of the solids particles therein. A number of studies [73] [87] [91] [90] proposed a linear dependence between the critical speed for solid suspension under aerated conditions, N_{SG}, and the gas induction rate as

$$N_{SG} = N_{JS} + \kappa Q_G \tag{2.11}$$

where κ is a constant. However, the reported values of κ significantly change amongst the latter studies mentioned, indicating the system-dependence of N_{SG}. With the intention of overcoming that issue, Zhu and Wu [51] have correlated N_{SG} independently from vessel/impeller sizes, particle size, and concentration of suspended particles, making it suitable for scale-up applications:

$$N_{SG} = N_{JS}\left[1 + 2.6\left(\frac{Q_G}{N_{JS}\, d_I^3}\right)^{0.7}\right] \tag{2.12}$$

This correlation was developed under impeller clearance-to-tank diameter ratios varying between 0.25 and 0.40, which is close to the industrial system studied.

Gas Holdup

The estimation of the gas holdup in agitated vessels is described in the literature through several correlations considering the impeller-vessel configuration, the operating conditions, and the physical properties of the system. However, like in the prediction of mass transfer coefficients, most of gas holdup correlations are based on either dimensionless groups, or on the power input per unit mass, which are limited to a small range of system geometries and operating conditions [99] [100]. To overcome this issue, Yamalkar et al. [101] correlated the gas holdup as a function of the relative gas dispersion ($\frac{N}{N_{CD}}$), arguing that N_{CD} uniquely describes the turbulence intensity at the completely gas dispersion condition, under a given impeller-vessel combination [100]

$$\epsilon_G = 0.122\left(\frac{N}{N_{CD}}\right)^{0.62}\left(\frac{60\, Q_G}{V_D}\right)^{0.69} {d_R}^{0.22}\left(\frac{d_I}{d_R}\right)^{0.14} \tag{2.13}$$

where ϵ_G is the gas holdup (volumetric fraction), and V_D is volume of the mixture, comprising the gas and liquid phases of the system.

2.3.3 Kinetic studies

The understanding of the kinetics of nitrobenzene hydrogenation to aniline took its initial steps in the studies performed by Haber [102], where the first proposal of a reaction scheme was established (see Figure 2.5). According to this reaction scheme, aniline can

be formed via the formation of Nitrosobenzene (NSB) and N-phenylhydroxylamine (PHA) intermediates; however, these compounds can undergo a condensation route producing dimeric molecules of Azoxybenzene (AZXB), Azobenzene (AZB) and Hydrazobenzene (HB). In addition, a few studies [103] [104] have reported the identification of the reaction intermediates during hydrogenation, which provided further supporting evidence for Haber's reaction scheme. Even so, this mechanistic scheme did not totally explain the experimental results. Therefore, other authors proposed alternative mechanistic schemes to describe the process of MNB hydrogenation. For instance, some studies [105] [106] indicate the formation of the dimeric compounds Azoxybenzene (AZXB) and Azobenzene (AZB) from either the remaining intermediates, or from nitrobenzene or aniline. Recent studies [107] claimed two different routes to the intermediate Nitrosobenzene (NSB) (e.g., dehydrogenation and condensation) towards aniline synthesis.

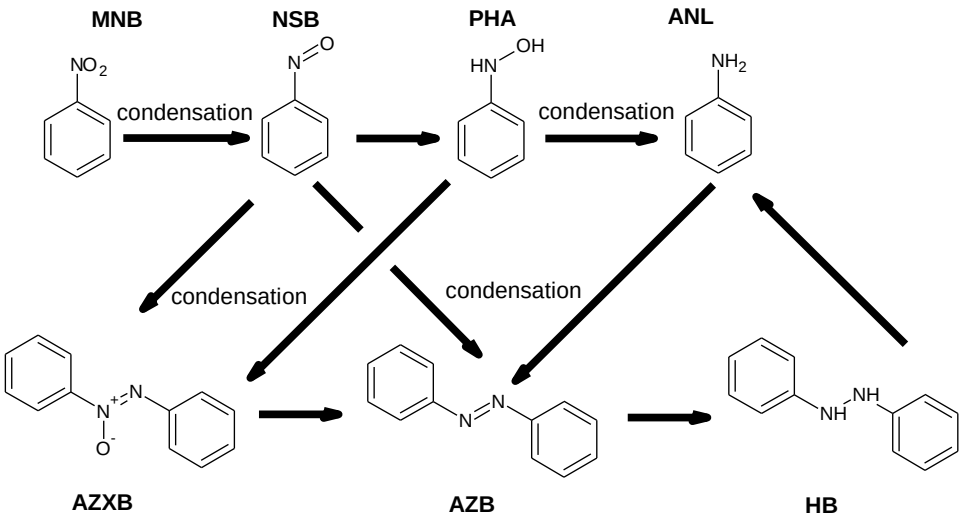

Figure 2.5 – Reaction mechanism proposed by Haber [102].

Apart from the hydrogenation of nitrobenzene, it should be noted that additional secondary reactions can also occur in the underlying system. A number of studies [22] [108] [109], including PhD theses developed at Bondalti [110] [111] [112], addressed this issue, proposing other reaction mechanisms to describe the nitrobenzene hydrogenation in the liquid-phase under distinct different heterogeneous catalysts.

Relvas [110] and Sousa [111] reported their results in laboratory-scale agitated reactors, using catalysts similar to the ones used in the industrial productive process under

study. Although these studies provide a better understanding of the industrial reaction system, the authors claim that the kinetic behaviour observed in laboratorial scaled reactors can differ from the industrial scale. Relvas [110] concluded that the activation state of the catalyst has a major influence on the reaction conversion and selectivity. In addition, he mentioned that the catalyst make-ups performed in the industrial unit can promote the heterogeneity of catalyst activation states, which, in turn, influences the formation of the secondary compounds, thereby hindering the kinetic modelling of the underlying reactions. On the other hand, Sousa [111] mentions that the prediction accuracy of the secondary compounds can be affected significantly at the industrial scale, due to the greater influence of mass transfer limitations therein, in comparison with the laboratorial system. In addition to this, it is worth mentioning that the total amount of hydrogenation by-products formed in the Bondalti industrial reactors represents a very low percentage of the reactants converted. Given this statement and the former issues pointed by Sousa [111] and Relvas [110], only the main reaction was considered (nitrobenzene hydrogenation) in the mechanistic model developed for the industrial reactor (see section 2.4).

A reference study of the kinetics of the liquid-phase hydrogenation of nitrobenzene to aniline in agitated slurry units was developed by Turek and co-workers [113]. Their experimental setup consisted in a laboratorial agitated autoclave containing suspended particles of Ni/Al_2O_3 catalyst, where the effect of temperature, pressure, nitrobenzene concentration, and pH on the reaction rate were evaluated. These authors adjusted a Langmuir-type model to describe the intrinsic kinetics of the reaction system (see Equation 2.14). Table 2.1 presents the experimental conditions used.

$$\begin{cases} r_{MNB} = \dfrac{kK_{MNB}C_{S,MNB}}{1 + K_{MNB}C_{S,MNB}} \cdot \dfrac{K_{H_2}\alpha_{H_2}P_{H_2}}{1 + K_{H_2}\alpha_{H_2}P_{H_2}} \\ k = 4.128 \times 10^{6} \exp\left[-\dfrac{53.25 \times 10^{3}\ J \cdot mol^{-1}}{RT}\right] \\ K_{MNB} = 3.503 \times 10^{11} \exp\left[-\dfrac{71.7 \times 10^{3}\ J \cdot mol^{-1}}{RT}\right] \\ K_{H_2} = 1.097 \times 10^{-5} \exp\left[\dfrac{28.29 \times 10^{3}\ J \cdot mol^{-1}}{RT}\right] \\ \alpha_{H_2} = 9.97 \times 10^{-5} \exp\left[-\dfrac{612}{T}\right] \end{cases} \quad (2.14)$$

Here r_{MNB} is the reaction rate $[mol \cdot kg_{cat}^{-1} \cdot s^{-1}]$, k the kinetic constant, K_{MNB} and K_{H_2} are the adsorption equilibrium constants of nitrobenzene and hydrogen $\left[m_{liquid}^{3} \cdot mol^{-1}\right]$, respectively, P_{H_2} the partial pressure of hydrogen $[Pa]$, α_{H_2} the hydrogen solubility $\left[mol \cdot m_{liquid}^{-3} \cdot Pa^{-1}\right]$, and $C_{S,MNB}$ the concentration of nitrobenzene in the surface of the catalyst $\left[mol \cdot m_{liquid}^{-3}\right]$.

Table 2.1 – Experimental conditions of the studies conducted by [113].

Parameter	Value
Liquid volume [L]	0.5-1.0
Catalyst	Ni/Al_2O_3
Operating temperature [°C]	50-150
Catalyst loading [g]	0.82
Average particle size [μm]	15
Operating pressure [barg]	2-20
Initial concentration of nitrobenzene [mol/m^3]	4.3 – 43
Solvent	Ethanol
Agitation rate [rpm]	150-800
Liquid-phase initial composition [wt.%]	Aniline (50%) Water (20%) Ethanol (30%)

These authors also analysed the mass transfer phenomena in the laboratory system noticing the existence of liquid-solid mass transfer limitations for nitrobenzene bulk concentration values below 0.1 mol·m^{-3} and reaction temperatures above 130°C. A strong influence of the agitation rate on the gas-liquid mass transfer of hydrogen was observed, whereas a small impact on the liquid-solid mass transfer of nitrobenzene was noticed.

Striving to further evaluate the liquid-phase hydrogenation of nitrobenzene in agitated slurry units, the same authors developed another study [114], where the kinetic model was correlated to data corresponding to an industrial-scaled vessel. In this study, the authors suggest the inclusion of a corrective factor to predict the reaction rate. This way, the effect of the catalyst particle size and of the activity on the reaction rate at the industrial scale are considered.

These kinetic studies were performed using ethanol as a solvent. From the industrial standpoint, this option is not very attractive, as the downstream separation between a solvent and the reaction products could reduce the economic viability of the operation.

In the case of the underlying industrial system studied, a fraction of the reaction products is recycled to the reactor feed to be used as a solvent. The reactor outlet stream, mainly composed by aniline and water can, in turn, form two immiscible liquid phases for temperatures below 120°C, allowing the downstream separation of the liquid phase. To ensure a homogenous reaction mixture in the industrial reactor, temperatures above 140°C should be employed [115] [116] [117].

Machado [115] studied the mass transfer and kinetics involved in the liquid-phase hydrogenation of nitrobenzene using a laboratory-scale gas-inducing reactor with Raney nickel-type catalysts. In this case, an aniline-water mixture was used as a solvent. The experimental conditions used are presented in Table 2.2. The determination of the reaction rate was performed through calorimetry measurements, while taking advantage of the exothermic nature of the reaction, in contrast to the studies performed by Turek et al. [113] [114], where the reaction rate was determined through the measurement of the hydrogen consumption rate in the reactor headspace.

Table 2.2 - Experimental conditions of the studies conducted by [115].

Parameter	Value
Liquid volume [L]	1.0
Catalyst	Raney nickel
Operating temperature [°C]	100-160
Catalyst loading [g]	0.45
Average particle size [μm]	34.2
Operating pressure [barg]	8-14
Initial concentration of nitrobenzene [mol/m^3]	16
Solvent	Aniline (85.7 wt.%) Water (14.3 wt.%)
Agitation rate [rpm]	1000
Liquid-phase initial composition [wt.%]	Aniline (50%) Nitrobenzene (50%)

Machado [115] confirmed that the overall kinetic rate constants are weak functions of the temperature between 140 and 160°C, also presenting a low activation energy. In addition, the author recalled that the overall kinetic constant obtained is close to the liquid-

solid mass transfer coefficient, evidencing that, under these conditions, the process is controlled by liquid-solid mass transfer. On the other hand, the kinetic constants are strongly influenced by temperature in the range of 120 to 140°C.

By assuming a simple rate model with a first order dependence on the nitrobenzene concentration and a zero-order related to hydrogen, the author determined the overall kinetic constants for different temperatures and pressures. These values were calculated and plotted according to the conventional Arrhenius model in [115]. For a temperature range from 140 to160°C and a hydrogen pressure of 14 barg, the pre-exponential and energy of activation can be estimated from the data provided, thereby leading to the following kinetic model:

$$\begin{cases} r_{MNB} = k \cdot X \cdot {C_{L,MNB}}/{C_{cat}} \\ k = 57.863 \exp\left[-\dfrac{1.589 \times 10^4}{RT}\right] \end{cases} \quad (2.15)$$

Here k is the overall kinetic constant, expressed in $[1/(\text{wt.\% catalyst} \cdot s)]$, X is the mass percentage of catalyst in the mixture $[\text{wt.\% catalyst}]$, C_{cat} is the catalyst mass concentration $\left[kg_{cat} \cdot m_{liquid}^{-3}\right]$, and $C_{L,MNB}$ is the concentration of nitrobenzene in the bulk phase $\left[mol \cdot m_{liquid}^{-3}\right]$.

The author evidenced that, at sufficiently high reaction temperatures and nitrobenzene concentrations in the liquid phase below 1000 ppm (≈ 8.13 mol·m^{-3} at 140ºC), liquid-solid mass transfer controls the reaction rate. On the other hand, it was observed that, beyond that threshold concentration of nitrobenzene in the bulk phase, the reaction order becomes zero with respect to the nitrobenzene concentration, thus suggesting that the reaction system becomes limited by the surface-reaction rate.

Relvas and co-workers [110] [118] also assessed the liquid-phase hydrogenation of nitrobenzene in a laboratorial batch agitated reactor with powdered Ni/SiO_2 catalyst. In this case, the reaction was conducted under initial concentrations of nitrobenzene about 100 times higher than those used in the previous studies referred. In this study, a significant induction period at the beginning of each catalyst trial was observed. These authors attributed this phenomenon to the possible inhibition of the catalyst due to the excessive content of nitrobenzene in the initial mixture, and/or to the activation process related to the hydrogenation itself that could enhance the reaction rate with time. This result showed that

the catalyst activation state could significantly change while contacting with the reaction mixture. This assumption was sustained by other authors [119] [120] that confirmed that similar catalysts can be activated over reducing atmospheres. Relvas and co-workers [110] [118] developed a semi-empirical kinetic model for the liquid-phase hydrogenation of nitrobenzene to aniline as:

$$\begin{cases} r_{MNB} = \dfrac{k\left(C_{L,MNB} \times 10^{-3}\right)^{9/7}\left(P_{H_2} \times 10^{-5}\right)^{2/7}}{1 + K_{MNB}\left(C_{L,MNB} \times 10^{-3}\right)^{4/3} + K_{H_2}\left(P_{H_2} \times 10^{-5}\right)^{7/13}}\ \chi_{AS} \\ k = 11.55 \times 10^{6} \exp\left[-\dfrac{34.52 \times 10^{3}\ J \cdot mol^{-1}}{RT}\right] \\ K_{MNB} = 371.89 \times 10^{-3} \exp\left[\dfrac{35.10 \times 10^{3}\ J \cdot mol^{-1}}{RT}\right] \\ K_{H_2} = 30.23 \times 10^{3} \exp\left[-\dfrac{28.62 \times 10^{3}\ J \cdot mol^{-1}}{RT}\right] \end{cases} \quad (2.16)$$

Here, χ_{AS} represents the fraction of active sites on the catalyst particles, and K_{MNB} and K_{H_2} represent the adsorption constants for nitrobenzene and hydrogen, respectively.

The evolution of the number of active sites with time and the corresponding initial condition were defined as

$$\frac{d}{dt}\chi_{AS}(t) = r_{MNB}\frac{(\chi_{AST} - \chi_{AS})}{\chi_{AST}}k_f \quad (2.17)$$

$$\chi_{AS}(t = 0) = \chi_{AST} \times f_0, \qquad (\chi_{AST} = 1) \quad (2.18)$$

where k_f represents the reaction rate constant for the activation of the catalyst, χ_{AST} is the total fraction of the sites on the catalyst particles, and f_0 is the fraction of sites available at t=0. The values of f_0 and of k_f are reported in [110] [118]. The experimental conditions are displayed in Table 2.3.

Table 2.3 – Experimental conditions of the studies conducted by [110] [118].

Parameter	Value
Liquid volume [L]	0.38-0.40
Catalyst	Ni/SiO_2
Operating temperature [°C]	50-250
Catalyst loading [g]	6.7
Average particle size [µm]	17
Operating pressure [barg]	5-50
Initial concentration of nitrobenzene [mol/m^3]	2400-2600
Solvent	Aniline
Agitation rate [rpm]	1200

Comparison of kinetic models

Considering that the kinetic studies of Machado [115], Relvas et al. [110] [118] and Turek et al. [113] were all developed in agitated vessels with comparable liquid volumes and operating conditions, the corresponding reaction rates can be compared for each case. Since the design details of the reactor used by Turek et al. [113] and Machado [115] are unknown, the design specifications of the laboratory apparatus used by Relvas and co-workers [110] [118] are here considered.

Regarding the kinetic modelling of the corresponding reaction, the previous work developed by Neves [23] at Bondalti Chemicals S.A. should be also mentioned. During this investigation, where two modelling approaches were proposed: (1) an isothermal and macroscopic model based on algebraic equations encompassing the global mass/energy balances and the partial mass balances of the underlying system, and (2) a non-isothermal microscopic model based on differential-algebraic equations, where the diffusional and conductive phenomena across the catalyst particle are considered. The corresponding sensitivity analysis corroborate similar results in both approaches, showing that the reaction rate was mainly influenced by the liquid-solid mass transfer of nitrobenzene. This result also indicates the small impact of intraparticle mass transfer on the reaction performance.

Considering the simulation results derived from Neves [23], this present comparison exercise assumes that all active sites are under catalyst-surface conditions in terms of nitrobenzene concentration. In addition, the isothermal behaviour of the particle is also assumed.

Here, the operating parameters include a catalyst concentration of 10 g/L, a catalyst particle size of 15 µm, an agitation rate of 1200 rpm, and an operating pressure of 15 barg. Here, ranges of temperature from 140 to 150°C and of nitrobenzene bulk concentration from 1 to 1000 ppm are considered.

For this purpose of comparison, further assumptions also include spherical-shaped catalyst particles, perfect-mixed reaction, constant activation state with time. In case of the kinetic model proposed by Turek et al. [113], the concentration of hydrogen in the catalyst surface can be estimated assuming the steady state between the gas-liquid/liquid-solid mass transfer and the surface-reaction rates. As mentioned previously, the gas-side film resistance can be ignored in this case, since hydrogen presents a low solubility in the liquid-phase. The concentration of nitrobenzene in the catalyst surface can be also estimated assuming the steady state between the liquid-solid mass transfer and the surface reaction rates. Equating the mass transfer and reaction terms in steady state for the reactants leads to:

$$k_L a_b \left(\frac{C_{G,H_2}}{He} - C_{L,H_2}\right) - \vartheta_{H_2} r_{S,MNB}\, C_{cat} = 0 \qquad (2.19\ A)$$

$$k_{LS,H_2}\, a_{cat} \left(C_{L,H_2} - C_{S,H_2}\right) - \vartheta_{H_2} r_{S,MNB}\, C_{cat} = 0 \qquad (2.19\ B)$$

$$k_{LS,MNB}\, a_{cat} \left(C_{L,MNB} - C_{S,MNB}\right) - r_{S,MNB}\, C_{cat} = 0 \qquad (2.19\ C)$$

Here, $k_L a_b$ is the gas-liquid mass transfer coefficient related to hydrogen $[s^{-1}]$ (Equation 2.5), $k_{LS,MNB}$ and k_{LS,H_2} are the liquid-solid mass transfer coefficients of nitrobenzene and of hydrogen, respectively $\left[m_{liquid}^3 \cdot m_{cat}^{-2} \cdot s^{-1}\right]$ (Equation. 2.6), a_{cat} is the external area of the catalyst per volume unit $\left[m_{cat}^2 \cdot m_{liquid}^{-3}\right]$, C_{cat} is the catalyst concentration $\left[kg_{cat} \cdot m_{liquid}^{-3}\right]$, $\frac{C_{G,H_2}}{He}$ is the saturation concentration of hydrogen in the liquid-solid interface $\left[mol \cdot m_{liquid}^{-3}\right]$, He is the Henry constant, $C_{L,MNB}$ and C_{L,H_2} are the concentrations of nitrobenzene and of hydrogen in the liquid phase, respectively $\left[mol \cdot m_{liquid}^{-3}\right]$, $C_{S,MNB}$ and C_{S,H_2} are the concentrations of nitrobenzene and of hydrogen in the catalyst surface, respectively, $\left[mol \cdot m_{liquid}^{-3}\right]$, $r_{S,MNB}$ is the surface-reaction rate of nitrobenzene $[mol \cdot kg_{cat}^{-1} \cdot s^{-1}]$, ϑ_{H_2} and is the stoichiometric coefficient of hydrogen. Assuming spherical shaped particles, the external area of the catalyst, a_{cat}, with size d_{cat} $[m]$ and density ρ_{cat} $[kg_{cat} \cdot m_{cat}^{-3}]$ is defined as:

$$a_{cat} = \frac{6\, C_{cat}}{\rho_{cat}\, d_{cat}} \tag{2.20}$$

The catalyst density is assumed the same as in Relvas et al [110] [118] work since this parameter is also unknown in the remaining studies.

For this analysis, the predicted reaction rate of nitrobenzene in each case is compared to the corresponding maximal mass transfer rate of nitrobenzene, MTR_{MNB} $[mol \cdot kg_{cat}^{-1} \cdot s^{-1}]$, assuming $C_{S,MNB} \approx 0$.

$$MTR_{MNB} = k_{LS,MNB}\, a_{cat}^{*}\, C_{L,MNB} = \frac{6\, k_{LS,MNB}}{\rho_{cat}\, d_{cat}}\, C_{L,MNB} \tag{2.21}$$

Here, $a_{cat}^{*}\ \left(= \frac{a_{cat}}{C_{cat}}\right)$ $[m_{cat}^{2} \cdot kg_{cat}^{-1}]$ corresponds to the specific external area of the catalyst.

As Machado [115] calculated the liquid-solid mass transfer coefficients based on the Kolmogorov's Theory, Table 2.4 shows a comparison between the values obtained for nitrobenzene and for hydrogen based on Machado work and on Equation 2.6, assuming the same experimental conditions The predicted liquid-solid mass transfer coefficients for nitrobenzene and for hydrogen according to the Kolmogorov-based equations used by Machado [115] are higher by a factor of 1.40 and of 1.80, respectively, when compared to the values obtained by Equation 2.6. This numerical difference can be possibly justified through the distinct hydrodynamics of the laboratorial apparatuses used by these authors, resulting from several factors that intervene in the calculation of $k_{LS,MNB}$. These include both the physical dimensions and clearances of the apparatus, and slightly different catalyst materials. Due to the limited differences observed in Table 2.4, Equation 2.6 will be used for comparing the comparing the various kinetic studies here assessed.

Table 2.4 – Predictions of liquid-solid mass coefficients for nitrobenzene and hydrogen, according to Machado [115] and to Equation 2.6.

Temperature [°C]	Nitrobenzene			Hydrogen		
	$k_{LS,MNB}\left[m^3_{liquid}\cdot m^{-2}_{cat}\cdot s^{-1}\right]\times 10^3$			$k_{LS,H_2}\left[m^3_{liquid}\cdot m^{-2}_{cat}\cdot s^{-1}\right]\times 10^3$		
	Machado (1)	Eq. 2.6 (2)	Ratio (1)/(2)	Machado (1)	Eq. 2.6 (2)	Ratio (1)/(2)
140	1.02	0.73	1.40	1.97	1.10	1.81
150	1.12	0.79	1.42	2.17	1.20	1.81

Table 2.5 and Figure 2.6 present the reaction rate and the maximal mass transfer rate according to the previous kinetic studies for different values of nitrobenzene bulk concentration and of temperature.

Table 2.5 – Reaction and maximal mass transfer rates predicted by [113], [115] and [118] for different values of nitrobenzene concentration and of operating temperature.

Laboratorial scale 140°C	Reaction rate [mol kg^{-1} s^{-1}] × 10^3				Maximal mass transfer rate [mol kg^{-1} s^{-1}] × 10^3
$C_{L,MNB}$ [ppm]	$C_{S,MNB}$ [ppm]	Turek	Machado	Relvas	
1	0.001	1	0	0	1
10	0.010	9	5	2	9
20	0.020	19	9	5	19
50	0.054	47	23	15	47
100	0.122	94	46	35	94
200	0.337	188	92	83	189
500	42	432	231	241	472
1000	538	436	461	473	943

Laboratorial scale 150°C	Reaction rate [mol kg^{-1} s^{-1}] × 10^3				Maximal mass transfer rate [mol kg^{-1} s^{-1}] × 10^3
$C_{L,MNB}$ [ppm]	$C_{S,MNB}$ [ppm]	Turek	Machado	Relvas	
1	0.000	1	1	0	1
10	0.005	10	5	2	10
20	0.010	20	10	5	20
50	0.027	51	26	15	51
100	0.059	102	51	37	102
200	0.150	203	103	89	203
500	2	506	257	265	508
1000	435	574	515	554	1017

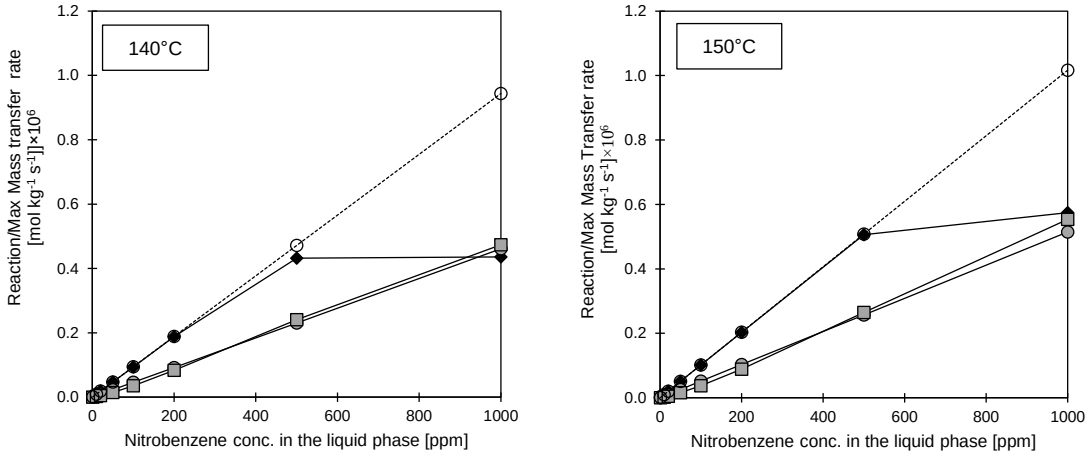

Figure 2.6 – Predicted values of the reaction and maximal mass transfer rates, according to the various kinetic models assessed, (-◆- Turek et al. [113], -●- Machado [115] -□- Relvas et al. [110] [118] and -○- maximal mass transfer rate).

In case of the kinetic model proposed by Turek et al. [113], the reaction rate shows a linear behaviour with the nitrobenzene liquid concentrations up to 200 and 500 ppm, when temperatures of 140 and 150°C are considered, respectively. Under these conditions, the reaction corresponds to the maximal mass transfer rate of nitrobenzene, suggesting that the reaction is limited by mass transfer. For higher concentrations of nitrobenzene in the liquid phase, the reaction rate becomes inhibited, while the catalyst surface becomes saturated with the adsorbed reactant; under these conditions, surface-reaction rate controls the reaction system.

In case of the kinetic expressions derived from the studies of Machado [115] and of Relvas et al. [110] [118], the predicted reaction rates are similar, describing both a linear behaviour throughout the entire range of nitrobenzene liquid concentrations and of temperatures considered. Although the kinetic model developed by Relvas et al. [110] [118] describes a the reaction rate through a Langmuir-type equation (see Equation 2.16), it was observed that the corresponding inflection of the kinetic curve occurs for nitrobenzene bulk concentrations around 2000-3000 ppm; for that reason, only the linear contribution of the kinetic curve is observed, giving the operating window considered. According to the former kinetic expressions, the predicted reaction rates are inferior to the predictions derived from the kinetic model of Turek et al. [113] for nitrobenzene bulk concentrations below 900 ppm. However, it is worth mentioning that all kinetic expressions describe a linear behaviour with nitrobenzene liquid concentrations below 200 ppm. Given this scenario, the saturation of

the catalyst active sites is not significant under those conditions. Bearing this in mind, mass transfer limitations of nitrobenzene are also pointed in the kinetic systems studied by Machado [115] and of Relvas et al. [110] [118].

In contrast to the kinetic model of Turek et al. [113], where the intrinsic kinetics at the catalyst surface are described, the kinetic expressions derived from the studies of Machado [115] and of Relvas et al. [110] [118] depict the overall reaction rate as a function of the nitrobenzene bulk concentration; because of this, steady state balance between mass transfer and chemical reaction rates cannot be mathematically applied to these kinetic expressions to determine the nitrobenzene concentration at the catalyst surface. Nevertheless, by plotting the predicted overall reaction rates against the maximal mass transfer rate of nitrobenzene ($\mathrm{MTR_{MNB}}$) assumed in this exercise (see Table 2.5), a comparable order of magnitude is observed (see Figure 2.7). This result supports the significance of mass transfer limitations of nitrobenzene in both cases.

Figure 2.7 indeed shows slopes between the overall reaction and the maximal mass transfer rates inferior to unity - Machado [115] (=0.507) and Relvas et al. [110] [118] (=0.489). Nevertheless, it should be noted that the parameters defined in Equation 2.21 ($\mathrm{k_{LS,MNB}}$ and $\mathrm{a^*_{cat}}$) may not accurately describing the hydrodynamics of the laboratorial apparatuses where both kinetic studies were developed. According to Equation 2.6, the value of $\mathrm{k_{LS,MNB}}$ relies on a proper estimation of $\mathrm{N_{SG}}$ (see Equation 2.12), which, in turn, depends significantly on the specific design features of the system (i.e., impeller submergence, impeller/tank size). Since only the design specifications of the laboratory reactor used by Relvas and co-workers [110] [118] are known, the predicted value of $\mathrm{k_{LS,MNB}}$ may not accurately describe the hydrodynamics of the system used by Machado [115]. On the other hand, the predicted value of $\mathrm{a^*_{cat}}$ can also be distinct among the catalysts used in both studies since the related particle size distributions were also unknown.

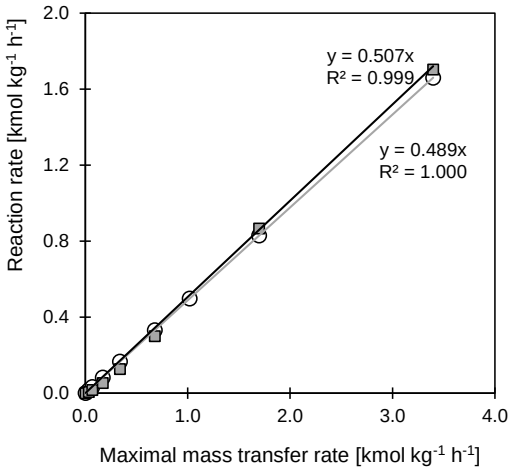

Figure 2.7 – Relationship between predicted reaction and maximal mass transfer rates (-○- Machado [115] -□- Relvas et al. [110] [118]).

Despite the difficulties in characterising the hydrodynamics of the laboratorial systems of the former kinetic studies, additional evidence that supports the significance of mass transfer limitations of nitrobenzene is available. As mentioned before, Machado [115] confirmed that the mass transfer of nitrobenzene through the liquid-solid interface controls the reaction rate in similar ranges of temperature and of nitrobenzene bulk concentrations assumed here. This author supported his claim by confirming that the measured overall rate constants were comparable to the predicted liquid-solid mass transfer coefficient of nitrobenzene. In addition to this, he reports a low apparent activation energy (17 $kJ \cdot mol^{-1}$), corroborating the strong effect of mass transfer limitations on the reaction rate. In case of Relvas et al. [110] [118], a Langmuir-type equation was adjusted to the experimental data, where a similar apparent activation energy (23 $kJ \cdot mol^{-1}$) was also obtained under comparable temperature conditions as those used by Machado [115]. According to [121] [122], for apparent activation energies around 20 kJ/mol, mass transfer phenomena have a significant impact on the overall reaction rate. Therefore, it is highly probable that the parameters derived from the kinetic model of Relvas et al. [110] [118] are also significantly influenced by the mass transfer limitations of nitrobenzene observed

As mentioned before, the kinetic model proposed by Turek et al. [113] describes the surface-reaction rate of the corresponding catalytic system. Therefore, the impact of mass transfer limitations of nitrobenzene can be further evaluated through the evaluation of the second Damköhler number (Da_{II}):

$$\mathrm{Da_{II}} = \frac{\text{Chemical reaction rate}}{\text{Maximal mass transfer rate}} \tag{2.22}$$

Table 2.6 shows the Da_{II} values obtained in the kinetic model of Turek et al. [113], considering the same operating conditions assumed previously.

Table 2.6 – Second Damköhler numbers obtained for kinetic study model of Turek et al. [113].

Laboratorial scale	Second Damköhler number (Turek et al. [113])	
$C_{L,MNB}$ [ppm]	140ºC	150ºC
1	435	602
10	60	75
20	31	38
50	12	15
100	6	8
200	3	4
500	1	2
1000	1	1

Here, it is possible to observe that Da_{II} values are particularly high for nitrobenzene concentrations below 20 ppm. Under these conditions, the corresponding chemical reaction rate is much higher than the maximal mass transfer rate observed, meaning that mass transfer is significantly limiting the overall reaction rate. On the other hand, for higher concentrations of nitrobenzene in the liquid phase, the Da_{II} values tend to decrease, denoting a reduction of the mass transfer limitations, as the active sites at the catalyst surface become gradually saturated by absorbed reactant, which is coherent with the surface-reaction inhibition.

Given the latter results, if a high conversion of nitrobenzene is demanded, small concentrations of this compound in the liquid phase are thus required to prevent a surface-reaction inhibition. Under these conditions, mass transfer limitations of nitrobenzene are expected to become dominant. To evaluate this scenario, the mass transfer coefficients of hydrogen and of nitrobenzene for the same operating conditions are calculated (see Table 2.7). In addition, the reduction of the concentration of hydrogen at the gas-liquid and liquid-solid interphases and of nitrobenzene at the liquid-solid interface are evaluated through

Equations 2.19 A-C (see Table 2.8). In this case, a nitrobenzene concentration in the liquid phase of 10 ppm is assumed.

Table 2.7 – Gas-liquid and liquid-solid mass transfer coefficients estimated in this exercise.

Temperature [°C]	$k_L a_b$ $[s^{-1}]$	$k_{LS,H_2} a_{cat}$ $[s^{-1}]$	$k_{LS,MNB}\ a_{cat}$ $[s^{-1}]$
140	0.122	1.897	1.263
150		2.065	1.375

Table 2.8 – Mass transfer limitations predicted at the laboratorial scale, considering the kinetic model proposed by Turek et al. [113] .

$C_{L,MNB}$ [ppm]	Hydrogen absorption to liquid phase [%] $\left(\frac{C^*_{G,H_2} - C_{L,H_2}}{C^*_{G,H_2}}\right)$ [1]	Hydrogen transport to catalyst surface [%] $\left(\frac{C_{L,H_2} - C_{S,H_2}}{C_{L,H_2}}\right)$	Nitrobenzene transport to catalyst surface [%] $\left(\frac{C_{L,MNB} - C_{S,MNB}}{C_{L,MNB}}\right)$
10	7.22	0.50	99.90

In this case, although the liquid-solid mass transfer coefficients of nitrobenzene, $k_{LS,MNB}\ a_{cat}$, and of hydrogen, $k_{LS,H_2} a_{cat}$ are greater than the corresponding gas-liquid mass transfer coefficient of hydrogen, $k_L a_b$, only the significant mass transfer limitations of nitrobenzene from liquid to solid are noticed (above 99%) (see Table 2.8). Minor reductions on the hydrogen concentration through the gas-liquid and liquid-solid interfaces – below 10% and 1%, respectively – are observed. Therefore, the external mass transfer of nitrobenzene as the major limiting step can be supported by these results.

In addition, it should be noted that the value of $k_L a_b$ obtained is low when compared to the values indicated in the studies of Machado [115] (0.235 s^{-1} at 1000 rpm) and of Turek [113] (0.750 s^{-1} at 800 rpm). Despite the low value of $k_L a_b$, the gas-liquid resistance is not significant. This can be justified through Equation 2.19-A which indicates that hydrogen

[1] C^*_{G,H_2} corresponds to the saturation concentration of hydrogen in the gas-liquid interface $\left(= \frac{C_{G,H_2}}{He}\right)$, where C_{G,H_2} is the hydrogen concentration in the gas phase and He is the Henry constant (see Appendix A).

absorption from gas to liquid $\left(\frac{C^*_{G,H_2}-C_{L,H_2}}{C^*_{G,H_2}}\right)$ is only affected if high reaction rates ($r_{S,MNB}$>>) and low partial pressures of hydrogen (C^*_{G,H_2}<<) are applied. Recall that $k_L a_b$ does not depend on the catalyst properties, but rather on the agitation efficiency. To improve this parameter, more efficient impellers should be applied to increase the power input per volume unit of the reaction mixture and, in turn. the specific area of the gas bubbles, a_b [123].

It should be noted that the underlying mass limitations of nitrobenzene were accepted assuming that heat transfer limitations are neglected. However, due to the significant exothermicity of the underlying reaction, this premise can also be checked. In this case, laminar flow in the liquid-solid interface is assumed, due to the small size of the catalyst particles [123]. Under these conditions, the particle-to-fluid heat transfer coefficient, h_{LS} $[W \cdot m^{-2} \cdot K^{-1}]$, can be estimated through the relationship:

$$Sh \approx Nu \Leftrightarrow \frac{k_{LS,i}\, d_p}{D_{L,i}} \approx \frac{h_{LS}\, d_p}{\lambda_L} \tag{2.23}$$

Here Sh is the Sherwood number representing mass transfer, Nu is the Nusselt number representing the heat transfer, D_L $[m^2 s^{-1}]$ is the diffusion coefficient of the component i in the liquid phase, λ_L $[W\, m^{-1}\, K^{-1}]$ is the thermal conductivity of the liquid phase (see Appendix A).

At steady state, the heat produced by the reaction on the surface of the catalyst equals the rate of energy transferred from the solid to the liquid phase:

$$(-\Delta H_R)\, r_{S,MNB} = h_{LS}\, a^*_{cat}\, (T_{cat} - T_L) \tag{2.24}$$

Here, ΔH_R is the enthalpy of the reaction $[J \cdot\ mol^{-1}]$, T_{cat} and T_L $[K]$ are the temperatures in the surface of the catalyst and in the liquid phase, respectively, and $r_{S,MNB}$ is the surface-reaction rate $[mol \cdot kg_{cat}^{-1} \cdot s^{-1}]$. Table 2.9 shows the values of λ_L, under the range of temperatures here considered and assuming a liquid phase composition of 86 wt.% aniline and 14 wt.% water.

Table 2.9 – Thermal conductivities of the liquid phase, under the range of temperature considered.

Temperature [°C]	λ_L [W m^{-1} K^{-1}]
140	0.176
150	0.174

By applying Equation 2.24, the relative temperature difference between the catalyst surface and the liquid phase $\left(\frac{T_{cat}-T_L}{T_L}\right)$ can be determined, considering the range of nitrobenzene concentration in the liquid phase (see Table 2.10), and $r_{S,MNB}$ was determined according to Turek et al. [113]. In this case, the low values obtained in $\frac{T_{cat}-T_L}{T_L}$ confirm the isothermal conditions in the underlying system.

Table 2.10 – Evaluation of heat transfer limitations considering the kinetic model proposed by Turek et al. [113].

140°C					
$C_{L,MNB}$ [ppm]	$r_{S,MNB}$ $[mol \cdot kg_{cat}^{-1} s^{-1}]$	$k_{LS,MNB}$ $\left[m_{liquid}^3 \cdot m_{cat}^2 \cdot s^{-1}\right] \times 10^4$	$D_{L,MNB}$ $\left[m_{liquid}^2 \cdot s^{-1}\right] \times 10^9$	h_{LS} $[W \cdot m^{-2} \cdot K^{-1}] \times 10^{-4}$	$\frac{T_{cat}-T_L}{T_L}$
1	0.001	7.321	4.115	3.131	2.40E-07
10	0.009	7.321	4.115	3.131	2.16E-06
20	0.019	7.321	4.115	3.131	4.56E-06
50	0.047	7.321	4.115	3.131	1.13E-05
100	0.094	7.321	4.115	3.131	2.26E-05
200	0.188	7.321	4.115	3.132	4.51E-05
500	0.432	7.322	4.114	3.132	1.04E-04
1000	0.436	7.322	4.114	3.133	1.05E-04

150°C					
$C_{L,MNB}$ [ppm]	$r_{S,MNB}$ $[mol \cdot kg_{cat}^{-1} s^{-1}]$	$k_{LS,MNB}$ $\left[m_{liquid}^3 \cdot m_{cat}^2 \cdot s^{-1}\right] \times 10^4$	$D_{L,MNB}$ $\left[m_{liquid}^2 \cdot s^{-1}\right] \times 10^9$	h_{LS} $[W \cdot m^{-2} \cdot K^{-1}] \times 10^{-4}$	$\frac{T_{cat}-T_L}{T_L}$
1	0.001	7.970	4.542	3.053	3.62E-07
10	0.010	7.970	4.542	3.053	3.62E-06
20	0.020	7.970	4.542	3.053	7.24E-06
50	0.051	7.971	4.542	3.053	1.85E-05
100	0.102	7.971	4.542	3.053	3.69E-05
200	0.203	7.971	4.542	3.054	7.35E-05
500	0.506	7.971	4.542	3.054	1.83E-04
1000	0.574	7.972	4.541	3.055	2.08E-04

As mentioned before, the parameters of the kinetic expressions derived from the studies of Machado [115] and Relvas et al. [110] [118] do not separate the mass transfer and chemical reaction characteristics. Mass transfer processes are specific to the scale/design and to the hydrodynamics of the reaction vessel. In the case of the industrial scale reactors, the agitation rate is typically lower than in a comparable laboratorial system. Therefore, mass transfer limitations are here expected to occur in a larger extent and the kinetic expressions derived from these authors may not be directly applicable to the industrial reactor studied in this work.

In contrast, the kinetic model proposed by Turek et al. [113] discriminates the intrinsic kinetics of the corresponding catalytic system, since gas-liquid and liquid-solid mass transfer processes were evaluated separately through empirical correlations applicable to the scale and geometry of the related laboratory apparatus. Although this kinetic expression is suitable for scale-up design, it is specific to a different catalyst from the one used in the industrial system here considered.

For this industrial process, high nitrobenzene conversions are required, to decrease the processing costs in the purification units to satisfy the quality standards of the final product. Consequently, low liquid concentrations of nitrobenzene need to be maintained in the reactor, and this is likely to induce the appearance of mass transfer limitations for nitrobenzene, as observed in the laboratory units. To confirm this behaviour, the nitrobenzene concentration rate evaluated from industrial data can be correlated with the corresponding estimated mass transfer coefficient, unit the specific properties of the catalyst and the remaining values of the relevant operating conditions. This information can later be assembled in a complete mechanistic model for the unit, to predict and interpret this behaviour. This is considered in the next section.

2.4 Mechanistic model of the industrial reactor

This section presents a mechanistic model for an industrial reactor used for producing aniline through the nitrobenzene hydrogenation in liquid-phase. This model comprises a system of nonlinear algebraic equations corresponding to the steady state mass and energy balances of the process. The solution of the model equations was performed using the *Wolfram Mathematica*® software through the constrained Newton's method.

As mentioned in the previous section, this study follows the former work developed by Neves [23] at Bondalti Chemicals S.A., where the kinetic behaviour of the underlying reaction system was assessed through distinct mathematical approaches. The corresponding sensitivity analyses revealed that the reaction rate was mainly influenced by the liquid-solid mass transfer of nitrobenzene, evidencing that the impact of intraparticle mass transfer on the reaction performance was not significant. In addition, the author claimed that the isothermal macroscopic model demanded significantly smaller CPU times, when compared to the non-isothermal microscopic model, that requires special initialisation and scaling procedures. Following these observations, the isothermal and macroscopic approach was considered in the model of the underlying industrial unit. This model comprises the global and partial mass balances related to the gas, liquid, and solid phases. In addition, the global energy balance is also included, where the operation of the heat exchanging devices is regarded in the removal of the heat produced by the reaction. Further features here considered include the gas induction rate through the hollow shaft of the impeller and the gas holdup term. This contrasts with the model developed by Neves [23], where only the hydrogen intake through the reactor headspace is accounted. Nevertheless, it should be noted that both models assume that no chemical reaction occurs inside the decanter vessel, due to the low availability of hydrogen therein.

The schematic representation of the reactor is outlined in Figure 2.7. The reactor total volume includes the reactor headspace (V_{HS}) and by the reaction mixture (V_D). The reaction volume comprises the gas-liquid-solid mixture, where the induced gas is either transferred to the liquid phase or returned to the reactor headspace as bubbles. The mass transfer of the reactants is performed from the gas/liquid bulk phases to the catalyst surface, where the hydrogenation occurs. In case of the industrial reactor, the gas hold up is around 10 to 20 vol.%

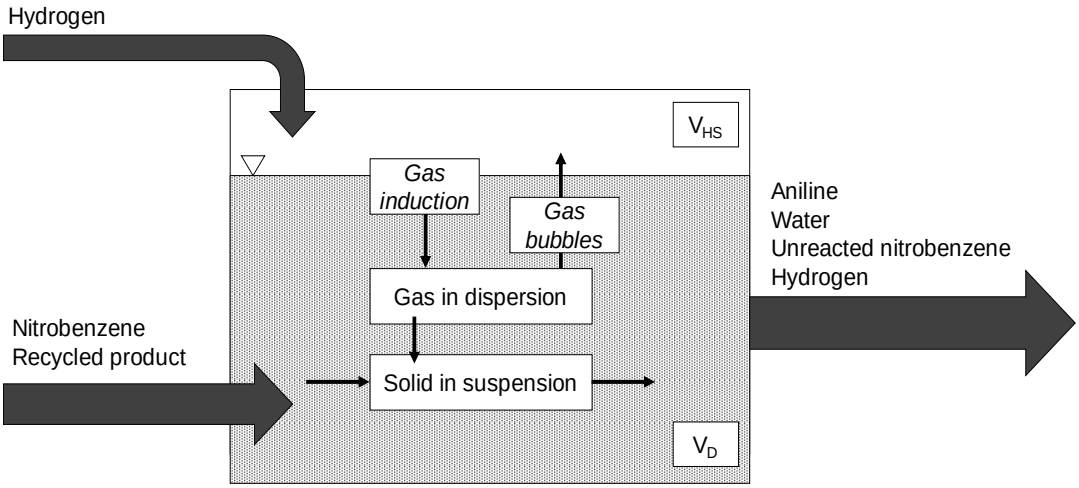

Figure 2.8 – Schematic representation of the industrial reactor.

This model is based on the following main assumptions:

- The reaction mixture is perfectly mixed (i.e., there is a uniform distribution of gas bubbles and catalyst particles).
- The operation is isothermal, with the reaction heat being removed through heat exchanger devices.
- Hydrogen is transferred from the gas to the liquid phase, while the remaining components are at equilibrium between the liquid and the gas phases.
- The hydrogenation reaction occurs at the catalyst surface.
- The activation state is the same for all catalyst particles and throughout the observation period.
- No interaction between the catalyst particles is assumed (i.e., agglomeration phenomena is not considered).
- Steady state operation for the mass transfer and reaction phenomena is considered.

The hydrogen partial pressure in the gas phase is estimated assuming vapour-liquid equilibrium between the reaction liquid mixture and the reactor headspace. Therefore, the hydrogen partial pressure is calculated as follows:

$$P_{H_2} = P_T - \sum_{i=1}^{3} P_{V,i} x_i \qquad i = \text{Aniline, Water, Nitrobenzene} \tag{2.25}$$

where $P_{V,i}$ and x_i are, respectively the vapour pressure and the molar fraction of component i, and P_T is the total pressure of the system. The values of $P_{V,i}$ for each component were determined by the Antoine equation (see Appendix A).

The mechanistic model is described by the following balances:

- Global mass balance:

$$\sum_{\substack{i \\ i = \text{Aniline, Water, Nitrobenzene}}}^{3} G_{in,i} + Q_{H_2} \beta \, MW_{H_2} = Q_{out} \, \rho_L \tag{2.26}$$

Here, $G_{in,i}$ is the feed mass rate of component i $[kg \cdot s^{-1}]$, Q_{out} and ρ_L are the volumetric flowrate $\left[m^3_{liquid} \cdot s^{-1}\right]$ and the density of the liquid phase $\left[kg_{cat} \cdot m^{-3}_{liquid}\right]$, respectively, $w_{L,i}$ is the fraction of the component i in the liquid phase, Q_{H_2} is the volumetric hydrogen consumption in the reactor $[Nm^3 \cdot s^{-1}]$, β is a volume-to-mole conversion factor for the gas phase, and MW_{H_2} is the molecular weight of hydrogen.

- Mass balance to hydrogen in the liquid phase:

$$k_L a_b \left(\frac{C_{G,H_2}}{He_{H_2}} - C_{L,H_2}\right) MW_{H_2} V_D (1 - \epsilon_G) = \\ = k_{LS,H_2} a_{cat} (C_{L,H_2} - C_{S,H_2}) MW_{H_2} V_D (1 - \epsilon_G) + Q_{out} \, \rho_L w_{L,H_2} \tag{2.27}$$

Here, C_{G,H_2}, C_{L,H_2} and C_{S,H_2} are the molar concentrations of hydrogen in the gas, liquid and solid phase $\left[mol \cdot m^{-3}_{liquid}\right]$, respectively, He_{H_2} is the Henry constant for hydrogen, V_D is the volume of the gas-liquid mixture $\left[m^3_{liquid}\right]$, ϵ_G is the gas hold up $[vol/vol]$, $k_L a_b$ $[h^{-1}]$and k_{LS,H_2} $\left[m^3_{liquid} \cdot m^{-2}_{cat} \cdot s^{-1}\right]$ are the gas-liquid and liquid-solid mass transfer

coefficients related to hydrogen (Equations 2.5 and 2.6, respectively), and a_{cat} is the external area of the catalyst $\left[m_{cat}^2 \cdot m_{liquid}^{-3}\right]$.

- Mass balances to the liquid compounds in the liquid-phase:

$$G_{in,i} = k_{LS,i}\, a_{cat}\left(C_{L,i} - C_{S,i}\right) MW_i\ V_D(1-\epsilon_G) + Q_{out}\, \rho_L w_{L,i}$$
$$i = \text{Aniline, Water, Nitrobenzene} \tag{2.28}$$

- Partial mass balances to the solid phase, where equilibrium between the liquid-solid mass transfer and the catalyst surface reaction rates is assumed:

$$k_{LS,i}\, a_{cat}\left(C_{L,i} - C_{S,i}\right) = \vartheta_i\, r_{MNB}\, C_{cat}$$
$$i = \text{Aniline, Water, Nitrobenzene, Hydrogen} \tag{2.29}$$

Here, r_{MNB} is the reaction rate of nitrobenzene $[mol \cdot kg_{cat}^{-1} \cdot s^{-1}]$ and C_{cat} is the concentration of catalyst $\left[kg_{cat} \cdot m_{liquid}^{-3}\right]$, ϑ_i is the stoichiometric coefficient of the component i.

- Global energy balance:

$$\Delta H_{prod} = \Delta H_{OUT} + \Delta H_{HC} + \Delta H_{VB} \tag{2.30}$$

The terms in this equation are given by:

$$\Delta H_{prod} = r_{MNB}\, C_{cat}\, V_D(1-\epsilon_G)\,(-\Delta H_R) \tag{2.31}$$

$$\Delta H_{OUT} = Q_{out}\, \rho_L \int_{T_R}^{T} c_{p,L}\, dT \tag{2.32}$$

$$\Delta H_{HC} = Q_{cw}\, \rho_{cw} \int_{T_{wc,in}}^{T_{wc,out}} c_{p,H_2O}\, dT \tag{2.33}$$

$$\Delta H_{VB} = G_C \left(\Delta H_{vap,H_2O} + \int_{T_{cond}}^{T_{steam}} c_{p,H_2O} dT\right) \tag{2.34}$$

Here, T and T_R $[K]$ are the operating and reference temperatures, respectively. ΔH_{prod}, $(-\Delta H_R)$, ΔH_{OUT}, ΔH_{HC} and ΔH_{VB} are, respectively, the heat produced by the

reaction, the reaction enthalpy, the enthalpy of the outlet stream, the heat removed by the helical coils, and the heat removed by the vertical steam bundles $[\mathrm{kW}]$. $\mathrm{Q_{cw}}$, ρ_{cw}, are, respectively, the volumetric flowrate $[\mathrm{m^3 \cdot s^{-1}}]$ and the density of the cooling water $[\mathrm{kg \cdot m^3}]$. $\mathrm{c_{p,H_2O}}$ and $\mathrm{c_{p,L}}$ are the mass specific heats of the cooling water in the helical coils and of the liquid product stream $[\mathrm{J \cdot kg^{-1} \cdot K^{-1}}]$, respectively. $\mathrm{G_C}$, $\Delta \mathrm{H_{vap,H_2O}}$, $\mathrm{T_{steam}}$ and $\mathrm{T_{cond}}$ are the condensate mass flowrate $[\mathrm{kg \cdot s^{-1}}]$, the vaporisation enthalpy for water $[\mathrm{J \cdot kg^{-1}}]$, and steam/condensate temperatures $[\mathrm{K}]$ in the vertical tube bundles, respectively.

The defined value of $\mathrm{T_R}$ corresponds to the temperature of the feed stream of the reactor (that considers the combined streams of nitrobenzene and of recycled aniline to the reaction vessel). By these means, the enthalpy of the feed stream is zero, which justifies its absence in the global energy balance defined in Equation 2.30.

The volumetric flowrate of the refrigeration helical coils ($\mathrm{Q_{cw}}$) in Equation 2.33 was obtained through in-field measurements performed during this work. The cooling water valve of the helical coils is usually kept fully open to guarantee a more efficient removal of the reaction heat. For this reason, a constant value for the refrigeration flowrate of the helical coils is considered.

As reported in the previous section, the liquid phase hydrogenation of nitrobenzene to aniline at the laboratorial scale tends to be limited by mass transfer if specific experimental conditions are applied. Assuming comparable conditions, the same is expected at the industrial scale. To confirm this scenario, the overall consumption rate of nitrobenzene observed in the industrial reactor will be compared to the corresponding maximal mass transfer rate. In this case, the former value will be determined using the model developed, while considering a data set collected from the process operation.

2.4.1 Overall nitrobenzene consumption rate

To evaluate the mass transfer limitations of nitrobenzene in the industrial reactor, a data set of 138 observations from the process operation was gathered during a period of approximately 700 days. In each observation, the catalyst concentration was measured through samples collected in the reactor outlet. The accuracy of these measurements was ensured by first evaluating the sample collection procedure, as well as different laboratorial techniques to determine this variable. In this case, filtration was the selected technique, due to its smaller error and better precision, in comparison with other techniques assessed (see

Appendix B). Note that, whenever a sample collection was performed, the stability of the process operation was also confirmed in the control room beforehand. In addition, the nitrobenzene bulk concentration was also measured at the same sampling point; the related data was reported by the Quality Control laboratory, that analysed the underlying samples through gas chromatography with a flame ionisation detector (GC-FID).

By considering, in each observation, the state of the process variables and the offline measurements of the catalyst concentration/nitrobenzene bulk concentration in the reactor outlet stream, the process model developed is used to estimate the overall nitrobenzene consumption rate, $n_{MNB}\ [mol \cdot s^{-1}]$:

$$\begin{cases} \dfrac{G_{in,i} - Q_{out}\,\rho_L w_{L,i}}{MW_i} = \vartheta_i\, n_{MNB} \\ Q_{H_2}\,\beta = \vartheta_{H_2} n_{MNB} \\ \left(\sum_i^3 G_{in,i}\right) + Q_{H_2}\,\beta\, MW_{H_2} = Q_{out}\,\rho_L \end{cases} \qquad (2.35)$$

$$i = \text{Aniline, Water, Nitrobenzene}$$

Here, $G_{in,i}$ is the feed flowrate of the component i $[kg \cdot s^{-1}]$, Q_{out} is the volumetric outflow of the reactor $\left[m^3_{liquid} \cdot s^{-1}\right]$ ρ_L is the density of the liquid phase $\left[kg_{cat} \cdot m^{-3}_{liquid}\right]$, $w_{L,i}$ is the fraction of the component i in the liquid phase, Q_{H_2} is the volumetric hydrogen consumption in the reactor $[Nm^3 \cdot s^{-1}]$, β is a volume-to-mole conversion factor for the gas phase, MW_{H_2} is the molecular weight of hydrogen, and ϑ_i is the stoichiometric coefficient of the component i. Based on these data, the observed nitrobenzene consumption rate per unit mass of catalyst, $r_{MNB,obs}\ [mol \cdot kg^{-1}_{cat} \cdot s^{-1}]$, is determined while considering the measured values of the catalyst concentration, C_{cat}, and the liquid volume of the industrial reactor, V_L:

$$r_{MNB,obs} = \frac{n_{MNB}}{C_{cat} V_L} \qquad (2.36)$$

If mass transfer limitations of nitrobenzene in the industrial reaction are significant, Equation 2.36 should provide comparable results with the maximal mass transfer rate of nitrobenzene, MTR_{MNB}, determined to the industrial scale. To evaluate this, the specific

external area of the catalyst, a_{cat}^{*} , is first calculated based on the solid density and particle size distribution from a catalyst sample collected in the outlet stream of the industrial reactor. The particle size distribution was measured through laser diffraction, where each particle size, d_i, is attributed to a differential volume percentage of the sample collected, f_i. By these means, the specific external area of the catalyst is defined as:

$$a_{cat}^{*} = \sum_{i=1}^{N} \left(a_{cat}^{*} f_i \right) = \frac{6}{\rho_{cat}} \sum_{i=1}^{N} \left(\frac{f_i}{d_i} \right) \tag{2.37}$$

Combining Equations 2.21 (see section 2.3.3) and 2.37, the maximal mass transfer rate of nitrobenzene, MTR_{MNB} $[mol \cdot kg_{cat}^{-1} \cdot s^{-1}]$, is calculated according to the following expression:

$$MTR_{MNB} = \left(k_{LS,MNB} \; a_{cat}^{*} \right) C_{L,MNB} = \frac{6}{\rho_{cat}} \left[\sum_{i=1}^{N} \left(\frac{k_{LS,MNB,i} \times f_i}{d_i} \right) \right] \times C_{L,MNB} \tag{2.38}$$

Here, $k_{LS,MNB,i}$ is the liquid-solid mass transfer coefficient of nitrobenzene based on Equation 2.6 for a catalyst particle with size d_i, while assuming the dimensions of the industrial reactor.

The mass transfer limitations of nitrobenzene in the industrial reactor can be assessed by comparing the corresponding average rates of the nitrobenzene consumption and of the related maximal mass transfer; if similar results are obtained, the nitrobenzene concentration at the catalyst surface could be neglected $\left(C_{L,MNB} - C_{S,MNB} \approx C_{L,MNB} \right)$. Bearing this in mind, $k_{LS,MNB}$ can be estimated through a simple rate model, where the overall reaction rate, r_{MNB}, is correlated with the specific external area of the industrial catalyst, a_{cat}^{*} and the measured nitrobenzene bulk concentration, $C_{L,MNB}$:

$$r_{MNB} = \frac{n_{MNB}}{C_{cat} V_L} \approx k_{LS,MNB} \, a_{cat}^{*} \times C_{L,MNB} \tag{2.39}$$

Attending to the current industrial practice, fresh catalyst make-ups can routinely occur, especially if the concentration of nitrobenzene starts to increase. This procedure,

however, can influence the available specific area of the catalyst for mass transfer. For this reason, the industrial data set used for the estimation of $k_{LS,MNB}$ considered an observation period where a stable values of catalyst concentration and a constant addition of fresh catalyst were verified. This will be addressed next.

Estimation of $k_{LS,MNB}$ based on industrial data

Figure 2.9 presents the overall nitrobenzene consumption rate, n_{MNB} $[mol \cdot s^{-1}]$ determined in each observation of the industrial reactor. The corresponding values remain mostly stabilised between 0.6 and 1.0 a.u. This variation can be caused by the measurement accuracy of the process variables derived from the instrumentation installed (i.e., feed flowrates, hydrogen consumption, operating temperature/pressure).

Figure 2.10 shows the evolution of the catalyst concentration during the same observation period, alongside with the cumulative of catalyst make-ups performed. During the first 168 days of observation, stable values of the catalyst concentration are verified, alongside with a moderate frequency of catalyst make-ups. Simultaneously, a high and stable conversion of nitrobenzene is observed (see Figure 2.11). After that period, however, the catalyst concentration varies significantly, whilst an increased addition of fresh catalyst is performed to the system; in this case, the stability of the nitrobenzene conversion is also affected (see Figure 2.11).

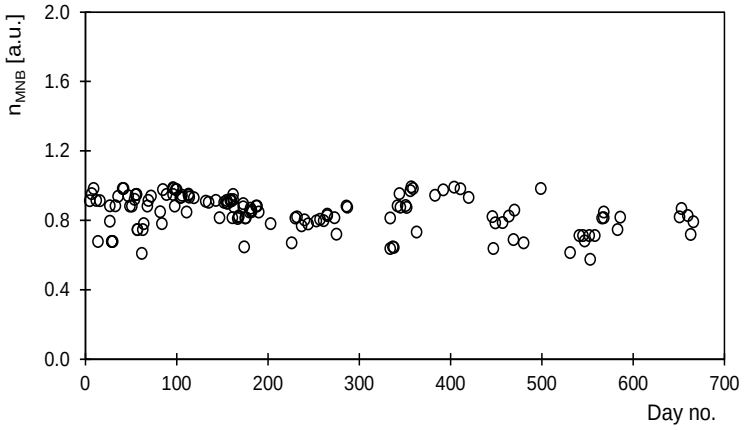

Figure 2.9 – Overall nitrobenzene consumption rate (n_{MNB}) during the overall observation period.

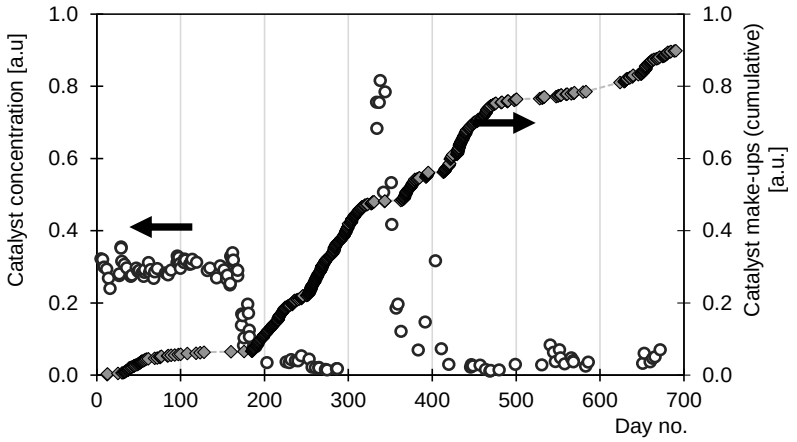

Figure 2.10 – Measured catalyst concentration (○) and cumulative of catalyst make-ups (◇).

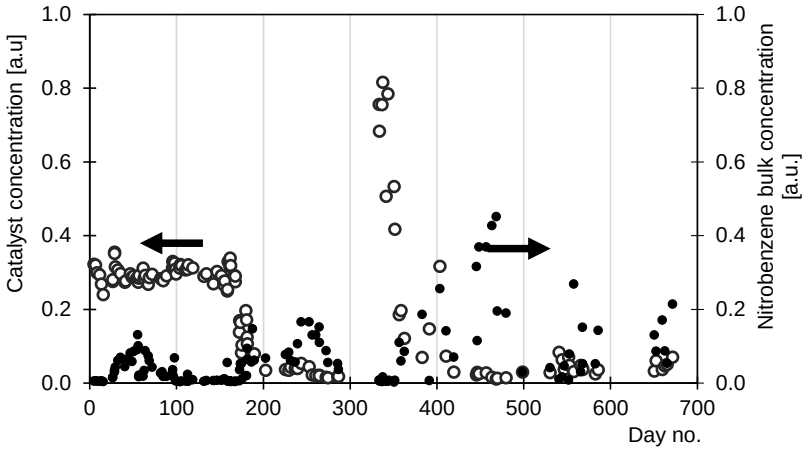

Figure 2.11 – Measured catalyst concentration (○) and nitrobenzene bulk concentration (●).

Under the premise that catalyst deactivation is here minimised due to the frequency of catalyst make-ups, it is plausible that the reaction conversion is mainly dependent on the stability of the catalyst concentration. Representing the observed nitrobenzene consumption rate per unit mass of catalyst $\left(\frac{n_{MNB}}{C_{cat}V_L}\right)$ during the overall period of observation (see Figure 2.12), constant values are noticed until day 168, period where the consistency of the catalyst concentration values is reported. During this interval, it is plausible that the specific external area of the catalyst, a^*_{cat} $[m^2_{cat} \cdot kg^{-1}_{cat}]$, remained more uniform and, in turn, the same is expected relatively to the mass transfer of nitrobenzene to the catalyst surface. Following this idea, the same observation period (1-168) is selected to further evaluate the significance of mass transfer limitations of nitrobenzene on the overall reaction rate.

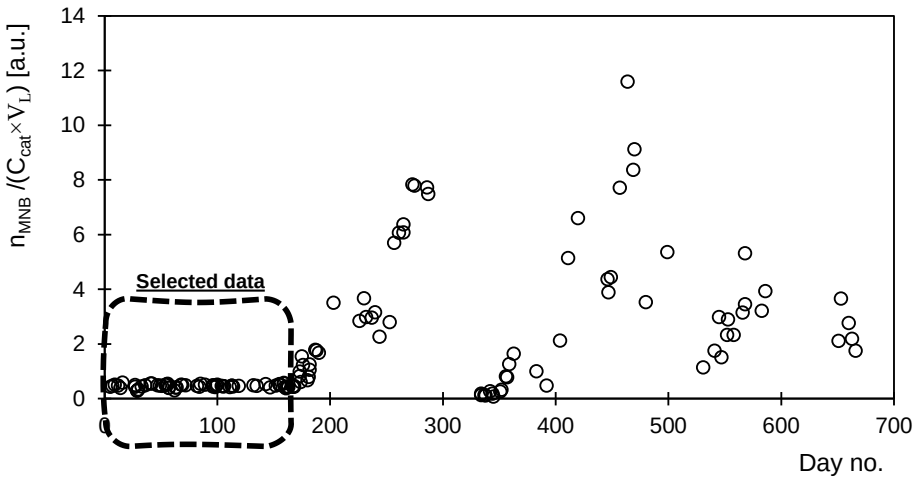

Figure 2.12 – Observed values of nitrobenzene consumption rate per unit mass of catalyst.

Figures 2.13-14 provide a more detailed view of the selected data, presenting the collection date of the catalyst sample here considered, together with the corresponding measurements of the catalyst concentration/nitrobenzene bulk concentration, and record of catalyst make-ups performed. It is possible to verify that the nitrobenzene conversion remains most stabilised between days 99-168, where the stability of the catalyst concentration coincides with a more moderate addition of fresh catalyst to the system, in comparison with the first half of the selected data.

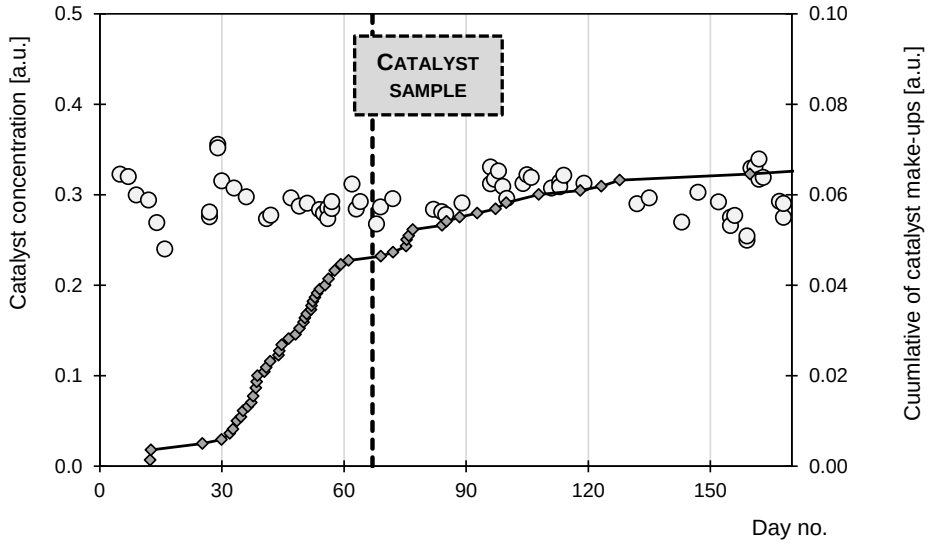

Figure 2.13 – Catalyst concentration (○) and record of catalyst make-ups (-◇-) (days 1-168).

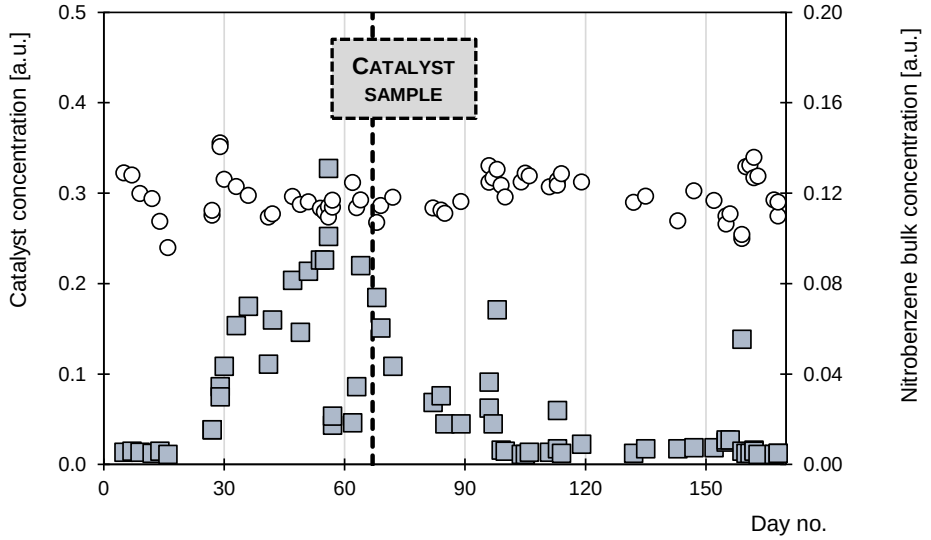

Figure 2.14 – Catalyst concentration (○) and nitrobenzene bulk concentration (■) (days 1-168).

Given these results, the average rates of the nitrobenzene consumption per unit mass of catalyst, $\overline{r_{MNB,obs}}$, (Equation 2.36) and the maximal mass transfer of nitrobenzene, $\overline{MTR}_{MNB}$, (Equation 2.38) were determined, while considering separately the overall period 1-168 and the specific time interval between days 99-168 (Table 2.11). As expected, the values of $\overline{r_{MNB,obs}}$ did not vary significantly among the periods here considered (see Figure 2.12); on the other hand, it is observed that the predicted $\overline{MTR}_{MNB}$ is substantially lowered during period 99-168, when compared to the overall period 1-168. Considering that the

predicted value of $k_{LS,MNB}$ does not depend significantly on the physical properties of the liquid mixture (according to Equation 2.6), the value $\overline{MTR}_{MNB}$ should here be mainly influenced by the nitrobenzene bulk concentration. Selecting the period 99-168 where stable and lower nitrobenzene bulk concentrations are verified, similar values between $\overline{r_{MNB,obs}}$ and $\overline{MTR}_{MNB}$ are obtained. This result suggests that mass transfer limitations of nitrobenzene are also pointed to control the overall reaction at the industrial scale. Given this, the observation period between days 99-168 will be considered to estimate the liquid-solid mass transfer coefficient, $k_{LS,MNB}$. To achieve this, Equation 2.39 is considered (see section 2.4.1), where the corresponding observed nitrobenzene consumption rate per unit mass of catalyst, $\frac{n_{MNB}}{C_{cat}V_L}$ $[mol \cdot kg_{cat}^{-1} \cdot s^{-1}]$ is correlated with the measured value of nitrobenzene bulk concentration, $C_{L,MNB}$. For this purpose, the measured specific catalyst external area of the industrial catalyst , a_{cat}^{*}, is also considered.

Table 2.11 – Average values of the nitrobenzene consumption and maximal mass transfer rates in the industrial reactor (days 1-168).

	$\overline{r_{MNB,obs}}$ [a. u.]	$\overline{MTR}_{MNB}$ [a. u.]
Overall period (days 1-168)	0.472	1.345
Days 99-168	**0.464**	**0.360**

Table 2.12 presents the estimated value of $k_{LS,MNB}$, together with the corresponding p-value and coefficient of determination (R^2). R^2 provides a statistical measurement, ranging from 0 to 1, of how close the data are to a given fitter linear regression. The p-value represents the probability at which the data lead to the null hypothesis, that is, to the rejection of a given parameter; therefore, the model is statistically significant whether the p-value of a given estimate is equal or inferior to the level of significance set in advance [124]. In this case, the high value of R^2 (>0.900) proved a good fit quality of the linear regression, observing that the corresponding estimate is statistically significant as indicated by the low p-value (<0.05).

Table 2.12 – Estimated liquid-solid mass transfer coefficient of nitrobenzene for the industrial reactor.

Parameter	Estimate	R^2	p-value	Confidence interval
$\left(k_{LS,MNB} \times a^*_{cat}\right) \left[m^3_{liquid}\, kg^{-1}_{cat}\, s^{-1}\right]$	0.180	0.975	2.158E-18	[0.167;0.193]
Number of points	22			
$a^*_{cat}\ [m^2 \cdot kg^{-1}_{cat}]$	184			
$k_{LS,MNB}\left[m^3_{liquid} \cdot m^{-2}_{cat} \cdot s^{-1}\right] \times 10^4$	9.77			

Due to the approximately isothermal conditions of the reaction unit, during this period the analysis of the Arrhenius equation cannot be applied to estimate the apparent activation energy. Regardless of that, the significance of nitrobenzene mass transfer limitations at the industrial scale is also highlighted by noticing the similarity between the estimated $k_{LS,MNB}$ and the corresponding prediction at the laboratorial scale previously advanced $(7.30 - 7.90) \times 10^4\ \frac{m^3_{liquid}}{m^2_{cat} \times s}$ (see Table 2.4).

Furthermore, the prediction of $k_{LS,MNB}$ in the industrial reactor is also calculated through Equation 2.6 considering the dimensions and operating conditions of the industrial vessel, together with the specific density and particle size distribution of the industrial catalyst sample collected. Table 2.13 shows the predicted value of $k_{LS,MNB}$ for the industrial scale and the corresponding estimated value based on the industrial data previously presented in Table 2.12.

Table 2.13 – Predicted (Eq. 2.6) and estimated $k_{LS,MNB}$ for the industrial reactor.

	$k_{LS,MNB}$ $\left[m^3_{liquid} \cdot m^2_{cat} \cdot s^{-1}\right] \times 10^4$
Industrial scale (predicted) (Eq. 2.6)	4.77
Industrial unit (estimated) (Table 2.12)	9.77

It is observed that the estimated value of $k_{LS,MNB}$ based on the industrial data is higher than the corresponding prediction based on Equation 2.6, although both values

present the same order of magnitude. On the other hand, recall that, according to the authors [67] that developed Equation 2.6, additional studies on large-sized vessels are required to check the dependence of k_{LS} on additional geometric parameters and physical properties. Given the quality-of-fit of the linear regression presented at Table 2.11, the estimated $k_{LS,MNB}$ should be representative of the present unit. Nonetheless, the update of this value is recommended as future work through the collection of more extensive data sets under steady operating conditions and specific catalyst management features.

This way, the overall reaction rate in the industrial unit, r_{MNB} $[mol \cdot kg_{cat}^{-1} \cdot s^{-1}]$ is determined by the mass transfer rate of the limiting reactant, which, in turn, is defined by the estimated liquid-solid mass transfer coefficient, the specific external area of the catalyst, and the liquid concentration of nitrobenzene as:

$$r_{MNB} = k_{LS,MNB} \times a_{cat}^{*} \times C_{L,MNB} = 0.180\ C_{L,MNB} \tag{2.41}$$

Here, the value 0.180 $\left[m_{liquid}^{3} \cdot kg_{cat}^{-1} \cdot s^{-1}\right]$ corresponds to the overall rate constant ($k_{LS,MNB}\ a_{cat}^{*}$) of the industrial reactor.

Once this kinetic expression is included in the process model of the industrial reactor, the reaction outcome can be readily predicted under a specified operating window. This enables the development of process monitoring tools, which, in turn, could serve as a basis for process optimisation. Because of this, the model validation is also here addressed by evaluating the deviation between the predicted and measured values of nitrobenzene bulk concentration during the overall observation period performed in the present work. This is detailed in the model results next.

2.4.2 Model results

Table 2.14 presents the system parameters, the input variables and the output variables considered in the model developed to predict the nitrobenzene bulk concentration in the industrial reactor.

Table 2.14 – Input/output variables and system parameters defined in the model developed.

Parameters	Input variables	Output variables
d_{cat}	C_{cat}	G_{out}
ρ_{cat}	P_T	$w_{L,ANL}$
Q_{cw}	T	$w_{L,Water}$
G_C	$G_{in,MNB}$	$w_{L,MNB}$
N	$G_{in,ANL}$	w_{L,H_2}
V_D	P_{steam}	$T_{cw,out}$
d_I	G_C	
d_R	$T_{wc,in}$	
S	Q_{H_2}	

Figure 2.15 shows the deviation between the predicted and measured values of nitrobenzene bulk concentration obtained during the together with observation period, the cumulative of fresh catalyst additions, together with the frequency of system shutdowns derived from high contents of unconverted nitrobenzene detected in the reactor outlet stream.

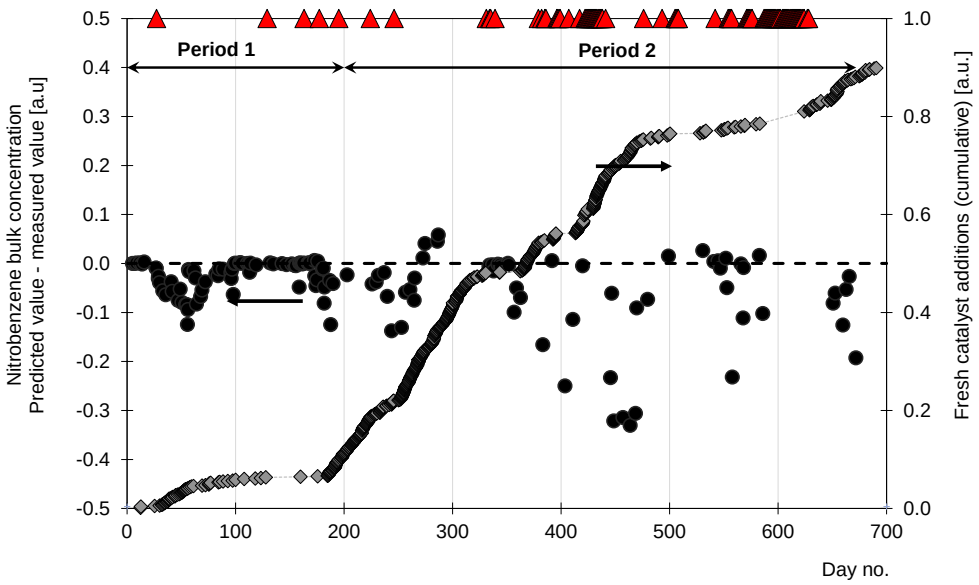

Figure 2.15 – Model predictions of nitrobenzene bulk concentration in the industrial reactor (● model deviation, ◇ fresh catalyst additions, △ system shutdowns).

Overall, the predicted values of the nitrobenzene bulk concentration are mostly below the corresponding measures verified in the industrial reactor. Considering the whole-time lapse of observation, two main periods are distinguished: “Period 1”, (days 1 to 200), where the deviation between the predicted and measured values of nitrobenzene bulk concentration varies between -0.125 and +0.006 a.u., and “Period 2” (days 200 to 672), where the same deviation is more significant (-0.330 to +0.058 a.u.). As shown in Figure 2.16, the higher deviations between the predicted and the measured values of nitrobenzene bulk concentration coincide with catalyst concentrations below 0.1 a.u, when frequent additions of fresh catalyst are also performed. This scenario is mainly observed during “Period 2” where the several changes on the blend composition of fresh catalyst used are also performed (see Figure 2.17), in contrast to “Period 1”. During Period 2, the system shutdowns (induced with the detection of high nitrobenzene contents in reactor outlet) are also more frequent, in comparison with Period 1.

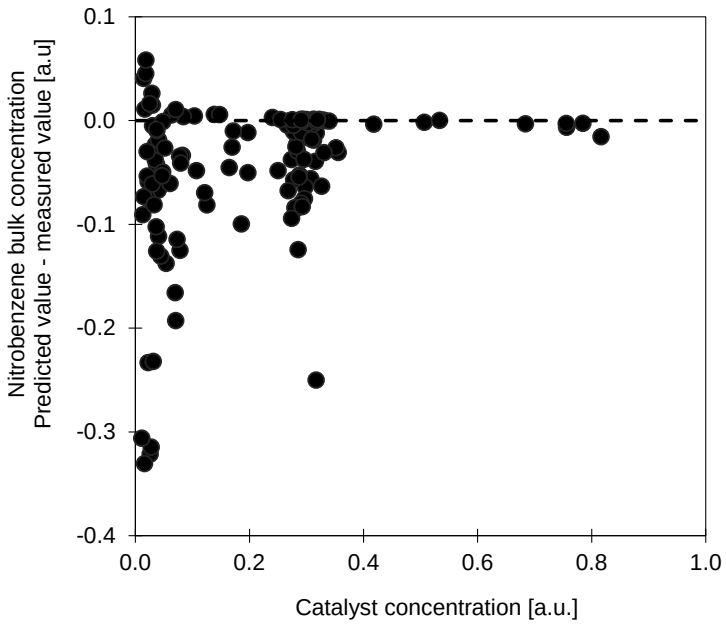

Figure 2.16 - Deviations between the predicted and measured nitrobenzene bulk concentration versus catalyst concentration.

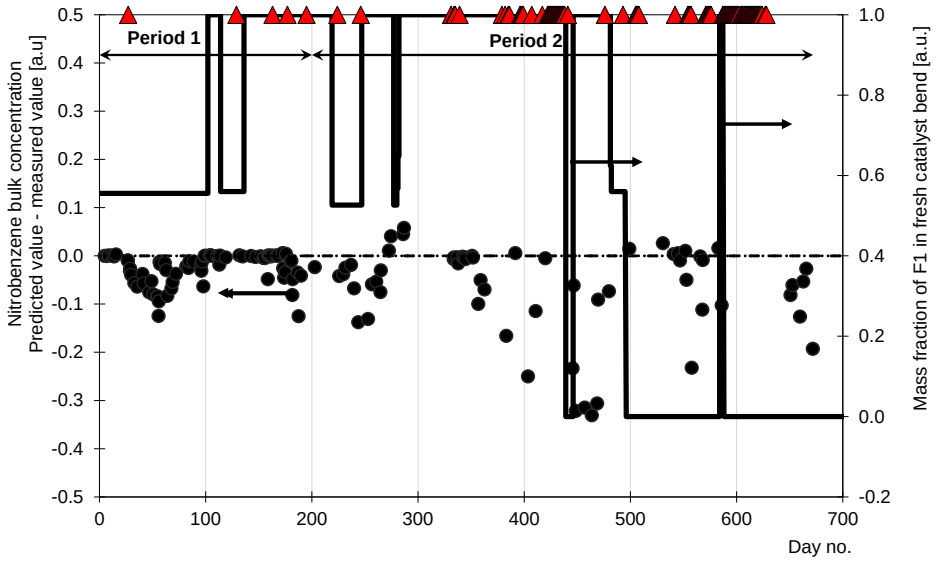

Figure 2.17 - Model predictions of the nitrobenzene bulk concentration in the industrial reactor and composition of fresh catalyst blends (● model deviation, ▬ composition of fresh catalyst blend, ---- baseline).

These remarks indicate that during this period, when low catalyst concentrations are combined with high frequencies of catalyst make-up, the model predictability was hindered.

This result can be explained by the unexpected modification of the specific area of the catalyst affecting the mass transfer rate of nitrobenzene. On the other hand, if the concentration of catalyst remains controlled with moderate addition of fresh catalyst, the specific area of the catalyst should be less disturbed, enabling a better prediction of the mass transfer rate and, therefore, of the nitrobenzene bulk concentration based on the model developed.

Due to the mass transfer limitations of the limiting reactant on the present industrial unit, the improvement of the system productivity should not rely in the increase of the catalyst activity, but rather on reducing the liquid-solid mass transfer resistance. Major factors to mitigate this issue include improving the physical properties of the catalyst suspension, including the catalyst concentration and catalyst size. Minor factors include the agitation rate and the operating temperature [125].

Next, a sensitivity analysis is presented. This includes the effect of key process variables on the predicted values of nitrobenzene concentration in the liquid phase.

2.4.3 Sensitivity analysis

To perform this analysis, a case is selected from the observation period considered in section 2.4.1, where a small deviation between the predicted and measured values of nitrobenzene bulk concentration is verified. Table 2.15 presents the reference and ranges of the process variables considered for this exercise.

Table 2.15 – Reference values and ranges used in the sensitivity analysis performed.

Reference variable	Value [a.u.]	Range [a.u.]
Catalyst concentration	0.28	0.02-1.00
Reactor temperature	0.77	0.70-0.90
Nitrobenzene flowrate	0.54	0.30-1.00
Recycled aniline flowrate	0.60	
Agitation rate	1.00	0.70-1.50
Nitrobenzene bulk concentration		
Industrial data	0.016	
Predicted value	0.021	

Figure 2.18 presents the effects of the process variables on the predicted values of nitrobenzene bulk concentration. The recommended value of 0.05 a.u. to nitrobenzene bulk

concentration is also represented in the same figure. This value is here assumed, attending to the quality specifications of the final product and to the separation capacity of the purification units downstream related to the reaction stage.

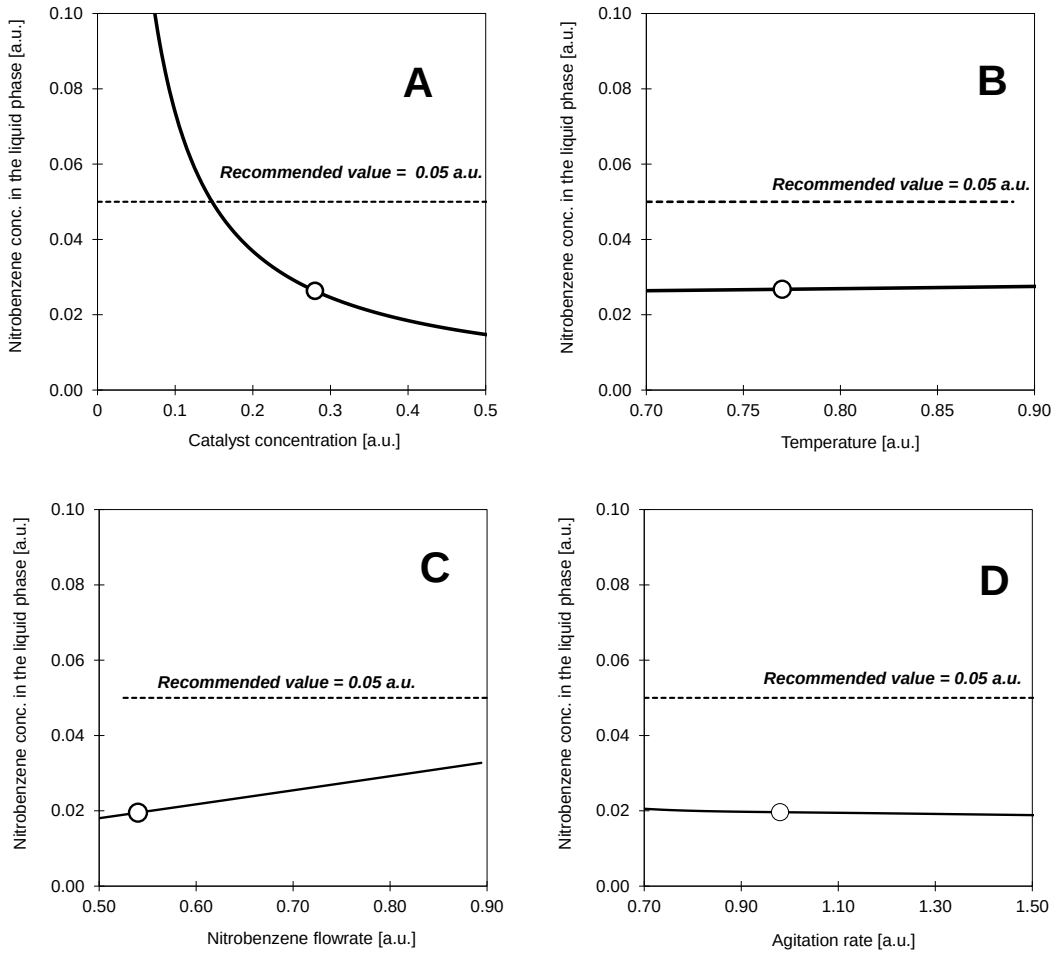

Figure 2.18 – Effect of (A) catalyst concentration, (B) of temperature, (C) of nitrobenzene feed flowrate, and of (D) agitation rate on the predicted values of nitrobenzene bulk concentration (○ reference values presented in Table 2.15).

The catalyst concentration directly influences the overall external area of the catalyst for mass transfer. For this reason, the stability of this variable should be maintained to improve the catalyst addition policy. In this case, the sensitivity analysis indicate that the catalyst concentration ought to be maintained around 0.10-0.20 a.u to ensure the stabilisation of the reaction conversion; however, note that this range is attributed to a

specific blend composition of fresh catalyst used in the time that the underlying observation was conducted to the industrial reactor. Given this, it becomes probable that the desired range of catalyst concentration could differ depending on the catalyst addition policy applied. For that reason, the kinetic model should encompass further process data sets, under steady and specified catalyst make-up features.

Temperature influences directly on mass transfer and chemical reaction steps. However, the corresponding effect is pronounced in different extents. In case of mass transfer processes, temperature only has influence on the fluid properties, while chemical kinetics is especially sensitive to this variable, according to the Arrhenius equation [38]. In this case, due to the mass transfer limitations on the overall reaction rate, a minor effect on the conversion of nitrobenzene is observed. In addition to this, it should be noted that the production of secondary compounds is promoted with temperature [110] [111], which demands higher processing costs in the downstream purification units.

Nitrobenzene feed flowrate directly affects the conversion of nitrobenzene, as it influences the hydraulic retention time in the reaction vessel. As expected, the predicted nitrobenzene concentration tends to increase when high feed flowrates of nitrobenzene are applied. In this case, although the corresponding nitrobenzene concentration remains below the maximal recommended value, note that the steadiness of the catalyst suspension is also verified. Nonetheless, if an unexpected reduction of the catalyst concentration occurs, the reaction performance can be compromised if high feed flowrates of nitrobenzene are applied. Bearing this in mind, a control strategy of the hydraulic retention time is also addressed in the present work (see section 4.4), with the intention of promoting the stability of the process.

To describe the effect of the agitation rate on the predicted values of the nitrobenzene concentration in the liquid phase, its influence on the mass transfer coefficients is considered. To accomplish this, the ratio between the estimated and predicted values of $k_{LS,MNB}$ at the industrial scale is considered (≈ 2.05) (see Table 2.13), which was then used as a factor to the prediction of $k_{LS,MNB}$ (Equation 2.6) and employed to the process model developed. In this case, a neglectable effect on the reaction conversion is noticed. Although, from an industrial standpoint, this result could theoretically benefit the energy consumption costs by reducing the agitation rate, this action is not recommended since it could compromise the induction of gas in the reaction mixture, as well as the recovery of catalyst from the decanter through the recirculation stream (see

section 2.2). Alternatively, the agitation efficiency could be improved by increasing the power per unit volume of the agitation system by using more effective impellers (e.g. Smith-type turbines). Another possibility would be enhancing the gas superficial velocity [126]. However, this action would require the reduction of the impeller submergence, which, in turn, could hinder the gas-liquid mass transfer.

This sensitivity analysis evidences that, apart from the conventional key operating variables of the process, the catalyst concentration should be especially regarded for process monitoring. On the other hand, the catalyst properties should be further understood regarding the physico-chemical changes that this material might undergo during its lifetime. This issue is addressed in Chapter 3.

In Chapter 4, the analysis of the process operation is addressed, together the practices involved with the catalyst management. Based on these remarks, the statistical control of the industrial unit based on the process model is also presented. In addition, guidelines for process monitoring and control are also detailed.

3. Catalyst characterisation

In this chapter, the characterisation of the catalyst used in the process is addressed. This study aims to assess the physico-chemical changes that the catalyst might undergo during its usage. Therefore, samples of fresh catalyst were compared with those of used catalyst collected in different sampling points of the industrial unit.

This work also includes the characterisation of the deposited catalyst collected from the internals of the reaction vessel during a downtime period. The results obtained were then compared with the samples of suspended catalyst, with the purpose of evaluating the possible causes to the agglomeration/deposition of this material.

Finally, the magnetic properties (e.g., coercivity and magnetisation saturation) of the samples of fresh catalyst batches and of the used catalyst collected from different reactors in the process are also assessed. The goal is to provide new highlights regarding the improvement of the catalyst management.

3.1 Objectives of the catalyst characterisation

As observed in Chapter 2, the catalyst behaviour can influence the performance of the underlying system. Catalyst activity within the system is maintained through the reposition of fresh catalyst, this way compensating the decay of the catalytic properties. Because of this, the importance of further understanding the physico-chemical features of this material is here advanced through the application of several characterisation techniques. By doing this, new insights regarding the catalyst management in the productive process can be attained.

In the case of the aniline production process of Bondalti, powdered nickel supported on silica is used as catalyst. The related quality standards of the fresh catalyst required to the external suppliers are outlined in Table 3.1.

Table 3.1 – Catalyst specifications for the aniline production process of Bondalti.

Parameter	Value
Nickel content [a.u.]	>0.30
Specific area [a.u.]	>0.60
Mean particle size, Dv(50) [a.u.]	>0.67

Apart from the overall catalyst specifications referred, characterisation techniques can provide addition measurements regarding the physico-chemical profile of the catalyst material. Examples of these characteristics include [132]:

- ✓ the chemical composition of the bulk and surface of the material;
- ✓ the catalyst textural and morphological properties (e.g. solid particle size and distribution, crystalline morphology, porosity, and surface area);
- ✓ the chemical properties measured at the surface of the material including valence state, acidity, reactivity with different molecules, surface energy, and surface electronic states;
- ✓ the aggregation properties (e.g., aggregate size, magnetic properties, density, mechanical strength, and resistance towards attrition);
- ✓ the catalytic performance such as activity, selectivity, and activity stability.

Next, a description of the characterisation techniques used in the present study are presented.

3.2 Characterisation techniques

The characterisation of the physico-chemical properties of the catalyst will be addressed considering the following techniques outlined in Table 3.2.

Table 3.2 – Characterisation techniques used in the catalyst studied.

Catalyst characteristic	Characterisation Technique
Physical properties	
Surface area	Nitrogen adsorption (BET)
Particle size, and size distribution	Laser diffraction
Surface texture and morphology	Scanning electron microscopy (SEM)
Magnetic properties	Vibrating sample magnetometry (VSM)
Chemical properties	
Bulk composition	Atomic absorption (AAS)
	CHNS elemental analysis
Surface chemical composition	Energy dispersive X-ray spectroscopy (EDS)
Crystallographic structure	X-ray diffraction (XRD)
Oxidation state	Temperature programmed reduction (TPR)

The surface morphology of the material was analysed through scanning electron microscopy (SEM) on a Hitachi® SU-70 electronic microscope with an image resolution scale varying between 600 nm and 60 μm. The same equipment also provided the measurement of local surface chemical composition through energy dispersive X-ray spectroscopy analysis (EDS).

The crystallographic structure was determined by X-Ray diffraction analysis (XRD), performed on a JEOL® 2200FS transmission electronic microscope in the angular range of 10° to 100° (2θ). This average size of the crystallites was also assessed by applying the Scherrer equation

$$d_{Ni} = \frac{K\lambda}{\beta \cos\theta} \quad (3.1)$$

where d_{Ni} is the crystallite size [nm], K is the shape factor [-], λ the X-ray wavelength [nm], β the line broadening at half maximum intensity (FWHM) already with the instrumental baseline subtracted [rad], θ is the Bragg angle [rad]. These parameters were provided by the XRD reports of the different samples studied.

The granulometric analysis was performed by laser diffraction, on a Malvern® Mastersizer 3000 whose size range varies between 0.01 and 3500 µm.

The determination of the specific area was performed by nitrogen adsorption, on a Micromemeritics® ASAP 2000, using nitrogen at 77K.

The oxidation state of the solid surface, which evidences the metal-support interaction of the supported catalyst, was analysed by Temperature Programmed Reduction (TPR). This analysis was performed on an Altamira Instruments® AMI-200. The applied heating rate was 10°C/min under a volumetric flowrate of 30 cm^3(STP)/min of argon with 5 vol.% hydrogen. The hydrogen consumption was monitored through a thermal conductivity detector (TCD).

The nickel content of each sample was determined through atomic absorption spectroscopy (AAS). This technique was performed on a Perkin-Elmer® 3000 using a Perkin-Elmer® Intensity Hallow Cathode lamp with a wave length of 323.2 nm. Each sample was digested on an HCl 6N solution at 150°C.

The quantification of lighter elements (i.e. carbon, hydrogen, nitrogen, sulphur) in the bulk of the solid samples was determined through CHNS elemental analysis. This characterisation technique was performed on a Truspec® 630-200-200 equipment with sample weight of 2 mg. The combustion furnace temperature used was 1075°C and the detection methods used included infrared absorption for carbon, hydrogen and sulphur, together with thermal conductivity for nitrogen.

The magnetic properties of the catalyst were measured on a vibrating-sample magnetometer (VSM) *Dynacool Quantum Design* at room temperature (300K), where each sample was subjected to a magnetic field varying up to 9T.

All catalyst samples were analysed in laboratorial facilities external to Bondalti Chemicals S.A. Before measuring each physico-chemical property, the preparation of each catalyst sample followed the documented standard procedures related to the characterisation equipment abovementioned.

In section 3.3, the characterisation study addresses the physico-chemical differences between the fresh catalyst and the used catalyst in suspension throughout the reaction stage. To achieve this, one sample in each of the sampling points distributed over the various streams of the process was collected on the same date. These samples were then subjected to a filtration procedure to separate the corresponding solids from the liquid phase. Afterwards, the solids were treated with ethanol to remove any organic residuals and dried in a stove. In addition, two samples of dried fresh catalyst derived from different catalyst suppliers were also collected from specific batches used in the production process during the same period; these samples were collected on the same date, this way providing a comparison under the same time basis. Apart from the latter set of samples, another sample collected about five months earlier at the reactor outlet stream was also characterised with the same techniques. In section 3.4, the characterisation of three other samples collected from the deposited material founded in the internals of the reactor is also presented. These samples were withdrawn about three months after the collection date of the former samples referred. By these means, the characterisation also provides an overlook of the physico-chemical changes of the catalyst during its lifetime inside the reaction vessel.

In section 3.5, the magnetic properties of the catalyst (e.g., coercivity and magnetisation saturation) are evaluated in more detail considering several samples from the lots provided by two different suppliers, previously used in the production process. In this case, one sample per lot was considered. In addition, the effect of the reduction temperature on the magnetic properties of the fresh catalyst was also evaluated. For this purpose, ten samples from a selected lot were considered; while one served as blank sample, the remaining nine were reheated at different reduction temperatures.

The latter section also addresses the effect of different blend compositions of fresh catalyst on the coercivity. Besides that, the temporal evolution of the coercivity in the suspended catalyst was also evaluated measuring this property from several samples collected from the outlet stream of different reactors; in this case, each reactor was fed with a specific blend composition of fresh catalyst. By doing this, the improvement of the catalyst

management by suggesting an improved blend composition of fresh catalyst to add to the system.

3.3 Characterisation of the fresh catalyst and of the suspended catalyst

The sampling sites of the different process streams are represented in Figure 3.1, from where the catalyst samples were collected and characterised.

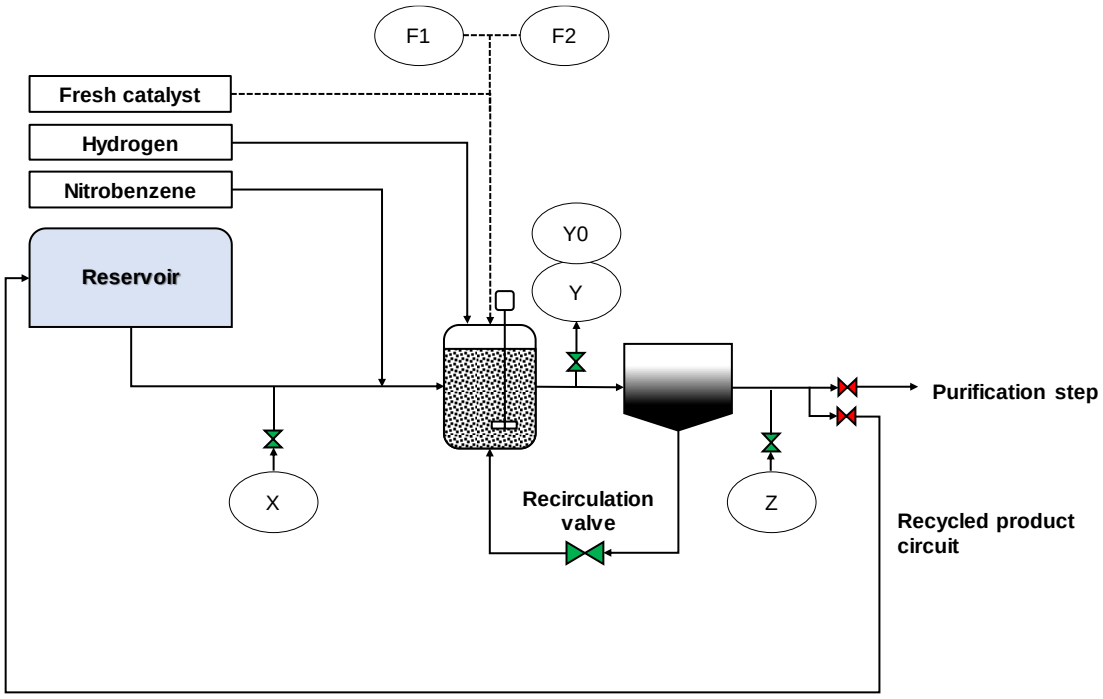

Figure 3.1 – Representation of the sampling sites in the reactor-decanter system.

F1 and F2 represent two different samples of fresh catalyst used in the underlying process. Each one is specific different catalyst supplier. X, Y, and Z refer to different samples of used catalyst withdrawn from the streams of the recycled aniline circuit, the reactor outlet, and the decanter outlet, respectively. These samples, together with samples F1 and F2, were collected on the same date. On the other hand, sample Y0, derived from the reactor outlet stream, was collected about five months earlier than the remaining samples referred.

3.3.1 Scanning Electron Microscopy/Energy Dispersive X-ray emission spectroscopy (SEM-EDS)

The SEM-EDS technique allows examining the surface morphology of the material and the analysis of the chemical composition in a semi-quantitative way. The SEM images obtained for the fresh and used catalysts are shown in Figure 3.2. In the 0.5K-magnified images, catalyst particles collected at the outlet stream of the reactor (Y0/Y) are visibly distinguishable from those of the remaining streams, showing higher homogeneity either in size, or in shape. As can be seen, the main difference inferred from these pictures is that sample Y0 has a smaller particle size, when compared to sample Y. In the 10K- and 50K-magnified images, sample Y presents needle-shaped nanostructures, in contrast to the particles from sample Y0, whose surface is similar to the samples of the remaining streams, revealing rounded-shaped nanoparticles.

Sample	× 0.5K (4.00 a.u.)	× 10K (0.20 a.u.)	× 50K (0.04 a.u.)
F1	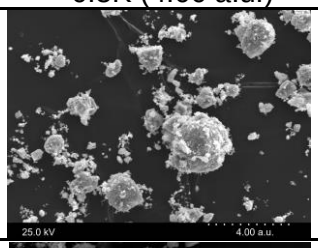	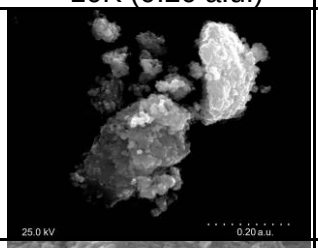	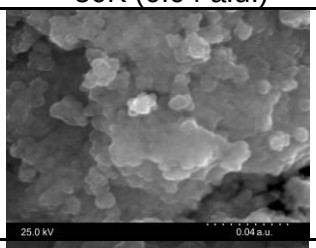
F2	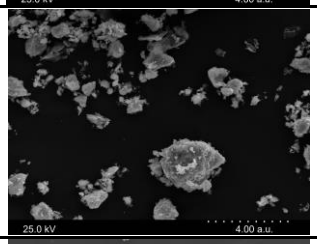	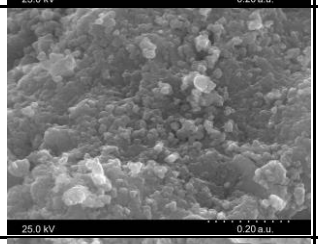	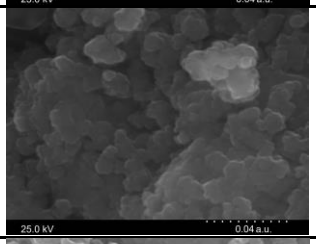
X	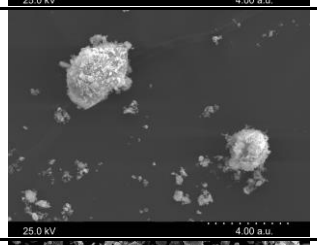	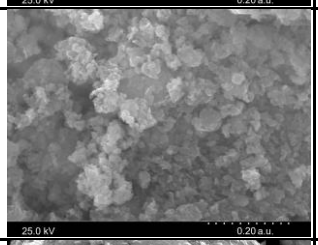	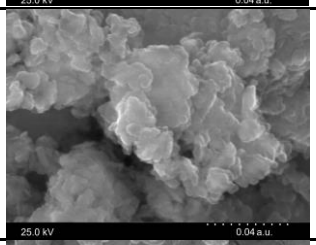
Y0	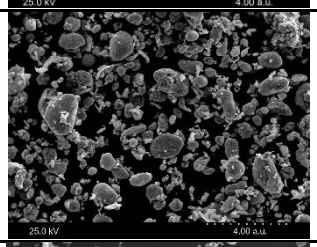	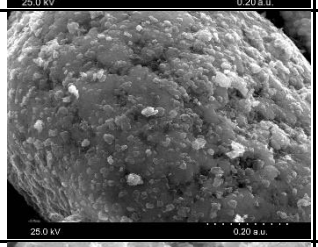	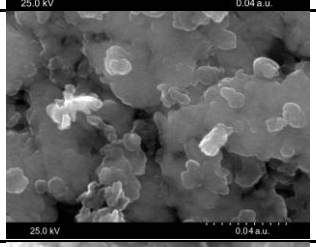
Y	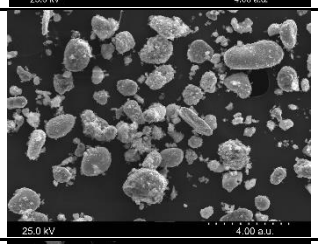	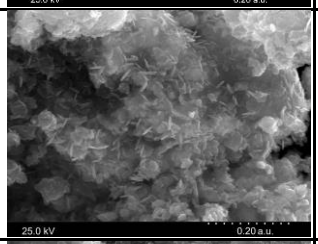	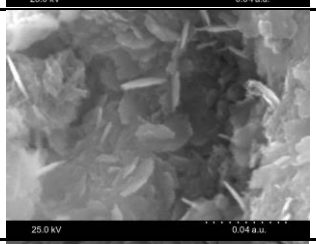
Z	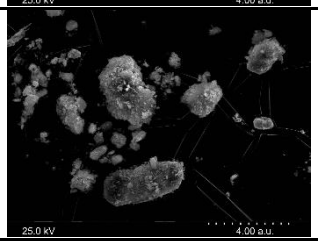	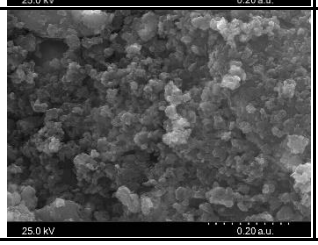	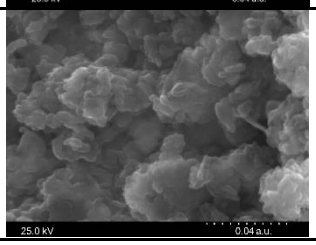

Figure 3.2 – SEM images of the samples of catalyst studied: fresh catalyst – F1/F2-, and used catalyst collected from recycled aniline stream (X), reactor outlet (Y0/Y), and decanter outlet (Z).

The EDS spectra and the corresponding chemical composition are outlined in Figure 3.3 and Table 3.3. In the case of the samples of fresh catalyst, the presence of aluminum

is observed only in F2. This result was expected, as the F2 catalyst presents alumina in its catalyst support formulation. Comparing the catalyst collected from the recycled aniline (X) and the decanter outlet (Z) streams, it can be observed that the contents of nickel and aluminum in sample X are, respectively, 5% and 14% lower than those observed in sample Z. On the other hand, the silicon content is 15% higher in sample X than that of sample Z.

Considering the samples collected at the reactor outlet stream, sample Y0 displays a Ni/Si ratio about one order of magnitude greater than sample Y, wherein Y0 presents a content of silicon about 86% lower than Y. On the other hand, note that Y presents a Ni/Si ratio like in fresh catalysts F1/F2. This result may suggest the loss of silica support, due t to the milling of catalyst particles caused by the reactor agitation [23]. In fact, this phenomenon is normally attributed to fluid or slurry beds [133]. In contrast, the smaller Ni/Si ratios found in both recycled aniline and the decanter outlet streams (samples X and Z) can indicate that the catalyst silica-based support exits the reaction stage, and it is maintained on the recycled aniline stream. However, note that EDS is a semi-quantitative technique that uniquely quantifies the chemical composition at a specific point on the surface; therefore, atomic absorption was used to determine the nickel content of each sample, as this technique enables the measurement of the bulk composition of the material. The corresponding results are presented next.

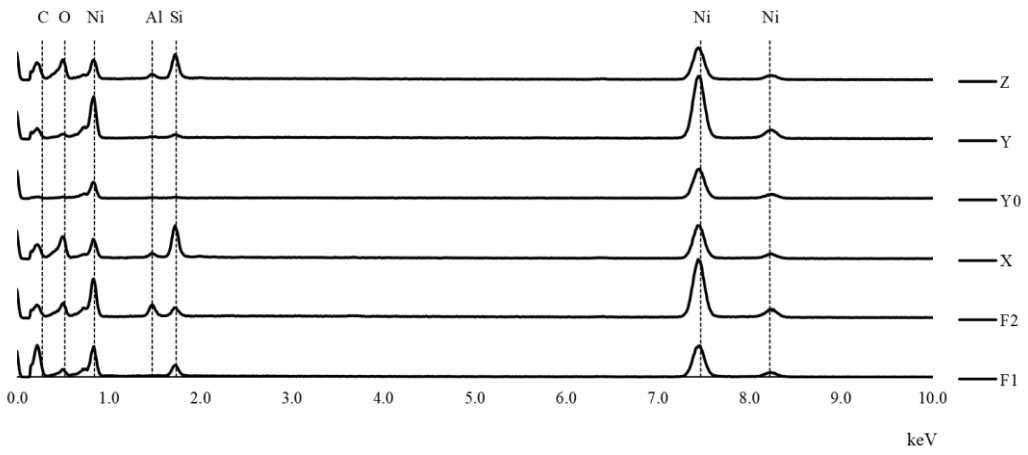

Figure 3.3 – EDS spectra of the samples of catalyst studied: fresh catalysts F1/F2 and used catalyst collect from the process streams X/Y0/Y/Z.

Table 3.3 – Elemental analysis determined through EDS of the samples of catalyst studied.

Sample	EDS [a.u.]						Ni/Si [a.u.]
	Ni	Al	Si	Fe	C	O	
F1	0.423		0.020		0.044	0.014	1.10
F2	0.449	0.014	0.009		0.013	0.015	2.65
X	0.368	0.006	0.046	0.002	0.029	0.049	0.40
Y0	0.446		0.002		0.024	0.029	12.40
Y	0.456	0.002	0.014		0.021	0.008	1.60
Z	0.388	0.007	0.040	0.002	0.029	0.033	0.50

3.3.2 Atomic absorption

The technique of atomic absorption provides the quantification of the bulk nickel composition in each sample. Table 3.4 exhibits the nickel content obtained through atomic absorption in the different samples studied. In the case of fresh catalysts F1 and F2, the corresponding values of nickel content meet the technical specification required by Bondalti (>0.30 a.u.). Note that the nickel content of F2 is 8% higher than that of F1. Considering the data reported in the inspection certificates of the batches from where F1 and F2 samples were collected, the measured nickel content in F1 (0.312 a.u.) is lower than of the corresponding batch provided by the supplier (0.360 a.u.), whereas in the case of F2 the measured value (0.337 a.u.) is slightly higher than the corresponding batch provided by the supplier (0.320 a.u.).

These values are lower than the corresponding values obtained through EDS. As said before, EDS only evaluates the composition at a specific point on the material surface, besides being semi-quantitative, whereas atomic absorption quantifies the bulk composition of the sample. However, both techniques display an analogous trend of results: higher nickel content in the catalyst exiting the reactor, followed by the fresh catalysts F1/F2, the catalyst in the decanter outlet (Z) and finally the catalyst collected in the recycled aniline stream (X). This result reinforces the scenario of nickel enrichment of the catalyst particles in suspension in the reaction vessel, together with the loss of silica support through the decanter outlet and recycled aniline streams.

Table 3.4 – Nickel content determined through atomic absorption of the samples of catalyst studied.

Sample	Atomic absorption Ni [a.u.]
F1	0.312
F2	0.337
X	0.232
Y0	0.447
Y	0.391
Z	0.260

3.3.3 X-Ray diffraction (XRD)

This characterization technique enables the crystallographic analysis of the material. Figure 3.4 shows the corresponding XRD diffractograms of the fresh and used catalyst samples. In the case of the fresh catalysts, only the sample F2 shows a peak of crystalline silica (SiO_2) (2θ≈27°); on the other hand, the corresponding peaks of metallic nickel (Ni) (2θ positions of 45°, 52°, 76°, 92° and 98°) are less intense when compared to the XRD diffractogram of the F1 sample. This result, together with the corresponding ones obtained through EDS and atomic absorption analyses, suggests that the F2 catalyst may have a higher fraction of nickel in its amorphous form. In the case of used catalyst, the peak of nickel silicate (3:4) ($Ni_3Si_2O_5(OH)_4$) (2θ≈12°) is always detected. Amongst the samples studied, the metallic-nickel peaks are more relevant in the case of the used catalyst withdrawn from the reactor outlet. Furthermore, it should be mentioned that the corresponding peak for metallic nickel is more intense in sample Y0 than in sample Y. This result complements those from EDS and atomic absorption analyses, suggesting that the suspended particles in the reaction vessel may undergo a process of nickel enrichment, presenting a higher fraction of nickel crystallites.

The quantification of crystalline species obtained by the Reference Intensity Ratio method (RIR) is registered in Table 3.5. In the case of fresh catalysts, one observes a higher fraction of NiO and a lower fraction of Ni in the F2 catalyst, in comparison with F1. This result is consistent with the higher intensity peak of metallic nickel obtained in the F1 diffractogram.

In the case of the used catalyst, the species $Ni_3Si_2O_5(OH)_4$ is detected in all sampling sites, especially at the recycled aniline (X) and at the decanter outlet (Z) streams. Since this species is attributed to a stronger metal-support interaction when compared to the other nickel-derivate species detected, this result corroborates the latter analyses that indicated the incidence of silica catalyst support on these streams.

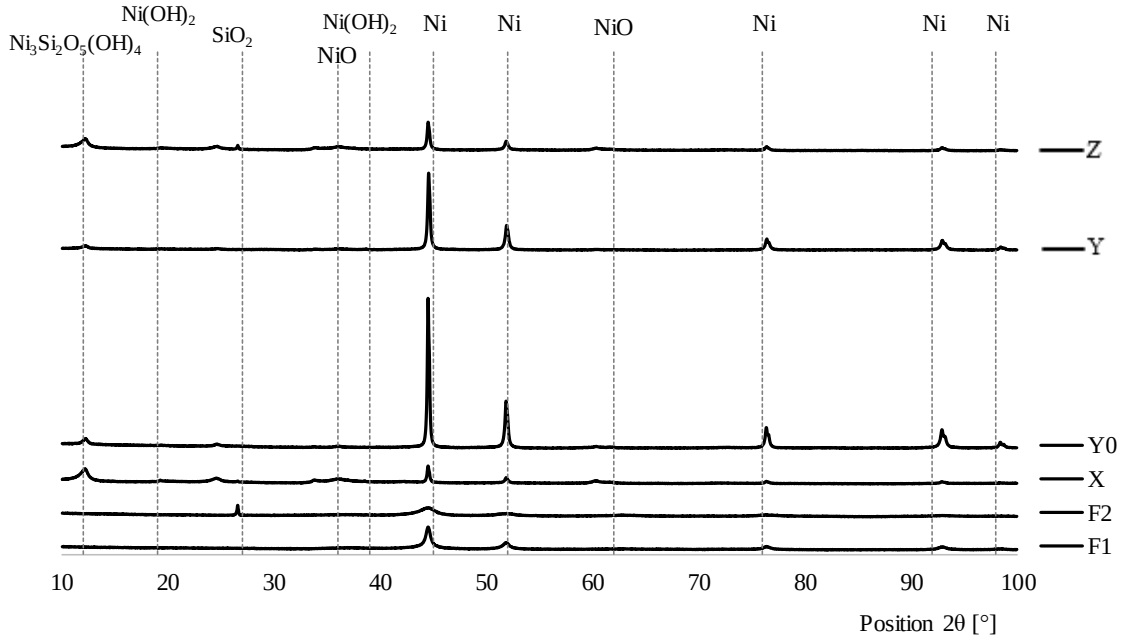

Figure 3.4 – XRD diffractograms of the fresh catalysts F1 and F2 and used catalysts collected at X, Y, Y0, and Z sampling points.

Table 3.5 - Quantitative analysis of the crystalline species identified through XRD (RIR method).

Sample	Crystallographic composition [a.u.]				
	Ni	NiO	SiO_2	$Ni(OH)_2$	$Ni_3Si_2O_5(OH)_4$
F1	0.340	0.160			
F2	0.155	0.220	0.125		
X	0.105		0.310		0.085
Y0	0.480				0.020
Y	0.465			0.015	0.020
Z	0.415		0.020		0.070

3.3.4 Granulometric analysis

The granulometric analysis using laser diffraction allows the determination of particle size distribution (PSD) of a given material. This technique measures the intensity of the light

scattered, as a laser beam passes through a dispersed particulate material; the gathered data is then analysed with the purpose of calculating the size of the particles, based on the scattering pattern created. The PSD results obtained could be either expressed in volume, surface, or number basis. This method is particularly useful for classifying catalyst powders whose particle size may vary significantly, depending on their origin [132] [134].

The particle size distributions and mean particle size obtained are presented in Figure 3.5 and Table 3.6, respectively. In general, the particle size distributions of samples F1, X, Y0 and Y revealed monomodal profiles, while samples F2 and Z present a bimodal profile.

The cumulative curves of the fresh catalysts show that catalyst F1 presents a higher fraction of particle fines than catalyst F2. The monomodal profiles obtained for samples Y0 and Y is coherent with the homogeneity of particle sizes observed by SEM analysis. Nonetheless, sample Y0 has an average particle size approximately 12% lower than sample Y. The cumulative size distributions show that all particles from samples X and Z have an average size below 1.67 a.u. In contrast, the same size grade gathers approximately 90 vol.% of the particles from samples Y and Y0. This result shows that the smaller particles from the reactor outlet tend to exit through the outlet stream of the decanter.

For particle sizes below 1.00 a.u., the catalyst particles collected in the recycled aniline stream (X) tend to be finer, in comparison with those withdrawn from the decanter outlet (Z). This fact evidence that the reservoir, present in the recycled aniline stream (see Figure 3.1), may work as a secondary settling unit, sending particle fines to the recycled aniline stream.

The volumetric average sizes outlined in Table 3.6 allow to evidence that both fresh catalysts studied meet the technical specifications of Bondalti (>0.67 a.u.). However, it should be noted that the average size of F1 is around 24% smaller than that of F2. The measured average sizes of catalysts F1 and F2 are, respectively, about 21% and 50% below the corresponding values reported in the inspection certificates of the related batches.

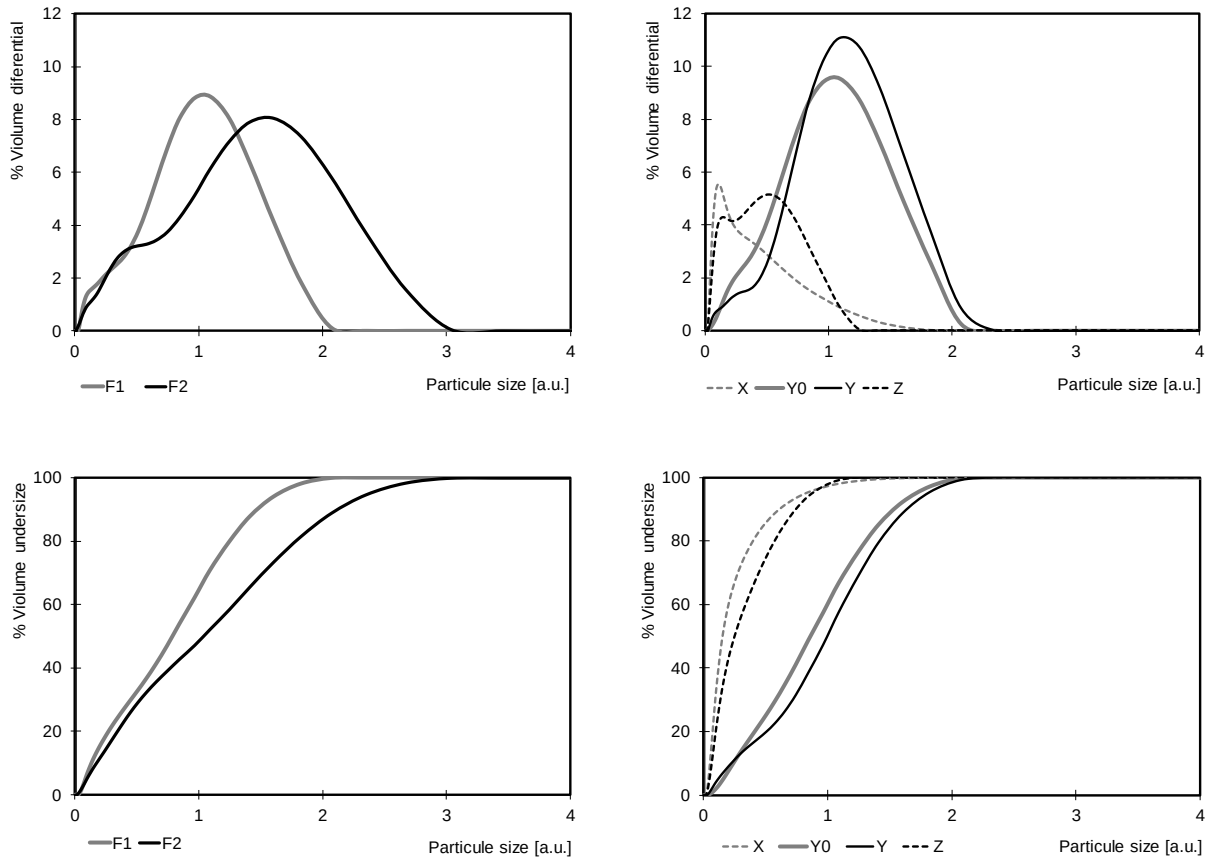

Figure 3.5 – Particle size distributions (particle volume distribution (top) and cumulative volume distribution (bottom)) of fresh catalysts F1 and F2 and of used catalysts collected at recycled aniline (X), reactor outlet (Y0/Y), and decanted outlet (Z) streams.

Table 3.6 – Mean particle size of the samples studied.

Sample	Dv(50) [a.u.]
F1	0.79
F2	1.03
X	0.15
Y0	0.87
Y	0.99
Z	0.25

3.3.5 BET analysis

This technique is widely used for measuring the internal surface area of mesoporous solid materials in the range of 1 to 1200 m^2/g. The concept of this analysis is based on the adsorption and condensation of nitrogen on the porous structure under relatively low pressures [132].

The results of the specific area, pore volume and pore size are in Table 3.7. Both samples of fresh catalyst meet the technical specification required (>0.60 a.u.). According to the inspection certificates of the fresh catalysts F1 and F2, the reported values of specific area (0.87 and 0.94 a.u., respectively) are above the measured values (0.76 and 0.75 a.u., respectively).

The BET specific area of the catalyst collected in the process streams is significantly lower than in the fresh catalyst samples studied. In the case of the catalysts collected at the recycled aniline and decanter outlet streams, the specific area is 34% lower, whereas for the catalyst withdrawn from the reactor outlet the specific area is 90% lower, in comparison with the fresh catalysts studied.

This significant decrease of the specific area of the suspended catalyst particles in the reaction vessel suggests the occurrence of substantial modifications on their pore structure, in comparison with the fresh catalyst. The results obtained through EDS, atomic absorption and XRD analyses indicate that these particles tend to lose their silica support due to the mechanical attrition, thus enhancing their composition in crystalline nickel [135]. The same reason justifies the reduction of the pore volume to about one tenth on the samples Y0 and Y; another possible cause for the reduction of both specific area and pore volume is pore blockage by organic material derived from the reaction mixture [35].

Table 3.7 – BET analysis results of the catalyst samples studied.

Sample	BET analysis	
	Specific area [a.u.]	Pore volume [a.u.]
F1	0.76	0.38
F2	0.75	0.56
X	0.49	0.72
Y0	0.05	0.06
Y	0.08	0.10
Z	0.31	0.46

3.3.6 Temperature Programmed Reduction (TPR)

The TPR characterisation technique is one of the most used thermo-analytical techniques in the characterisation of solid materials. In general, these techniques allow the measurement of the energy/mass consumed or released by the solid under study, while varying the temperature. In this technique, a flow of a reducing gas mixture (i.e., nitrogen or argon with a small fraction of hydrogen or carbon monoxide) is applied to a solid material, while the temperature is linearly increased. This experiment allows the measurement of the consumption of the reducing agent, thus the degree of reduction and, consequently, the surface oxidation state of the solid material [136]. The peak temperatures observed in a TPR profile of supported catalysts can be used to evaluate the strength of metal–support interactions [137].

Figure 3.6 shows the TPR profiles obtained with the catalyst samples studied. In general, two main peaks of hydrogen consumption can be observed: a low-temperature peak (250-350°C) and another at a high-temperature range (600-800°C). The former is typically associated to the reduction of species with higher oxidation potential, possibly attributed to the reduction of NiO to Ni. The unique presence of NiO in the fresh catalyst samples observed by XRD is coherent with the TPR low-temperature peak detected only in the TPR of the same catalyst samples.

The second peak may be related to the reduction of the species $Ni_3Si_2O_5(OH)_4$, whose interaction with the catalyst support is stronger. Although this species is not identified in the fresh catalyst through XRD analysis, it may still be present in its amorphous form, thus explaining the TPR profiles in these samples. It should be noted that the high-temperature peak is larger in the used catalyst than in the fresh catalyst samples, which matches the greater fraction of crystalline $Ni_3Si_2O_5(OH)_4$ detected through XRD in the former ones.

Attending to the TPR profiles of the catalyst exiting the reactor, it is observed that the sample Y0 is far more reduced than in sample Y. This result can be explained by the higher content of crystalline Ni detected in the sample Y0 through XRD analysis. On the other hand, the higher H_2 consumption in the sample Y is coherent with the presence of the species $Ni(OH)_2$ evidenced by XRD.

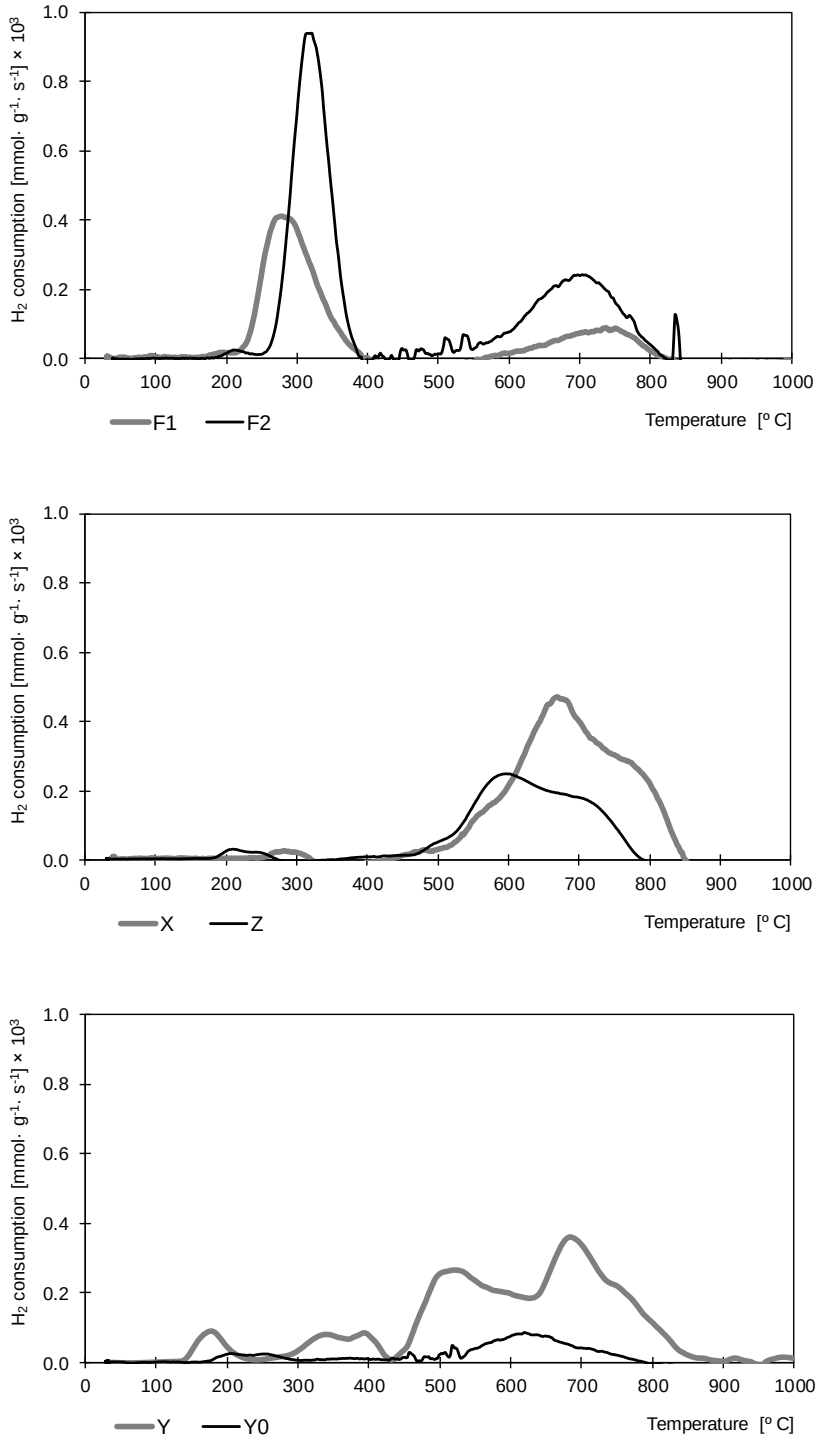

Figure 3.6 - TPR profiles for the fresh catalysts (F1/F2) and used catalyst collected at the recycled aniline (X), decanter outlet (Z), and reactor outlet (Y0/Y) streams.

3.3.7 Magnetic analysis

Magnetism is related to the motion phenomena of electric charges in materials whenever these are exposed to a magnetic field. The magnetic behaviour of a material relies on its capacity of revealing collective interaction of magnetic moments along its atomic structure [138]. The orientation of these magnetic moments will consequently describe the magnetic behaviour of the material. In general, five types of magnetic behaviour can be distinguished: diamagnetism, paramagnetism, antiferromagnetism, ferromagnetism, and ferrimagnetism. While the first two refers to materials with no (or insignificant) collective magnetic interaction, the latter groups are attributed to large-order net magnetisation [138].

In the case of ferromagnetic materials, these materials display permanent magnetic moments in the absence of an external field. This property is usually referred to as *spontaneous magnetisation*, which is attributed to transition metals such as nickel, iron, cobalt, and some alloys of rare earth elements [138]. The alignment of magnetic moments in these materials is confined to a certain volume fraction designated as *domain*. Each domain has its own magnetic dipole, and it can be adjacent to other domains depending on the grain size of the ferromagnetic material (see Figure 3.7). The net alignment of all domains will then determine the degree of magnetisation of a ferromagnetic material [139].

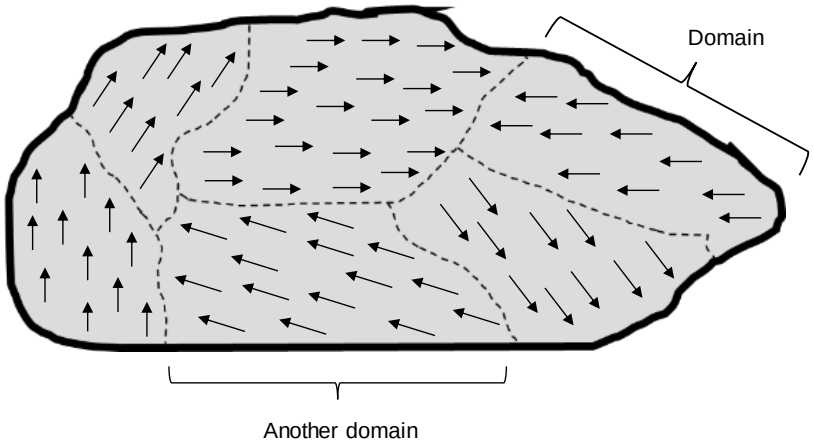

Figure 3.7 – Representation of magnetic domains in a ferromagnetic material (absence of external field).

The behaviour of a ferromagnetic material is also influenced by the temperature. Increasing temperatures enhance the thermal vibration of atoms, thereby inhibiting

magnetisation; this tendency reaches a maximum, where no magnetisation occurs – the corresponding temperature is called the Curie Temperature. This parameter depends on the type of material. Iron, cobalt, and nickel present values of 768°C, 1120°C, and 358°C, for this parameter, respectively [138].

Analogously to the effect of temperature, the alignment of magnetic moments can be hindered due to the size of ferromagnetic crystallites. If this size goes below a certain critical value, no magnetisation occurs, and the material is superparamagnetic [140]. In addition to this, magnetisation can be also conditioned by the crystallinity degree of the ferromagnetic material which constrains the alignment of the magnetic moments. This property is called magnetic anisotropy [139] [141].

Oxidised forms of typical ferromagnetic elements have their magnetic atomic moments distributed in an antiparallel alignment, thereby leading to zero magnetisation. These compounds are designated as antiferromagnetic and examples include NiO, MnO, and Fe_2O_3 (hematite) [140].

The magnetic properties of the material can be obtained through the magnetic hysteresis loop (M-H curve), representing the magnetisation (M) of a material towards a magnetic field applied (H) (see Figure 3.8). By inducing an external magnetic field (H), each domain of the material begins to be oriented towards the direction of the applied field (initial magnetisation). When no further magnetisation is possible, the full alignment of all domains of the material is obtained - saturation magnetisation (M_S); from this point, the magnetic field is reversed, gradually demagnetising the material, wherein a distinct profile from the previous magnetisation step is observed. This behaviour is called hysteresis, and it may be derived from the motion of the domain boundaries from which new domains are formed and developed at the expense of the previous magnetic alignment. Once all the field is removed, the ferromagnetic material displays a new configuration of domains thus exhibiting a magnetisation of remanence (M_r). To fully demagnetise the material, a magnetic field must be applied in the opposite direction of the original one, which is denominated as coercivity or coercive force (H_c) [141].

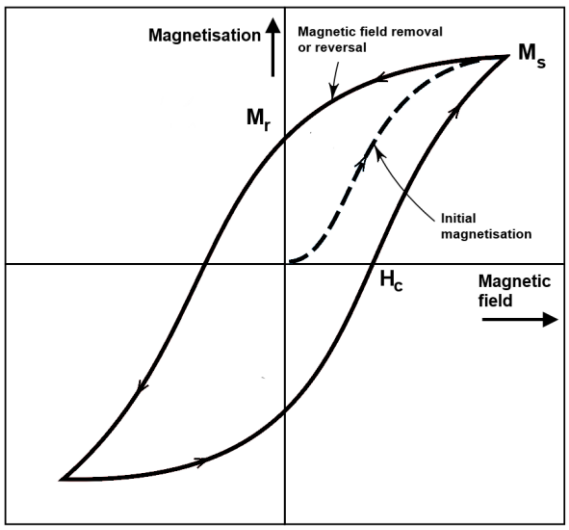

Figure 3.8 – Schematic representation of a M-H curve of a ferromagnetic material (adapted from [141]).

Ferromagnetic materials can be classified either as *hard*, *semi-hard*, or *soft magnets*, depending on their characteristic hysteresis [141]. Generally, hard magnets (or permanent magnets) are attributed to materials that present significant resistance to demagnetisation. The latter materials have coercivities above 125 Oe. Semi-hard magnets, on the other hand, have lower coercivities (13-125 Oe) than permanent magnets, thus being suitable for producing magnetic recording materials - their coercivity still enables them to retain information (magnetic memory), however it is low enough to allow the demagnetisation of the material with relatively low magnetic fields (e.g., erasable magnetisation). Soft magnets are easily magnetised and demagnetised, due to their low coercivity (less than 13 Oe) [141].

In other words, the coercivity dictates how resistant a material can be towards demagnetisation. This property is dependent on the ferromagnetic grain size, the crystalline structure, the presence of antiferromagnetic compounds and the temperature conditions [141]. Figure 3.9 outlines the coercivity-size dependency of a ferromagnetic material, along with the critical diameters for the superparamagnetic behaviour (d_{SP}) and multidomain state (d_C). For particle sizes below d_{sp}, the thermal energy is greater than the magnetic dipole energy. In this case, the material is unable to sustain any magnetic domain and therefore it has no net alignment of magnetic moments, thus presenting zero coercivity (superparamagnetic state). For particle sizes between d_{sp} and d_c, a single domain prevails

and the coercivity increases with particle size. For particle sizes larger than d_c, the ferromagnetic material presents multi magnetic domains and a decreasing coercivity with size is observed, owing to the lower net magnetisation. Examples of ferromagnetic materials and the corresponding values of d_{SP} and d_C are presented in Figure 3.10. In the case of nickel, it is verified that the corresponding nanoparticles can display a single ferromagnetic domain from sizes up to 30 nm, and multi ferromagnetic domains are formed for sizes ranging from 30 to 85 nm.

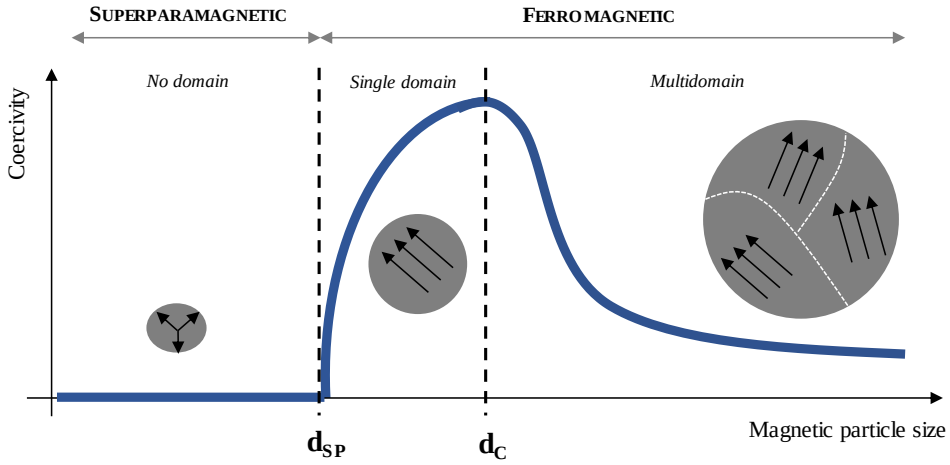

Figure 3.9 – Coercivity size-dependence within magnetic particles (adapted from [142]).

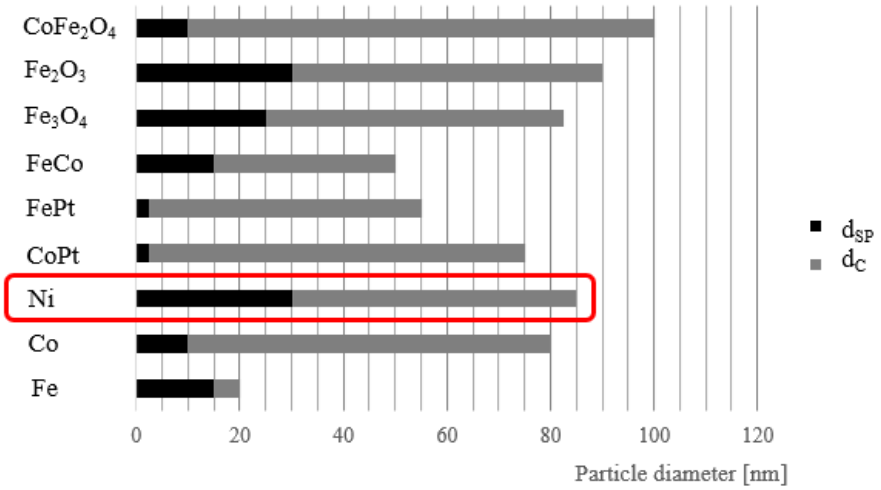

Figure 3.10 – Critical magnetic particle sizes related to the superparamagnetic and single domain behaviour (adapted from [142]).

As previously stated, the magnetic behaviour of nickel nanoparticles can be measured depending on their (1) mass, (2) crystalline structure, (3) temperature conditions and (4) grain size. The results obtained through EDS, atomic absorption, and XRD evidenced that the catalyst particles inside the reactor tend to display an increasing content of crystalline nickel with time. On the other hand, note that the temperature conditions of the reaction vessel are considerably below the temperature of Curie for nickel; therefore, the factors (1), (2) and (3) can favourably contribute towards a ferromagnetic behaviour of nickel nanoparticles. The average size of the nickel crystallites can be obtained by applying the Scherrer equation (see section 3.2) considering the peak related to metallic nickel in the XRD-diffractogram of each sample; Table 3.8 outlines the average size of the nickel crystallites in the of fresh and used catalysts samples studied.

Table 3.8 - Average size of nickel crystallites in the samples of fresh catalyst (F1/F2) and of used catalyst (X/Y0/Y/Z).

Sample	Nickel crystallite [nm]
F1	16
F2	19
X	41
Y0	50
Y	44
Z	26

According to Figure 3.10, bulk nickel nanoparticles can display a single ferromagnetic domain from sizes up to 30 nm, and multi ferromagnetic domains appear for sizes ranging from 30 to 85 nm. It should be noted that, in the single domain region, the resistance towards demagnetisation (coercivity) increases with nickel nanoparticle size, whereas in the multidomain region the opposite tendency is verified. Therefore, considering the results displayed in Table 3.8, fresh catalysts F1/F2 can be either superparamagnetic (i.e., neglectable coercivity), or ferromagnetic (single domain); on the other hand, in the case of used catalysts, nickel nanoparticles can be ferromagnetic (single or multi domain). To confirm this hypothesis, magnetic measurements on the latter catalyst samples were performed. M-H curves obtained at 300K for the samples F1, F2, X, Y0, Y, and Z, together with the corresponding values of coercivity and of saturation magnetisation are presented in Figure 3.11.

Amongst the various samples studied, note that the values of the saturation magnetisation of the catalyst withdrawn from the reactor (samples Y0/Y) are close to what is expected for bulk nickel (55 $A \cdot m^2/kg$ [138]). This result is consistent with the significant nickel content found on these samples, evidenced by the atomic absorption and EDS analyses. Considering the fresh (F1/F2) and used catalysts collected at the recycled aniline and decanter outlet streams (X/Z), these samples coarsely display the same saturation magnetisation, whose values are lower than bulk nickel; in the case of the fresh catalysts, this result can be attributed to the significant content of crystalline NiO (antiferromagnetic specie); in the case of the samples X and Z, their lower values of saturation magnetisation can be explained by the lesser content of bulk nickel, in comparison with the remaining samples.

As for the coercivity results, samples F1, X, Y0, Y, and Z presented values one order of magnitude higher than in F2. In the case of samples F1, Y0, Y and Z, these results are justified by the higher fraction of crystalline nickel determined through XRD (0.34, 0.48, 0.47 and 0.42 a.u., respectively), in comparison with the sample F2 that accounts for only 0.16 a.u. In the case of sample X, the greater coercivity is possibly attributed to the higher size of the nickel crystallite, in comparison with sample F2.

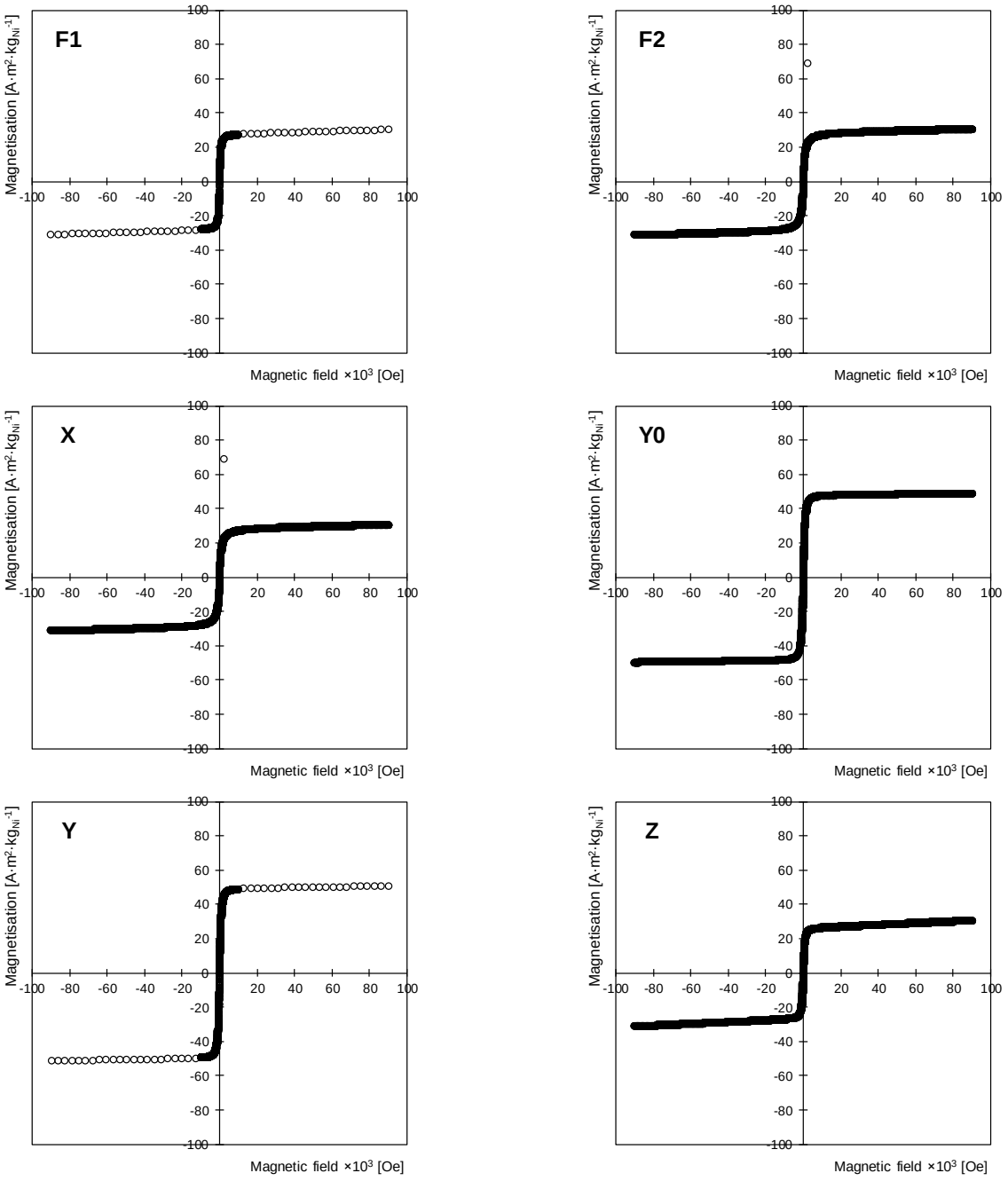

Sample	Coercivity [Oe]	Saturation magnetisation [$A \cdot m^2 \cdot kg_{Ni}^{-1}$]
F1	102	31
F2	23	31
X	116	22
Y0	93	49
Y	103	51
Z	146	31

Figure 3.11 – Magnetic analysis performed at 300K for the samples of fresh and used catalyst studied.

Considering the latter coercivity measurements, all catalyst samples studied can be classified as semi-hard magnetic materials, except sample Z, whose coercivity is characteristic of a hard magnet. This scenario highlights the likelihood of nickel particles becoming resistant to demagnetisation with time, thus potentially promoting their agglomeration and deposition within the system.

3.3.8 Global analysis of the characterisation studies

The characterisation of the catalyst collected from the different process streams allowed to evidence the physico-chemical changes of this material throughout the reactor-decanter system. According to the SEM analysis, the suspended catalyst particles exiting the reactor display greater homogeneity in size and shape, when compared to the fresh catalyst. According to the granulometric analysis, the catalyst particles from the reactor outlet display a greater average size, presenting a lesser fraction of particle fines, in comparison with the samples collected in the remaining streams of the process. EDS and atomic absorption analyses indicate, respectively, a higher Ni/Si ratio and Ni content, in the reactor outlet stream than in the other streams of the process. Therefore, it is plausible that the catalyst may lose its silica support within the reactor, possibly due to the reactor agitation.

According to the XRD results, the average size of the nickel crystallites (≈50nm) in the catalyst suspended in the reactor is about twice the average size of the nickel crystallites in the catalyst collected at the decanter outlet. Therefore, if the catalyst particles are progressively reduced due to the attrition caused by the reactor agitation, *catalyst fragments* with larger nickel crystallites tend to be retained inside the reaction vessel, whilst catalyst fines with smaller nickel crystallites escape easily from the decanter outlet. This hypothesis of catalyst attrition is also evidenced by the granulometric analysis performed in the catalyst collected at the decanter outlet, where a higher fraction of particle fines was found, in comparison with the catalyst particles inside the reaction vessel. In turn, the catalyst collected at the recycled aniline stream presented a higher fraction of particle fines than in the decanter outlet. Such result further indicates that the reservoir of recycled aniline circuit may function as a secondary settling tank.

Apart from the reduction in particle size, a decrease of the specific area in the catalyst collected at both the reactor (Y0/Y) and the decanter outlet (Z) streams was observed, in comparison with the fresh catalyst samples; this result, together with the higher

fraction of crystalline nickel determined on the former samples through XRD analysis, suggests that the packing of metallic particles is more significant in samples Y0,Y and Z. In the case of catalyst collected at the recycled aniline stream (X), the reduction of the specific area was less significant, in comparison with the fresh catalysts; the smaller fraction of crystalline nickel in sample X evidenced by XRD analysis, in comparison with the fresh catalysts, indicates that nickel present therein is mainly amorphous, thereby promoting a less significantly packing of the metallic particles. Another possible cause for the specific area reduction is pore blockage, owing to the thermic decomposition of organic compounds. However, this hypothesis was not confirmed in the present study due to the lack of additional analyses performed on these samples (e.g., CHNS elemental analysis).

TPR profiles show that hydrogen consumption on the fresh catalyst occurred mainly at lower temperatures, in contrast to the used catalyst, where the consumption of hydrogen is only significant at higher temperatures. This result indicates that the latter are more reduced than the fresh catalysts studied.

The magnetic measurements performed evidence further differences among the catalyst samples studied. In the case of fresh catalysts, F1 presents a coercivity value one order of magnitude greater than in F2; despite displaying the same average size of nickel crystallites, F1 presents a higher fraction of crystalline nickel, which suggests that magnetic anisotropy is more significant, thereby explaining the greater coercivity in F1. Nevertheless, both fresh catalysts present the same saturation magnetisation, which is coherent with the similar fractions of bulk nickel (ferromagnetic material) and crystalline NiO (antiferromagnetic specie), obtained through atomic absorption and XRD analyses, respectively. In the case of used catalysts, the coercivity values are of the same order of magnitude as F1; this result can be explained by their significant fraction of crystalline nickel, except with the catalyst collected at the recycled aniline stream, whose coercivity can be attributed to its average size nickel crystallite, which is comparable to the catalyst particles collected at the reactor outlet. Note that the catalyst samples withdrawn from the reactor outlet stream show a higher saturation magnetisation than in the catalyst collected at the recycled aniline and decanter outlet streams, and close to the corresponding value of bulk nickel. This result is coherent with the greater nickel content of the catalyst inside the reaction vessel, as evidenced through the results of atomic absorption.

As mentioned before, all catalyst samples studied can be denoted as *semi-hard* magnetic materials, except for catalyst sample collected at the decanter outlet which can

be categorised as a *hard magnet*. This scenario suggests that, in general, the catalyst material tends to be magnetised over time which, in turn, may justify the formation of catalyst deposits in the internals of the reactor studied. The characterisation of these materials will be presented next.

3.4 Characterisation of the deposited catalyst

This section presents a characterisation of the solids deposited in the internals of the reactor, detected during a shutdown period. With that purpose, two samples (A/B) were collected from the outer surface of the tube bundles, and another one (C) from the temperature probe, located above the level of the mixture, as represented in Figure 3.12. The samples A and B are distinguishable from sample C, wherein the former ones presented a muddy appearance, in contrast to the latter which exhibited a greater rigidity.

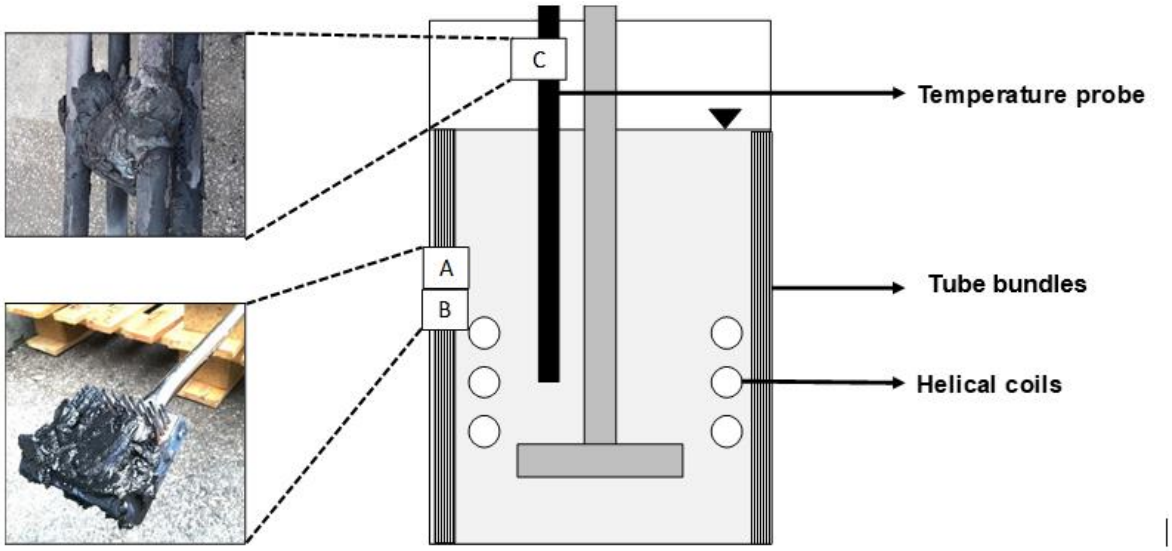

Figure 3.12 – Location of the samples of deposited solids collected at the internals of the reactor.

The preparation of each sample for physico-chemical characterisation is important so that they can be properly introduced in the analytical equipment. The analysis also intends to evaluate uncommon components present in the solid phase. Therefore, each sample was submitted to a laboratorial procedure, as shown in Figure 3.13. Firstly, each sample was introduced in a agitated vessel with aniline at 150°C. Then, a filtration step was applied which allows the separation of the initial sample in two main fractions: the soluble (liquid) and the insoluble (solid) in aniline.

The aniline-soluble fraction was distilled at 150°C and 100 mbar, with the purpose of evaluating the existence of non-volatile compounds in such conditions. No bottom residue was observed. As such, the corresponding distillate was analysed through gas chromatography with a flame ionisation detector (GC-FID). The aniline-insoluble fraction, after being carefully washed with ethanol and conditioned in a stove for 8h, was characterized through SEM-EDS, atomic absorption, XRD diffraction, laser diffraction, CHNS elemental analysis, and magnetic analysis.

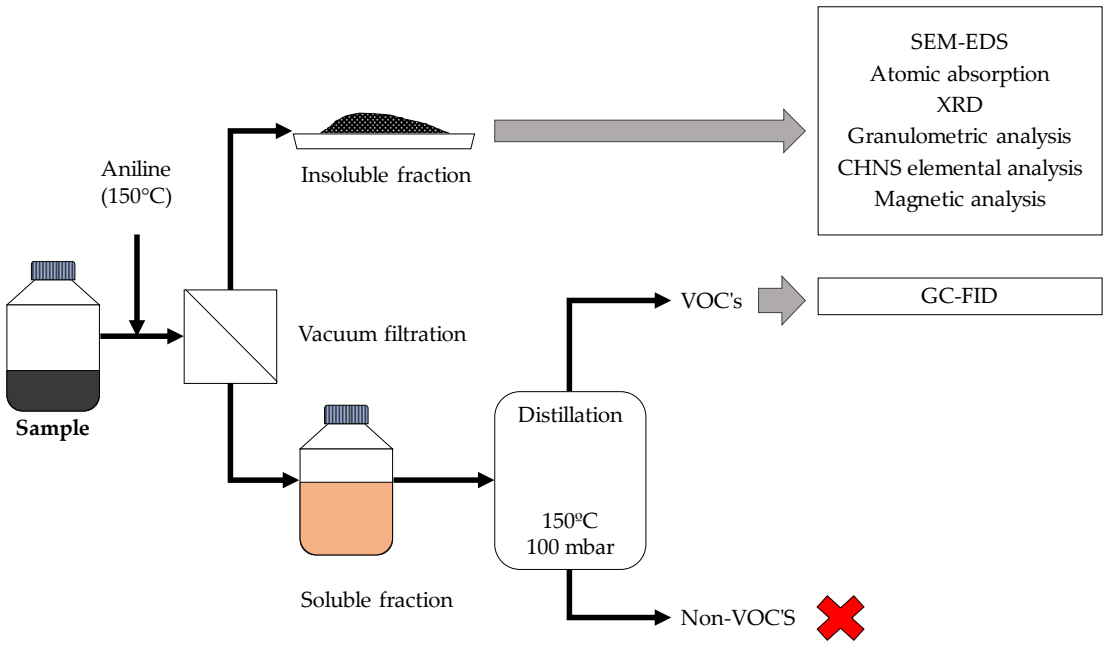

Sample	Aniline-soluble fraction [wt. %]
A	56
B	52
C	80

Figure 3.13 – Laboratorial pre-treatment of the samples collected at the internals of the reactor.

3.4.1 Characterisation of the aniline-soluble fraction of the samples A/B/C

The aniline-soluble fraction of the samples A/B/C was analysed through GC-FID, using processed aniline as the extraction solvent. The corresponding composition was determined through mass balances, by knowing the composition of the processed aniline beforehand (see Table 3.8). The values of Dicyclohexylamine (DICHA) in all samples, and the amount of Cyclohexylidene-aniline (CHENO) in sample C, were omitted (*), since the

values obtained were below the ones measured in the processed aniline (blank); this result was possibly derived from a procedure/analytical error.

The mass composition of aniline-soluble fractions of samples A/B are similar, whereas sample C differs by presenting lower concentrations of cyclohexylamine and cyclohexanol and a significant content of MNB.

Since no abnormal peaks were detected in these samples, apart from the typical compounds found in the process, a plausible cause for catalyst deposition could not be attributed to the compounds present in the aniline-soluble fraction.

Table 3.9 - GC-FID results of the aniline-soluble fraction of A/B/C samples.

Compound	Composition [a.u.]			
	A	B	C	Blank (Aniline)
Benzene	0.002	0.002	0.000	0.000
Cyclohexylamine	0.157	0.138	0.022	0.022
Cyclohexanol	0.229	0.212	0.043	0.065
Cyclohexanone	0.056	0.084	0.002	0.040
Nitrobenzene	0.000	0.000	0.426	0.004
Dicyclohexylamine	*	*	*	0.071
Cyclohexylidene-aniline	0.026	0.037	*	0.262
Cyclohexyl-Aniline	0.030	0.027	0.007	0.036

3.4.2 Characterisation of the aniline-insoluble fraction of the samples A/B/C

SEM-EDS

The SEM images of the aniline-insoluble fraction are outlined in Figure 3.14. In the 0.5K-magnified images, one verifies that samples A/B present higher homogeneity both in size and shape, as well a smaller average size when compared to sample C. In the 10K- and 50K-magnified images, the material displays a regular surface, except in sample C that presents sharp-shaped nanostructures, similar to the ones observed in sample Y (Figure 3.2).

The EDS spectra and the corresponding chemical composition are represented in Figure 3.15 and Table 3.10, respectively. Although the given spectra identify low atomic

number elements such as carbon, nitrogen and oxygen, this technique is not particularly sensible towards the absorption of low energy photons, leading to significant errors on the quantification of these elements [143].

The EDS results display the presence of nickel and silicon, which are typically found in the catalyst formulation, revealing no traces of aluminium derived from the support of the fresh catalyst F2. Other elements with a poisoning nature (e.g., sulphur) were not detected. Although EDS is a semi-quantitative analysis, the solid deposits tend to have a lower fraction of silicon when compared to the suspended catalyst particles collected at the various process streams. Hence, the loss of silica and alumina from the catalyst support seems more significant in the deposited solids, comparatively to the suspended catalyst particles in the reaction vessel.

Sample	× 0.5K (4.00 a.u.)	× 10K (0.20 a.u.)	× 50K (0.04 a.u.)
A	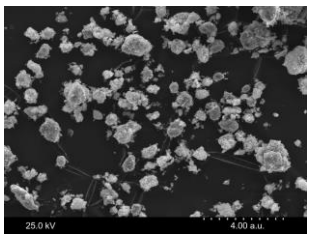	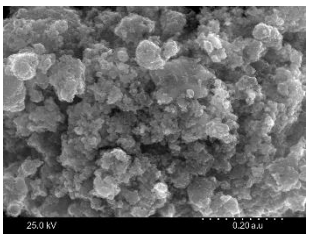	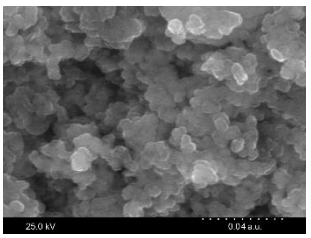
B	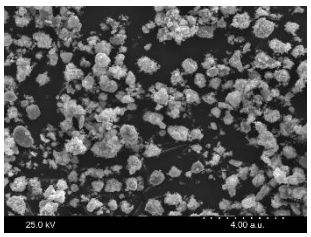	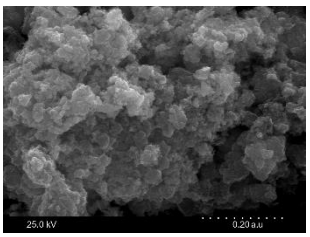	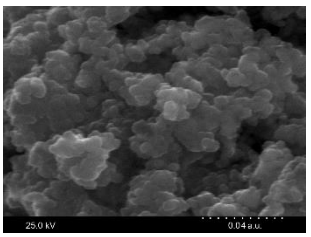
C	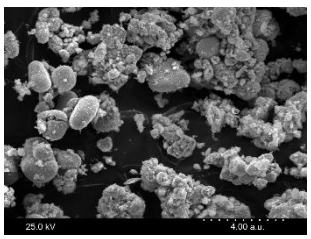	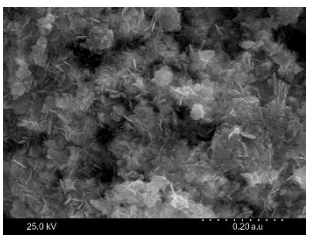	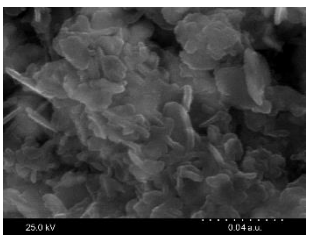

Figure 3.14 – SEM images magnified of the aniline-insoluble fraction of the samples collected at the internals of the reactor: tube bundles (A/B) and temperature probe (C).

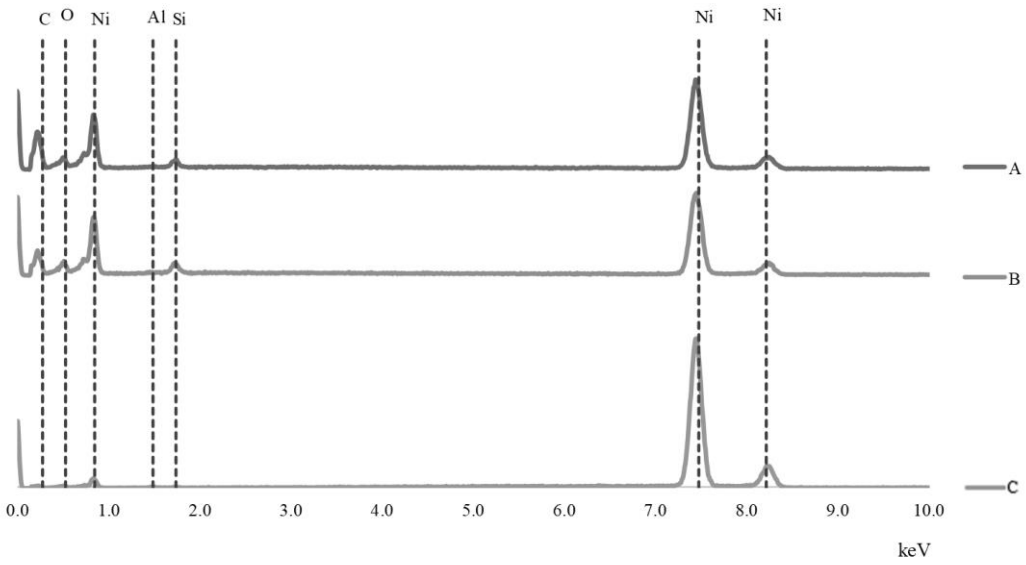

Figure 3.15 – EDS spectra of the aniline-insoluble fraction of the samples A/B/C.

Table 3.10 - Elemental analysis determined through EDS of samples A/B/C.

Sample	EDS [a.u.]			
	Ni	Si	C	O
A	0.311	0.005	0.117	0.066
B	0.337	0.011	0.084	0.068
C	0.499	0.000	0.001	0.001

Atomic absorption

As mentioned before, the technique of atomic absorption allows the quantification of the bulk composition of a given material. Table 3.11 outlines the nickel contents obtained for samples A, B, and C, varying between 0.415 and 0.437 a.u. The corresponding average value (0.424 a.u.) is about 31% higher than in the fresh catalysts studied (F1 – 0.312 a.u. and F2 – 0.337 a.u.). On the other hand, the average nickel content of samples A/B/C is closer to the samples collected from the reactor outlet (Y0 - 0.447 a.u. and sample Y - 0.391 a.u.), suggesting the loss of silica support and nickel enrichment of the catalyst particles inside the reactor.

Table 3.11 – Nickel content of samples A/B/C obtained through atomic absorption.

Sample	Atomic absorption Mass fraction of Ni [a.u.]
A	0.420
B	0.437
C	0.415

CHNS elemental analysis

Given the low accuracy of the EDS technique towards quantifying lighter elements (i.e., carbon, hydrogen, nitrogen and sulphur), the CHNS elemental analysis was used. This combustion analysis is more suitable for the quantification of the latter compounds [144] [145].

The corresponding results are shown in Table 3.12. No traces of sulphur were detected in any of the samples studied as expected, since this element is not present in the formulation of the fresh catalysts. Concerning the content of carbon, hydrogen, and nitrogen, samples A and B practically show the same profile. The corresponding average contents of carbon and hydrogen in the samples A/B are about half of what is observed in the sample C. Although these results may suggest the presence of insoluble organic material, it should be necessary to perform the same analysis on the fresh catalysts (F1/F2) to confirm this hypothesis.

Table 3.12 – CHNS elemental analysis results of samples A/B/C.

Sample	CHNS elemental analysis [a.u.]			
	C	H	N	S
A	0.006	0.003	0.001	0.000
B	0.006	0.002	0.001	0.000
C	0.013	0.005	0.002	0.000

X-Ray Diffraction

The XRD diffractograms and the quantification of the composition of the crystalline species are shown, respectively, in Figures 3.16 and Table 3.13. Samples A and B display the same crystallographic composition, from which only Ni and $Ni_3Si_2O_5(OH)_4$ are detected.

This result contrasts with the profile obtained in the catalyst samples collected in the process streams, wherein crystalline forms of SiO_2 (recycled aniline and decanter outlet) and of $Ni(OH)_2$ (reactor outlet) were detected. Sample C also presents the species of Ni and $Ni_3Si_2O_5(OH)_4$, but the content of crystalline Ni is 25% less than in samples A and B. In sample C, crystalline $Ni(OH)_2$ is also observed. This species may be formed due to the NiO hydrolysis to $Ni(OH)_2$, or by oxidation of Ni^0 to Ni^{2+} due to the alkaline conditions of the system.

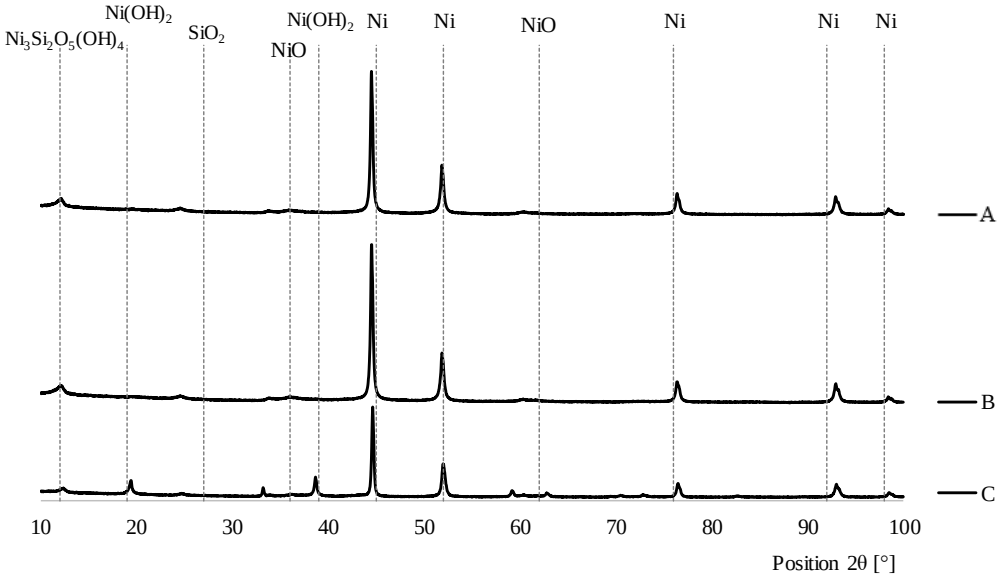

Figure 3.16 – XRD diffractograms of the aniline-insoluble fraction of samples A/B/C.

Table 3.13 - Quantitative analysis of the crystalline species identified through XRD (RIR method).

Sample	Crystallographic composition [a.u.]				
	Ni	NiO	SiO_2	$Ni(OH)_2$	$Ni_3Si_2O_5(OH)_4$
A	0.480				0.020
B	0.480				0.020
C	0.355			0.115	0.030

Granulometric analysis

The results of the granulometric analysis, obtained through laser diffraction, are presented in Figure 3.17 and Table 3.14. The volumetric distributions of the particles sizes of samples A/B are similar and coherent with the corresponding SEM images. Although these samples present bimodal profiles, the corresponding first mode is less significant than the second one; according to the cumulative curve size distribution, A and B have their sizes below 1.67 a.u., corresponding to 90 vol.% of the particles from sample C. The latter displays a monomodal distribution, which is similar to the profile obtained for the samples Y0/Y withdrawn from the reactor outlet stream. Furthermore, it should be noted that sample C shows a significant similarity with samples Y0/Y, in terms of average particle size. Attending to these results and considering that sample C was collected in the headspace of the reactor, it is possible that the deposition of this material was promoted by abnormal rises of the liquid level, promoting the once suspended particles in the reaction mixture to be retained from where the sample C was collected. The latter hydrodynamic behaviour of the system shall be considered in more detail in Chapter 4.

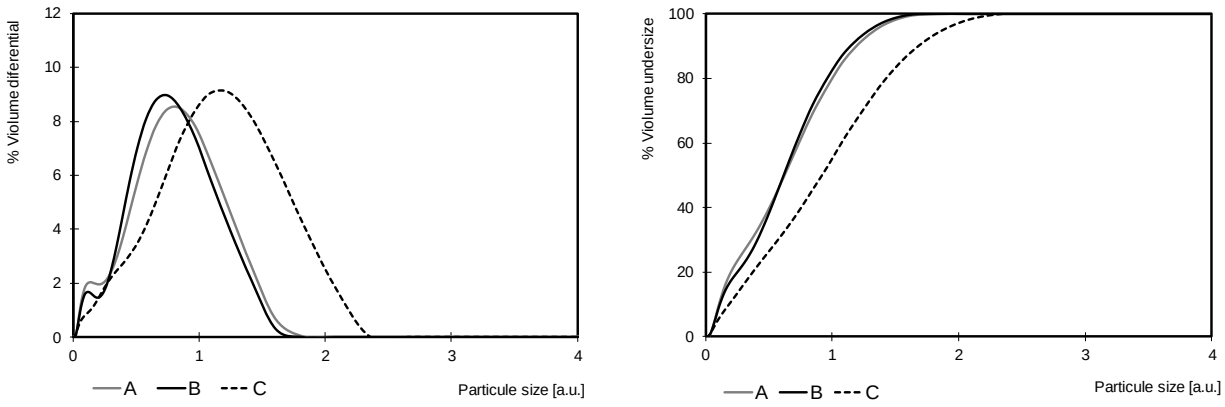

Figure 3.17 – Particle size distributions of the aniline-insoluble fraction of samples A/B/C.

Table 3.14 – Average particle sizes of samples A/B/C.

Sample	Dv(50) [a.u.]
A	0.62
B	0.61
C	0.91

Magnetic analysis

Considering the magnetic characterisation of the fresh and used catalysts collected in the process streams, the magnetic properties of the solid deposits were also measured and compared, with respect to the nickel crystallite size, crystalline composition, and bulk nickel content.

Table 3.15 outlines the average size of nickel crystallites in the samples A/B/C obtained through XRD analysis. Nickel crystallites are larger in the sample C, when compared to the samples A/B, although all values are similar to those obtained in the samples withdrawn from the reactor outlet (samples Y0/Y). Therefore, it is plausible that the nickel nanoparticles in the solid deposits are also ferromagnetic.

Table 3.15 - Average size of nickel crystallites in the samples A/B/C.

Sample	Nickel crystallite [nm]
A	39
B	40
C	43

M-H curves of samples A/B/C at 300K and the corresponding values of coercivity and saturation magnetisation are displayed in Figure 3.18. It can be observed that the samples A/B present the greatest coercivity, in comparison with the samples of fresh and used catalysts previously assessed. Although A and B also show similar contents of crystalline and bulk nickel as the catalyst particles collected at the reactor outlet (Y0/Y), the smaller nickel crystallites in the samples A/B are likely to promote less number of magnetic domains, thereby explaining their higher coercivity comparing with the samples Y0/Y.

On the other hand, the sample C presents considerably lower coercivity than in the samples A/B, and samples Y0/Y; this result can be attributed to the smaller fraction of crystalline nickel in the sample C, thereby reducing its magnetic anisotropy.

In addition, note that the coercivity values obtained in the samples A/B surpass the critical value of 125 Oe, above which the related materials are identified as *hard* or *permanent magnets,* owing to their high resistance to be demagnetised. Therefore, it is

possible to conclude that this coercivity increase of the catalyst particles with time is a potential cause for their incremental deposition in the internals of the reactor.

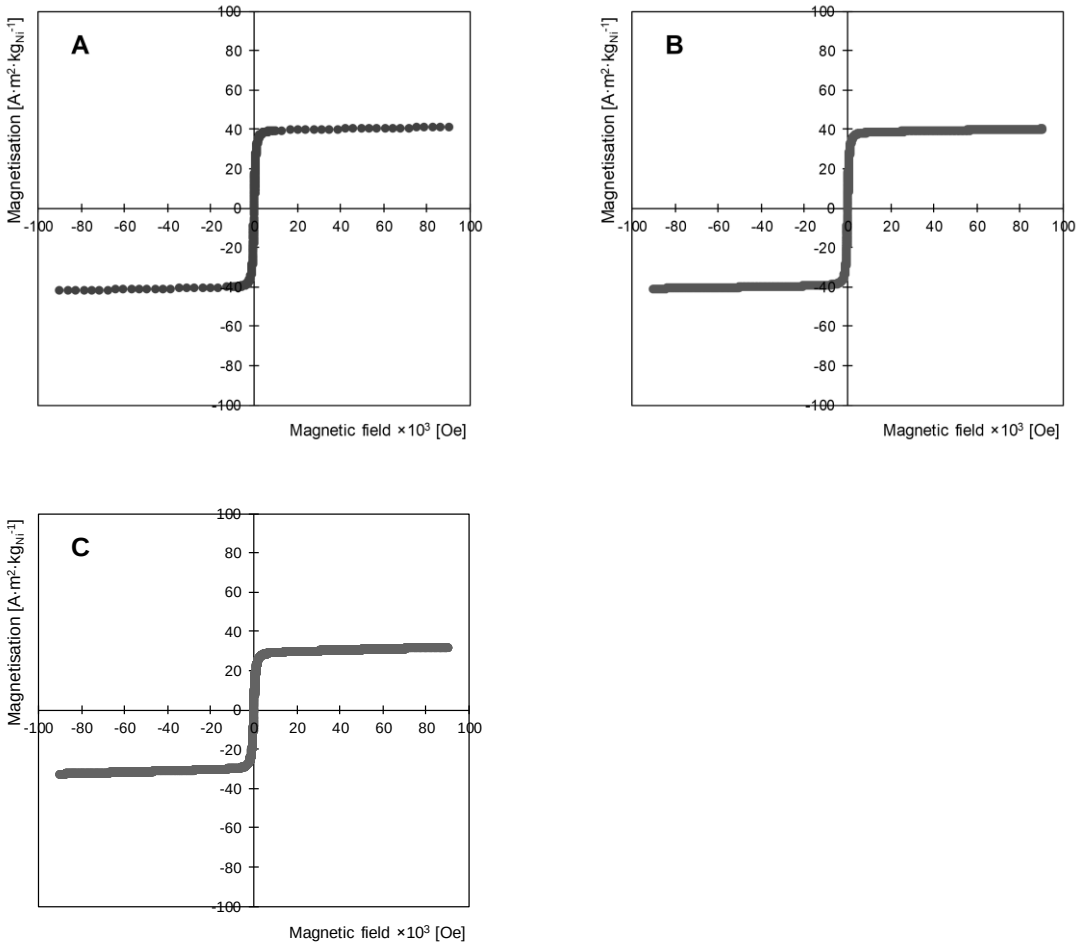

Sample	Coercivity [Oe]	Saturation magnetisation [$A \cdot m^2 \cdot kg_{Ni}^{-1}$]
A	153	42
B	149	41
C	61	32

Figure 3.18 – Magnetic analysis performed at 300K for the samples of fresh and used catalyst studied.

3.4.3 Discussion

In the previous section, the physico-chemical characterisation of the solid deposits was addressed. In general, the nickel content and the crystallinity of this material is higher than in the samples of fresh and used catalysts collected at different streams of the underlying process. Additionally, the solid deposits displayed a smaller fraction of silicon, and no trace of aluminium. Since the latter elements are derived from the catalyst support formulation, this suggests that the loss of support is more significant in the deposited material than in the suspended catalyst.

The physico-chemical differences between the solid deposits and the suspended catalyst particles did not evidence a cause for the accumulation on the internals of the reaction vessel. The solid deposits withdrawn from the vertical steam bundles revealed interesting similarities to sample Y0, collected from the reactor outlet stream several months before of the former ones. In fact, both materials presented the highest Ni/Si ratio, as well as the highest fraction of crystalline nickel. This result may suggest that the nickel enrichment, together with the increase of related crystallinity over time could have an impact on the magnetic properties of the catalyst, thus explaining its agglomeration/deposition in the reaction vessel.

The magnetic analysis confirmed that the deposited material collected in the tube bundles displays higher resistance to demagnetisation (coercivity) when compared to the suspended catalyst particles found in the reaction vessel and the fresh catalyst samples studied. Moreover, distinct magnetic profiles were observed amongst the fresh catalyst samples studied, noting that fresh catalyst F1 displays a coercivity one order of magnitude greater than fresh catalyst F2. This result is consistent with the higher content of crystalline nickel of F1, in comparison with F2.

3.5 Magnetic characterisation of the fresh and of the suspended catalysts

In this section, the magnetic properties of the fresh catalyst are evaluated in more detail considering several samples from lots provided by two different suppliers previously used in the productive process. Afterwards, the effects of the reduction temperature and of different blending compositions on the magnetic properties of the fresh catalyst are also advanced.

Next, the coercivity of the suspended catalyst was also evaluated by measuring this property on several samples collected from the outlets of different reactors that were fed with a specific blend composition of fresh catalyst.

3.5.1 Coercivity assessment of distinct lots of fresh catalyst

According to the results displayed in the previous section, the magnetic properties of the catalyst material changed during its usage in the system. Namely, the coercivity of catalyst particles suspended in the reaction vessel tends to increase, as the amount of crystalline nickel in enhanced over time.

As stated before, F1 displayed a coercivity significantly greater (102 Oe) than F2 (23 Oe). Since these catalysts exhibit similar-sized nickel crystallites and similar contents of bulk nickel, their different coercivities can be attributed to the higher fraction of crystalline nickel in F1 – this property provides a higher magnetic anisotropy and, in turn, more resistance to demagnetisation, when compared to F2. To prove the consistency of this scenario, the record of F1/F2 catalyst batches used in the underlying process was assessed, and several samples were collected, with the intention of measuring their coercivity, and thereby analysing the evolution of this parameter over time (see Figure 3.19).

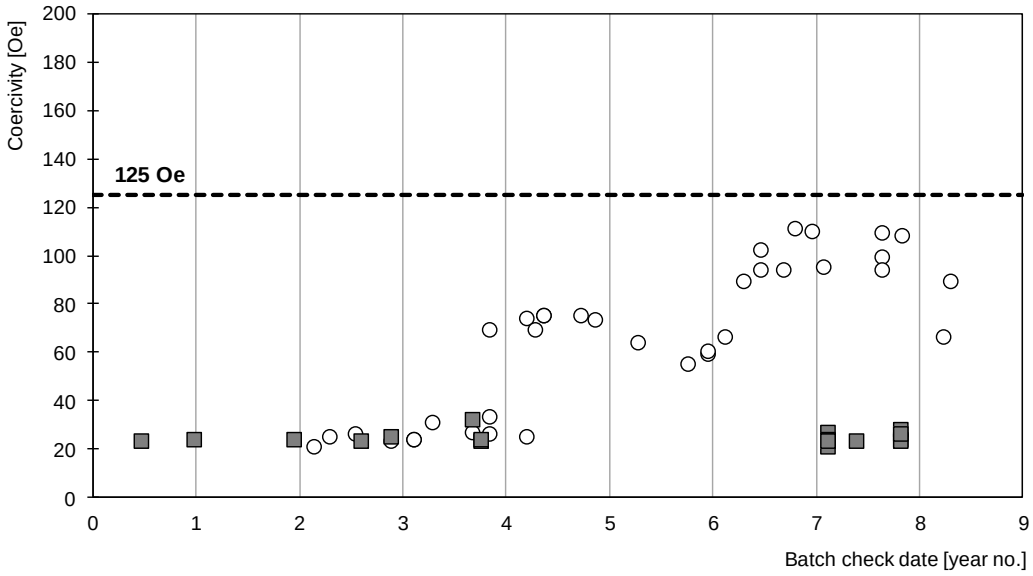

Figure 3.19 – Coercivity of several fresh catalyst batches provided by different suppliers (○ fresh catalyst F1 and ■ fresh catalyst F2, **----** minimum coercivity value of *hard magnets*).

As can be observed, the coercivity measured from the suppliers of catalysts F1 and F2 remained below 40 Oe up to the year 4. After that period, however, the fresh catalyst batches from supplier F1 revealed two distinct coercivity thresholds: a first one with 55-75 Oe (year 4 to 6) and a second one with 94-109 Oe (year 6 to 8), which closely approximates the critical value of 125 Oe attributed to “hard magnet” materials. On the other hand, the batches from supplier F2 mostly exhibited the same coercivity (around 20 Oe). This result suggests that the properties of the F1 catalyst have significantly changed after year 4.

3.5.2 Coercivity assessment of the fresh catalyst with different reduction temperatures

The increasing coercivity detected in the batches of fresh F1 catalyst could indicate a significant change of the operating conditions used in the preparation of this material. For this procedure high temperatures are typically used (e.g., calcination and activation steps) to ensure the well-dispersion of metallic nanoparticles and the mechanical resistance of the support [135]. As mentioned before, temperature can significantly affect the crystalline structure and, thus, the magnetic alignment of ferromagnetic materials. This way, the effect of temperature on the coercivity of the catalyst was evaluated by conditioning a selected sample from a F1-catalyst batch under a hydrogen-containing atmosphere. The coercivity of the material was then measured at room temperature.

For this study, a sample from batch of F1 catalyst was collected and divided into nine other samples, each one reduced at different temperatures (100°C, 200°C, 300°C ,350°C, 400°C, 450°C, 500°C, 600°C, 700°C) during 4h, with a heating rate of 10°C/min. After this procedure, each sample was cooled down to room temperature with nitrogen. Afterwards, all samples were analysed through XRD from which the average size of the nickel crystallites was obtained.

The corresponding coercivity measurements and Ni crystallite average size are outlined in Table 3.16 and Figure 3.20. For reduction temperatures between 100 to 300°C, the size of nickel crystallite and coercivity practically remains unchanged when compared to the blank sample. This evidences that the reduction conditions are not enough to significantly affect the conversion of NiO to Ni, or the distribution of metallic Ni particles that already existed before the reduction treatment. For reduction temperatures higher than 350°C, however, an almost linear decrease of the coercivity values is verified, while higher average sizes of Ni crystallites are observed. The increase of nickel crystallites could be

attributed to the sintering of nickel particles, specially promoted by temperature; consequently, the larger nickel nanoparticles tend to display multi magnetic domains, thereby explaining the reduction of coercivity observed.

Table 3.16 -Coercivity and XRD results obtained of the fresh catalyst F1 before and after reduction at different temperatures.

Temperature of reduction [°C]	Nickel crystallite [nm]	Coercivity [Oe]
Blank	16	99
100	14	101
200	23	101
300	18	86
350	17	118
400	5	160
450	34	114
500	39	119
600	52	45
700	73	10

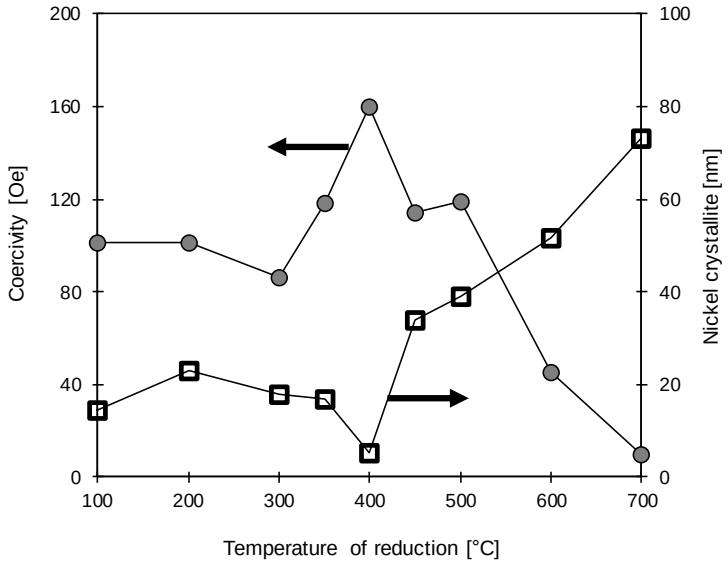

Figure 3.20 – Effect of reduction temperature on the values of coercivity and nickel crystallite size of fresh catalyst F1.

Figure 3.20 shows that the coercivity of this material could be reduced by using higher temperatures of reduction during its manufacturing process. However, note that the number of active sites is likely to be significantly reduced, because of the sintering of nickel crystallites, which, in turn, hinders the active area of the catalyst. Therefore, an alternative solution should be accessed to reduce the coercivity of the fresh catalyst added to the system, without compromising its catalytic potential.

As fresh catalyst F2 tends to exhibit lesser coercivity than F1, different blends containing both fresh catalysts were tested to reduce the coercivity of the catalyst added to the system. This issue will be considered in the next section.

3.5.2 Coercivity assessment of different blends of fresh catalyst

Considering the different coercivity values observed in the fresh catalysts F1 and F2, three different blends made from both catalysts were prepared (A, B and C), with the intention of measuring their coercivity (see Table 3.17).

Table 3.17 – Different blends of fresh catalyst.

Identification	Composition
Blend A	25 wt.% F1 + 75 wt.% F2
Blend B	50 wt.% F1 + 50 wt.% F2
Blend C	75 wt.% F1 + 25 wt.% F2

The coercivity measurements obtained as a function of the mass percentage of F2 are represented in Figure 3.21. Here the coercivity of the catalyst mixture is significantly reduced for contents of F2 above 50 wt.%. Note that the coercivity of Blend C (containing 75 wt.% of F2) equals the coercivity of F2.

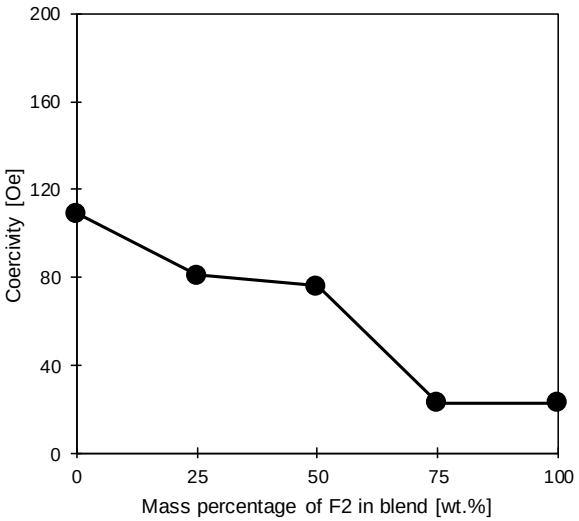

Figure 3.21 – Coercivity measurements of fresh catalysts F1 and F2 and of the related blends.

However, it is also important to notice that, once a load of fresh catalyst enters the reaction vessel, their catalyst particles will undergo several physico-chemical changes, that ultimately increase their coercivity over time (see section 3.3). As such, the behaviour of the coercivity in the used catalyst should be also evaluated. This issue shall be considered in the next section.

3.5.3 Coercivity assessment of the used catalyst

Since the coercivity of the used catalyst tends to be higher than in the fresh catalysts added to the underlying system, this evolution of the coercivity of the suspended catalyst particles was assessed by collecting samples from different reactors of the industrial process after their start-up. In Table 3.18, the selected reactors are outlined, together with the corresponding procedure performed before their start-up and during operation.

In reactor I only fresh catalyst F2 was added before the start-up and during operation if necessary. In the case of reactors II and IV, a mixture of 50 wt.% of fresh F1 and 50 wt.% of fresh F2 (Blend B), was added before the start-up and during operation. In the case of reactor III, a load of used catalyst was added before start-up and during the operation the blend B was added. In addition, note that the internals of the reactor II were not cleaned; therefore, the solid deposits eventually present were not removed during the same shutdown period.

Table 3.18 –Planning for different reactors after being subject to maintenance.

Reactor	Before start-up	During operation
I	Internals cleaned Loaded w/ fresh F2	Only fresh F2 added
II	Internals not cleaned Loaded w/ 50-50 wt.% F1/F2 (Blend B)	Fresh Blend B added
III	Internals cleaned Loaded w/ used catalyst	Fresh Blend B added
IV	Internals cleaned Loaded w/ 50-50 wt.% F1/F2 (Blend B)	Fresh Blend B added

After the start-up of each reactor, several catalyst samples were collected at the reactor outlet stream during the three months that followed. Figure 3.22 outlines the coercivity measurements obtained.

In the case of reactors I/III/IV, one notices that the coercivity increases until the second month of observation and tends to decrease on the third month. This result can be attributed to the retention of catalyst particles with larger nickel crystallites inside the reaction vessel, while the catalyst fines with smaller nickel crystallites are progressively discarded through the decanter outlet; the larger crystallites tend to display multi magnetic domains, thereby explaining the coercivity reduction observed.

In the case of reactor II, the coercivity of catalyst particles remains virtually unchanged, standing above the critical point of 125 Oe. Since the internals of this reactor were not cleaned, it is plausible that the used catalyst with greater coercivity remained inside the reaction vessel after the start-up.

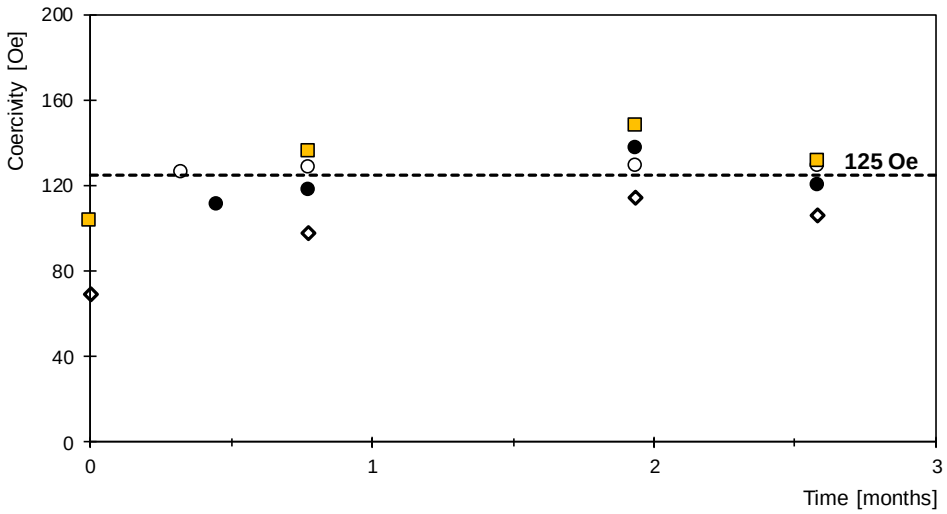

Figure 3.22 – Coercivity of used catalysts collected at the reactor outlet stream (□ reactor I, ○ reactor II, ● reactor III , ◇ reactor IV).

Attending to the latter results, it appears that the coercivity of the used catalyst stabilises around 100-130 Oe, independently of the initial load employed before start-up, and fresh catalyst added during operation. Considering that the high coercivity values were obtained in the solid deposits withdrawn from the tube bundles (≈150 Oe), it was not possible to conclude if the suspended catalyst particles in the latter reactors studied would display even greater coercivity values beyond the period assessed. However, it should be noted that any 100 wt.% F1-based blends of fresh catalyst were added to the same reactors before start-up and during this period of operation. Therefore, the evolution of the coercivity on the suspended catalyst in the industrial reactors with only F1 fresh catalyst additions remains to be comprehended.

Considering the latter issue, in a study performed by Espírito Santo [146], it was concluded that fresh catalyst F1 presents a higher sedimentation rate than fresh catalyst F2. Attending to the granulometric results presented in section 3.3.4, the F1 particles are, on average, smaller, besides exhibiting a greater fraction of fines (especially for particle sizes above 0.67 a.u.), when compared to the fresh catalyst F2. As smaller particles are more likely to aggregate owing to lower energy barriers [147], the higher sedimentation rate can be justified due to this phenomenon.

Catalyst deposition can affect the dispersion of catalyst particles throughout the reaction vessel and significantly reduce the number of available active sites in the catalyst.

For that reason, the monitoring of the operation of the process will be addressed in Chapter 4, where the catalyst concentration will be related to the process variables, and nitrobenzene conversion. The goal is the improvement of industrial practices, including the management of catalyst make-ups.

4. Process monitoring and control

This chapter addresses the monitoring of the operation of an industrial reactor used to produce aniline at Bondalti Chemicals S.A.

As previously reported, the performance of the underlying process relies in the behaviour of the catalyst used. Here, the periodic catalyst make-ups are performed allowing not only compensate the decay of the catalyst properties, but also the catalyst losses that are likely to occur over time. For that reason, the present work addresses the monitoring of suspended catalyst concentration, together with the online/offline measurements of the process variables, while considering the frequency of fresh catalyst repositions. Moreover, this study also encompasses several tests performed in the industrial reactor to evaluate the catalyst deposition and loss phenomena, as well as the control practices that can be used to regulate the catalyst concentration in the underlying system.

Following the former remarks, a process monitoring tool based on the model developed is advanced. This approach provides the identification of external disturbances affecting the predictability of reaction conversion. After that, a new strategy applied to the regulatory control system is detailed, where the related impact on the steadiness of the industrial unit is discussed. Ultimately, a procedure for process monitoring and control is presented, oriented to standardise the industrial practice regarding the catalyst management.

4.1 Process variables

The distributed control system (DCS) installed in the control room of the underlying industrial unit allows to remotely monitor the process operation. Besides that, the control room has also access to the record of offline measurements from the quality control laboratory, including the composition of the process streams (e.g., nitrobenzene and reaction by-products), together with the catalyst concentration at the reactor outlet. Here, the nitrobenzene concentration in the outlet stream needs to be maintained below a certain threshold value to prevent high processing costs in the downstream purification units. For that reason, if an increasing concentration of nitrobenzene is detected, catalyst make-ups are usually preferred.

The control of the operating temperature is also crucial for the process. since the extent of undesired side reactions derived from aniline can also be promoted with higher temperatures. In this case, the reactor is equipped with heat exchangers that ensure the removal of the heat produced by the reaction. This energy, in turn, is used for steam production. Therefore, the measured values of the steam flowrate and the steam pressure can be useful to monitor the performance of the heat transfer system over time.

The operating pressure is another important process variable. This is usually controlled by the hydrogen intake in the reactor headspace. The hydrogen consumption of the system is usually proportional to the nitrobenzene feed flowrate. However, if a significant the hydrogen consumption and the operating temperature decrease simultaneously under a given nitrobenzene feed flowrate, reaction failure might occur. Under such scenario, the shutdown of the system is required. This procedure has been claimed [148] to be executed as quickly as possible, to avoid the “damage to the catalyst by an excessively high concentration of nitroaromatics in the reactor”.

Another important process aspect is the level balance between the reactor-decanter system. A level difference between these two vessels ensures the flow from the reactor outlet to the decanter, while the gas-inducing agitator on the reactor side promotes the recirculation flow from the decanter bottom to the reaction vessel through the recirculation stream (see Figure 4.1). The level in the decanter is also controlled by a valve, located in the decanter upflow stream, that regulates the liquid level of the decanter dike. The decanter downflow stream is regulated by a valve located in the decanter-reactor bottom connection (recirculation valve), ensuring the recovery of catalyst back to the reactor. This recirculation valve should not be excessively opened, otherwise it could impair the decantation efficiency [41]. Moreover, if the recirculation flowrate is too high, the agitator of the reactor can be overloaded, causing an excessive current intensity at the electric motor. Under such conditions, the agitation system is automatically stopped.

As already stated in Chapter 2, monitoring the catalyst concentration, together with other key process variables can provide a better understanding of the reaction system, and thereby provide new guidelines for process diagnosis. In addition, the characterisation study reported in Chapter 3 evidenced the physico-chemical changes of the catalyst material during its usage in the reaction vessel. Therefore, this study aims to evaluate the dynamics of the catalyst behaviour by exploiting and analysing industrial data sets, together with the conduction of industrial trials.

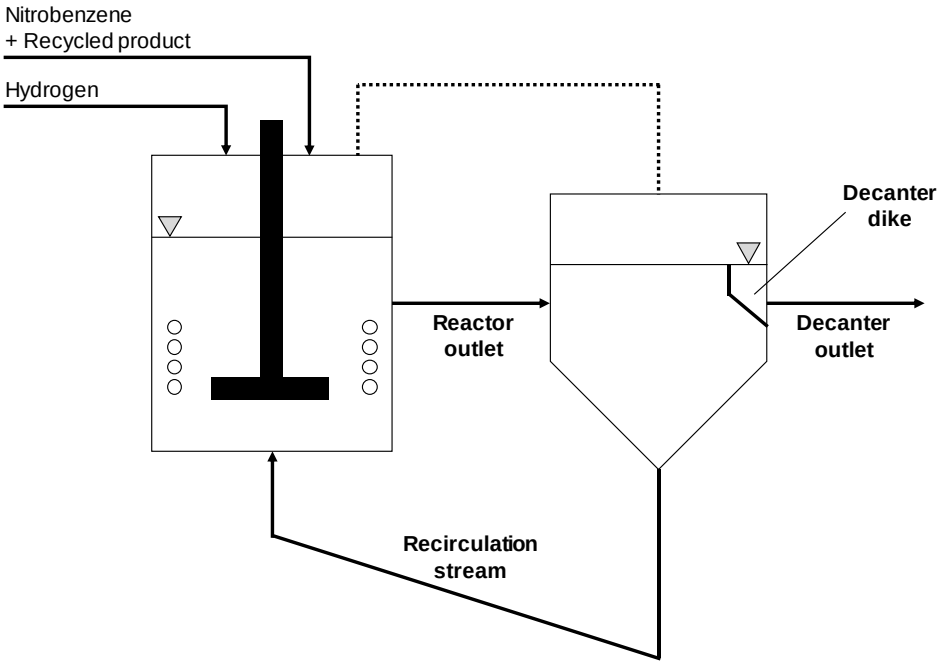

Figure 4.1 – Schematic representation of the reactor-decanter system.

4.2 Analysis of the process operation

The operation of the industrial reactor was assessed by following the online measurements of the process variables, together with the offline measurements of the catalyst concentration and of the nitrobenzene bulk concentration. In addition to this, the cumulative of the catalyst make-ups and corresponding blend composition, the heat transfer performance, and the energy consumption of the reactor agitator are also considered.

The catalyst concentration in the industrial reactor was assessed through filtration of samples collected in the reactor outlet. This procedure includes the measurement of the sample volume, followed by the liquid-solid separation. After that, the solid fraction is previously dried, and the corresponding mass measured. This procedure was selected among a group of other laboratorial techniques by performing tests with known weights of catalyst. The filtration methodology provided the highest precision thereby justifying its use in the present work (see Appendix B). Nevertheless, this filtration procedure can be more time-consuming when compared to the decantation method currently used in the laboratory of quality control, due to the drying step included in the former case. Because of this, an upgraded version of the current decantation method currently was tested. The outcome provides a smaller measurement error and improved precision. Besides that, the procedure

for collecting samples in the industrial reactor was also evaluated, where an improvement was made to provide results of the catalyst concentration as representative as possible (see Appendix B).

Figure 4.2 shows the follow-up of the catalyst concentration in the industrial reactor, together with the behaviour of the process variables and record of process shutdowns. Three phases of operation are verified: period A (between days 1 and 300), period B (between days 300 and 600), and period C (between days 620 and 750). Each of these periods will be analysed separately.

During period A, a significant decrease in the catalyst concentration is observed, which coincides with an increased concentration of nitrobenzene in the reactor outlet stream. The reduction of the nitrobenzene conversion followed the standard procedure of increasing the make-ups of fresh catalyst to the system.

In period B, the reactor is subjected to a maintenance procedure (around day no. 350) where the internals of the equipment were cleaned. Intentionally, the deposited solids were maintained inside the reaction vessel. After that, the system was restarted, observing that the catalyst concentration increased significantly, suggesting that the catalyst amount formerly settled, was placed again in suspension. However, the catalyst concentration returned rapidly to its former values, noticing a new increase of nitrobenzene bulk concentration, obligating to further additions of fresh catalyst.

In period C, the reactor is restarted, after a global maintenance procedure, where the internals of the reactor were cautiously cleaned including the removal of the solid deposits from the reaction vessel. Here, the catalyst concentration appears to respond favourably to the fresh catalyst additions performed.

Overall, it is possible to notice that, for higher values of catalyst concentration, the content of nitrobenzene tends to decrease, coinciding with lesser repositions of fresh catalyst. On the other hand, for values of catalyst concentration below 0.10 a.u., the conversion of nitrobenzene is unstable, demanding a greater addition of fresh catalyst.

Next, the evolution of the catalyst concentration is compared to the current intensity of the agitator and to the performance of the heat exchanging devices. These issues are considered later.

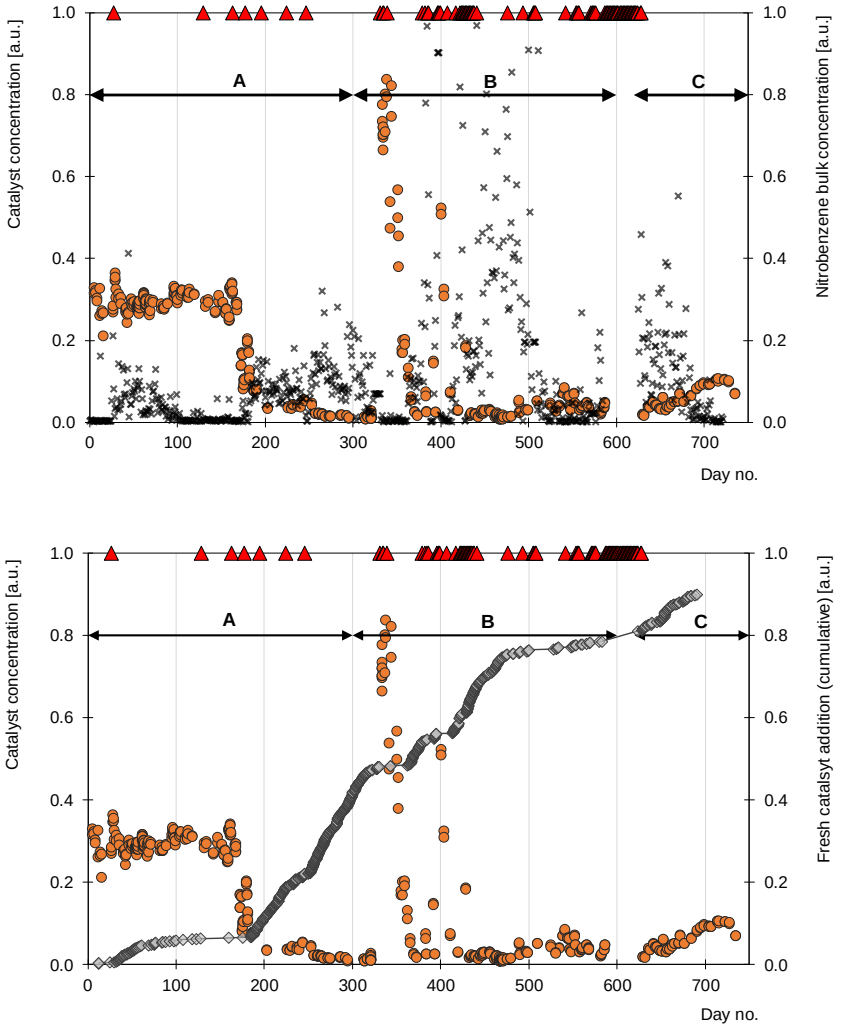

Figure 4.2 – Monitoring results for an industrial hydrogenation reactor (● catalyst concentration, × nitrobenzene bulk concentration, ◇ cumulative of fresh catalyst addition, ◆ overall heat transfer coefficient (tube bundles), and ▲ system shutdowns).

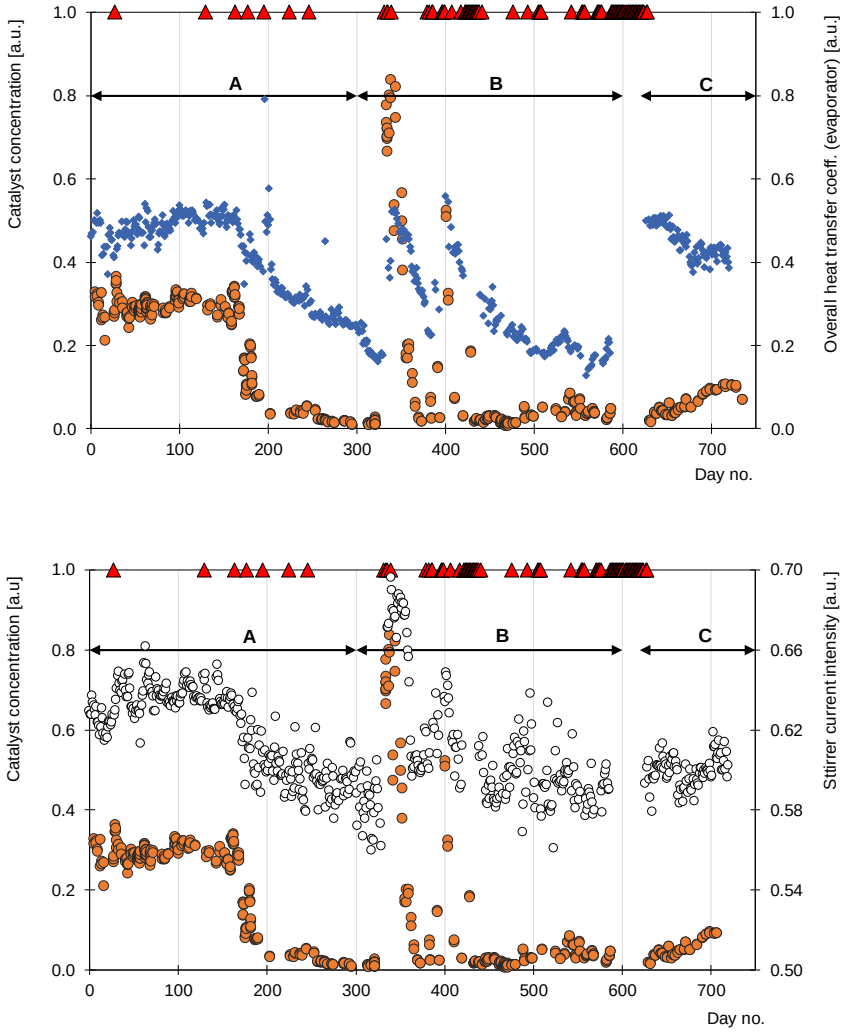

Figure 4.2 (cont.) – Monitoring results for an industrial hydrogenation reactor (● catalyst concentration, ○ agitator current intensity, and ▲ system shutdowns).

4.2.1 Period A: Decrease of catalyst concentration

During this period, a significant decrease in the catalyst concentration between days 150 and 200 is observed. Since this could be attributed to either catalyst deposition or catalyst loss, these phenomena need to be quantified.

Just before the reduction in the concentration of suspended catalyst from 0.30 to 0.10 a.u., several abnormal peaks on the agitator current intensity were observed, causing the shutdown of the reactor due to the stoppage of the agitator (see Figure 4.3). In this case, the current intensity of the agitator increased unexpectedly without any manipulation in the recirculation valve, while a simultaneous decrease in the decanter level was observed.

These occurrences suggest that either the recirculation stream increased due to the unclogging of solid deposits therein, or due to the sudden clogging between the reaction-decanter upper connection.

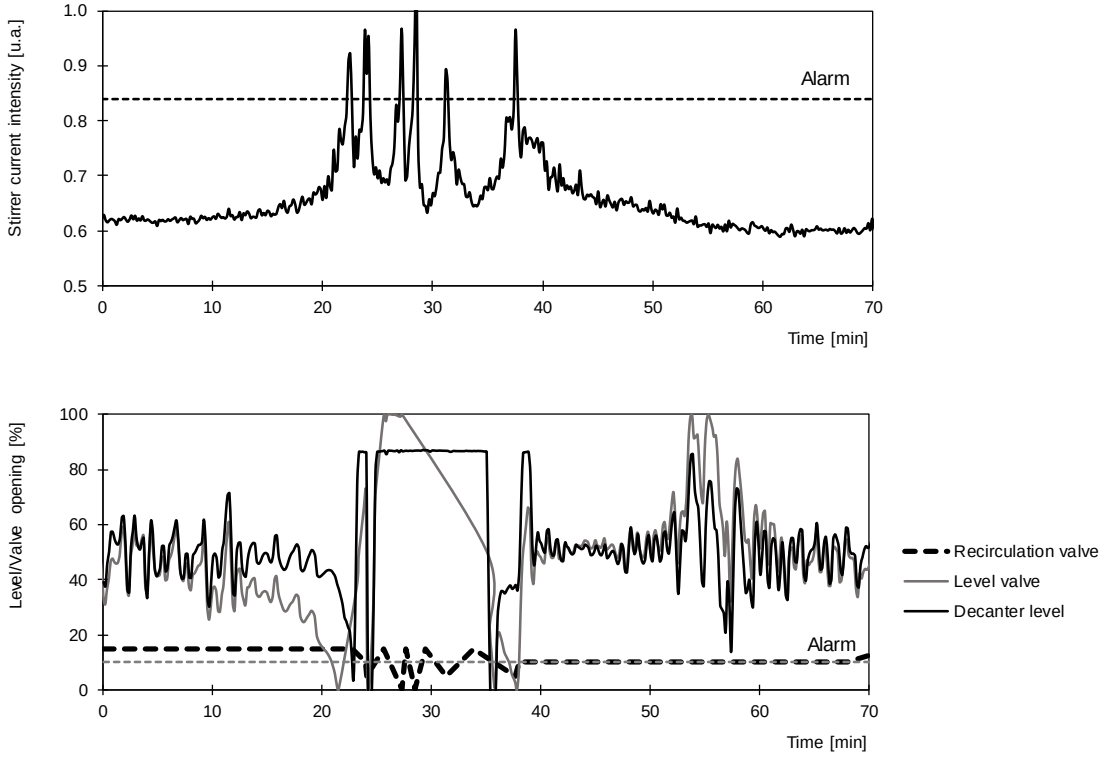

Figure 4.3 – Abnormal behaviour of the agitator current intensity registered and the related effect on the decanter level control between days 180 and 190.

In comparison with the latter example, Figure 4.4 presents a typical response of the current intensity to an increase in the recirculation flowrate, with a temporary total opening of the recirculation valve. In this case, the reduction of the decanter level only occurred when the recirculation valve was fully open; at the same time, the current intensity of the agitator increased due to the higher recirculation flowrate induced. During that period, the decanter level dropped below 10% - a threshold at which a safety valve in the decanter outlet is automatically closed; after repositioning the recirculation valve, the decanter level control responded favourably by stabilising the decanter dike level in the 10 min that followed.

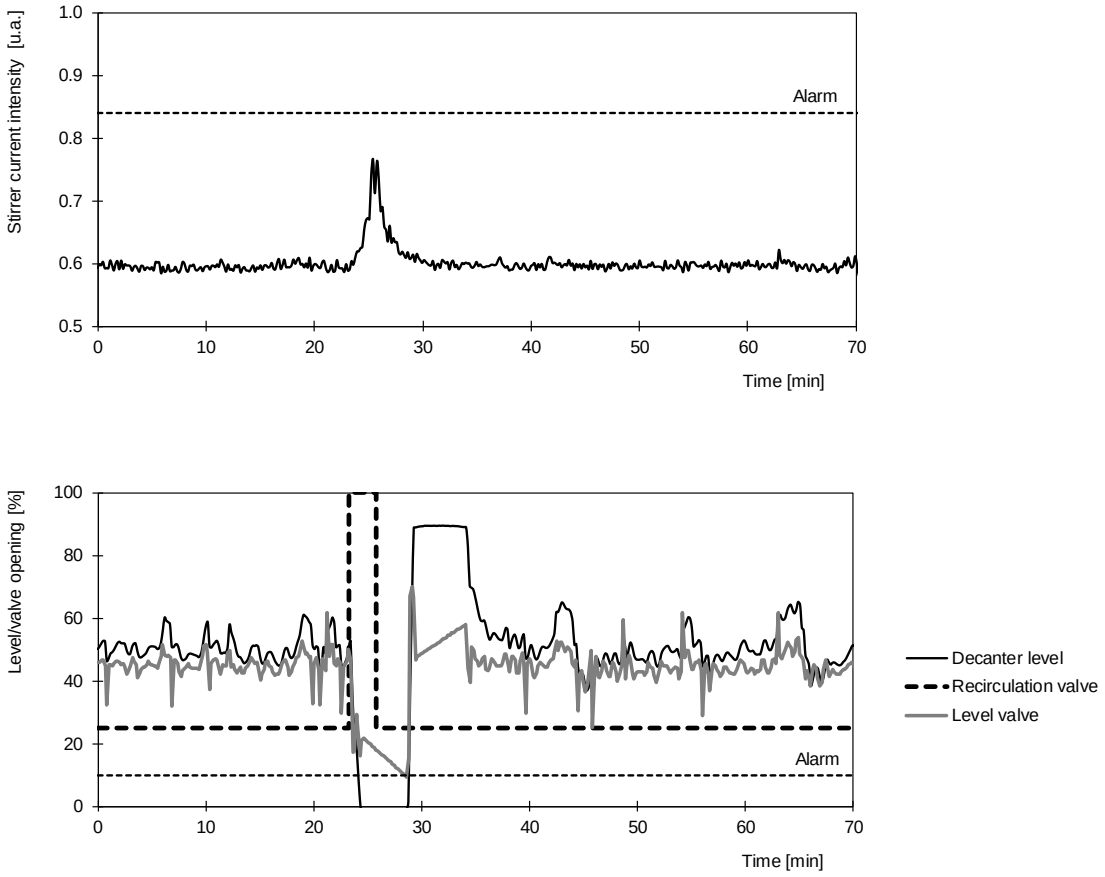

Figure 4.4 – Behaviour of the agitator current intensity and the decanter dike level with the manipulation of the recirculation valve (fully opened and returned to the previous level).

Considering these cases, we can notice that the level of the decanter dike decreased more rapidly in the previous abnormal event than in the case of the total opening of the recirculation valve. In addition, note that the increase of the agitator current intensity in the former case occurred before the decrease of the decanter level. This might suggest that the abnormal peaks of the current intensity may not be caused by a sudden flow increase in the recirculation stream. To reinforce this hypothesis, a comparison between the abnormal behaviour of the agitator current intensity and an operation event where the manipulation of the recirculation valve involved a smaller opening (see Figure 4.5). In this case, the recirculation valve is open from 18 to 20% observing that, approximately 7-8 min after that action, the current intensity of the agitator slightly increases while, simultaneously, the level of the decanter dyke decreases. By comparing this event with the abnormal event

shown in Figure 4.3, it is plausible that an eventual catalyst unclogging of the recirculation pipeline is not enough to justify the anomalies observed.

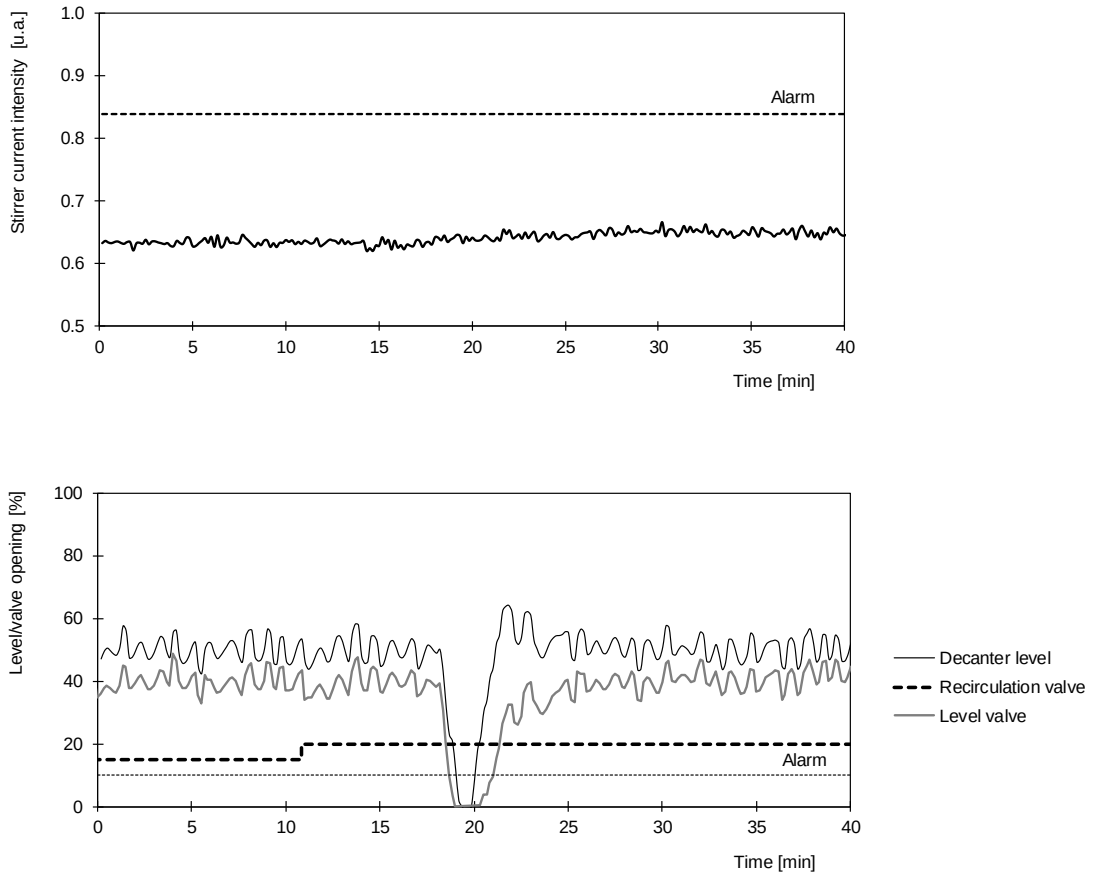

Figure 4.5 - Behaviour of the agitator current intensity and the decanter dike level towards the manipulation of the recirculation valve (smaller opening variation).

In Figure 4.6, the response of the operating pressure and hydrogen intake in the reactor headspace is presented, during the events portrayed in Figures 4.3 and 4.4. In both cases, the variation of the agitator current intensity coincided with the increase of the operating pressure, which promoted the decrease of the hydrogen flowrate. This phenomenon may be related to a sudden rise in the reactor level. However, it should be noted that the oscillations in the operating pressure were far more significant during the abnormal behaviour reported of the current intensity. This indicates a greater variation in the reactor level might occurred in the abnormal event, when compared to the case of the full opening of the recirculation valve.

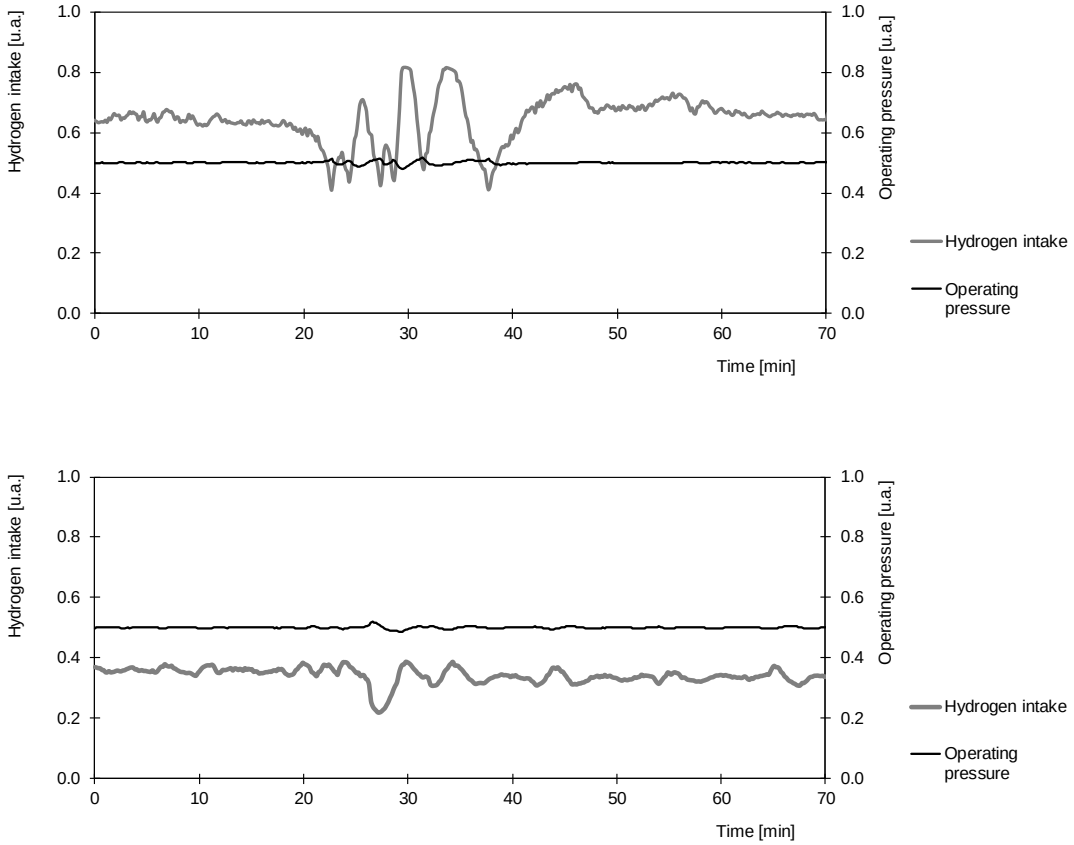

Figure 4.6 – Behaviour of hydrogen intake and operating pressure: (top) abnormal event registered in agitator current intensity, and (bottom) example of full opening of the recirculation valve.

Attending to the previous anomalous behaviour of the agitator, the potential factors behind the energy consumption of the agitation mechanism were evaluated. According to Equation 4.1, the agitation power input ($\mathrm{Pot_0}$) only depends on the mixture density ρ_m, assuming a constant agitation rate (N) and size of the agitator (d_I):

$$\mathrm{Pot_0} = \mathrm{N_p}\ \rho_m\ \mathrm{N^3 d_I^5} \qquad (4.1)$$

Here, $\mathrm{N_p}$ is the power number, which value is specific to the type of agitator, agitation rate, and fluid properties. Assuming a turbulent regime, $\mathrm{N_p}$ is constant and only limited to the impeller design [51].

Regarding the present case-study, the mixture density is influenced by the induction of hydrogen through the impeller. In Figure 4.7, the feed of liquid and gas phases into the

reaction vessel is illustrated. The liquid phase, containing the feed flowrates of nitrobenzene and the recycled aniline streams, is conducted through an annulus distributor close to the impeller region, whereas the gas phase can be either induced through the impeller, or introduced through a gas sparger located at the reactor base.

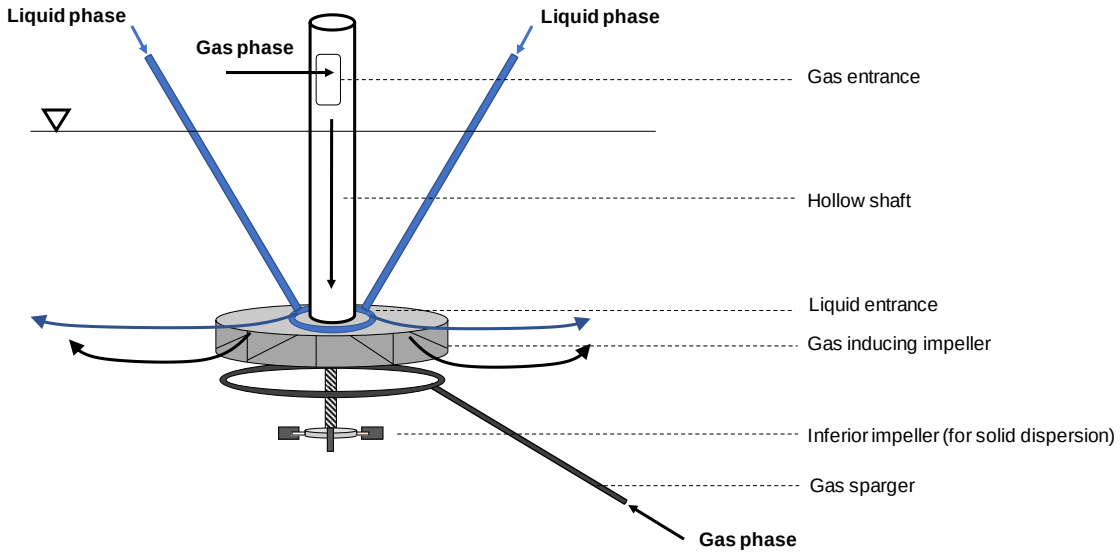

Figure 4.7 – Scheme of the agitator of the industrial reactor.

As the gas phase promotes is induced in the reaction mixture, a reduction of the density is expected in the surroundings of the impeller. This should decrease the movement resistance of the blades and, in turn, the current intensity of the agitator. Examples of the calculation of the mixing power input under aerated conditions for different impeller types are reported in the literature [79] [80] [81] [149]. These studies show that the aerated power input depends on the gas induction rate which, in turn, depends on the fluid properties, the impeller submergence, and the impeller dimensions. Nonetheless, these examples are attributed to agitated vessels without recirculation streams, in contrast to the present system. Therefore, the present case-study is evaluated qualitatively. Based on the above-mentioned authors, the rise of the liquid level in the reactor should increase the impeller submergence, promoting a decrease of the gas induction rate and, in turn, the energy consumption of the agitator. Assuming a temporary blockage of the reactor outlet sudden occurs, the level of the reactor could rise excessively. This scenario could explain the anomalies on the current intensity of the agitator.

In addition, if an excessive rise of the reactor level occurs, the mixture overflow through the gas entrance of the agitator shaft could occur, compromising even more the induction rate of gas. Figure 4.8 outlines the gas entrance of the agitator showing that the solid deposits tend to accumulate in this area, thereby supporting this claim.

Next, the phenomena of catalyst deposition and catalyst losses will be addressed, with the intention of assessing the most plausible cause for the above-mentioned decrease of catalyst concentration.

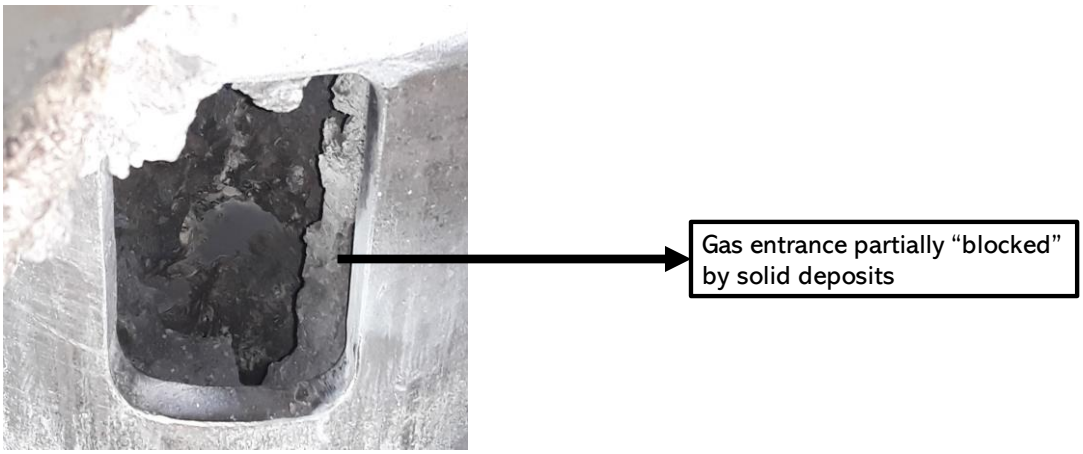

Figure 4.8 - Detail of the gas entrance of the impeller shaft.

Evaluation of the catalyst deposition

Considering the behaviour of the agitator current intensity before and after the abnormal peaks were registered, globally, this variable tends to decrease with the catalyst concentration, despite its abnormal behaviour occasionally registered (see Figure 4.9). As mentioned previously, the agitation power input depends on the density of the reaction mixture.

In this case, the reaction mixture represents a three-phase system, where the solid catalyst particles are suspended over a gas-liquid dispersion. Therefore, the overall density, should consider the corresponding densities and the volumetric fractions of each phase involved. Assuming a constant composition of gas-liquid dispersion, it is expected that the overall density of the reaction mixture only varies with the catalyst concentration. To

calculate this parameter, the density of the gas-liquid mixture, ρ_{GL} was first determined considering the densities of the liquid, ρ_L, and gas, ρ_G, fractions and the corresponding gas holdup ϵ_G (volumetric fraction) (Equation 2.13) as

$$\rho_{GL} = \rho_G \epsilon_G + \rho_L (1 - \epsilon_G) \tag{4.2}$$

Next, the density of the reaction mixture, ρ_m, was determined, considering the presence of the solid phase though the following expression:

$$\rho_m = \frac{1}{\frac{w_{cat}}{\rho_{cat}} + \frac{(1 - w_{cat})}{\rho_{GL}}} \tag{4.3}$$

Here w_{cat} is the mass fraction of catalyst $\left[kg_{cat}/kg_{gas-liquid\ mixture}\right]$, ρ_{cat} is the catalyst density $[kg_{cat}/m^3_{cat}]$, and ρ_{GL} is the density of the gas-liquid fraction $\left[kg_{gas-liquid\ mixure}/m^3_{gas-liquid\ mixure}\right]$.

Combining the Equations 2.3 and 4.1, the corresponding relation is obtained:

$$\frac{I_2}{I_1} = \frac{\rho_{m,2}}{\rho_{m,1}} \tag{4.4}$$

where the subscripts 1 and 2 are, respectively, related to the conditions before and after the abnormal peaks observed in the current intensity of the agitator between days 150 and 200, respectively (see Figure 4.9). During this period, the catalyst concentration reduced from 0.30 to 0.10 a.u., whereas the current intensity of the agitator reduced from 0.63 to 0.60 a.u. From Equation 4.3, this reduction on the catalyst concentration promotes a decrease of 4.6% in the overall mixture density. On the other hand, the agitator current intensity decreases 5.0%, which is close to the estimated variation of the mixture density. Therefore, it is quite plausible that the decrease of the agitator current intensity observed during period A was caused by the reduction of the mixture density.

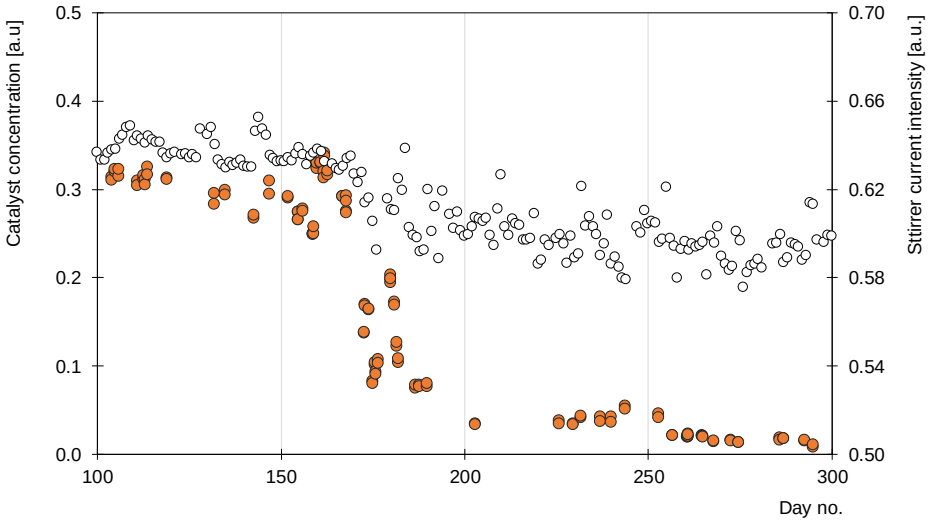

Figure 4.9 – Current intensity of reactor agitator and corresponding catalyst concentration of the reaction vessel (● catalyst concentration, ○ agitator current intensity).

As mentioned above, the performance of the underlying process also relies on the efficiency of the heat exchangers. The overall heat transfer coefficient can be monitored considering the online measurements of flowrate/pressure of the steam produced, and the operating temperature of the reactor. Neglecting the contribution of the sensible heat in the condensate entering the tube bundle, the production of saturated steam is assumed. This way, the overall heat transfer coefficient (U_{VB}) of the tube bundle can be determined as:

$$U_{VB} = \frac{G_C \, H_{V,H_2O}}{A \, (T - T_{steam})} \tag{4.5}$$

Here U_{VB} is the overall heat transfer coefficient $[W/(m^2 \cdot K)]$, G_C is the condensate flowrate $[kg/s]$, H_{V,H_2O} is the vaporisation enthalpy $[J/kg]$, A is the heat transfer area $[m^2]$, T_{steam} and T are the saturation temperature of steam and the reactor temperature $[K]$, respectively.

Figure 4.10 shows the evolution of the overall heat transfer coefficient of the tube bundle, and of the catalyst concentration. It is observed that U_{VB} also decreases with the catalyst concentration. Hence, it is possible that the reduction of catalyst concentration may be linked to the catalyst deposition in the internals of the heat exchanger device.

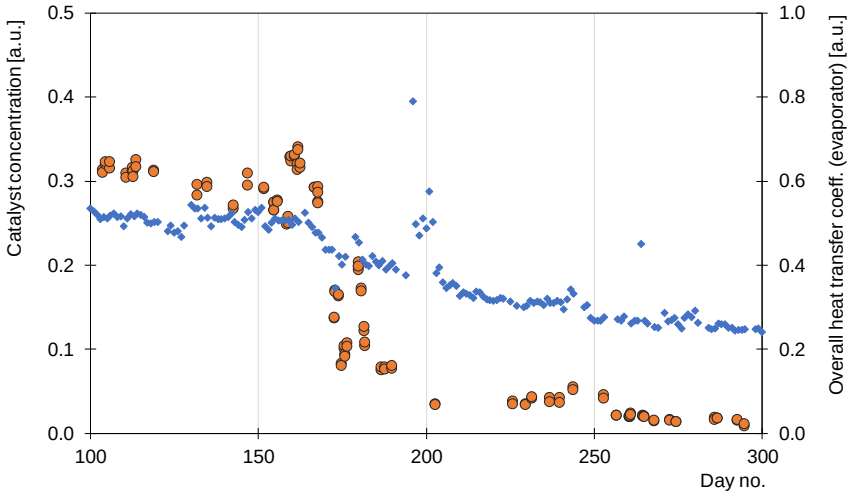

Figure 4.10 – Evolution of catalyst concentration, together with the heat transfer of the tube bundles (● catalyst concentration and ◆ overall heat transfer coefficient).

Considering that the catalyst deposition may justify the variation of catalyst concentration observed between days 150 and 200, the following observations should be highlighted:

- Globally, the behaviour of the agitator current intensity, during the reduction of catalyst concentration, matches its theoretical dependency with the mixture density. On the other hand, noted that, during the same period, abnormal events were registered, where the agitator current intensity increased significantly without any previous action on the recirculation valve. This fact may indicate a hindered circulation among the reactor-decanter vessel system.

- The overall heat transfer coefficient of the tube bundles reduced simultaneously with catalyst concentration. The phenomenon may suggest the increase of the thermal resistance due to the deposition of catalyst in the internals of heat exchanging devices (solid fouling).

Evaluation of catalyst losses

The scenario of catalyst loss through the decanter outlet stream was also evaluated by performing two industrial tests. The first test addressed the evaluation of the effect of

catalyst addition, whereas the in second one the effect of feed flowrate variations on the catalyst loss was analysed.

- ***Effect of catalyst addition***

Figure 4.11 shows the results of the industrial test performed to evaluate the effect of catalyst addition on the catalyst concentration measured in the decanter outlet stream. In this case, several samples were collected at the process streams that contain catalyst: the recycled aniline inlet and the decanter outlet. The operating conditions were maintained constant, as well as the position of the recirculation valve. Fresh catalyst was added into the reactor between 6 and 13 minutes after the beginning of the industrial test. Five minutes after the catalyst addition period, the catalyst concentration measured at the decanter outlet increased 63%. Attending to the average volumetric flowrate of the decanter outlet stream, this peak of catalyst concentration would represent about 0.1 wt.% of the load of fresh catalyst added to the system.

Considering the average flowrates of the recycled aniline and the decanter outlet, together with the corresponding measurements of the catalyst concentration therein, it is estimated that an equivalent mass of catalyst to what was added to the system would be lost in 12h, assuming the same operating conditions.

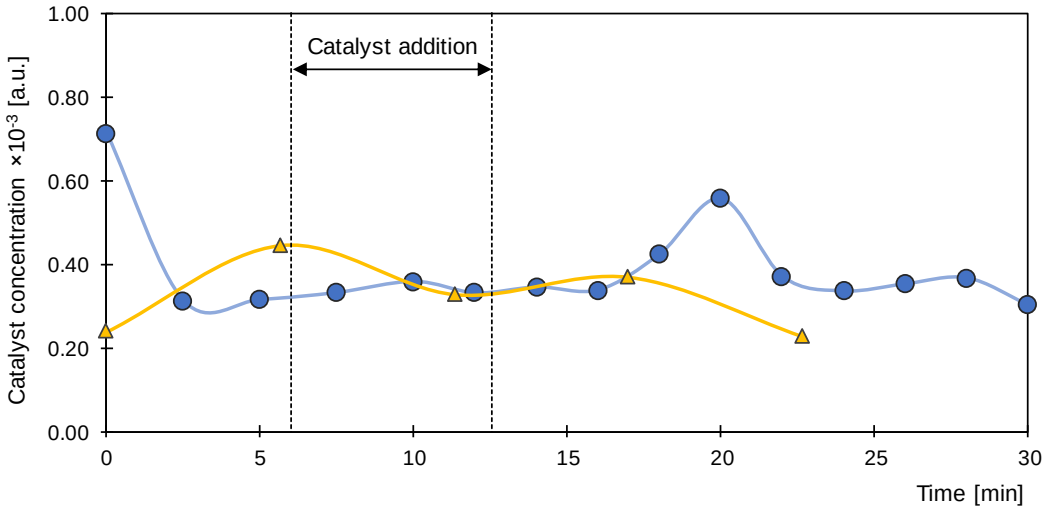

Figure 4.11 – Catalyst concentration measured in both (▲) recycled aniline and (●) decanter outlet streams, during the addition of fresh catalyst in the reactor studied.

- ***Effect of the feed flowrate on catalyst losses***

The effect of the feed flowrate was also studied, since it directly influences the decanter outlet stream flowrate, and thereby can also affect the catalyst losses therein. In this case, the catalyst concentration in the recycled aniline and decanter outlet streams was measured in different regimes of nitrobenzene feed flowrate, while maintaining the same nitrobenzene-recycled aniline feed flowrate ratio. It should be mentioned that, in each trial, neither new fresh catalyst loads were added to the system, nor manipulations on the recirculation valve were performed. Samples were collected at the recycled aniline and the decanter outlet streams every 20 min, during a total period of 4 h. The operating conditions observed in each trial are presented in Table 4.1.

Table 4.1 - Operating conditions of each regime of the reactor studied.

Regime	Nitrobenzene flow [a.u.]	Recycled aniline flow [a.u.]	Recirculation valve [%]
A	0.42	0.50	25
B	0.48	0.58	25
C	0.55	0.66	15

Figure 4.12 shows the total flowrate of recycled aniline, the decanter outflow, and the corresponding measurements of the catalyst concentration. Regarding the recycled aniline stream, noted that the amount of catalyst therein is influenced by the combined output of several industrial reactors that feed the recycled aniline circuit. This influence was, therefore, considered during the realisation of these trials.

Figure 4.13 presents the outflow of each reactor feeding the recirculation product circuit, as well as the level of the recycled aniline tank. As can be observed, the level of the recycled aniline tank remained mostly stable, thus indicating its independence from the catalyst concentration measured in the recycled aniline stream. Moreover, it is verified that reactor II had the highest and most unstable outflow, among the reactors that feed the recycled aniline circuit. A decreasing tendency of the catalyst concentration measured in the recycled aniline stream is observed in regimes A and B, in contrast to regime C. These results are coincident with a lower outflow of reactor II, in the case of regimes A and B.

Therefore, it is plausible that the catalyst losses derived from reactor II may have affected the amount of suspended catalyst in the recycled aniline stream.

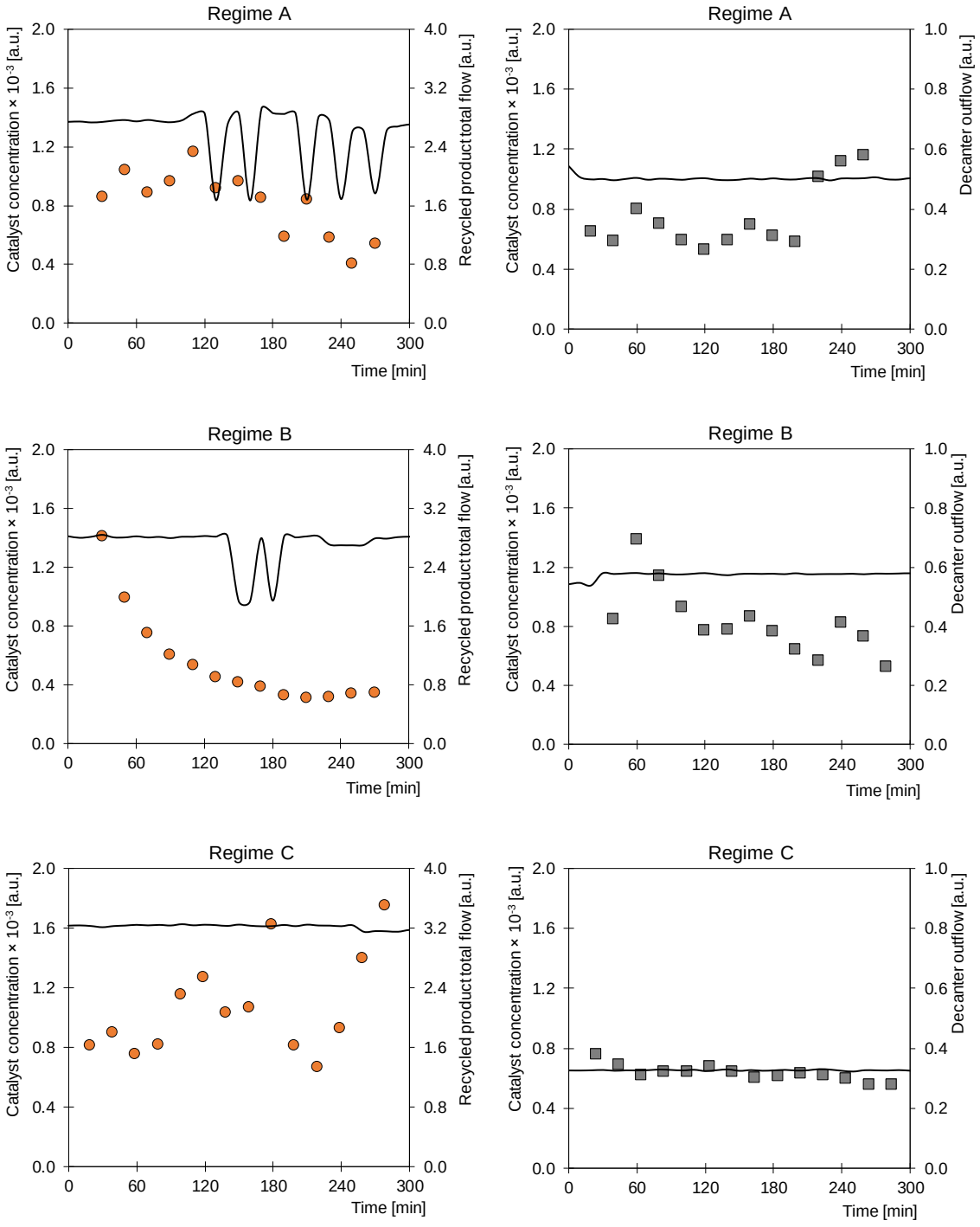

Figure 4.12 - Catalyst concentration measured in the recycled aniline (●) and in the decanter outflow (■) (— recycled aniline total flow/decanter outflow).

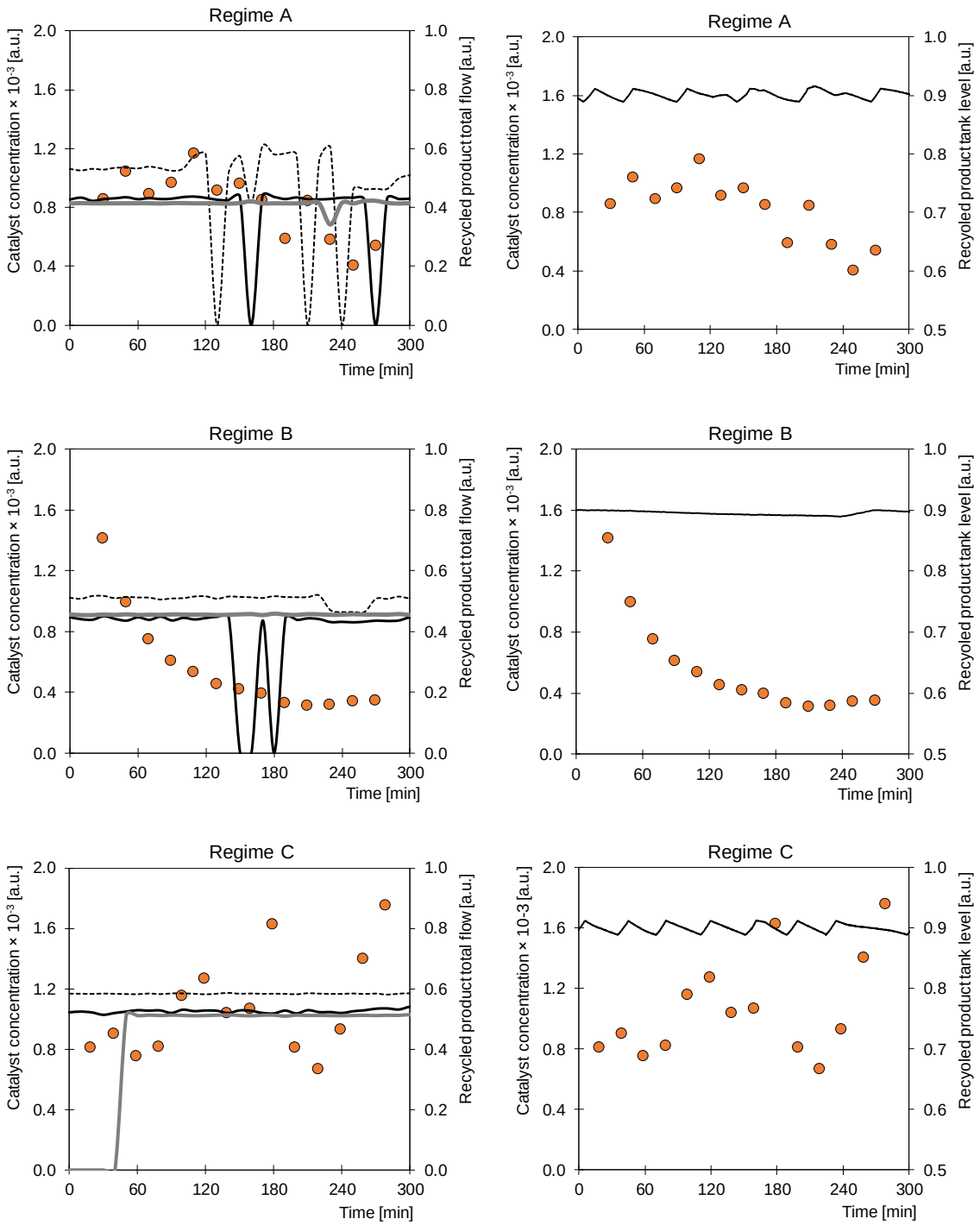

Figure 4.13 - Catalyst concentration measured in the recycled aniline, together with the outflow of the reactors that feed the recirculation product circuit (left), and level of the recycled aniline reservoir (right) (● catalyst concentration, ——— reactor II, - - - - - reactor III, ——— reactor IV).

For each measurement of the catalyst concentration, the mass input and output flowrates of catalyst were determined considering, respectively, the average volumetric flowrates of the recycled aniline and decanter outlet streams. By these means, the average catalyst loss obtained for regimes A, B and C were 0.14, 0.26 and 0.07 a.u., respectively (see Figure 4.14). For the regimes A and B, a greater dispersion of results in the catalyst mass outflow values is observed, when compared to regime C. However, one notices that the feed flowrate used in the regime B promotes a catalyst loss almost two times higher than in regime A. Therefore, it is evidenced that an increase on reactor feed flowrate increases the amount of catalyst in the decanter outlet stream.

On the other hand, the lowest average catalyst loss is observed in regime C, despite its higher flowrate conditions, in comparison with the remaining regimes. In this case, a lower opening of the recirculation valve is used, suggesting that a higher separation efficiency of the decanter, which, in turn, might have contributed to a smaller dispersion on the values of the catalyst mass outflow.

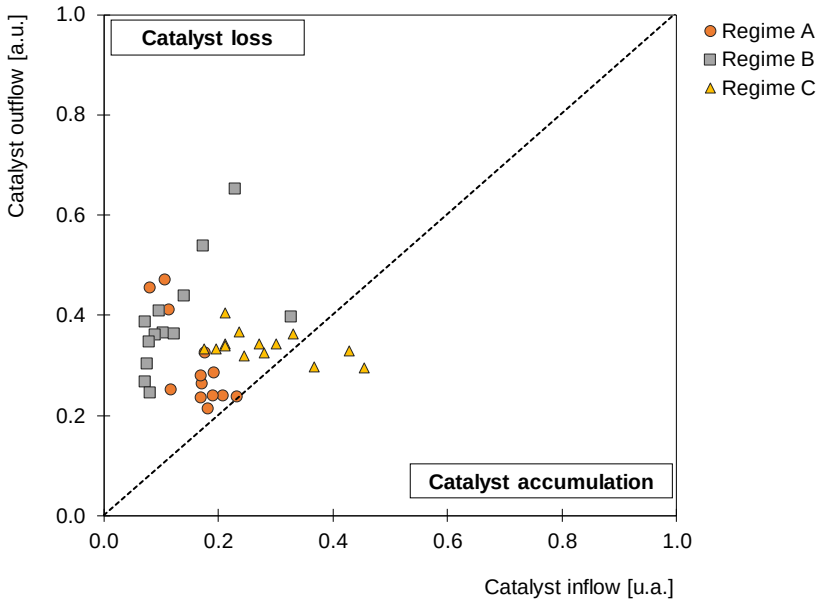

Regime	Nitrobenzene flow [a.u.]	Recycled aniline [a.u.]	Recirc. valve [%]	Avg. catalyst loss [a.u.]
A	0.42	0.50	25	0.14
B	0.48	0.58	25	0.26
C	0.55	0.66	15	0.07

Figure 4.14 – Mass inflow and outflow of catalyst and the corresponding average catalyst loss for each regime tested.

Considering the average catalyst loss obtained in these industrial trials, the next step was to check whether these results could justify the observed reduction in the catalyst concentration in the industrial reactor between the days 150 and 200. In Table 4.2, the average catalyst loss necessary for the variation of the catalyst concentration is determined, considering that the catalyst concentration decreased 67% in the first 8 days of the period abovementioned. In this case, the average catalyst loss obtained is considerably higher than in any of the regimes tested (8, 4, and 18 times higher, respectively, for the regimes A, B and C). Hence, the former reduction of catalyst concentration registered in the reactor is unlikely to be justified by the loss of catalyst.

Table 4.2 – Estimation of the average catalyst loss necessary for the reduction of catalyst concentration observed in the reactor (days no. 150-200).

Variable	**Value**
Nitrobenzene flowrate [a.u.]	0.51
Recycled aniline flowrate [a.u.]	0.62
Recirculation valve [%]	15
Reduction of catalyst concentration observed [%]	67
Period of catalyst concentration reduction [d]	8
Average catalyst loss [a.u.]	1.08

By determining the reduction of the catalyst concentration in the reactor that occurred during the period A, the catalyst deposition is identified as the most plausible cause that can explain such a variation. In addition, noted that the frequent repositions of fresh catalyst registered during that period were not enough to increase the catalyst concentration. For that reason, the reactor was shut down afterwards, during a period where the internals of the reactor were cleaned with the intention of improving the heat transfer performance. The consequent restart of the system is considered in the next period of observation discussed next.

4.2.2 Period B: Reactor cleaning and consequent restart of the process operation

As previously mentioned, the reactor cleaning was performed at the end of period A with the goal of improving the performance of the heat exchangers. This procedure was applied to the reactor studied around day 330 of the present study. As the reactor headspace was opened to perform this cleaning procedure, a significant fouling was found in the internals of the equipment. This evidences the scenario already considered, involving catalyst deposition. In this case, the deposited solids were removed from the equipment by using a high-pressured water washing machine; however, noted that the material was not removed from the reaction vessel, with the intention of enhancing the catalyst concentration afterwards. Consequently, after the restart of the system, the concentration of suspended catalyst was significantly higher than the values observed in period A. This led to an increase in the contents of by-products, derived from the aniline hydrogenation, demanding greater processing in the downstream purification stages.

Figure 4.15 shows the process monitorisation during the period B. Despite the cleaning procedure applied, the amount of suspended catalyst in the reactor rapidly decreased in the 100 days that followed this start-up. Simultaneously, the nitrobenzene content increased, as well as the frequency of system shutdowns, regardless of a constant reactor regime applied. Consequently, a greater addition of fresh catalyst was verified in the same period.

Besides that, the overall heat transfer coefficient of the heat exchanger and the current intensity of the agitator are reduced, coinciding with the reduction of catalyst concentration. This behaviour suggests that catalyst deposition was also promoted, as identified in period A.

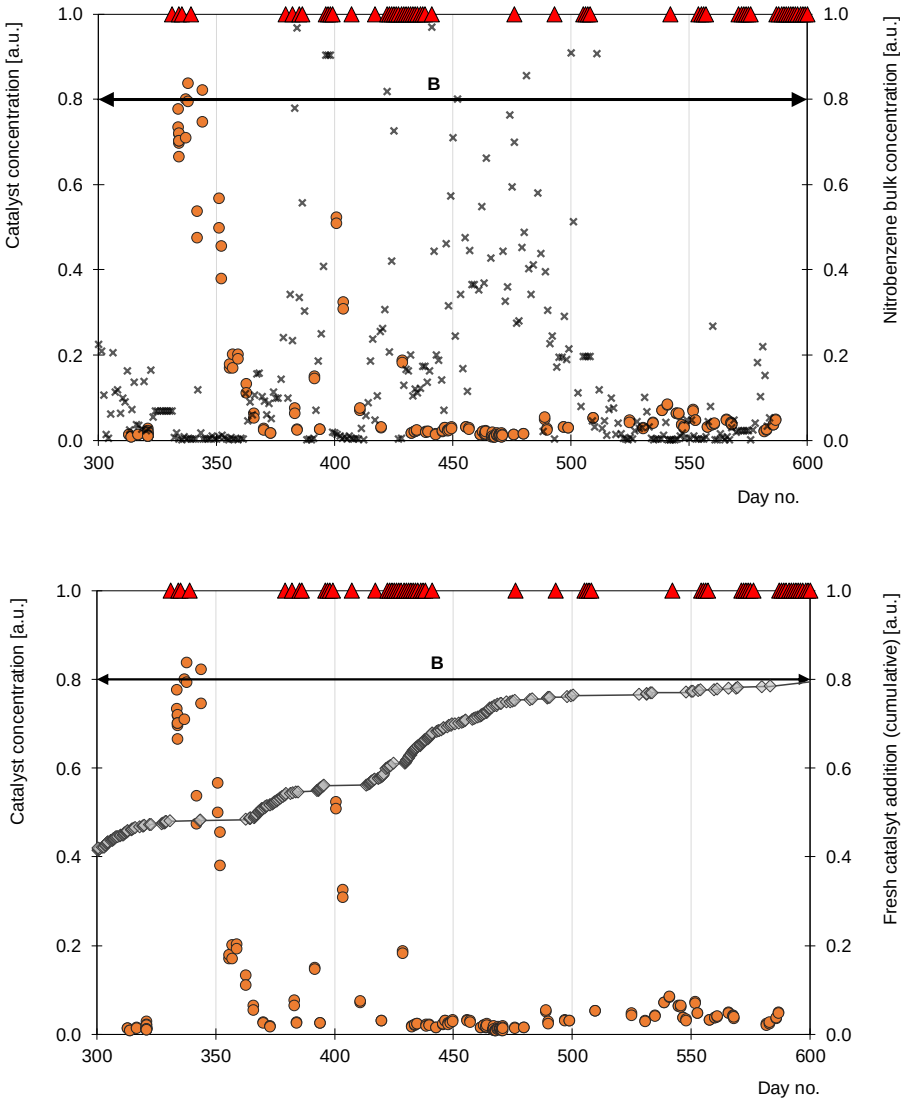

Figure 4.15 – Monitoring study of the industrial reactor during period B (● catalyst concentration, × nitrobenzene bulk concentration, ◇– cumulative of fresh catalyst addition, ◆ overall heat transfer coefficient, ○ current intensity of the reactor agitator, and ▲ system shutdowns).

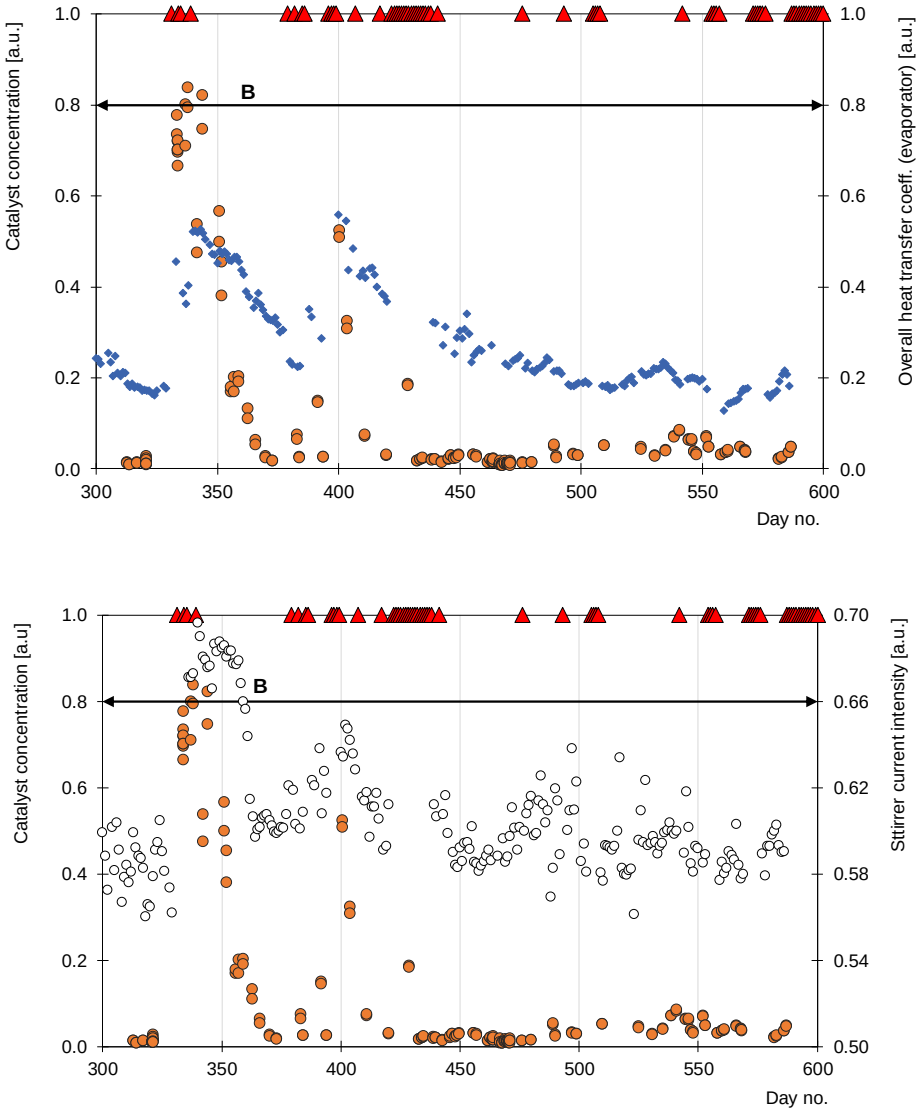

Figure 4.15 (cont.) – Monitoring study of the industrial reactor during period B (● catalyst concentration, ◆ overall heat transfer coefficient, ○ current intensity of the reactor agitator, and ▲ system shutdowns).

These results point to considerable limitations in the industrial practice of keeping a mass of used catalyst inside the reaction vessel after a cleaning procedure. As described in Chapter 3 (section 3.3.7), the magnetic properties of the catalyst material tend to change over time, as the amount of ferromagnetic nickel promotes higher coercivity values; this result, may thus explain the rapid formation of the solid deposits found in the reaction vessel in period A.

By measuring the coercivity of several batches of fresh catalyst already used in the productive process, a higher coercivity of F1 relatively to F2 was evidenced. Figure 4.16 shows the blend composition of the fresh catalyst added to the reactor, together with the catalyst concentration measured and the cumulative amount of fresh catalyst added. It is possible to remark that, whenever the fresh catalyst blend was exclusively composed by F1, the catalyst additions were more frequent. Further, one notices that the exclusive use of F1 in the additions of fresh catalyst coincided with the significant reduction of catalyst concentration when high contents of unreacted nitrobenzene were also detected.

Hence, it is plausible that exclusively adding fresh catalyst F1 may promote, and even accelerate, the agglomeration/deposition of catalyst inside the reactor. Based on these observations, the addition of uniquely F2-based blends was performed. This experiment was performed after the global shutdown of the plant, a period when the internals of the reactor were cleaned, and the catalyst deposits were totally removed from the interior of the reaction vessel. This is considered in the next section.

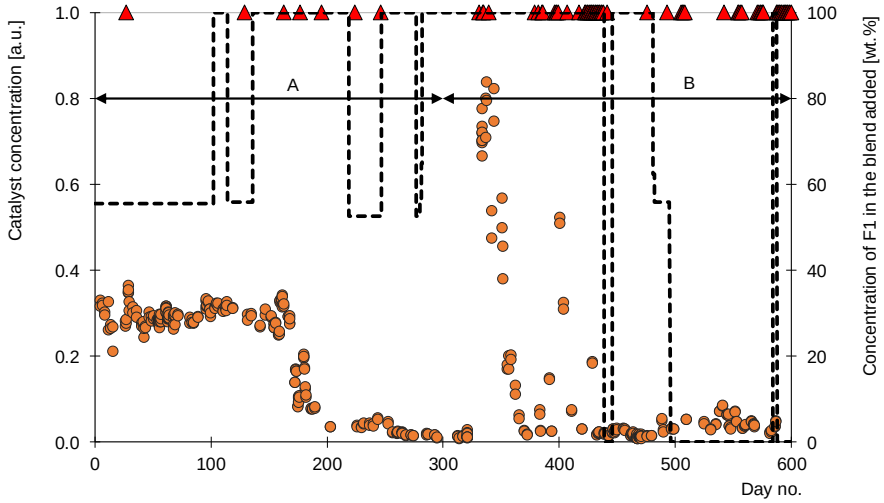

Figure 4.16 - Composition of the fresh catalyst blends added to the reactor studied, together with the catalyst concentration and the cumulative of fresh catalyst additions (● catalyst concentration, ▬ composition of F1 in the blend of fresh catalyst, ◆ cumulative of fresh catalyst addition, and ▲ system shutdowns).

4.2.3 Period C: Improving the fresh catalyst blend

As mentioned before, only fresh catalyst F2 was added to the reactor in period C. Figure 4.17 outlines a comparison of the process behaviour between periods B and C. An increase of the catalyst concentration is observed with the addition of F2-based blends. In period C, the stabilisation of nitrobenzene bulk concentration is attained with a lower frequency of catalyst make-ups, under similar feed flowrate regimes, in comparison with the intervals of period B, where only fresh catalyst F1 was used. Besides that, note that, after day 700, the catalyst concentration values on the reactor have stabilised for 35 days, even without any addition of fresh catalyst. In parallel, the heat transfer coefficient and the electrical current intensity of the agitator driver was maintained constant during the same period. This suggests that adding fresh catalyst F2 should provide the steadiness of the catalyst suspension.

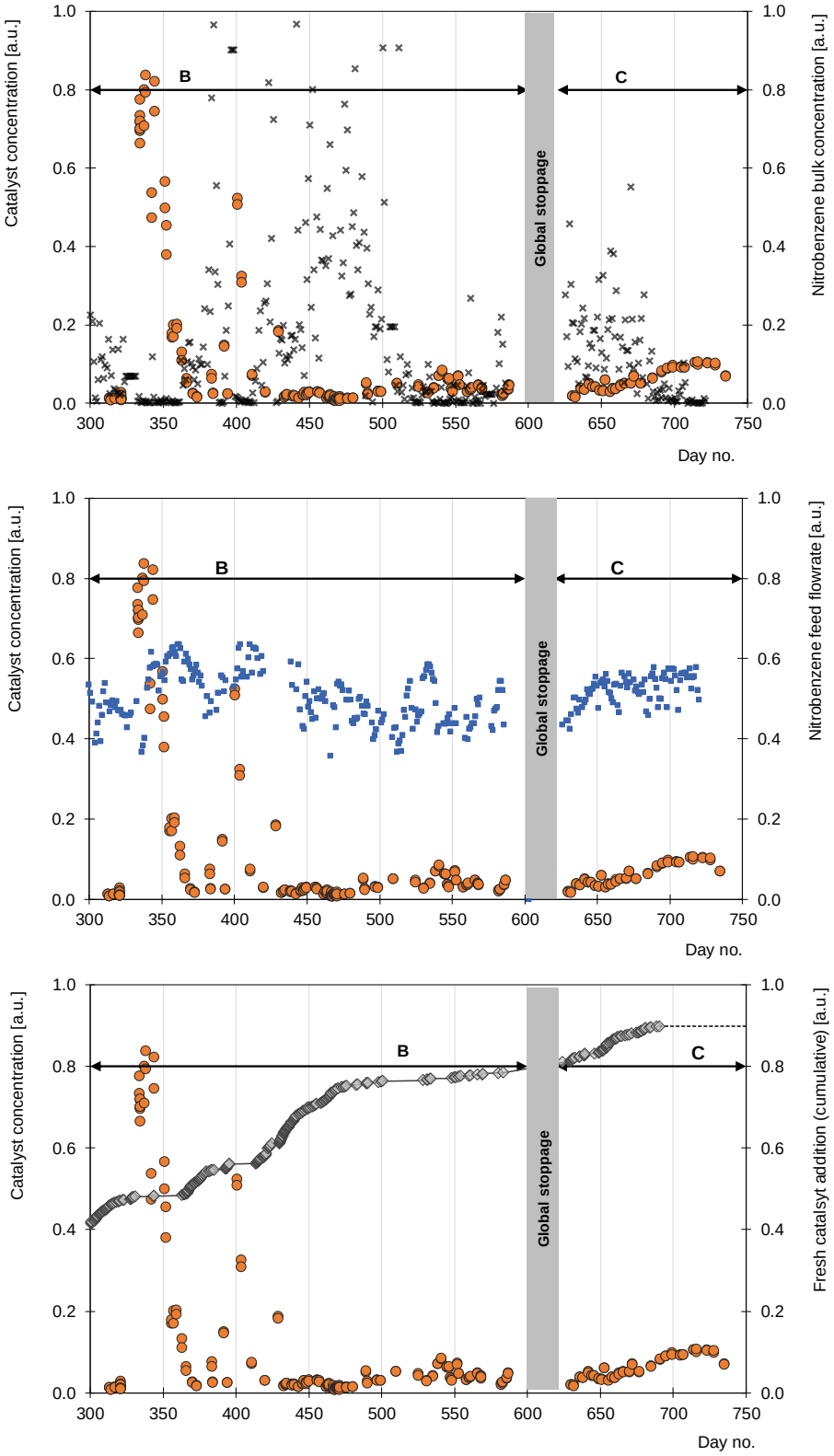

Figure 4.17 – Monitoring study during periods B and C of the industrial reactor (● catalyst concentration, × nitrobenzene bulk concentration, ◈ cumulative of fresh catalyst addition, ■ nitrobenzene feed flowrate.

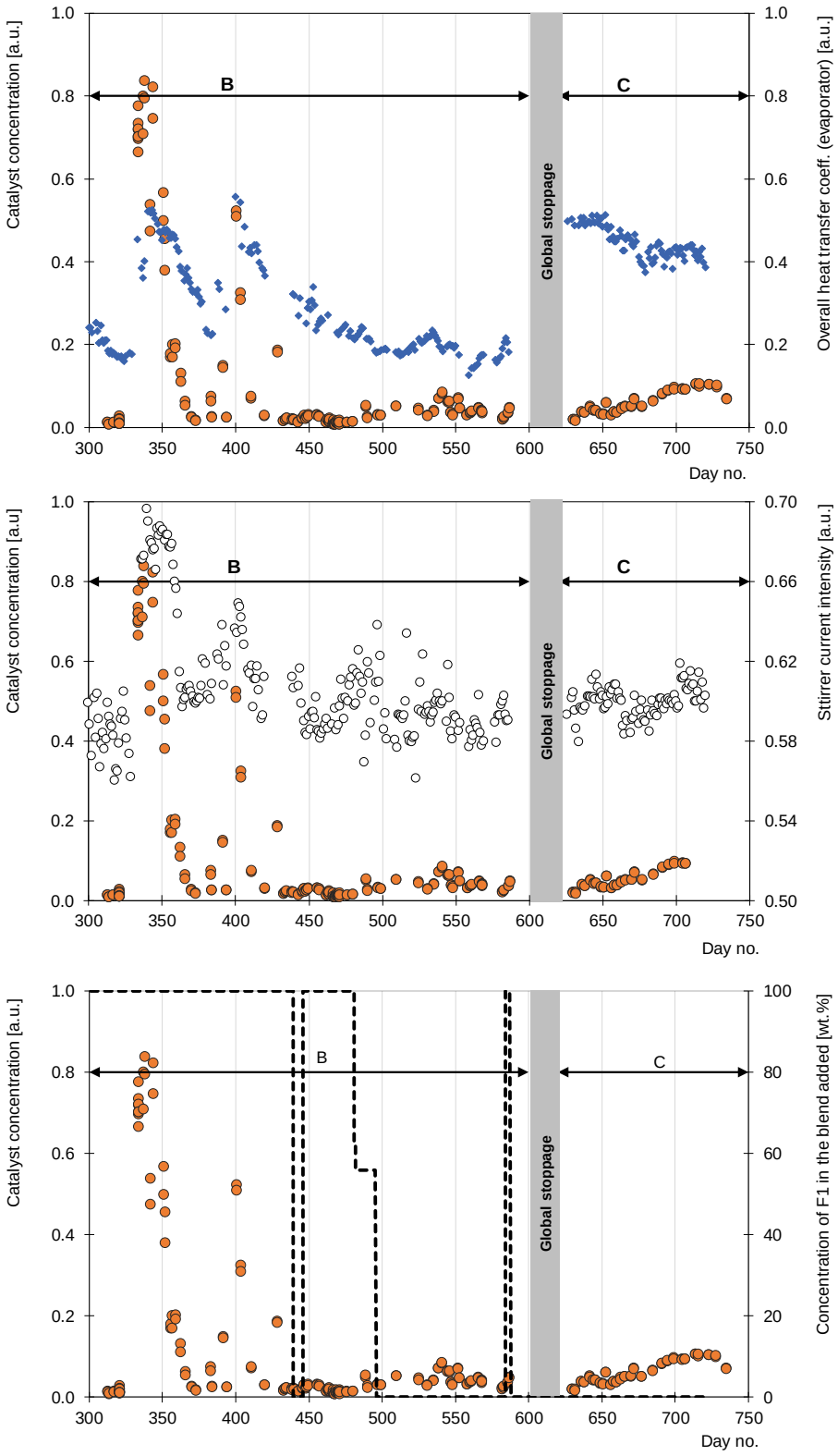

Figure 4.17 (cont.) – Monitoring study during periods B and C of the industrial reactor (● catalyst concentration, ■ nitrobenzene feed flowrate, ◆ overall heat transfer coefficient, ○ current intensity of the agitator, --- F1 concentration in the blend of fresh catalyst).

This operated period confirms that the catalyst concentration values can be stabilised with a low content of nitrobenzene detected in the reactor outlet stream. This leads to a reduced demand of fresh catalyst repositions. Besides this industrial practice, several actions are typically performed with the purpose of controlling the catalyst in the reaction mixture. In the next section, this issue will be addressed, encompassing a set of industrial tests performed also in the present work.

4.3 Evaluation of the industrial practices to control the catalyst concentration

Catalyst deposition can reduce the amount of catalyst in the suspension, and thereby affecting the conversion of nitrobenzene in multiple ways. An example of an anti-fouling procedure applied to polymerisation slurry reactors was reported in [150], which involves the rapid heating of the internals of the reactor, thus ensuring the disaggregation of the deposited material therein. However, this practice cannot be applied in the industrial reactor studied due to safety reasons. As such, alternative strategies were assessed that are typically applied to the current industrial practice aimed at keeping the catalyst suspended in the reaction vessel.

These strategies include nitrogen injection in the reactor-decanter recirculation stream, rapid changes on the recirculation valve, and increased repositions of fresh catalyst. The first two practices assume that catalyst is accumulated in the decanter-reactor bottom connection, whereas the second practice assumes that the amount of suspended catalyst can be enhanced through an intensified period of catalyst addition. These actions were assessed thought several industrial tests described next.

4.3.1 Nitrogen injection/Manipulation of the recirculation valve

The industrial practices of nitrogen injection and manipulation of the recirculation valve were evaluated, considering their effect on the catalyst concentration in the reactor. Several tests (T1-T5) are described in Table 4.3. During the performance of each test, samples from the reactor outlet were collected to determine its catalyst concentration. These tests were performed according to the following recommendations:

- nitrogen injection into the recirculation stream should not exceed 10 s, so that the pressure in the reactor headspace is not affected significantly.

- fully opening the recirculation valve should be performed under a short period to avoid the runaway of the current intensity and, therefore, the shutdown of the system.

In Table 4.3, the tests T1-T5 performed in the industrial reactor are described. Figure 4.18 shows the behaviour of catalyst concentration during each test. It is possible to observe that none of these actions were effective in increasing the catalyst concentration in the reaction vessel. This result evidence two possibilities: either these actions were inefficient to release the catalyst deposits to the recirculation stream, or the catalyst accumulation therein was not significant at the time that these industrial tests were performed.

Table 4.3 – Industrial tests performed in the industrial reactor, involving nitrogen injection and recirculation valve manipulation.

Test	Description
T1	Nitrogen injection on the recirculation stream (10 s)
T2	i. Close the recirculation valve (30 s) ii. Nitrogen injection on the recirculation stream (10 s) iii. Return the recirculation valve opening to its initial state
T3	i. Close the recirculation valve ii. Nitrogen injection on the recirculation stream (10 s) iii. Recirculation valve fully open iv. Return the recirculation valve opening to its initial state (Repeat this procedure 3 times)
T4	i. Close the recirculation valve ii. Recirculation valve fully open iii. Return the recirculation valve opening to its initial state (Repeat this procedure 3 times)
T5	i. Close the recirculation valve ii. Return the recirculation valve opening to its initial state

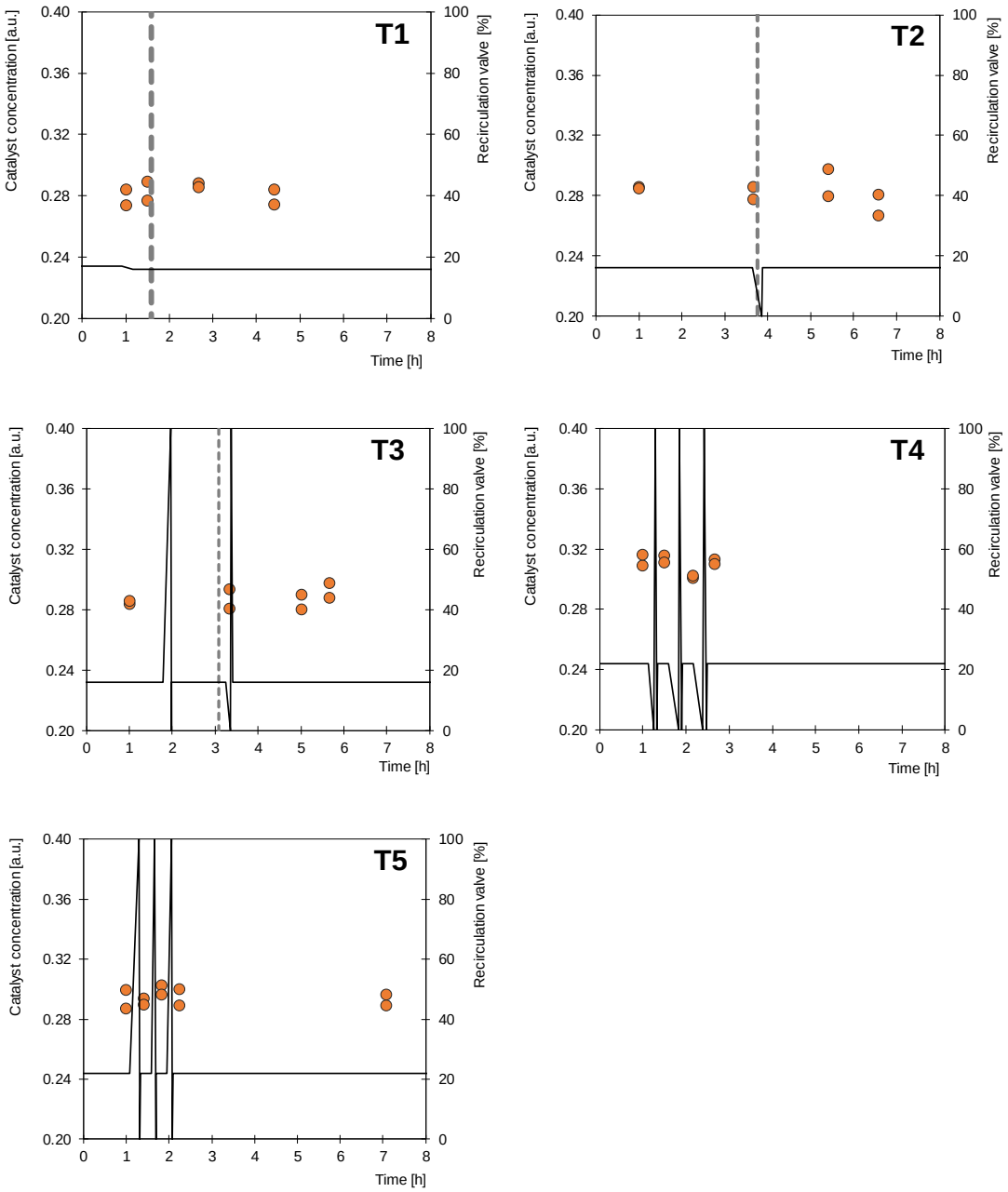

Figure 4.18 - Industrial tests T1 to T5 performed in the reactor K510 (● catalyst concentration, - - - nitrogen injection, ── recirculation valve).

As mentioned in section 4.2, the performance of the reaction stage tends to be improved for catalyst concentration values above 0.10 a.u.. Bearing this in mind, since the tests T1 to T5 were performed at the beginning of period A, precedent of the decrease of

catalyst concentration reported between days 150 and 200 (see section 4.2.1, it is plausible that the catalyst deposition was not significant at that time.

Considering the latter issue, an additional test was carried during the end of period A, when the catalyst concentration values were much lower than in the former case (around 0.01 a.u.). In this case, we intended to perform a full opening of the recirculation valve, while collecting samples from the reactor outlet before, during and after this manipulation. The recirculation flowrate was also measured by using a portable ultrasonic flowmeter installed *in situ*. The corresponding results are presented in Figure 4.20. One notices that, although the catalyst concentration values enhanced during the increase of the recirculation flowrate, they rapidly returned to the initial state. In addition, note that the heat transfer was not affected. This result indicates that, despite this action might be useful to avoid excessive accumulation of catalyst on the recirculation channel, above it seems unlikely to be effective in significantly removing the solid deposits from the internals of the reactor.

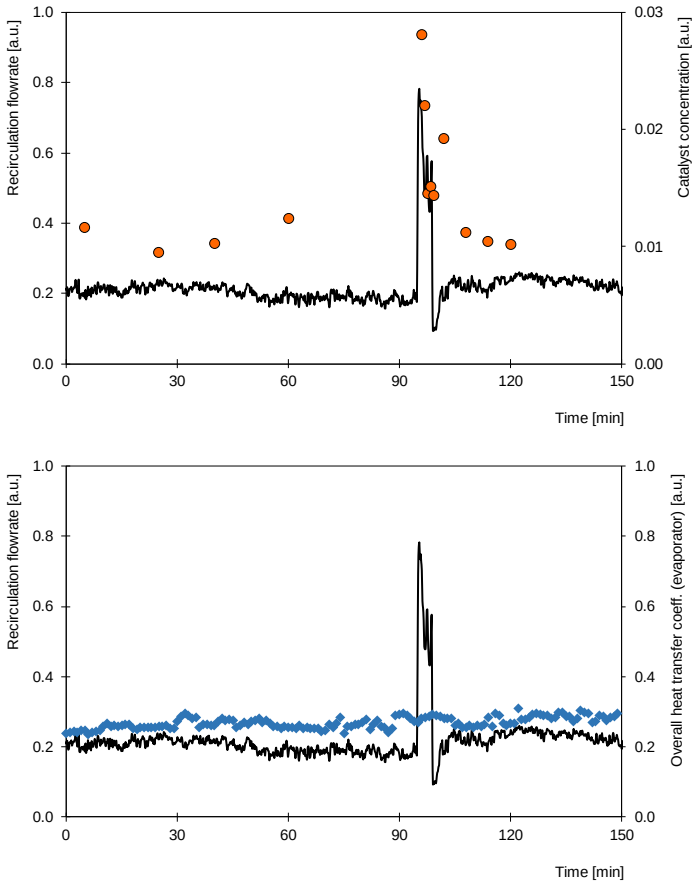

Figure 4.19 – Behaviour of the (—) recirculation flowrate, (●) catalyst concentration and (◆) heat transfer performance, during the test where the recirculation valve was briefly placed in the fully open position in the industrial reactor.

4.3.2 Catalyst addition

The addition of fresh catalyst is commonly used in the industrial practice for controlling the conversion of unconverted nitrobenzene in the reactor. Due to the recurrence of this action, catalyst addition is expected to influence the concentration of suspended catalyst. This way, the effect of catalyst addition on the concentration of suspended catalyst was also evaluated through an industrial test performed on a distinct reactor (reactor II) with identical design and scale as reactor I, where the referred observation periods A, B and C were conducted.

In the case of reactor II, the catalyst concentration and the conversion of nitrobenzene were at the time very low, regardless of the constant catalyst make-ups performed therein. Because of that, the addition of catalyst intensified with the purpose of increasing the catalyst concentration from 0.01 to 0.13 a.u. in reactor II. Table 4.4 shows the estimated amount of fresh catalyst necessary to add to reactor II to achieve that variation in the catalyst concentration. In this case, the estimated value is about 100 times higher than the equivalent amount typically used in a fresh catalyst make-up.

Table 4.4 – Estimated amount of fresh catalyst to add to the reactor II.

Variable	Value
Initial catalyst concentration [a.u.]	0.01
Target value of catalyst concentration [a.u.]	0.13
Addition of fresh catalyst [a.u.]	0.06

Figure 4.21 outlines the measurements of the catalyst concentration and of the nitrobenzene bulk concentration before and after the intensified addition of fresh catalyst was performed to the reactor II. Although an increase of the catalyst concentration was achieved, the corresponding value only reached 0.03 a.u., which was below than the desired value (0.13 a.u.). In addition, the catalyst concentration rapidly returned to its initial value two days after the same fresh catalyst addition, observing that the nitrobenzene bulk concentration in the reactor outlet also increased.

These results suggest that the amount of fresh catalyst added to the system was either lost downstream (from the decanter outlet) or deposited in the internals of the equipment. It should be mentioned that the reduction of catalyst concentration observed in after the fresh catalyst addition period also coincided with the decrease of the overall heat transfer coefficient and of the electrical current intensity of the agitation driver (see Figure 4.22). Because of this, it is plausible that the catalyst deposition was also promoted during this test.

Note that several manipulations in the recirculation valve were performed, during the period when the same reduction of the catalyst concentration was verified. This suggests that the catalyst added during this industrial test was unlikely to accumulate significantly on the decanter-reactor recirculation channel.

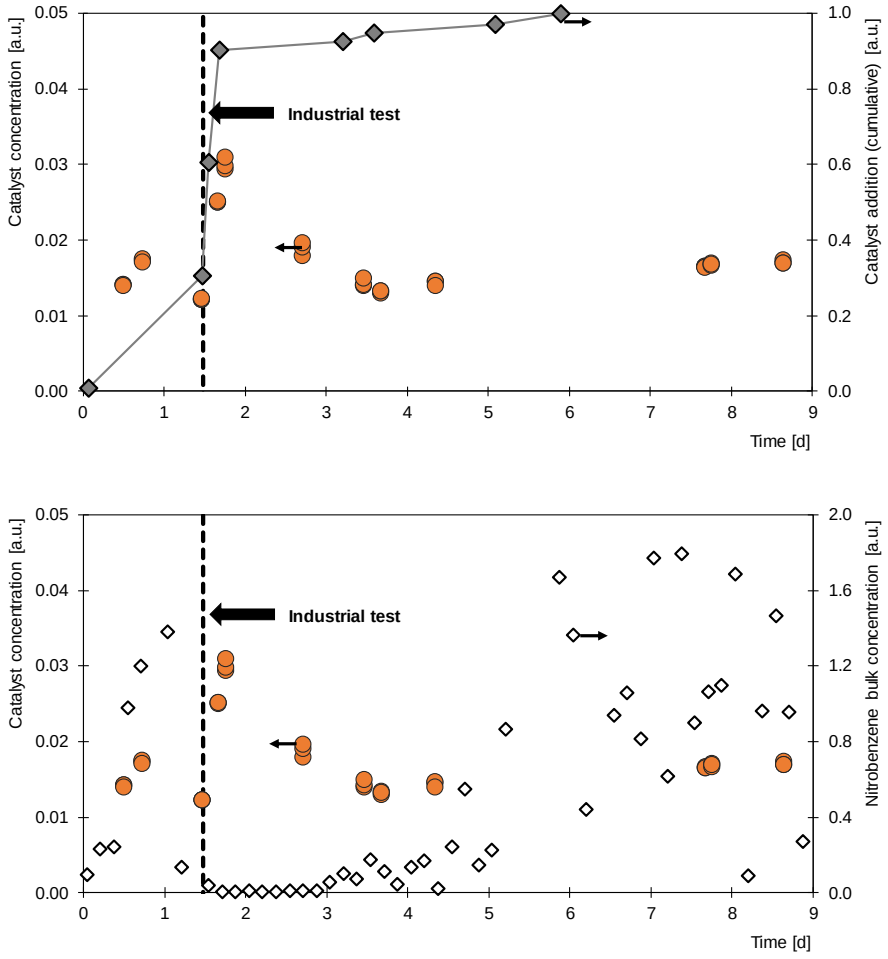

Figure 4.20 – Results of the industrial test performed in the reactor II (● catalyst concentration, ◆ catalyst addition (cumulative), ◇ nitrobenzene bulk concentration).

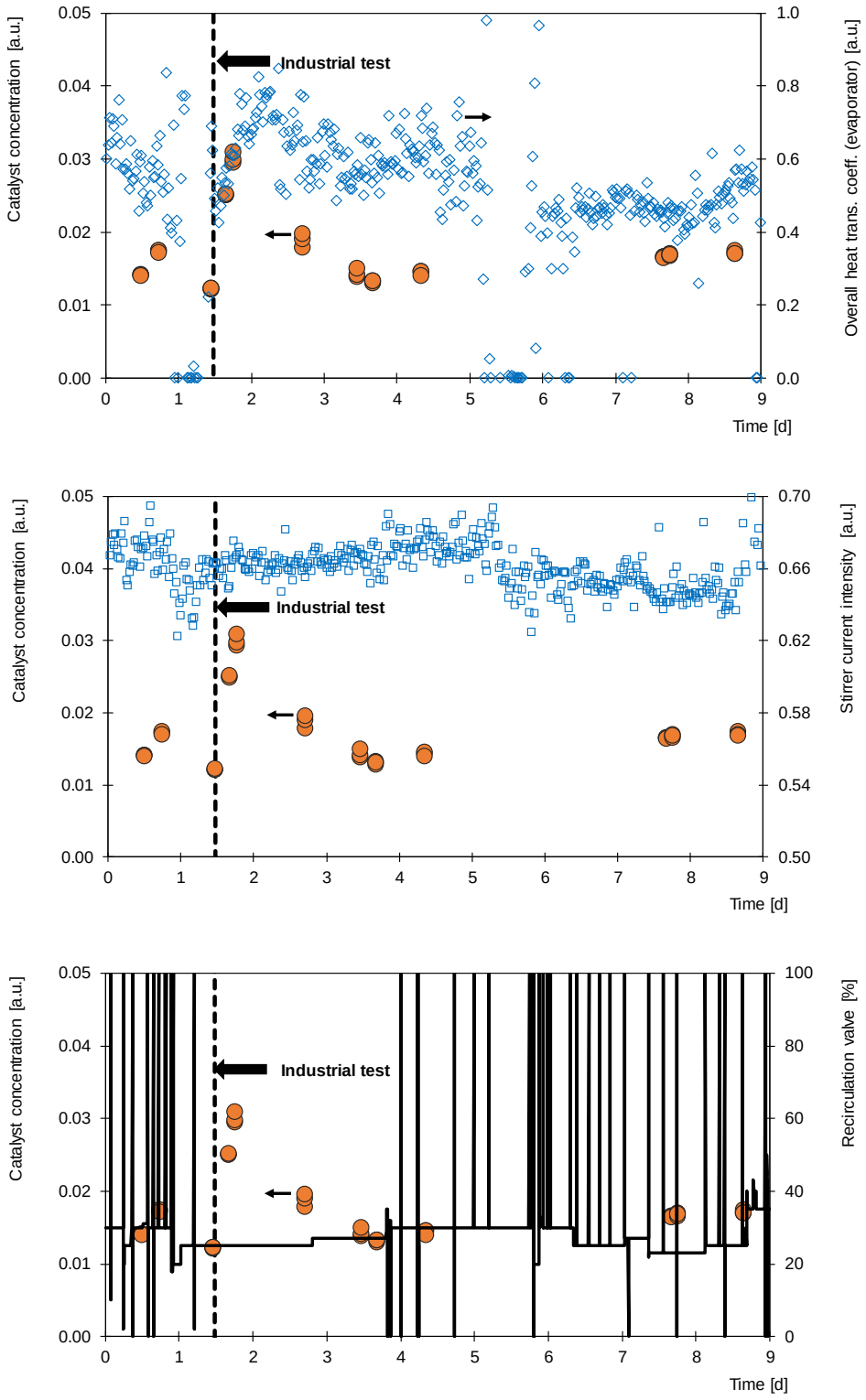

Figure 4.21 - Results of the industrial test performed in the industrial reactor II (● catalyst concentration, ◇ overall heat transfer coefficient (tube bundle), □ agitator current intensity, and ── recirculation valve).

On the other hand, it should be pointed that only fresh catalyst F1 was added during the industrial test performed to the reactor II. Likewise, this catalyst was also applied to reactor I from day 150 to 450 (see Figure 4.16), when the catalyst concentration was difficult to control, regardless of the frequency of catalyst addition. In contrast, when the blend composition of the fresh catalyst used was at least 50 wt.% F2, the catalyst concentration was more readily controlled.

According to section 3.3.7, the magnetic measurements performed on the deposited material collected from the internals of reactor I showed a higher coercivity (150 Oe), when compared to the most recent batches of fresh catalyst used in the process - F1 (around 102 Oe) and F2 (around 20 Oe). The withdraw of the sample of deposited material was performed after the second half of period A (day 150-300), when mostly F1 catalyst was added to the system. The magnetic measurements performed on this material indicated a coercivity around 150 Oe. On the other hand, the magnetic measurements performed on samples of used catalysts collected from different reactors fed with at least 50 wt.% of F2 indicate that the coercivity tends to stabilise around 125 Oe with time (section 3.5.3). Therefore, it is quite plausible that the exclusive use of F1 make-ups promoted the phenomenon of catalyst deposition observed during this investigation.

Overall, this evaluation on the current industrial practices for controlling the catalyst concentration in the industrial reactor allows to highlight the following remarks:

- The nitrogen injection/manipulation of the recirculation valve did not appear to effectively remove the catalyst deposits from the internals of the reaction unit. However, these practices may be useful to prevent an excessive accumulation of catalyst in the recirculation channel.

- The frequency of catalyst make-ups can indeed enhance and stabilise the catalyst concentration, if an appropriate blend composition of fresh catalyst is applied; in particular, fresh catalyst batches with low resistance to demagnetisation are recommended to prevent the deposition/accumulation of catalyst within the reaction vessel in a short term.

Although these practices can promote the steadiness of the catalyst suspension, their efficiency may not ensure the stability of the reaction conversion in the long term. This issue should be especially regarded if a proper prediction of the system outcome is intended through the process model developed. For that reason, a more systematic approach of the

process operation should be defined to identify the influence of unexpected disturbances affecting the prediction of the system outcome. Having said that, the statistical process control of the industrial reactor is detailed in the next section. This solution offers a process monitoring tool to promote the preventive maintenance of the reaction unit.

4.4 Statistical control of the industrial reactor

Process monitoring involves ensuring the process stability with time by reducing its variability. For this purpose, a set of problem-solving tools are usually used in several manufacturing industries denoted as statistical process control (SPC) [150].

A process is under *statistical control* when only the inherent variability of the operation is verified. Whenever an unexpected event disturbs the normal operation of the process (i.e., operator errors, defective raw material, incorrectly controlled machines), the common process variation is considered to be affected by *special causes* [151] [152], leading to an *out-of-control* state of the operation; SPC helps to identify the influence of those disturbances, so that the corrective actions are performed on time to keep the process under reduced variability. This way, SPC offers a means towards the process diagnosis and the preventive maintenance. Note that SPC should not be confused with quality control, since it does not measure quality directly, but rather indicates the probability of some correctable condition affecting an undesirable variation in product quality/process stability [151] [152].

The statistical control of the process is typically represented through control charts, where the process variation is plotted against a defined tolerance of the variable that is intended to monitor. This tolerance is specified by the target value (centre line CL), and the upper and lower control limits (UCL and LCL, respectively). These characteristics are determined considering a sample data collected of the process operation, where only common variation of the process is observed. Assuming that the population of the quality variable is normally distributed, the control limits are typically set at ±3 standard deviations of the population. This way, the values of CL, UCL and LCL are defined as:

$$\bar{x} = CL \tag{4.6}$$

$$UCL = CL + 3\frac{\bar{S}}{\sqrt{n}} \tag{4.7}$$

$$LCL = CL - 3\frac{\bar{S}}{\sqrt{n}} \tag{4.8}$$

Here $\bar{x}$ is the mean value taken from a sample of n observations of the process, and $\bar{S}$ is the standard deviation of the sample data.

These control limits are defined so that, if the process is in-control, nearly all the sample points will fall between them. Nevertheless, if a non-random pattern among a sequence of observations is detected within the specified tolerance, it is an indicator that a special cause is affecting the common variation of the process. Considering this, a set of decision rules suggested by [151] for identifying non-random patterns on control charts and, this way, ensuring the preventive maintenance of the process.

The determination of the statistical tolerance is based on a sample process data set, which should be representative of the operating window applied. To collect this data, the steady state of the process variables should be attained. For this reason, it is not surprising that process understanding usually represents the most time-consuming step during the implementation of a SPC procedure [150].

The further development of the process understanding tendentially results in the prediction of the system outcome based on a process model. By these means, a sample process data set can be collected from the process operation to validate a determined output variable that is susceptible to monitor. Consequently, SPC can be applied to define the statistical tolerance of the model predictability.

Attending to the present case-study, the outlet stream composition of the reaction unit provides a description of the system outcome in terms of the nitrobenzene conversion and of the selectivity to aniline based on the secondary compounds detected therein. As detailed in Chapter 2, only the main chemical reaction (nitrobenzene hydrogenation) is considered in the present study. Therefore, once the nitrobenzene bulk concentration is predicted by the process model developed, the monitoring of the model predictability becomes possible for a given operating window. To achieve this, a process data set from the industrial unit was collected during an extensive observation period, where the deviation

between the predicted and measured values of nitrobenzene bulk concentration was evaluated (see section 2.4.2). This deviation was smaller for catalyst concentrations above 0.20 a.u., observing that, under these conditions, a moderate addition rate and a constant blend composition of fresh catalyst was applied. On the other hand, this deviation was mor significant when the catalyst concentration became unexpectedly unstable, reducing below the former value. This behaviour occurred after significant modifications on the blend composition of fresh catalyst were performed noticing that the frequency increase of catalyst-makeups did not promote the steadiness of the catalyst concentration values, as well as the nitrobenzene conversion.

Given the influence of the catalyst concentration and of the catalyst utilisation on the prediction of the system outcome, a sample data was selected to define the statistical tolerance establish the statistical control of the industrial reactor. To perform this, a SPC control chart was developed by selecting several observations where a small deviation between the predicted and measured values of nitrobenzene is observed (74 out of 138).

Figure 4.22 shows the control chart obtained to the deviation between the predicted and measured values of nitrobenzene bulk concentration during the total period of observation. The CL, UCL and LCL values are -0.001 a.u., +0.004 and -0.006 a.u., respectively. Overall, it is verified that the model predictability to the nitrobenzene bulk concentration remains under the statistical tolerance essentially between the days 1-29, 100-170. During these observations, it is observed that the catalyst concentration values remained stabilised mostly around 0.20-0.30 a.u., the addition of fresh catalyst was moderate, and the corresponding blend composition was mostly 50 wt.% of F2 minimum. On the other hand, the process was out of statistical control when the catalyst concentration remained unsteady and below 0.20 a.u., alongside with intensive F1-based catalyst make-ups to the system and reduced performance of the heat exchanging devices.

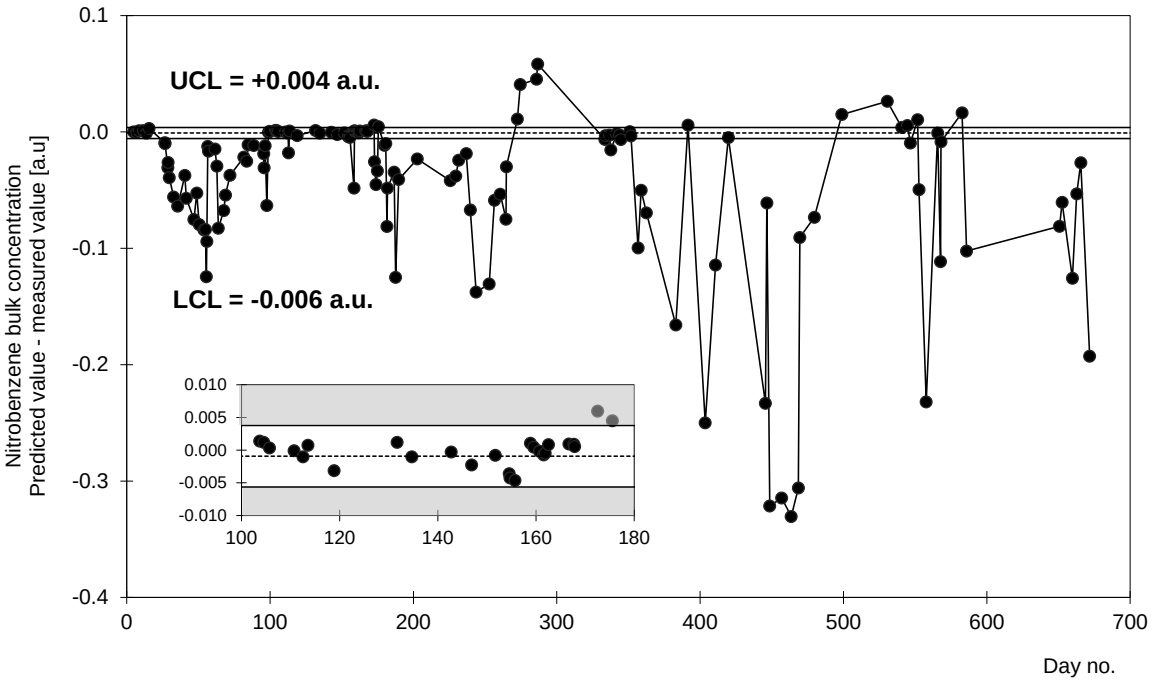

Figure 4.22 – Control chart of the deviation between predicted and measured values of nitrobenzene bulk concentration.

Overall, these results clearly evidence the importance of applying SPC in the present industrial unit in a near future. By providing a systematic approach based on the process model, the prediction of the nitrobenzene conversion can be monitored, rather than only attending to the current state of the process variables individually. If the model predictability on the nitrobenzene bulk concentration tends to move away from the statistical tolerance defined, an assignable cause is likely affecting the process common variation. Under this scenario, the current catalyst utilisation should be revised – this include either enhancing the catalyst concentration with an improved addition of fresh catalyst or checking if the deposition of catalyst is already significant.

Bearing in mind the continuous improvement of the underlying system, recall that the latter control limits could be updated by gathering new sample data sets from the industrial operation. This information should be collected under stricter operating windows and detailed features of the catalyst make-up policy to maximise productivity. By doing this, a more robust process monitoring tool can be developed in the future, this way beneficing, for instance, the reduction of downtime periods and/or of excessive fresh catalyst loads to the reaction unit.

In addition, it should be noted that the development of this monitoring tool can be extended the prediction of the secondary compounds involved in the underlying reaction system; considering that the related kinetics related to these reactions are still not fully understood, statistical models could be developed for this matter based on extensive collection of new process data sets. Likewise, this data acquisition should be performed under narrow operating windows and defined characteristics of the catalyst utilisation (e.g., addition rate, blend composition).

Besides the corrective measures applied to the catalyst management, the improvement of the nitrobenzene conversion also relies in the steadiness of the operation. Bearing this in mind, a new strategy was implemented to the regulatory control system of the industrial reactor. This is presented next.

4.5 Improvement of the regulatory control of the industrial reactor

The regulatory control loops allow the process to operate at a chosen target, providing a safe operation and minimising the effects of disturbances and of raw material variability. In present case-study, the regulatory control system mainly comprises the feedback control loops of the operating temperature and pressure, of the steam pressure, of the liquid level of the decanter dike, and of the feed flowrates of nitrobenzene and recycled aniline. In each loop, the measured process variable is compared to the corresponding setpoint. The obtained deviation results in a corrective action by the PID controller. For example, in case of the temperature control, the measured value is transmitted to the temperature controller which, in turn, acts on a valve that regulates the refrigerating water flowrate of the helical coil to remove the heat produced by the reaction.

In case of the nitrobenzene feed flowrate control, the corresponding setpoint is given by the production demand. Due to the formation of water during the hydrogenation of the nitrobenzene, a stream of recycled aniline is fed to the industrial reactor to avoid the formation of two liquid phases (organic and aqueous). Currently, the homogeneous reaction mixture is ensured by a constant ratio of recycled aniline to nitrobenzene flowrates. Thus, the recycled aniline flowrate is configured through ratio control, where the related setpoint value is given to the recycled aniline flow controller as function of the nitrobenzene flowrate regime. This procedure, however, has a drawback: it does not ensure a constant hydraulic

retention time (HRT) in the reaction zone, compromising the reaction conversion. Considering this issue, the control of the HRT in the industrial reactor is proposed by determining the setpoint of the recycled aniline flowrate, $G_{ANL,SP}$, based on the following mass balance:

$$G_{ANL,SP} = G_{out,SP} - G_{MNB,SP} \quad (4.9)$$

Here, $G_{out,SP}$ and $G_{MNB,SP}$ are the setpoints of the reactor outflow and nitrobenzene feed flowrate, respectively. In this strategy, it was necessary to determine previously the minimum value of $G_{out,SP}$ that ensures the homogenisation of the liquid phase for a given operating ranges of nitrobenzene flowrate and of temperature. To achieve this, the total water content in the reaction vessel was estimated by mass balance and compared to the expected water/aniline solubility limit. This strategy allows to keep the HRT of the industrial reactor constant, while the nitrobenzene flowrate is changed according to the production demand. Note that this strategy has the advantage of contributing to less disturbances to the overall system, namely on the liquid level of the decanter dyke, as well as on the pressure of the reactor headspace.

Figure 4.23 shows the control strategy applied to the HRT of the industrial reactor. Although the feedback control of the nitrobenzene and recycled aniline flowrates are kept in this configuration, the setpoint of the recycled aniline flowrate, $G_{ANL,SP}$, is now based on the setpoints of the reactor outflow, $G_{out,SP}$, and of the nitrobenzene feed flowrate, $G_{MNB,SP}$, specified, respectively, by the process engineer and by the control operator. This contrasts with the prior practice of applying a constant ratio of recycled aniline flow to nitrobenzene flow to obtain the value of $G_{ANL,SP}$. The mass balance described by Equation 4.9 is now incorporated into the distributed control system (DCS), where the values of $G_{out,SP}$ and of $G_{MNB,SP}$ to calculate $G_{ANL,SP}$ are set and sent to the feedback flow controller of the recycled aniline stream.

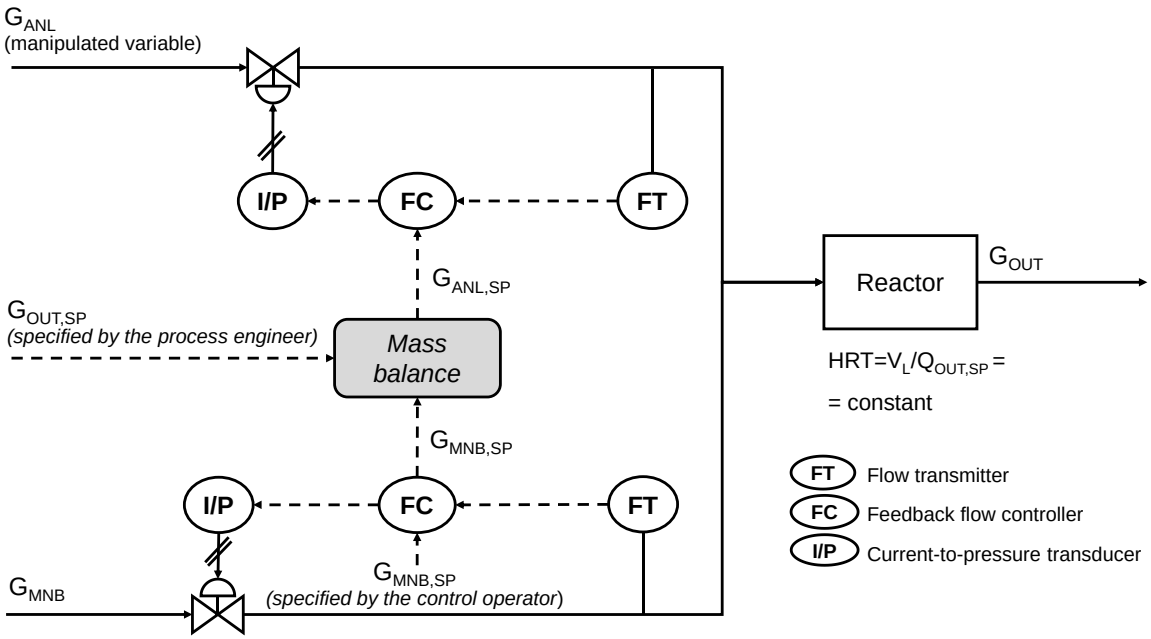

Figure 4.23 – Control scheme of the reactor outflow.

Figure 4.24 shows the behaviour of the system before and after the implementation of the control strategy presented previously. The initial date represented here (day 630) corresponds to the restart of the industrial plant that followed a cleaning procedure performed on the internals of the industrial reactor. From days 630 to 680, the industrial reactor was fed with only F2-based catalyst, noticing that the catalyst concentration had increased up to 0.05 a.u. Although the catalyst concentration responded favourably towards the catalyst make-ups performed, the measured values of the nitrobenzene bulk concentration did not stabilise in the same period. On the other hand, an improvement on the reaction conversion was verified after day 680, with the implementation of the HRT control of the industrial reactor; in this case, the value of 0.50 a.u. to the reactor outflow, $\mathrm{G_{out,SP}}$, was established as the minimal value that ensures the homogenisation of the reaction mixture. As expected, HRT control provides a constant reactor outflow, irrespective of the modifications performed on the regime of the nitrobenzene flow, through a proper manipulation of the recycled aniline flowrate.

The stabilisation of the nitrobenzene concentration values also justified the absence of further catalyst make-ups 10 days after the HRT control was implemented. Note that this catalyst addition policy maintained the same blend composition (F2), providing a further increase of the catalyst concentration up to 0.10 a.u., which was held constant from days

690 to 730. This behaviour of the catalyst concentration coincided with the steadiness of the overall heat transfer coefficient at around 0.40 a.u., suggesting that the deposition of catalyst in the internals of the reactor was not likely promoted.

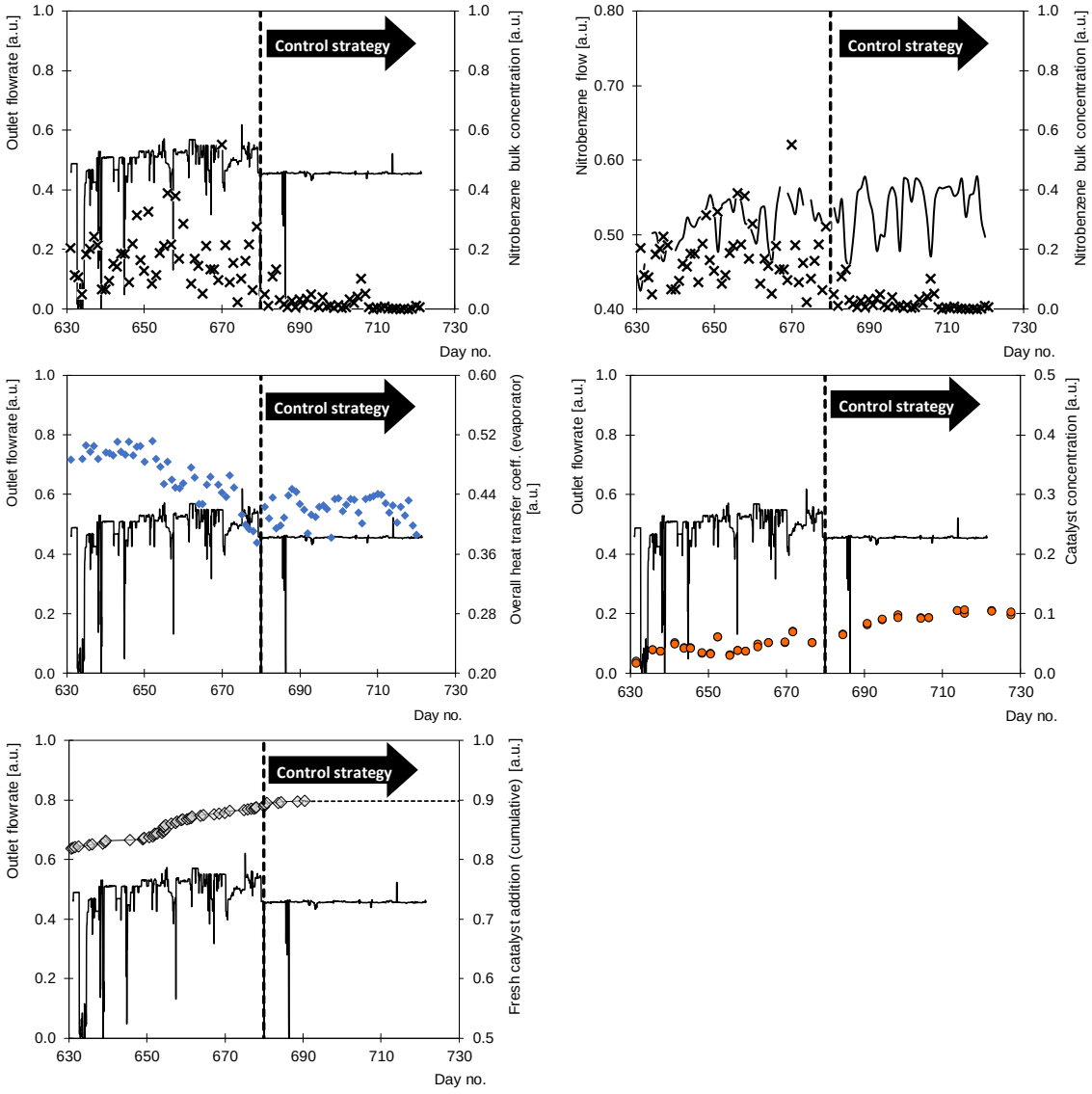

Figure 4.24 – Behaviour of the system before and after the control of the hydraulic retention time of the industrial reactor (── system outflow, ✕ nitrobenzene bulk concentration, ◆ heat transfer coefficient (bundle tubes), -◇- cumulative of fresh catalyst addition, and ● catalyst concentration).

Since the implementation of the HRT control strategy and the stabilisation of the catalyst concentration occurred simultaneously, it is not possible to conclude which of these

actions provided a greater impact on the improvement of the reaction conversion. Nevertheless, it should be noted that the stabilisation of the process operation here evidenced is crucial for the development of the statistical control of the industrial reactor by promoting better data acquisition conditions to upgrade the statistical control limits. This way, the detection of assignable causes affecting the model predictability can be improved.

Once the possibility of controlling the hydraulic retention time in the industrial reactor is confirmed, the process model developed also becomes useful in the future in optimising this variable towards the new operating conditions that maximises the productivity in the reaction vessel. By combining this with the preventive maintenance ensured by statistical control, process supervision should be promoted in the industrial routine.

Next, a procedure for process monitoring and control is advanced. This highlights several recommendations to apply to the industrial practice, based on the major findings obtained in the present investigation concerning the process understanding.

4.6 Procedure for integrating process monitoring and control

In this investigation several improvements on the operation of liquid-phase hydrogenation units were provided including:

- the highlight of catalyst concentration as a key process variable
- the highlight of planning of shutdown periods in the industrial reactor based on the evaluation of the overall heat coefficient.
- the manipulation of the blend composition of fresh catalyst in the industrial unit to promote a better control of the catalyst concentration
- the establishment of a control chart for process monitoring based on the process model developed. This way, a predictive tool is provided, allowing a better detection of disturbances affecting the reactor operation
- the control of the hydraulic retention time of the industrial reactor to improve the steadiness of the operation, and, in turn, the nitrobenzene conversion

Given the advances regarding the improvement of the industrial unit, a procedure for the industrial practice is proposed, combining both process monitoring and control (see Figure 2.25).

In this procedure, the process model has an important role, receiving the process/quality data, from which the deviation between the predicted and measured values of nitrobenzene bulk concentration is determined and, in turn, compiled into the monitoring control chart; here, an evaluation of the model predictability is performed. Once the statistical control of the process is confirmed, the predicted nitrobenzene bulk concentration should be compared to the corresponding recommended value – if predicted value is below the recommended value, no corrective measures are needed, considering the operating conditions applied.

If the nitrobenzene bulk concentration value surpasses the recommended value, the reactor outflow applied should be compared to the minimum value defined (0.50 a.u.) in the HRT control strategy applied. If the reactor outflow is above 0.50 a.u., this means that the hydraulic retention time can be increased to improve the nitrobenzene conversion.

The corrective measure of reducing the reactor outflow is also advised when the reactor is not under statistical control. In this case, it is assumed that the mass transfer of nitrobenzene may no longer support the current HRT used in the industrial reactor. Therefore, instead of performing a catalyst make-up immediately, the HRT can be first increased by reducing the setpoint of the reactor outflow. According to previous studies [111] [112], catalyst selectivity towards aniline is promoted with the catalyst lifetime. By doing this, unnecessary catalyst make-ups can be avoided, reducing not only the raw-material costs, but also the processing costs related to the content of secondary compounds that need to be separated from the reaction mixture.

If the reactor outflow cannot be longer reduced, the catalyst concentration should be checked by comparing the measured value with the recommended catalyst concentration based on the sensitivity analysis of the process model. If the measured catalyst concentration is above the minimum value recommended, a new catalyst make-up is advised to ensure the maintenance of the catalyst specific area for mass transfer. On the other hand, if the catalyst concentration is too low, the overall heat transfer coefficient should be first verified. This step should be supported with a new control chart, where the statistical control limits of the overall heat transfer coefficient should be defined in advance. If this variable is under statistical control, a new catalyst make-up should be also performed,

with the purpose of increasing the catalyst specific area and, in turn, the mass transfer of nitrobenzene catalyst to the catalyst surface. If the overall heat transfer coefficient is not under statistical control, catalyst deposition is pointed as significant. Under these conditions, the planning of the shutdown of the industrial unit for cleaning and removal of the catalyst deposits in the internals of the equipment is recommended.

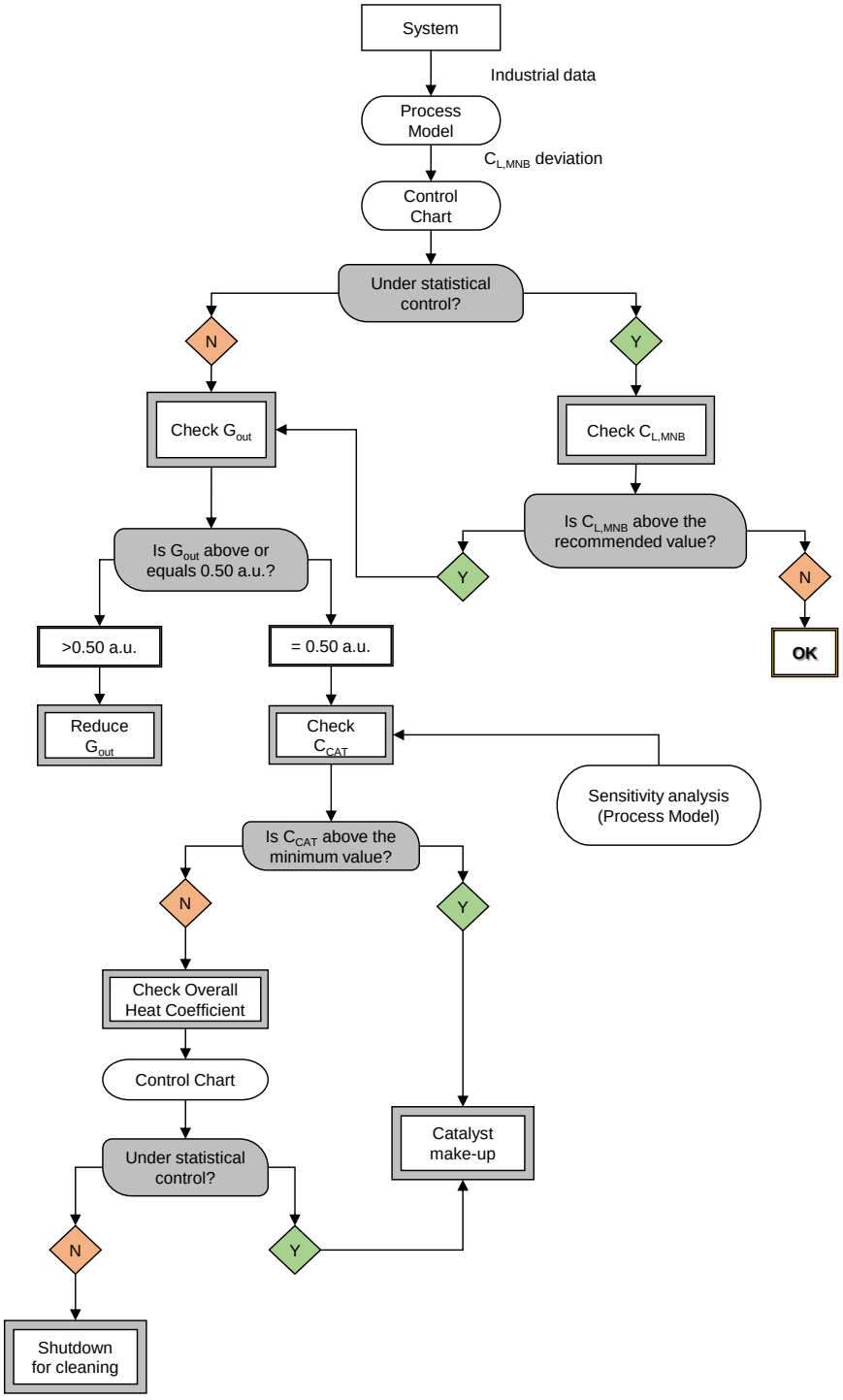

Figure 4.25 – Procedure for process monitoring and control.

5. Conclusions and Future Work

During this research, significant developments were provided regarding the process understanding of the industrial hydrogenators used for aniline manufacturing at Bondalti Chemicals. This was accomplished by combining the scientific insights attained in previous laboratorial studies with the industrial knowledge shared in-field during the timeline of this project. Overall, the obtained outcomes include:

- the correlation of the industrial reaction rate based on process data gathered under specific features of the catalyst management. This mathematical procedure can be updated towards new sample data sets to improve the continuous improvement of the catalyst utilisation.
- a mechanistic model of the industrial reactor able to predict the reaction conversion under a given operating window.
- the highlight of catalyst concentration as a key process variable for process monitoring.
- the improvement of the laboratorial method to determine the catalyst concentration in the Laboratory of Quality Control
- the stabilisation of the catalyst concentration in the reaction unit by improving the blend composition of the fresh catalyst used in the productive process. This was accomplished by performing several characterisation analyses on fresh and used catalyst samples.
- a detailed monitoring tool for the industrial operation based on the process model developed
- the stabilisation of the reaction conversion through the control of the hydraulic retention time of the industrial reactor.

Regarding the modelling of the industrial reactor, a mechanistic approach was adopted to predict the related physico-chemical properties, mass transfer coefficients and hydrodynamic parameters. To obtain a reliable prediction of the reaction rate, different kinetic studies developed at the laboratorial scale of liquid-phase nitrobenzene hydrogenation were first evaluated. By comparing these studies under the comparable ranges of temperature and of nitrobenzene liquid concentrations, it was possible to confirm that mass transfer of nitrobenzene limits the reaction rate. Because of this, the same was also pointed at the industrial scale. To confirm this, the predicted values of the liquid-solid mass transfer coefficient of nitrobenzene at the laboratorial and industrial scales were compared, together with the estimated value correlated with industrial data, while considering the specific area measured in catalyst sample withdrawn from the system. A reasonable similarity between the predicted and estimated values of the liquid-solid mass transfer coefficient of nitrobenzene, corroborating the significance of mass transfer limitations in the present industrial unit. By these means, the system productivity should involve the enhancement of the physical properties of the catalyst (e.g., particle size distribution and density) to potentiate the mass transfer of the limiting reactant. To accomplish this, the steadiness of the catalyst suspension is essential to ensure the specific area of the catalyst for mass transfer.

From an industrial standpoint, the measurement of the nitrobenzene bulk concentration in the reactor outlet stream represents a key indicator of the reaction performance. Given this, the model validation was carried comparing the predicted and measured values of the nitrobenzene bulk concentration verified during an extensive observation period. It was possible to observe that the model could readily predict the reaction conversion when a high and stabilised catalyst concentrations are observed, alongside with moderate addition of fresh catalyst and constant blend composition. In contrast, a higher mismatch between the predicted and measured values of nitrobenzene bulk concentration is obtained when significant modifications to the catalyst utilisation are performed.

Due to the importance of the catalyst utilisation on the overall performance, a characterisation study of the catalytic material was performed to describe the physico-chemical alterations during its lifetime in the industrial unit. In general, the suspended catalyst particles in the reaction vessel exhibit a greater nickel fraction when compared to the fresh catalysts. In contrast, the catalyst fines in the decanter outlet stream presented a smaller nickel content, in comparison with the suspended catalyst in the reaction vessel.

Thus, the nickel enrichment of the catalyst particles inside the reactor appears to be promoted with time.

During this investigation, samples of solid deposits found the internals of the industrial reactor were collected during a maintenance procedure. By characterising this material, a higher nickel content (especially in the crystalline form), lesser fraction of silicon and no traces of aluminium (attributed to the catalyst support formulation) were detected, in comparison with the remaining samples of fresh and used catalysts studied. The inexistence of aluminium on the solid deposits indicates that this material was subjected to a greater attrition than the suspended catalyst in the reaction vessel. The predominance of crystalline nickel on the solid deposits led to assume that its deposition/accumulation could be derived from a magnetic property. Therefore, several magnetic measurements were performed, confirming that this material presents a greater resistance towards demagnetisation (coercivity), in comparison with the suspended catalyst and the fresh catalysts. The coercivity of the deposited material was found to be above the critical point from which a given material is described as a *permanent magnet*. Therefore, it is plausible that the gaining coercivity in the catalyst with time may ultimately promote its deposition and accumulation in the reactor, and thereby inhibiting the accessibility of the reaction mixture to the active sites.

The detection of the solid deposits was followed by specific period of observation, where the catalyst concentration had decreased significantly, irrespective of the addition of fresh catalyst. During the same timeframe, the nitrobenzene conversion did not stabilise, while a performance decay of the heat exchanging devices was also observed. This sequence of events suggests that the accumulation of catalyst can promote serious implications in the reaction vessel. By assessing the catalyst management policy applied during the given period, only catalyst F1 was applied to the system. For that reason, additional magnetic measurements were performed on several batches of fresh catalyst, where the most recent batches of F1 showed a greater coercivity, in comparison with the old batches utilised in the process. On the other hand, the coercivity of F2 batches utilised by the company remained low and unaltered in the same timeframe. This result suggests that the operating conditions employed during the preparation of F1 were recently altered by the manufacturer, despite F1 and F2 catalysts agreeing with the technical specifications required by the company.

After the abovementioned period, the industrial reactor was shut down and the corresponding internals were properly cleaned, including the removal of the solid deposits. Given the lower coercivity of F2, in comparison with F1, only the F2 was added to the system thereinafter. It was possible to observe that the catalyst concentration values increased progressively and remained stabilised afterwards.

Since the catalyst utilisation can affect the model predictability, a statistical control of the industrial reactor was developed based on the model developed. Here, the statistical tolerance was defined based on the validated data. By doing this, the process diagnosis and preventive maintenance of the catalyst utilisation are enhanced. This solution provides a way of reducing the catalyst consumption, together with of the maintenance costs related to the system shutdowns caused by the catalyst deposition in the internals of the equipment.

In addition, the steadiness of the reaction conversion was also regarded by improving the regulatory control system. The strategy applied involved the control of the hydraulic retention time through a proper manipulation of the feed flowrate of recycled aniline. This was accomplished by defining the set-point of the aniline flowrate based on a mass balance between the set point values of the reactor outflow and of the nitrobenzene flowrate. After applying this strategy, the reduction and steadiness of the nitrobenzene bulk concentration is confirmed, which justified the decrease of fresh catalyst make-ups. It should be noted that this control solution was combined with an improved blend composition of the fresh catalyst. By ensuring the steadiness of the reaction conversion, the continuous improvement of the industrial unit is provided by promoting better conditions to gather new sample data sets to upgrade the process monitoring charts.

Finally, a procedure for process monitoring and control was proposed which combined the set of improvements advanced in the present work. This procedure involves the use of the statistical control chart based on the process model, together with a set of corrective measures to keep the model predictability under the defined tolerance. In case of in-control scenario, these corrective measures are only advised if the predicted nitrobenzene concentration remains above the recommended value. Under these conditions, the hydraulic retention time (HRT) can be readjusted to prevent unnecessary catalyst make-ups. This measure is also advised when an out-control state of the former control chart is verified. If the HRT control solution cannot ensure the reduction of the nitrobenzene concentration, nor an adequate prediction of the same variable by the process model, the catalyst state needs to be revised. If the measured catalyst concentration agrees

with the desired range provided by the sensitivity analysis of the model developed, a catalyst make-up is advised to ensure the mass transfer of nitrobenzene. If the catalyst concentration is below the desired range, the performance of the heat exchanging devices should be evaluated. This assessment can be provided with a new control chart to confirm whether catalyst deposition is or not likely occurring. If the heat exchanging devices reveal a good performance, catalyst make-ups should be performed to enhance the mass transfer of nitrobenzene. On the other hand, if a significant reduction of the heat transfer is confirmed, the shutdown of the industrial unit should be timetabled for cleaning procedures.

As future work, the collection and analysis of wider sample data sets from the process operation is recommended. This information should support the robustness of the model predictions, including not only the main reaction, but also the formation of secondary compounds. To accomplish this, each sample data set should be gathered under defined features of the catalyst utilisation in the productive process, namely the rate addition and blend composition of fresh catalyst. By doing this, the process monitoring charts can be further improved by defining refined statistical tolerances to specific features of the catalyst utilisation policy. This continuous improvement can be extended to the other reactors currently used in the industrial aniline manufacturing process of Bondalti to provide an optimised network of the reaction stage.

Furthermore, the dynamic behaviour of the process variables should be also considered in the same modelling studies. This way, advanced control strategies can be developed to optimise the set-points of the process variables (i.e. model predictive control). This way, an improved upper layer for process supervision can be provided to manage the regulatory control system already installed.

Bibliography

[1] J. C. Michaelson, “Aniline in history and technology,” *Endeavour,* vol. 17, no. 3, pp. 121-126, 1993.

[2] A. S. Travis, "Anilines: Historical background," in *Chemistry of Anilines*, West Sussex (United Kingdom), John Wiley & Sons, 2007, pp. 1-75.

[3] Imarc, “Aniline market: Global Industry Trends, Share, Size, Growth, Opportunity and Forecast (2018-2023),” IMARC Services Privated Limited, 2018.

[4] Technavio, “Global aniline market 2015-19,” 2015.

[5] IHS Markit, “CEH: Aniline,” 2017.

[6] Mordor Intelligence, “Aniline Market - Segmented by Application, End-user Industry, and Geography - Growth, Trends, and Forecast (2019-2024),” Mordor Intelligence, 2018.

[7] A. Afshar , “Chemical Profile: Aniline,” TranTech Consultants Inc, Westernville (EUA), 2014.

[8] A. S. Travis, “Manufacture and uses of the anilines: A vast array of processes and products,” in *The Chemistry of Anilines Part 1*, Jerusalem (Israel), Wiley, 2007, pp. 717-721.

[9] G. R. Maxwell, “Synthetic nitrogen products,” in *Kent and Riegel's Handbook of Industrial Chemistry and Biotechnology*, New York (USA), Springer Science+Business Media, 2007, p. 1073.

[10] T. Kahl, K. -W. Schröder, F. R. Lawrence, W. J. Marshall, H. Höke and R. Jäckh, “Aniline,” in *Ullmann's Encyclopedia of Industrial Chemistry*, Weinheim (Germany), Wiley-VCH, 2012, pp. 465-478.

[11] O. C. Karkalits, C. M. Plainfield, B. Vanderwaart and F. H. Megson, “New Catalyst for Reducing Nitrobenzene and the Process of Reducing Nitrobenzene thereover”. New York (USA) Patent US 2891094, 1955.

[12] H. Sperber, G. Poehler, H. J. Pistor and A. Wegerich, “Production of Aniline”. Ludwigshafen (Germany) Patent US 3136818, 1964.

[13] L. Seidemann, L. Koenigsmann, C. Scheneider, E. Schwab, D. Stuetzer and D. Liekens, “Process for Preparing Aromatic Amines in a Fluidized-Bed Reactor”. Ludwigshafen (Germany) Patent US 8044244 B2, 2011.

[14] S. Haase, D. Kadijevic, A. Merten, M. Zoellinger, A. Raichle, A. Schocker, S. Mühlbeyer, O. Wiedenhoff and J. C. Tsou, “Process for preparing aromatic amines”. Ludwigshafen (Germany) Patent US 2012/0215029 A1, 2012.

[15] K. Sommer, K. Wilke, P. Lehner, F. Gehlen, L. Mleczho, S. Schubert, E. Hizaler and E. Hoffman, “Process for the preperation of aromatic amines”. Leverkusen (Germany) Patent US 2010/0280271 A1, 2010.

[16] L. Szigeth, “Method for the Catalytic Hydrogenation of Organic Nitro Derivatives in the Gaseous State to Corresponding Anilines”. Basel (Switzerland) Patent US 3636152, 1972.

[17] M. Dugal, F. Von Gehlen, S. Wershofen, A. Lago, P. Lehner and B. Marotz, “Process for Preparing Aniline”. Leverkusen (Germany) Patent US 7692042 B2, 2010.

[18] R. Langer, H. J. Buysch, P. Wagner and U. Pentling, “Process for Producing Aromatic Amines”. Leverkusen (Germany) Patent US 5808157, 1998.

[19] C. J. Mitchell and D. H. Stewart, “Process for the conversion of aromatic nitro compounds into amines”. The Woodlands (USA) Patent US 9533939 B2, 2017.

[20] E. V. Cooke and H. J. Thurlow, “Catalytic Hydrogenation od Nitro Aromatic Compounds to Produce the Correponding Amino Compounds”. London (United Kingdom) Patent US 3270057, 1966.

[21] F. R. Lawrence, “Process for Preparing Aniline”. Wilmington (USA) Patent US 4415754, 1983.

[22] T. Nagata, K. Watanabe, Y. Kono, A. Tamaki and T. Kobayashi, “Process for Preparing High-Purity Aniline”. Tokyo (Japan) Patent US 5616806, 1997.

[23] F. Neves, “Modelling and Optimization of Large-Scale Processes: Application to the Liquid-phase aniline production (PhD Thesis),” Coimbra University, Coimbra (Portugal), 2007.

[24] W. H. Williams, R. D. Holmes, A. H. Widiger and M. Mich, “Method for production of aromatic amines”. Delaware (USA) Patent US 2432552, 1947.

[25] D. G. Jones and N. J. Cherry Hill, “Production of aromatic amines by ammonolysis”. New York (USA) Patent US 3231616, 1966.

[26] W. Prahl and W. Mathes, “Manufacture of aniline from chlorobenzene and ammonia”. Ludwigshafen-on-the-Rhine (Germany) Patent US 2001284A, 1935.

[27] N. K. Kochar and B. J. Ozero, “Coproduction of Aniline and Diphenylamine”. New York (USA) Patent US 4404399, 1983.

[28] M. Yasuhara and F. Matsunaga, “Preparation of Anilines”. Tokyo (Japan) Patent US 4987260, 1991.

[29] T. W. Del Peso, “Sythesis of aromatic amines by reaction compounds with ammonia”. Wilmington (USA) Patent US 4001260, 1977.

[30] D. M. Poojary, R. Borade, A. Hagemeyer, X. P. Zhou, C. E. Dube, U. Notheis, R. Armbrust, C. Rasp and D. M. Lowe, “Amination of aromatic hydrocarbons and heterocyclic analogs thereof”. Santa Clara (USA) and Leverkusen (Germany) Patent US 6933409 B1, 2005.

[31] F. V. Laar, E. Schwab, H. Voss, J. Anders, S. Crone and W. Mackenroth, “Direct hydrocarbon amination”. Ludwigshafen (Germany) Patent US 20090203941 A1, 2009.

[32] A. Mendes, A. Ribeiro, M. Catarino, A. Felix and M. Pinho, “Electrodes/electrolyte assembly, reactor and method for direct amination of hydrocarbons”. Estarreja (Portugal) Patent US 20160032469 A1, 2016.

[33] NetComposites Ltd., “Covestro Develops Bio-Based Aniline,” in *EcoComp 2019 - Composites for a Better Environment*, Conventry (United Kingdom), 2018.

[34] C. H. Bartholomew and R. J. Farrauto, “Hydrogenation and Dehydrogenation of Organic Compounds,” in *Fundamentals of Industrial Catalytic Processes*, New Jersey (USA), John Wiley & Sons, 2006, pp. 487-559.

[35] C. H. Bartholomew and R. J. Farrauto, "Catalyst deactivation: Causes, mechanisms, and treatment," in *Fundamentals of Industrials Catalytic Processes*, New Jersey (EUA), John Wiley & Sons, Inc., 2006, pp. 312-314.

[36] M. Baerns and G. Boskovic, "Catalyst deactivation," in *Basic principles in applied catalysis*, Berlin (Germany), Springer-Verlag, 2004, pp. 477-503.

[37] W. Himmelsbach, W. Keller, M. Lovallo, T. Grebe and D. Houlton, “Increase production through better gas-liquid mixing,” *Chemical Engineering,* vol. 114, no. 10, pp. 50-73, 2007.

[38] V. V. Buwa, S. Roy and V. V. Ranade, “Three-phase slurry reactors,” in *Multiphase Catalytic Reactors: Theory, Design, Manufacturing, and Applications*, New Jersey, Wiley, 2016, pp. 132-153.

[39] K. Conway, A. Kyle and C. D. Rielly, “Gas-Liquid-Solid Operation of a Vortex-Ingesting Stirred Tank Reactor,” *Chemical Engineering Research and Design,* vol. 80, no. 8, pp. 839-845, 2002.

[40] V. G. Pangarkar, “Gas-Inducing Reactors,” in *Design of Multiphase Reactors*, Mumbai (India), John Wiley & Sons, 2015, pp. 407-450.

[41] L. Alheritiere, G. Gobron, C. Falize, J. Diet, B. Roux and R. Bouchet, “Process for carrying out chemical reactions in heterogeneous medium”. Paris (France) Patent US3895065A, 1973.

[42] J. D. Seader, E. J. Henley and D. K. Roper, “Mass Transfer and Diffusion,” in *Separation Process Principles. Chemical and Biochemical Operations*, USA, John Wiley and Sons, Inc., 2011, p. 123.

[43] I. Houson, “Scale-up of Chemical Reactions,” in *Process Understanding*, Weinheim (Germany), Wiley-VCH, 2011, pp. 155-198.

[44] V. G. Pangarkar, “Principles of similarity and their application for scale-up of multiphase reactors,” in *Design of Multiphase Reactors*, New Jersey (USA), Wiley, 2015, pp. 93-104.

[45] N. Froessling, “Uber die Verdunstung fallender Tropfen,” *Gerlands Gerlands Beitrage zur Geophysik,* vol. 52, pp. 170-175, 1938.

[46] W. E. Ranz and W. R. Marshall, “Evaporation from drops (Part I),” *Chemical Engineering and Processing,* vol. 48, no. 3, pp. 141-146, 1952.

[47] W. E. Ranz and W. R. Marshall, “Evaporation from drops,” *Chemical Engineering and Processing,* vol. 4, no. 173-180, p. 48, 1952.

[48] A. N. Kolmogorov, “The local structure of turbulence in incompressible viscous fluids at very large Reynolds numbers,” *Doklady Akademiia Nauk SSSR ,* vol. 30, pp. 301-305, 1941.

[49] J. O. Hinze, Turbulence, 2nd ed., New York (USA): McGraw-Hill, 1975, pp. 460-471.

[50] M. F. Edwards and M. R. Baker, “Mixing of liquids in stirred tanks,” in *Mixing in the process industries*, Butterworth Heinemann, 1992, p. 137.

[51] Y. Zhu and J. Wu, “Critical Impeller Speed for Suspending Solids in Aerated Agitation Tanks,” *The Canadian Journal of Chemical Engineering,* vol. 80, no. 4, pp. 1-6, 2008.

[52] J. M. Smith , K. Van't Riet and J. C. Middleton , “Scale-up of agited gas-liquid reators for mass transfer,” in *Proceedings of Second European Conference on Mixing*, Cambridge (United Kingdom), 1977.

[53] K. Van't Riet, “Review of Measuring Methods and Results in Nonviscous Gas-Liquid Mass Transfer in Stirred Vessels,” *Industrial &*

Engineering Chemistry Process Design and Development, vol. 18, no. 3, pp. 357-364, 1979.

[54] V. Linek, V. Vacek and P. Benes, “A critical review and experimental verification of the correct use of the dynamic method for the determination of oxygen transfer in aerated agitated vessels to water, electrolyte solutions and viscous liquids,” *The Chemical Engineering Journal,* vol. 34, no. 1, pp. 11-34, 1987.

[55] A. D. Hickman, “Gas-liquid oxygen transfer and scale-up: a novel experimental technique with results from mass transfer in aerated agitated vessels,” in *Proceedings of Sixth European Conference on Mixing*, Pavia (Italy), 1988.

[56] J. M. Smith, “Simple performance correlations for agitated vessels,” in *Proceedings of Seventh European Conference on Mixing*, Brugge (Belgium), 1991.

[57] M. J. Whitton and A. W. Nienow, “Scale up correlations for gas hold up and mass transfer coefficients in stirred tank reactors,” in *Proceedings of Third International Conference on Bioreactor and Bioprocesses Fluid Dynamics*, Cambridge (United Kingdom), 1993.

[58] Y. Zhu, P. C. Bandopadhayay and J. Wu, “Measurement of Gas-Liquid Mass Transfer in an Agitated Vessel. A Comparison between Different Impellers,” *Journal of Chemical Engineering of Japan,* vol. 34, no. 5, pp. 579-584, 2001.

[59] D. M. Levins and J. R. Glastonbury, “Application of Kolmogorov's Theory to Particle-Liquid Mass Transfer in Agitated Vessels,” *Chemistry and Engineering Science,* vol. 27, p. 537, 1972.

[60] A. W. Nienow and D. Miles, “The effect of Impeller/Tank Configuration on Fluid-Particle Mass Transfer,” *Journal of Chemical Engineering,* vol. 15, p. 13, 1978.

[61] K. R. Screenivasan , “Fluid Turbulence,” *Reviews of Modern Physics,* vol. 71, no. 2, pp. 383-395, 1999.

[62] P. H. Calderbank and M. B. Moo-Young, “The continuous phase heat and mass transfer properties of dispersions,” *Chemical Engineering Science,* vol. 16, no. 1-2, pp. 39-54, 1961.

[63] P. Harriot, “Mass transfer to particles. Part I. Suspended in agitated vessels.,” *American Institute of Chemical Engineers,* vol. 8, no. 1, pp. 372-380, 1962.

[64] P. Harriot, “A random eddy modification of the penetration theory,” *Chemical Engineering Science,* vol. 17, no. 3, pp. 149-154, 1962.

[65] A. W. Nienow, “Dissolution Mass Transfer in a Turbine Agitated Baffled Vessel,” *The Canadian Journal of Chemical Engineering,* vol. 47, no. 3, pp. 248-258, 1969.

[66] R. Kuboi, I. Komasawa, T. Ohtake and M. Iwasa, “Fluid and Particle Motion in Turbulent Dispersion. Part III. Particle-Liquid HYdrodynamics and Mass Transfer in Turbulent Dispersion,” *Chemical Engineering Science,* vol. 29, no. 3, pp. 659-668, 1974.

[67] V. G. Pangarkar, A. A. Yamalkar, M. M. Sharma and A. A. C. M. Beenackers, “Particle-Liquid Mass Transfer Coefficient in Two/Three-Phase Stirred Tank Reactors,” *Industrial & Engineering Chemistry Research,* vol. 41, no. 17, pp. 4141-4167, 2002.

[68] R. B. Keey and J. B. Glen, “Mass transfer from solid spheres,” *The Canadian Journal of Chemical Engineering,* vol. 42, no. 5, pp. 227-232, 1964.

[69] G. A. Hughmark, “Hydrodynamics and Mass Transfer for Suspended Solid Particles in a Turbulent Liquid,” *American Institute of Chemical Engineers,* vol. 20, no. 1, pp. 202-204, 1974.

[70] S. V. Jadhav and V. G. Pangarkar, “Particle-liquid mass transfer in mechanically agitated contactors,” *Industrial & Engineering Chemistry Research,* vol. 30, no. 11, pp. 296-2503, 1991.

[71] K. B. Kushalkar and V. G. Pangarkar , “Particle-liquid mass transfer in mechanically agitated three phase reactors,” *Industrial & Engineering Chemistry Research,* vol. 33, no. 7, pp. 1817-1820, 1994.

[72] K. B. Kushalkar and V. G. Pangarkar, “Particle-Liquid Mass Transfer in Three-Phase Mechanically Agitated Contactors: Power Law Fluids,” *Industrial & Engineering Chemistry Research,* vol. 34, no. 7, pp. 2486-2492, 1995.

[73] N. N. Dutta and V. G. Pangarkar, “Critical impeller speed for solid suspension in Multi-Impeller Agitated Three Phase Agitated Contactors,” *The Canadian Journal of Chemical Engineering,* vol. 73, no. 3, pp. 273-283, 1995.

[74] A. A. Yawalkar, B. M. Heesink, G. T. Versteeg and V. G. Pangarkar, “Gas-Liquid Mass Transfer Coefficient in Stirred Tank Reactors,” *The Canadian Journal of Chemical Engineering,* vol. 80, no. 5, pp. 840-848, 2002.

[75] D. M. Levins and J. R. Glastonbury, “Application of Kolmogoroff's Theory to Particle-Liquid Mass Transfer in Agitated Vessels,” *Chemistry and Engineering Science,* vol. 27, p. 537, 1972.

[76] V. G. Pangarkar, “Stirred Tank Reactors for Chemical Reactions,” in *Design of multiphase reactors*, New Jersey (USA), Wiley, 2015, p. 154.

[77] J. B. Joshi and M. M. Sharma, “Mass transfer ans hydrodynamic chracteristics of gas inducing type of agitated contactors,” *The Canadian Journal of Chemical Engineering,* vol. 65, pp. 683-695, 1977.

[78] S. B. Sawant and J. B. Joshi, “Critical impeller speed for the onset of gas induction in gas-inducing tyes of agitated contactors,” *Chemical Engineering Journal,* vol. 18, pp. 87-91, 1979.

[79] K. Saravanan, V. D. Mundale and J. B. Joshi, “Gas inducing type mechanically agitated contactors,” *Industrial & Engineering Chemical Research,* vol. 33, pp. 2226-2241, 1994.

[80] G. M. Evans, C. D. Rielly, J. F. Davidson and K. J. Carpenter, “A fundamental study of gas inducing impeller design,” in *Institution of chemical engineers sysmposium series*, Rugby (United Kingdom), 1990.

[81] G. M. Evans, C. D. Rielly, J. F. Davidson and K. J. Carpenter, “Hydrodynamic characteristics of gas inducing impeller,” in *Proceedings of the Seventh European conference on mixing IV*, Brugge (Belgium), 1991.

[82] K. Saravanan and J. B. Joshi, “Gas-Inducing-Type Mechanically Agitated Contactors: Hydrodynamic Characteristics of Multiple Impellers,” *Industrial & Engineering Chemistry Research,* vol. 34, no. 7, pp. 2499-2514, 1995.

[83] S. Poncin, C. Nguyen, N. Midoux and J. Breysse, “Hydrodynamics and volumetric gas-liquid mass transfer coefficient of a stirred vessel equipped with a gas-induncing impeller,” *Chemical Engineerig Science,* vol. 57, no. 16, pp. 3299-3306, 2002.

[84] A. W. Nienow, D. J. Wisdom and J. C. Middleton, “The effect of scate and geometry on flooding, recirculation, and power in gassed stirred vessels,” in *Proceedings of Second European Conference on Mixing*, Cambridge (United Kingdom), 1977.

[85] T. N. Zwietering, “Suspending of solid particles in liquid by agitators,” *Chemical Engineering Science,* vol. 8, pp. 244-258, 1958.

[86] A. W. Nienow, “The suspension of solid particles,” in *Mixing in the Process Industries*, Oxford (United Kingdom), Butterworth Heinemann, 1992, pp. 364-392.

[87] C. M. Chapman, A. W. Nienow , M. Cooke and J. C. Middleton, “Particle-gas-liquid mixing in stirred vessels (Part III) Three phase mixing,” *Chemical Engineering Research and Development,* vol. 61, no. 3, pp. 167-181, 1983.

[88] J. J. Frijlink, A. Bakker and J. M. Smith, “Suspension of Solid Particles with Gassed Impellers,” *Chemical Engineering Science,* vol. 45, no. 7, pp. 1703-1718, 1990.

[89] C. Buurman, G. Resoort and A. Plaschkes, “Scaling-up Rules of Solids Suspension in Stirred Vessels,” *Chemical Engineering Science,* vol. 41, no. 11, pp. 2865-2871, 1986.

[90] C. W. Wong, J. P. Wang and S. T. Huang, “Investigations of Fluid Dynamics in Mechanically Stirred Aerated Slurry Reactors,” *Canadian Journal of Chemical Engineering,* vol. 65, no. 3, pp. 412-419, 1987.

[91] W. Bujalski, M. Konno and A. W. Nienow, “Scale-up of 45º Pitch-Blade Agitators for Gas Dispersion and Solid Suspension,” in *6th European Conference on Mixing*, Pavia (Italy), 1988.

[92] G. Ranjan and A. S. R. Rao, Basic and Applied Soil Mechanics, 2nd ed., New Delhi (India): New Age International Ltd., 2000.

[93] V. B. Rawalkar, K. S. M. S. Raghava Rao and J. B. Joshi, “Critical speed from Solid Suspension in Mechanically Agitated Three-Phase Reactors: 1. Experimental Part,” *Industrial & Engineering Chemical Research,* vol. 30, no. 8, pp. 1770-1784, 1991.

[94] G. R. Drewer, N. Ahmed and G. J. Jameson, “Suspension of High Concentration of Solids in Mechanically Stirred Vessels,” in *Proceedings in 8th European Conference on Mixing*, Warwickshire (United Kingdom), 1994.

[95] S. Ibrahim and A. W. Nienow, “Particle suspension in Turbulent Regime: The Effect of Impeller Type and Impeller/Vessel Configuration,” *Institution of Chemical Engineers,* vol. 74, no. A6, pp. 679-688, 1996.

[96] P. R. K. Pantula and N. Ahmed, “Solids Suspension and Gas Holdup in Three Phase Mechanically Agitated Contactors,” in *Chemeca '98*, Queensland (Australia), 1998.

[97] K. J. Myers and A. Bakker, “Solids Suspension with Up-pumping Pitched-blade and High-efficiency Impellers,” *Canadian Journal of Chemical Engineering,* vol. 76, pp. 4233-4440, 1998.

[98] M. C. Lehn, K. J. Myers and A. Bakker, “Agitation Design for Solids Suspension under Gassed Conditions,” *The Canadian Journal of Chemical Engieneering,* vol. 77, no. 5, pp. 1065-1071, 1999.

[99] M. Greaves and M. Barigou, “Estimation of Gas Hold-up and Impeller Power in a Stirred Vessel Reactor,” *Fluid Mixing,* vol. 108, pp. 235-255, 1988.

[100] V. G. Pangarkar, “Gas Holdup in Stirred Tanks,” in *Design of Multiphase Reactors*, New Jersey (USA), Wiley, 2015, pp. 155-165.

[101] A. A. Yamalkar, V. G. Pangarkar and A. A. C. M. Beenackers, “Gas Hold-up in Stirred Tank Reactors,” *The Canadian Journal of Chemical Engineering,* vol. 80, no. 1, pp. 158-166, 2002.

[102] F. Z. Haber, *Electrochemistry,* vol. 22, p. 506, 1898.

[103] H. D. Burge, D. J. Collins and B. H. Davis, “Intermediates in the Raney Nickel Catalized Hydrogenation of Nitrobenzene to Aniline,” *Industrial & Engineering Chemistry Product Reseach and Development,* vol. 19, no. 3, pp. 389-391, 1980.

[104] F. Figueras and B. Coq, “Hydrogenation and hydrogenolysis of nitro-, nitroso-, azo-, azoxy-, and other nitrogen-containing compounds on palladium,” *Journal of Molecular Catalysis A: Chemical,* vol. 173, no. 1-2, pp. 223-230, 2001.

[105] H. Debus and J. Jungers, “La cinétique quantitative en catalyse hétèrogéne. L'hydrogenation du nitrobenzene sur le nickel.,” *Bulletin de la Société Chimique de France,* p. 785, 1959.

[106] J. Wisniak and M. Klein, “Reduction of nitrobenzene to aniline,” *Industrial & Engineering Chemistry Product Research and Development,* vol. 23, no. 1, pp. 44-50, 1984.

[107] E. A. Gelder, S. D. Jackson and C. M. Lok, “The hydrogenation of nitrobenzene to aniline: a new mechanism,” *Chemical Communications,* pp. 522-524, 2005.

[108] S. Narayanan and R. Unnikrishnan, “Comparison of hydrogen adsorption and aniline hydrogenation over co-precipitated Co/Al2O3 and Ni/Al2O3 catalysts,” *Journal of the Chemical Society,* vol. 93, no. 10, pp. 2009-2013, 1997.

[109] M. Králik, M. Turákova, I. Macak and S. Wenchich, “Catalytic Hydrogenation of Aromatic Compounds in the Liquid Phase,” *Journal of Chemistry and Chemical Engineering,* vol. 6, no. 12, pp. 1074-1082, 2012.

[110] J. Relvas, “Modelação cinética da reação de hidrogenação do nitrobenzeno a anilina num reator trifásico industrial (PhD Thesis),” University of Lisbon (IST), Lisbon (Portugal), 2008.

[111] J. Sousa, “Intensificação da produção da anilina (PhD Thesis),” University of Lisbon (IST), Lisbon (Portugal), 2015.

[112] C. Sá Couto, “Impure Hydrogen Valorization for Chemicals Production in a Tubular Reactor (PhD Thesis),” Universidade do Porto (Faculdade de Engenharia), Porto (Portugal), 2016.

[113] F. Turek, R. Geike and R. Lange, “Liquid-phase hydrogenation of nitrobenzene in a slurry reactor,” *Chemical Engineering Processing,* vol. 20, pp. 213-219, 1986.

[114] F. Turek, R. Geike and R. Lange, “Problems Encountered in the Scale-up of a Gas-Liquid Reaction in a Stirred Reactor with Suspended Catalyst,” *The Chemical Engineering Journal,* vol. 36, no. 1, pp. 51-58, 1987.

[115] R. M. Machado, “Fundamentals of Mass Transfer ans Kinetics for the Hydrogenation of Nitrobenzene to Aniline,” *Air Products and Chemicals, Inc.,* vol. 1, pp. 1-14, 2007.

[116] G. Wegener, M. Brandt, L. Duda, J. Hofmann, B. Klesczewski, D. Koch, R. Kumpf, H. Orzesek, G. Pirkl, C. Six, C. Steinlein and M. Weisbeck, “Trends in industrial catalysis in the polyurethane industry,” *Applied Catalysis A: General,* vol. 221, no. 1-2, pp. 303-335, 2001.

[117] E. Klemm, B. Amon, H. Redlingshöfer and E. Dieterich, “Deactivation kinetics in the hydrogenation of nitrobenzene to aniline on the basis of a coke formation kinetics — investigations in an isothermal catalytic wall reactor,” *Chemical Engineering Science,* vol. 56, no. 4, pp. 1347-1353, 2001.

[118] J. Relvas, R. Andrade, F. G. Freire, F. Lemos, P. Araújo, M. J. Pinho, C. P. Nunes and F. R. Ribeiro, “Liquid-phase hydrogenation of nitrobenzene over an industrial Ni/SiO2 supported catalyst,” *Catalysis Today,* Vols. 133-135, pp. 828-835, 2008.

[119] S. -P. Lee and Y. -W. Chen, “Nitrobenzene hydrogenation on Ni-P, Ni-B and Ni-P-B ultrafine materials,” *Journal of Molecular Catalysis: Chemical,* vol. 152, no. 1-2, pp. 213-223, 2000.

[120] A. G. Boudjahem, S. Monteverdi, M. Mercy and M. M. Bettahar, “Study of nickel catalysts supported on silica of low surface area and prepared by reduction of nickel acetate in aqueous hydrazine,” *Journal of Catalysis,* vol. 221, no. 2, pp. 325-334, 2004.

[121] P. A. Ramachandran and R. V. Chaudhari, Three phase catalytic reactors, New York (USA): Gordon & Breach Science Publishers Inc., 1983.

[122] O. Levenspiel, Chemical reaction engineering, New York (USA): John Wiley & Sons, 1999.

[123] R. M. Machado , “Increasing Productivity in Slurry Hydrogenation Processes,” Air Products, Allentown (EUA), 2013.

[124] F. P. Incorpera, D. P. Dewitt, T. L. Bergman and A. S. Lavine, “Introduction to Convection,” in *Fundamentals of heat and mass transfer*, Danvers (USA), John Wiley & Sons, 2007, pp. 347-400.

[125] D. G. Montgomery, Introduction to Statistical Quality Control, Arizona (USA): Wiley, 2013.

[126] H. S. Fogler, Elements of Chemical Reaction Engineering, New Jersey (USA): Prentice-Hall, 1992.

[127] C. H. Bartholomew and R. J. Farrauto, “Catalyst Characterization and Selection,” in *Fundamentals of Industrial Catalytic Processes*, New Jersey (USA), John Wiley & Sons, 2006, pp. 118-196.

[128] C. H. Bartholomew, “Mechanisms of Catalyst Deactivation,” *Applied Catalysis A: General,* vol. 212, no. 1-2, pp. 17-60, 2001.

[129] HORIBA Scientific, “A Guidebook to Particle Size Analysis,” HORIBA, Irvine (USA), 2012.

[130] J. L. Figueiredo and F. R. Ribeiro, Catálise Heterogénea, Lisbon (Portugal): Fundação Calouste Gulbenkian, 2007.

[131] H. Knözinger, “Temperature-Programmed Reduction and Oxidation,” in *Handbook of Heterogeneous Catalysis*, Weineheim (Germany), Wiley-VCH, 2008, pp. 1080-1096.

[132] B. Mile, D. Striling, M. A. Zammit, A. Lovell and M. Webb, “The Location of Nickel Oxide and Nickel in Silica-Supported Catalysts: Two Forms of "NiO" and the Assigment of Temperature-Programmed Reduction Profiles,” *Journal of Catalysis,* vol. 114, no. 2, pp. 217-229, 1988.

[133] B. M. Moskowitz, “Classes of Magnetic Materials,” in *Hichhiker's Guide to Magnetism*, University of Minnesota, Institute of Rock Magnetism, 1991, pp. 5-15.

[134] R. K. Nutor, X. Fan, S. Ren, M. Chen and Y. Fang, “Research Progress of Stress-Induced Magnetic Anisotropy in Fe-Based Amorphous and Nanocrystalline Alloys,” *Journal of Electromagnetic Analysis and Applications,* vol. 9, pp. 53-72, 2017.

[135] D. R. Askeland, P. P. Fulay and W. J. Wright, “Magnetic Materials,” in *The Science and Engineering of Materials*, Stamford (USA), CENGAGE Learning, 2010, pp. 767-798.

[136] W. D. Callister, “Magnetic properties,” in *Materials Science and Engineering*, York (United Kingdom), John Wiley & Sons, Inc., 2007, pp. 76-113.

[137] A. Akbarzadeh, M. Samiel and S. Davaran, “Magnetic nanoparticles: preparation, physical properties, and applications in biomedicine,” *Nanoscale research letter,* vol. 144, no. 7, 2012.

[138] J. I. Goldstein, D. E. Newbury, J. R. Michael, N. W. Ritchie, J. H. Scott and D. C. Joy, “Analysis of Specimens with Special Geometry: Irregular Bulk Objects and Particles,” in *Scanning Electron Microscopy and X-Ray Microanalysis*, New York (USA), Spinger, 2017, p. 407.

[139] D. A. Skoog, F. J. Holler and S. R. Crouch, Principles of Instrumental Analysis, Belmont (USA): Thomson, 2007.

[140] D. C. Harris, “Mass Spectroscopy,” in *Quantitative Chemical Analysis*, New York (USA), W. H. Freeman and Company, 2007, pp. 474-500.

[141] S. Espírito Santo, “Monitorização de Reatores Trifásicos (Master Thesis),” University of Coimbra, Coimbra (Portugal), 2018.

[142] A. R. Petosa, D. P. Jaisi, I. R. Quevedo, M. Elimelech and N. Tufenkji, “Aggregation and deposition of engineered nanomaterials in aquatic

environments: role of physicochemical interactions," *Enrironmental Science and Technology,* vol. 44, pp. 6532-6549, 2010.

[143] A. Raiche, S. Haase, H. Braunsberg, J. Buettner, U. Penzel and S. Neto, "Monitoring of the stiochiometric ratio in the reaction of nitroaromatics with hydrogen". Ludwigshafen (Germany) Patent US 8,895,783 B2, 2014.

[144] D. A. White and J. U. de Villiers, "Rates of induced areation in agitated vessels," *Chemical Engineering Journal,* vol. 14, no. 2, pp. 113-118, 1977.

[145] N. N. Hochgraf, L. C. Kenyon Jr. and A. W. Langer Jr., "Anti-fouling procedure". Delaware (USA) Patent US2908671, 1957.

[146] J. A. Shaw, "Statistical Process Contol for the Process Industries," *ISA Transactions,* vol. 30, no. 1, pp. 100-106, 1991.

[147] D. S. Moore, Statistical Process Control, New York (USA): W.H. Freeman and Company, 2007.

[148] Western Electric, Statistical Quality Control Handbook, Indianopolis (USA): Western Electric Corporation, 1956.

[149] H. C. V. Ness and M. M. Abbott, Classical Thermodynamics of Noneelectrolyte Solutions, New York (USA): McGraw-Hill, 1982.

[150] T. E. Daubert and R. P. Danner, Physical and Thermodynamic Properties of Pure Chemicals. Data Compilation. Part I, Taylor & Francis, 1994.

[151] R. L. Rowley, W. V. Wilding, J. L. Oscarson, Y. Yang, N. A. Zundel, T. E. Daubert and R. P. Danner, "Data Compilation of Pure Chemical Properties," *American Institute of Chemical Engineers,* 2007.

[152] C. R. Wilke and P. Chang, “Correlation of diffusion coefficients in dilute solutions,” *American Institute of Chemical Engineers ,* vol. 1, no. 2, pp. 264-280, 1955.

[153] L. R. Perkins and C. J. Geankoplis, “Molecular diffusion in a ternary liquid system with the diffusing component dilute,” *Chemical Engineering Science,* vol. 24, no. 7, pp. 1335-1042, 1969.

[154] H. Yu and Z. Tan, “New Correlations of Volumetric Liquid-Phase Mass Transfer Coefficients in Gas-Inducing Agitated Tank Reactors,” *International Journal of Chemical Engineering,* vol. 10, no. 1, pp. 1-33, 2012.

[155] B. A. Ogunnaike and W. H. Ray, “Introductory concepts of process control,” in *Process Dynamics, Modeling, and Control*, New York (USA), Oxford University Press, 1994, pp. 5-33.

[156] G. Roberts, Catalysis in Organic Synthesis, New York (USA): Academic Press and Engelhard Industries, 1976.

[157] W. G. Whitman, “The two film theory of gas absorption,” *International Journal of Heat and Mass Transport,* vol. 5, no. 5, pp. 429-433, 1962.

[158] F. A. A. Kingdom and N. Prins , “Model Comparisons,” in *Psychopsysics: A Practical Introduction*, Oxford (Unided Kingdom), Elsevier, 2010, pp. 209-255.

[159] M. Schwaab and J. C. Pinto, “Optimum reference temperature for reparametrization of the Arrhenius equation. Part 1: Problems involving one kinetic constant,” *Chemical Engineering Science,* vol. 62, no. 10, pp. 2750-2764, 2007.

[160] F. A. L. Dullien, “Microscopic Pore Strutures Parameters,” in *Porous Media: Fluid Transport and Pore Structure*, Dallas (USA), Academic Press, 1992, p. 73.

[161] Z. I. Önsan and A. K. Avci, “Microkinetic analysis of heterogenous catalytic systems,” in *Multiphase Catalytic Reactors: Theory, Design, Manufacturing, and Applications*, New Jersey (USA), John Wiley & Sons, Inc., 2016, pp. 17-79.

[162] S. M. Ross, Introductory Statistics, San Diego (USA): Elsevier, 2010.

[163] M. E. Davis and R. J. Davis, “Effects of Transport Limitations on Rates of Solid-Catalyzed Reactions,” in *Fundamentals of Chemical Reaction Engineering*, New York (USA), McGraw-Hill , 2003, p. 208.

[164] H. T. Horsfield, “The strenght of asphalt mixtures,” *Journal of the Society of Chemical Industry,* vol. 53, no. 9, pp. 107-115, 1934.

[165] R. J. Wijngaarden, A. Kronberg and K. R. Westerterp, “Catalysis and External Transfer,” in *Industrial Catalysis*, Weinheim (Germany), Wiley, 1998, p. 69.

[166] D. G. Montgomery and G. C. Runger, “Adequacy of the Regression Model,” in *Applied Statistics and Probability for Engineers*, Danvers (EUA), John Wiley & Sons, Inc., 2011, pp. 426-428.

[167] J. Martin, D. R. Ruiz de Adana and A. G. Asuero, “Fitting Models to Data: Residual Analysis, a Primer,” in *Uncertainty Quantification and Model Calibration*, Zagreb (Croatia), INTECH, 2017, pp. 133-173.

Appendix A

A.1 Prediction of physical properties

The expressions for predicting the physical properties of each phase (gas, liquid, and solid) involved in the reaction mixture are here presented.

Gas phase

- Hydrogen solubility [115] :

$$S_{H_2} = 0.0997 \times 10^{-3} e^{(-612/T)} \qquad [\text{mol m}^{-3}\text{Pa}^{-1}] \qquad \text{A.1}$$

- Henry constant [152] :

$$He = {}^{1}\!/\!_{(S_{H_2} RT)} \qquad [\text{dimensionless}] \qquad \text{A.2}$$

- Hydrogen concentration [153] :

$$C_{H_2,G} = {}^{P_{H_2}}\!/\!_{RT} \qquad [\text{mol m}^{-3}] \qquad \text{A.3}$$

- Vapour pressure of each component :

$$P_{i,V} = \text{Exp}\left[C1 + \frac{C2}{T} + C3\ \text{Log}[T] + C4\ T^{C5}\right] \qquad [\text{Pa}] \qquad \text{A.4}$$

Table A.5 – Antoine coefficients of the liquid components.

	Aniline	Nitrobenzene	Water
C1	2.9128×10^{2}	7.3649×10^{1}	9.0445×10^{1}
C2	-1.6504×10^{4}	-7.2582×10^{3}	-9.7448×10^{3}
C3	-4.2763×10^{1}	-7.3037	-9.5228
C4	3.9918×10^{2}	4.1653×10^{-6}	7.5659×10^{18}
C5	1.0000	2.0000	6.0000
Equation	A.4	A.4	A.4
Reference	[154]	[154]	[154]

Liquid phase

- Density

The density of each component [155] is calculated by equations A.5 and A.6. In Table A.2 the coefficients of each component are presented. The density of the reaction mixture is determined through the equation A.7, that only assumes the participation of aniline and water.

Table A.2 - Coefficients for the prediction of density of pure compounds.

	Water	Aniline	Nitrobenzene
C1	3.5000×10^{-1}	1.0401	7.2599×10^{-1}
C2	6.6667×10^{-1}	2.8056×10^{-1}	2.4731×10^{-1}
C3	1.0000	6.9900×10^{2}	7.1900×10^{2}
C4	1.3334	2.9280×10^{-1}	2.857×10^{-1}
Equation	A.5	A.6	A.6
Reference	[155]	[154]	[154]

$$\rho_i = (17.863 + 58.606\,\tau^{C1} - 95.393\,\tau^{C2} + 213.89\,\tau^{C3} - 141.26\,\tau^{C4})\,MW_i \quad [\mathrm{kg\,m^{-3}}] \quad \text{A.5}$$

where $\tau = 1 - {}^{T}/_{647.096}$

$$\rho_i = \left(C1/C2^{[1+(1-T/C3)^{C4}]}\right) MW_i \quad [\mathrm{kg\,m^{-3}}] \quad \text{A.6}$$

$$\rho_L = \frac{1}{\sum_{i=1}^{n} \rho_i} \qquad [\mathrm{kg\ m^{-3}}] \qquad \text{A.7}$$

where n is the number of compounds.

- Viscosity

The viscosity of each component is given by equation A.8.

$$\mu_{i,L} = \mathrm{Exp}\left[C1 + \frac{C2}{T} + C3 \ln T + C4\ T^{C5}\right] \qquad [\mathrm{Pa\ s}] \qquad \text{A.8}$$

The corresponding coefficients are in Table A.3. The viscosity of the mixture is determined by equation A.9.

$$\mu_L = \mathrm{Exp}\left[x_{ANL,L} \ln\left(\mu_{ANL,L}\right) + x_{H_2O,L} \ln\left(\mu_{H_2O,L}\right) + 0.766\ x_{ANL,L}\ x_{H_2O,L}\right] \qquad [\mathrm{Pa\ s}] \qquad \text{A.9}$$

where $x_{ANL,L}$ and $x_{H_2O,L}$ are, respectively, the molar fractions of aniline and water in the liquid phase.

Table A.3 - Coefficients for prediction of viscosity of pure compounds.

	Aniline	Water
C1	-9.8301×10^{1}	-5.2843×10^{1}
C2	6.5244×10^{3}	3.7036×10^{3}
C3	1.2439×10^{1}	5.8660
C4	0.0000	-5.8790×10^{-29}
C5	0.0000	1.0000×10^{1}
Equation	A.7	A.7
Reference	[155]	[155]

- Diffusion coefficient assuming binary mixture of component A dissolved in a solvent B [156]

$$D_{AB} = \frac{7.4 \times 10^{-12} \sqrt{\varphi_i MW_B}\, T}{1000\, \mu_{B,L} \left(1000\, V_{m,A}\right)^{0.6}} \qquad [m^2\, s^{-1}] \qquad A.10$$

where φ_i is an association factor of solvent B (dimensionless), MW_B is the molecular weight of solvent B expressed in [g mol^{-1}], $V_{m,A}$ is the molar volume of component A expressed in [m^3 kmol^{-1}]. The latter parameters are represented in Table A.4.

Table A.4 – Physical parameters for prediction of diffusion coefficients [156].

	Aniline	Water	Nitrobenzene	Hydrogen
φ_i	1.0	2.6	1.0	1.0
$V_{m,A}$ [m^3 kmol^{-1}]	9.1603×10^{-2}	1.8067×10^{-2}	1.0272×10^{-1}	2.8604×10^{-2}

- Diffusion of component A in a multicomponent liquid mixture [157]

$$D_{A,m} = \frac{10^{-4}\, (1000\, \mu_L)^{-0.8}}{\sum_{\substack{i=1 \\ j \neq A}}^{n} \left[x_j \left(D_{Aj} \times 10^4\right) \left(1000\, \mu_j\right)^{0.8}\right]} \qquad [m^2\, s^{-1}] \qquad A.11$$

Appendix B

To determine representative values of the concentration of the suspended catalyst in the hydrogenation reactors, this present work addressed the procedures of sampling and distinct laboratorial methods to determine this variable. This assessment is presented next.

B.1 Evaluation of sample collection procedure

The sample collecting in hydrogenation units of Bondalti is typically performed in the outlet stream of the reactor (letter Y in Figure B.1). According to the standard instruction, the purge of the sampling site before the collection of the sample is not considered. However, the existence of residual deposits inside the sampling gear may affect the measurement of the catalyst concentration. The effect of sample purging on the determination of catalyst concentration was evaluated by collecting samples consecutively at sampling point Y and then determining its concentration of catalyst through filtration. This evaluation procedure was performed in four reactors (I, II, III, and V).

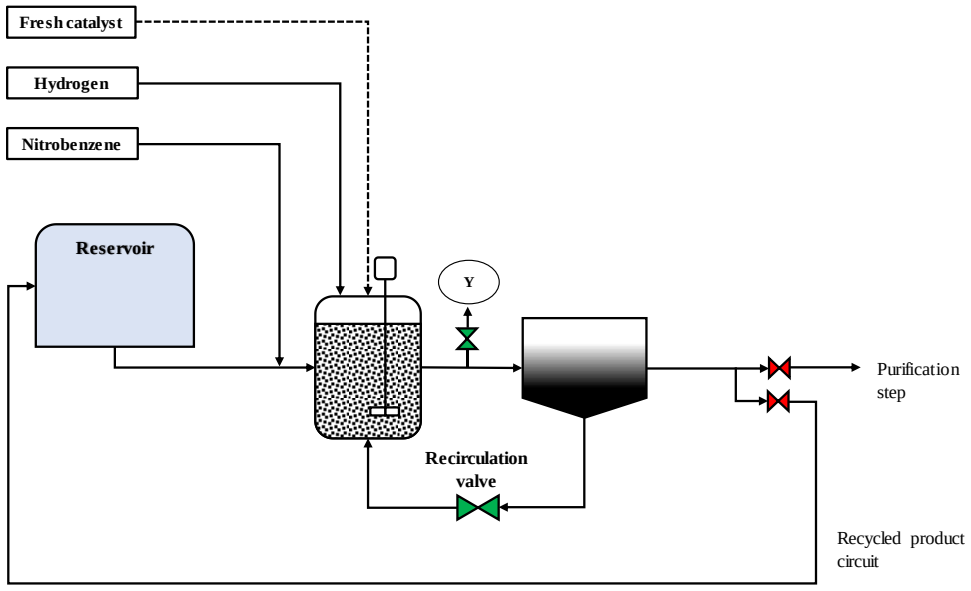

Figure B.1 – Representative scheme of the reactor-decanter system.

To evaluate the variability of results, three series of five consecutive samples per reactor were collected in the corresponding outlet stream. Noted that in each reactor, each series of samples was collected at separate days thus guaranteeing each series was statistically independent from the remaining ones. The values of the catalyst concentration obtained in the samples withdrawn from the different reactors studied are shown in Figure B.2. It is observed that the catalyst concentration is inferior to the second sample, when compared with the first sample collected in each series. In addition, it is observed that the catalyst concentration tends to stabilise from the third sample.

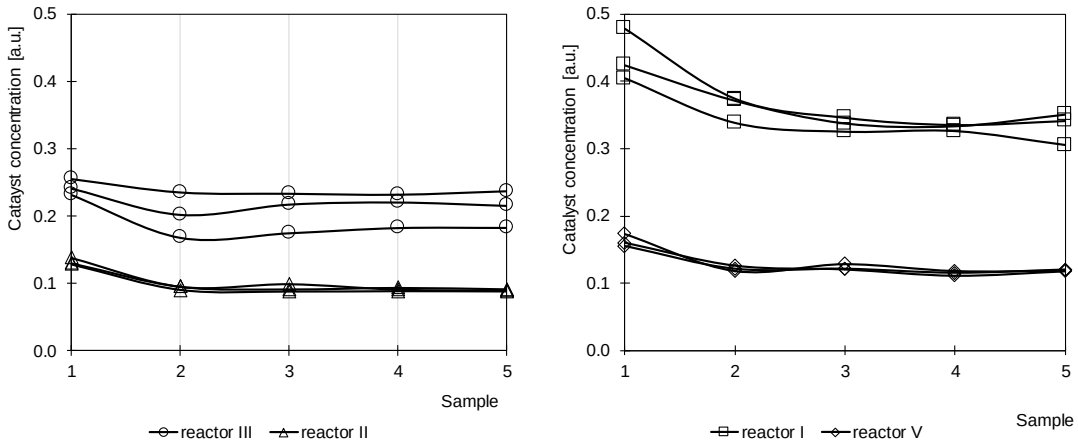

Figure B.2. – Purge test results: Catalyst concentration measured in the purge tests of the reactors I, II, III, and V.

The effect of sample purging on the catalyst concentration values was quantified by calculating the reduction between the average catalyst concentration in the last three samples of each series and the corresponding value obtained in the first sample collected (see Figure B.3) It is possible to observe that the reduction of catalyst concentration was more significant in the reactors I, II and V, in contrast with the reactor III. The average catalyst concentration decreased between 8% and 32%, when compared to the first sample collected. It is verified that the reactor III presented the greatest variability of results, among the reactors assessed.

These results indicate the importance of collecting two consecutive samples per sampler before collecting a more representative sample of the process, in terms of catalyst concentration. Hence, only the third sample collected should be considered for that

purpose. Another possibility consists in eliminating the stagnant volumes presented in the pipping connections of the sampling site.

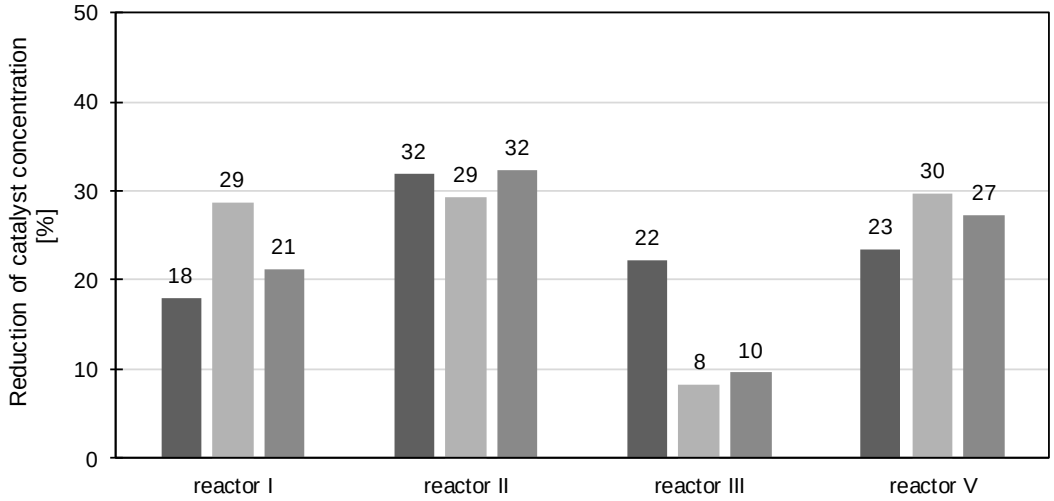

Figure B.3 – Reduction of catalyst concentration observed, in comparison with the first sample collected at each reactor.

B.2 Analytical techniques for evaluating catalyst concentration

Different laboratorial techniques for determining catalyst concentration were evaluated by quantifying the error of measuring a known mass of used catalyst, previously dried. Several aqueous suspensions were prepared with 5g, 10g and 20g of catalyst, corresponding to a catalyst concentration between range 0.05 and 0.34 a.u. This range agrees with the typical values of catalyst concentration observed in the industrial reactor. For each tested mass, it was performed 3 trials in each analytical technique, with the purpose of evaluating the variability of the results. The tested analytical techniques were (1) decantation/centrifugation, (2) decantation, and (3) filtration under vacuum.

B.2.1 Decantation/Centrifugation

In this procedure, the sample is maintained in a proper flask to promote decantation for three hours. Afterwards, the supernatant is removed and the remaining volume centrifugated and transferred to a volumetric flask. The volumetric flask is then made up to the mark with water and weighted (W_1). The mass of the same flask only with water (W_2) is also registered. The mass of catalyst (M_{cat}) is calculated through the following expression:

$$M_{cat} = f_c \times (W_1 - W_2) \quad \text{(B.1)}$$

where f_c is a corrective factor which is directly related to the real density of the catalyst (ρ_{cat}), and the density of the aqueous phase of the mixture (ρ_{liq}) as follows:

$$f_c = \frac{\rho_{cat}}{\rho_{cat} - \rho_{liq}} \quad \text{(B.2)}$$

B.2.2 Decantation

Since the latter analytical technique was still time-consuming, an alternative solution was developed by eliminating the centrifugation step. In this case, the sample is directly analysed in the sample flask.

Firstly, the collected sample is kept for three hours to be decantated being weighted afterwards (W_3). The supernatant is then removed, and the flask is made up with water until is filled and weighted once more. The masses of the empty flask (W_0) and filled with water are also registered. The mass of catalyst is also calculated through equation B.1.

The concentration of catalyst (C_{cat}) is calculated considering the mass of catalyst (M_{cat}), together with the volume occupied by the solid $\left({M_{cat}}/{\rho_{cat}}\right)$ and liquid fractions $\left({M_{liq}}/{\rho_{liq}}\right)$ of the sample. The corresponding calculation formula is described as

$$\begin{cases} M_{liq} = W_3 - M_{cat} - W_0 \\ C_{cat} = \dfrac{M_{cat}}{{M_{cat}}/{\rho_{cat}} + {M_{liq}}/{\rho_{liq}}} \end{cases} \quad \text{(B.3)}$$

B.2.3 Filtration

Alternatively, the concentration of solids can be determined through filtration. In this case, the volume of the sample is determined in a measuring cylinder (V) and it a filtration

membrane (properly dried) is also weighted (M_A). Then, a sample is filtrated using a vacuum filtration equipment. The filtration membrane with the retained solids is stored afterwards in a drying chamber at 35°C for 4h. Finally, the filtration membrane is once again weighted, and its mass recorded (M_B). Therefore, the concentration of catalyst is calculated through the following expression:

$$C_{cat} = \frac{M_B - M_A}{V} \quad \text{(B.4)}$$

B.2.4 Assessment of techniques for determining catalyst concentration

The error related to each known mass of catalyst and for each analytical technique is represented in Figure B.4. The corresponding mean value and deviation for each technique are outlined in Table B.1.

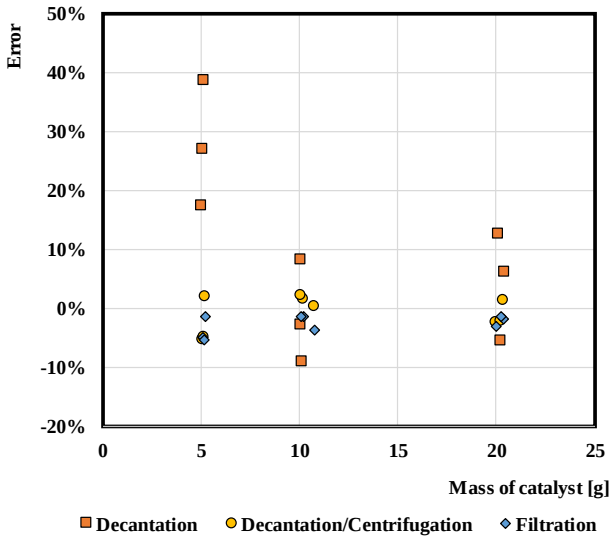

Figure B.4 – Errors obtained from different analytical techniques by using a known mass of catalyst.

Table B.1 - Mean and absolute deviation obtained in the evaluation tests of the analytical techniques for determining catalyst concentration.

	Mean value ± deviation [g]		
Expected value (g)	5	10	20
Decantation + Centrifugation	4.97 ± 0.16	10.46 ± 0.45	19.96 ± 0.39
Decantation	6.48 ± 2.02	9.94 ± 0.56	21.13 ± 2.42
Filtration	4.91 ± 0.02	10.09 ± 0.02	19.77 ± 0.21

In general, a decreasing error for higher concentrations of catalyst is observed, except for filtration that showed similar results in all tests. Decantation presented the highest error and dispersion of results among the analytical techniques studied. Despite decantation/centrifugation and filtration techniques showed similar errors, the latter exhibited higher precision, thereby justifying its utilisation in this investigation. Nonetheless, note that filtration presents greater time of execution due to the drying step.

Attending to the decantation procedure, the possible causes behind the significant errors obtained and the variability of the results were assessed. One remarks that that the volumetric measurement directly through the sample flask might be inaccurate, which, in turn, could hinder the calculation of the mass of catalyst. For this reason, an improvement of the latter technique was attempted, with the proviso that the simplicity and promptness of the overall procedure should not be compromised. Therefore, the use of a conical piece screwed on the top of the sample flask was suggested (see Figure B.5). This solution is commonly applied to determine the density of multiphasic mixtures, which is referred to as *pycnometer bottle* [94].

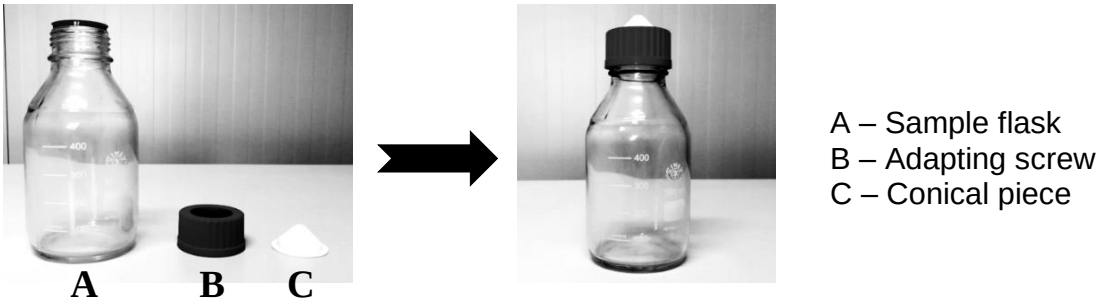

Figure B.5 – Pycnometer bottle prototype for determining catalyst concentration.

The pycnometer bottle-concept was then tested with the same mass of catalyst as in the latter techniques tested. Figure B.6 and Table B.2 provide a comparison between the conventional and improved (pycnometer) decantation techniques. It is clearly verified that the error and the precision of results were upgraded. Hence, this solution is recommended, as it does not affect the time of execution, nor the procedure applied.

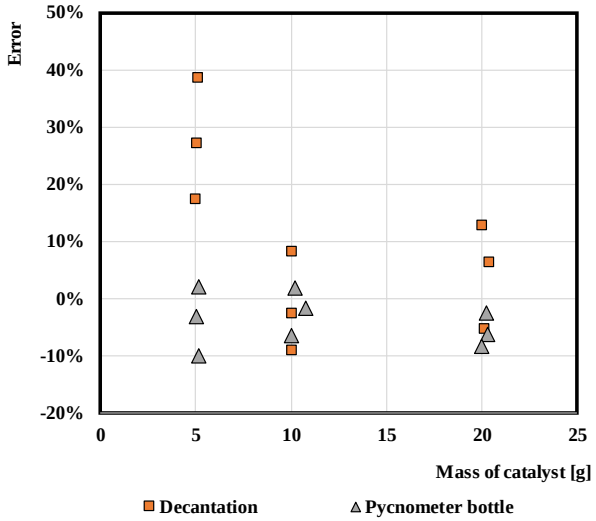

Figure B.6 – Errors obtained in the decantation and pycnometer bottle methods.

Table B.2 – Mean and absolute deviation obtained in the evaluation tests of decantation and pycnometer bottle methods for determining catalyst concentration.

	Mean value ± deviation		
Expected value [g]	5	10	20
Decantation	6.48 ± 2.05	9.94 ± 0.81	21.13 ± 2.38
Pycnometer bottle	4.92 ± 0.19	10.11 0.50	19.03±0.52